2021

The Role of Hippo Signalling in Merlin Null Tumours of the Nervous System

Laraba, Liyam

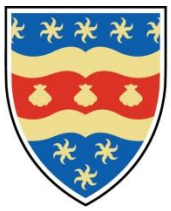

UNIVERSITY OF PLYMOUTH

The Role of Hippo Signalling in Merlin Null Tumours of the Nervous System

By

Liyam James Laraba

A thesis submitted to the University of Plymouth in partial fulfilment for the degree of

DOCTOR OF PHILOSOPHY

Peninsula Medical School

August 2021

Acknowledgements

First and foremost I must give my thanks to my director of studies, Professor David Parkinson. David you have given me excellent training, guidance and countless opportunities to grow as a scientist, all whilst working with refreshing optimism and enthusiasm. It has been a pleasure to work alongside you. Thanks also to the rest of my supervisory team, Dr Sara Ferluga and Professor Oliver Hanemann. There have been countless people in the lab who have supported and guided me during my time in the lab, it would be impossible to name everyone, but the support of people like Dr Jemma Dunn, Trish Woodley and Bora Agit has been invaluable during my PhD studies. I must also thank my mum and Len, my Dad, and the rest of my family and friends for their ever-present love and support, whether it be financial or emotional, I hope you know that your parenthood has played a huge part in me being able to work in scientific research, which I have such passion for.

Author's Declaration

At no time during the registration for the degree of Doctor of Philosophy has the author been registered for any other University award without prior agreement of the Doctoral College Quality Sub-Committee.

This thesis has been proofread by a third party; no factual changes or additions or amendments to the argument were made as a result of this process. A copy of the thesis prior to proofreading will be made available to the examiners upon request.

Work submitted for this research degree at the University of Plymouth has not formed part of any other degree either at the University of Plymouth or at another establishment.

Publications (or public presentation of creative research outputs): None

Presentations at conferences:

- CTF meeting – Paris, 2018 – Poster Presentation
- British Neuropathological Society – London, 2019: Oral Presentation
- CTF Meeting – Virtual, 2020 – Poster Presentation
- AACR Meeting – Virtual, 2020 – Poster Presentation

Word count of main body of thesis: 39 406

Signed: Liyam Laraba

Date: 30/09/2020

Liyam James Laraba

The Role of Hippo Signalling in Merlin Null Tumours of the Nervous System

Abstract

Meningiomas and schwannomas are mostly benign tumours of the nervous system that currently have no clinically approved treatments apart from surgical resection. The tumour suppressor Moesin-Ezrin-Radixin-Like Protein (Merlin) is deleted in 50-60% and 70% of meningiomas and schwannomas respectively. The Hippo pathway is an evolutionarily conserved pathway that has been shown to control tissue size by contact-mediated growth inhibition. Previous studies have shown that there is aberrant nuclear activity of yes-associated protein (YAP) and transcriptional coactivator with PDZ-binding motif (TAZ), the co-transcriptional activators of the Hippo pathway in Merlin-null meningioma and schwannoma. Nuclear YAP and TAZ activate transcription, primarily by binding to the TEAD family of transcription factors, which has been linked to multiple tumour phenotypes. Here we aim to show that aberrant Hippo pathway activity in Merlin null meningioma and schwannoma can be targeted either genetically or pharmacologically to reduce tumour proliferation. We used a combination of in vitro and in vivo approaches, including primary tumour cell culture and Merlin null mouse models, to establish the role of Hippo signalling in Merlin null meningioma and schwannoma and to identify therapeutic targets. We saw that there was increased nuclear localisation of YAP in primary meningioma cells, and that knockdown of YAP or TAZ reduces proliferation in both meningioma and schwannoma cells. We used novel inhibitors of TEAD palmitoylation which disrupted the interaction between TEAD proteins and YAP/TAZ, leading to reduction of proliferation in meningioma and schwannoma. Through an RNA sequencing screen, we identified that the cancer stem cell marker ALDH1A1 is strongly upregulated in multiple meningioma and schwannoma models;

inhibition of ALDH1A1 reduced proliferation in primary meningioma and schwannoma cells. YAP and TAZ both transcriptionally activate TEAD family members, leading to transcription of genes which drive tumour phenotypes. In summary, we have characterised aberrant Hippo pathway activity in Merlin null meningioma and schwannoma, exploring the mechanisms by which loss of Merlin drives tumour progression, and explored therapeutic options that target such pathways. This thesis has provided evidence that pharmacological disruption of TEAD transcription is an effective way of reducing proliferation in Merlin null schwannoma and meningioma, thus provides a foundation for further studies testing inhibitors of TEAD palmitoylation in a schwannoma and meningioma *in vivo* mouse models.

Abbreviations

Akt	Protein Kinase B
AMPD1	adenosine monophosphate deaminase 1
ANOVA	Analysis of Variance
ARID	AT-rich interaction domain
BM1	Ben-Men-1
BSA	Bovine serum albumin
CGS	Cambridge Genomic Services
CNTN6	Contactin 6
CPM	Counts Per Million
CRBP	Cellular retinol-binding protein
CRABP	Cellular retinoic acid-binding protein
DAB	3,3'-Diaminobenzidine
DMEM	Dulbecco's Modified Eagle's Medium
DMSO	Dimethyl sulphoxide
DPI	Days post-injury
EDTA	Ethylenediaminetetraacetic Acid
EdU	5-Ethynyl-2'deoxyuridine
ERM	Ezrin-Radixin-Moesin
FAK	Focal adhesion kinase
FAT4	Fat tumour suppressor homolog 4
FBS	Foetal Bovine Serum
FC	Fold Change
FDR	False Discovery Rate
FERM	4.1-Ezrin-Radixin-Moesin
FOXJ1	Forkhead box protein J1
GFM	Proliferation medium for Schwann cells and schwannoma
HMC	Human Meningeal Cells
HRP	Horseradish Peroxidase
IBMX	3-Isobutyl-1-methylxanthine
Igsf21	Immunoglobulin superfamily member 21
IHC	Immunohistochemistry

LB	Luria-Bertani
LZTR1	Leucine-zipper-like transcriptional regulator 1
MAPK	Mitogen-Activated Protein Kinase
Merlin	Moesin-Ezrin-Radixin-Like Protein
mTORC1	Mammalian target of rapamycin complex one
OCT	Optimal Cutting Temperature Compound
Nefh	Neurofilament heavy class promoter
NF2	Neurofibromatosis two
NRG-1	Neuregulin-1
PAGE	Polyacrylamide Gel Electrophoresis
PBS	Phosphate Buffered Saline
PDVF	Polyvinylidene Fluoride
PFA	Paraformaldehyde
PI3K	Phosphoinositide 3-kinase
PKA	Protein Kinase A
PLL	Poly-L-lysine
RAR	Retinoic acid receptor
RARE	Retinoic acid response element
RXR	Retinoid X receptor
RIPA	Radioimmunoprecipitation Assay
RPM	Revolutions per Minute
RTK	Receptor Tyrosine Kinase
SDS	Sodium Dodecyl Sulphate
Src	Proto-oncogene tyrosine-protein kinase
TAZ	Transcriptional coactivator with PDZ-binding motif
TBS-T	Tris-buffered saline containing 0.5 % Tween
X-ist	X-inactive specific transcript
YAP	Yes-associated protein

Contents

1 Introduction 1

1.1 Background 1

1.2 The Tumour Suppressor Merlin 2

1.3 The Hippo Pathway 10

1.3.1 Pathway Overview 10
1.3.2 Hippo Pathway and Contact Inhibition 12
1.3.3 Upstream Signalling and Merlin 17
1.3.4 Hippo Signalling in Meningioma and Schwannoma 17
1.3.5 Drugs Targeting the Hippo Pathway 20
1.3.6 The Biology of Meningioma and Schwannoma 21

1.4 Overview of the Clinical Treatment and Biology of Meningiomas and Schwannomas 22

1.4.1 Clinical Treatment of Meningiomas 22
1.4.2 Clinical Treatment of Schwannomas 23
1.4.3 Drug Treatments and Clinical Trials 23
1.4.4 Genetic Alterations in Schwannoma 24
1.4.5 Genetic Alterations in Meningioma 25
1.4.6 Epigenetics of Meningioma and Schwannoma 26

1.5 Meningioma and Schwannoma Mouse Models 28

1.5.1 Schwannoma Mouse Models 28

1.6 Meningioma Mouse Models 32

1.7 RNA Sequencing for Differential Expression Analysis 34

1.8 Cancer Stem Cells and ALDH1A1 36

1.9 Project Aims 40

2 Materials and Methods 42

2.1 Clinical Samples 42

2.2 Cell Culture 44

2.2.1 Immortalised Human Cell Lines 44

2.2.2 Primary meningioma and human meningeal cells 44
2.2.3 Primary schwannoma 45
2.2.4 Primary human Schwann cells 45
2.2.5 Primary mouse Schwann cells 46
2.2.6 Passaging Cells 46
2.3 Mice 47
2.3.1 Genotypes of transgenic mouse lines 47
2.3.2 Genotyping 48
2.3.3 Sciatic Nerve Injury 54
2.3.4 Vivace Oral Gavage 54
2.4 RNA Sequencing 54
2.4.1 Sample Preparation 54
2.4.2 Data Analysis 55
2.5 Antibodies 55
2.6 Western Blotting 56
2.6.1 Western Blot Sample Preparation 56
2.6.2 Western Blot Gel Running, Transfer and Detection 57
2.7 EdU Proliferation Assay 60
2.8 Immunofluorescence 62
2.8.1 Immunofluorescence for Cultured Cells 62
2.8.2 Tissue preparation, sectioning and immunofluorescence 63
2.9 Paraffin Embedded Immunohistochemistry (IHC) 64
2.9.1 Staining of Paraffin Sections 65
2.10 Lentivirus 71
2.10.1 Lentiviral Plasmid Preparation 71
2.10.2 Lentiviral Transfection and Production 71
2.10.3 Lentiviral Transduction 72
2.11 Drug Treatments 75
2.12 Statistical Analysis 76
3 Results 78

3.1 RNA Sequencing of Schwann cell conditional knockout nerves before and after injury identifies novel targets for human meningioma and schwannoma. 78

3.1.1 Introduction 78

3.1.2 Conditional deletion of NF2 and YAP in Schwann cells causes differential expression of genes before and after sciatic nerve crush injury. 79

3.1.3 Discussion 84

3.2 The Cancer Stem Cell Marker ALDH1A1 is Upregulated in Merlin Null Meningioma and Schwannoma Tumours 86

3.2.1 Introduction 86

3.2.2 ALDH1A1 is upregulated in NF2-Deficient Mouse Models 88

3.2.3 The Hippo Pathway Effector TAZ is Required for ALDH1A1 Expression in Mouse Schwann Cells 93

3.2.4 ALDH1A1 is upregulated in human meningioma and schwannoma 99

3.2.5 ALDH1A1 drives proliferation in Merlin Null meningioma and schwannoma cells in vitro. 105

3.2.6 Discussion 116

3.3 Hippo Pathway regulation in meningioma and schwannoma and the use of novel inhibitors to target YAP/TEAD activity. 121

3.3.1 Introduction 121

3.3.2 Expression of Hippo Pathway Proteins in Meningioma Cell Lines and Primary Meningioma cells 122

3.3.3 The YAP-TEAD Inhibitor Verteporfin Reduces Proliferation in Primary Meningioma Cells 125

3.3.4 Loss of Merlin Causes Translocation of YAP into the Nucleus in Meningioma 129

3.3.5 Knockdown of YAP or TAZ Proteins Reduces Proliferation of both the Meningioma cell line BM1 and Primary Human Meningioma Cells 132

3.3.7 Vivace Inhibitors are a Novel Selective Inhibitor of YAP and TAZ Mediated TEAD Transcriptional Activity 138

3.3.8 Vivace Compounds Inhibit Primary Meningioma and Schwannoma in Vitro .. 146

3.3.9 Preliminary Assessment of Vivace Inhibitors in the Postn-Cre Schwannoma Mouse Model 155

3.3.10 Discussion 160

4 Discussion 167

5 Future Work 172

6 Conclusion 173

7 References.....175

8 Appendix:.....190

List of Figures

Figure 1.1 – The domains of the tumour suppressor Merlin 5

Figure 1.2 – Signalling pathways affected by loss of Merlin 7

Figure 1.3 – Stages of Schwann cell development 11

Figure 1.4 - Overview of Merlin's influence on the mammalian Hippo Pathway 14

Figure 1.5 – YAP and TAZ protein structure 15

Figure 1.6 - Retinoic acid signalling 39

Figure 2.1 Typical PCR genotyping gel image 51

Figure 3.1.1 RNA sequencing diagram to show overlap of intact and injured NF2 null nerves 82

Figure 3.2.1 ALDH1A1 is upregulated in Merlin null mouse sciatic nerve 89

Figure 3.2.2 ALDH1A1 is upregulated in non-myelinating Merlin null Schwann cells 91

Figure 3.2.3 TAZ is required for expression of ALDH1A1 in mouse sciatic nerve 95

Figure 3.2.4 ALDH1A1 is upregulated in Postn-Cre NF2 null mice 97

Figure 3.2.5 ALDH1A1 is upregulated in human meningioma cell lines 100

Figure 3.2.6 ALDH1A1 is upregulated in primary meningioma tissue 102

Figure 3.2.7 IHC for ALDH1A1 in human schwannoma 104

Figure 3.2.8 Knockdown of TAZ reduces ALDH1A1 expression 108

Figure 3.2.9 ALDH1A1 inhibitors reduce proliferation in BM1 cells 109

Figure 3.2.10 ALDH1A1 inhibitors reduce proliferation in primary schwannoma 111

Figure 3.2.11 ALDH1A1 inhibitors increase Cisplatin sensitivity in BM1 cells 113

Figure 3.2.12 ALDH1A1 inhibitors reduce proliferation in primary schwannoma 115

Figure 3.2.13 ALDH1A1 is upregulated in NF2-deficient schwannoma and meningioma through a TAZ-dependent mechanism 120

Figure 3.3.1 Merlin status does not regulate Hippo pathway protein levels in meningioma 124

Figure 3.3.2 Verteporfin reduces proliferation in primary meningioma cells 127

Figure 3.3.3 Verteporfin does not affect YAP nuclear localisation in primary meningioma 130

Figure 3.3.4 Knockdown of YAP or TAZ in BM1 cells reduces proliferation 134

Figure 3.3.5 Knockdown of YAP or TAZ in primary Merlin negative meningioma reduces proliferation 136

Figure 3.3.6 Vivace inhibitors reduce proliferation in BM1 cells 140

Figure 3.3.7 Vivace inhibitors reduce proliferation in KT21 cells 142

Figure 3.3.8 Vivace inhibitors reduce TEAD expression in BM1 cells 145

Figure 3.3.9 Vivace compounds reduce proliferation in Merlin null primary meningioma cells 148

Figure 3.3.10 TEAD expression in heterogeneous in primary meningioma cells 150

Figure 3.3.11 Vivace compounds reduce proliferation in primary schwannoma cells 153

Figure 3.3.12 Vivace compounds decrease CTGF expression in primary schwannoma 154

Figure 3.3.13 Oral gavage with VT03989 reduces proliferation in NF2 null DRGs 158

Figure 3.3.14: Proposed mechanisms of verteporfin and Vivace therapeutics drugs inhibition in Merlin-null schwannoma 165

Figure 4.1 Aberrant Hippo pathway activity in Merlin null schwannoma and meningioma lead to increased proliferation and ALDH1A1 upregulation which can be targeted genetically or pharmacologically 168

List of Tables

Table 2.1 Primary tumour clinical information 43

Table 2.2 PCR genotyping reaction 50

Table 2.3 PCR reaction steps 51

Table 2.4 Primers for genotyping 52-53

Table 2.5 Reagents used for gel electrophoresis 59

Table 2.6 EdU reaction mix 61

Table 2.7 Primary antibodies 68-69
Table 2.8 Secondary antibodies 70
Table 2.9 Lentivirus constructs 74
Table 2.10 Drugs 75
Table 3.1 Top upregulated and downregulated RNAseq transcripts 83
Table 3.2.1 Clinical information for schwannomas assessed for ALDH1A1 expression by IHC 103
Table 3.3.1 Mouse oral gavage weights and adverse effects 157

1 Introduction

1.1 Background

Meningiomas and schwannomas are mostly benign tumours of the nervous system. Meningiomas are the most common intracranial tumour and they arise from the middle layer of the meninges, a thick membrane that protects and encapsulate the brain and spinal cord. Meningiomas are typically intracranial but can be spinal, and have a combined incidence of 97.5 / 100 000 based on a review of cases in the United States of America (Wiemels et al., 2010). A more recent 2012 review on meningioma epidemiology in the United Kingdom revealed meningiomas have an incidence of 5.3 /100 000 person years between 1996 and 2008, with incidence being twice as high in women compared with men (Cea-Soriano et al., 2012). Symptoms of meningiomas include but are not limited to: pain; changes in vision; headaches; hearing loss and seizures, depending on the site of the tumour. Schwannomas arise from Schwann cells, a type of glial cell that provides trophic support and myelin to peripheral nerves. Typically, schwannomas are vestibular [occurring on the 8th cranial nerve], although they can grow on peripheral nerves such as the sciatic nerve or within the brachial plexus. Vestibular schwannomas have an incidence of 1.2 / 100 000, based on cases in the United States of America (Babu et al., 2013). In the UK, at the time of writing, studies have only assessed schwannoma epidemiology regionally. One such study by Evans et al investigated schwannoma incidence in the north-west of England (4.1 million people) and found that incidence was 1.4 / 100 000 (Evans et al., 2005). Symptoms of schwannomas include but are not limited to: pain; loss of hearing; loss of coordination and balance; facial weakness and paralysis. Paralysis is caused by compression of the cranial nerves (Chen et al., 2014). Meningiomas and schwannomas are currently treated in similar ways, following diagnosis and monitoring, surgical resection occurs if tumours are symptomatic or fast growing, with occasional use

of radiotherapy. However, surgery is an intrusive procedure and inaccessible or incomplete resection of these tumours can lead to recurrence, progression, further morbidity and mortality.

Since the advent of Hanahan and Weinberg's "Hallmarks of cancer" (Hanahan and Weinberg, 2000, Hanahan and Weinberg, 2011) in 2000, there has been a mass shift in focus away from traditional cytotoxic chemotherapies, towards targeted therapies. The identification of phenotypes that are unique to tumour cells by Hanahan and Weinberg, as well as the development of much more accurate genomic and proteomic analytical techniques have allowed targeted therapies become the *de facto* approach for treating tumours pharmaceutically. Targeted therapies aim to disrupt specific genes, proteins or stases that facilitate a tumour's existence or growth. Tumour specific therapies are often transferable to other tumours if they share a common genetic background. Loss of function of the tumour suppressor gene neurofibromatosis two (NF2) which encodes the protein Moesin-Ezrin-Radizin-Like Protein (Merlin) is one such commonality between meningiomas and schwannomas. Among a number of roles, Merlin is important for modulation of the Hippo pathway, an evolutionarily conserved pathway that controls tissue size and is often dysregulated in tumours (Maugeri-Sacca and De Maria, 2018). This PhD uses mouse models, human immortalised cell culture and primary cell culture with an aim to identify novel therapeutic targets for meningioma and schwannoma. This introduction will provide an overview of the tumour suppressor Merlin and the Hippo pathway, meningioma and schwannoma, and discuss how targeted therapies are being developed for these tumours.

1.2 The Tumour Suppressor Merlin

Moesin-Ezrin-Radixin-Like Protein (Merlin) is an actin cytoskeleton-membrane linker that is well-characterised as a growth repressive tumour suppressor (Hanemann, 2008). Merlin is so called as it shows homology with the Ezrin-Radixin-Moesin (ERM) family

paralogues, which all contain a conserved 4.1-Ezrin-Radixin-Moesin (FERM) domain, with the FERM domain playing a role in signalling from the cell surface (McClatchey and Fehon, 2009). Merlin acts at various cell junctions to transduce signals which lead to contact-mediated inhibition of growth. The domain structure and phosphorylation sites of Merlin are depicted in Figure 1.1. Encoded by the NF2gene located on chromosome 22q 12.2, biallelic loss of Merlin was identified in 1993 as causative for the rare autosomal dominant genetic condition neurofibromatosis type 2 (Rouleau et al., 1993, Trofatter et al., 1993). Patients with neurofibromatosis type 2 develop multiple meningiomas and schwannomas throughout their lifetime. In neurofibromatosis type 2, 100 % of tumours arise due to loss of NF2, whereas in sporadic cases, biallelic Merlin mutations leading to tumourigenesis occur in 50-60% and 70% of sporadic meningiomas and schwannomas respectively (Petrilli and Fernandez-Valle, 2016).

Structurally, Merlin exists in multiple isoforms, with the canonical full length protein consisting of 595 amino acids (Cooper and Giancotti, 2014). X-ray crystallography of Merlin revealed an N-terminal FERM domain (Shimizu et al., 2002), conserved in ERM family members, a common feature of cytoskeletal-membrane scaffold proteins, focal adhesion kinases and Janus tyrosine kinases are two examples of other plasma membrane associated FERM domain containing proteins, which facilitate integrin and peptide hormone signalling respectively. The FERM domain of Merlin is followed by a helical domain in the middle of the secondary structure and a regulatory C-terminal domain, in which the critical regulatory Ser518 residue is located. The phosphorylation of Ser518 residue has been shown to be responsible for regulating Merlin's activity by triggering a conformational change to a less active closed conformation (Ye, 2007). Merlin's FERM domain is distinct from other ERM proteins; it can interact with components of the cytoskeleton such as F-actin through its FERM domain, as it lacks this functionality in its C-terminal domain (Xu and Gutmann, 1998). Phosphorylation of Ser518 by p21-

activated kinase (PAK) or Protein Kinase A (PKA) was found to disrupt the intramolecular interactions of Merlin, thus limiting the ability of Merlin to interact with various targets (Rong et al., 2004). Merlin activity is also attenuated by phosphorylation of other sites; AKT phosphorylates Merlin at residues Thr230 [FERM domain] and Ser315 [helical domain], phosphomimetic mutant studies have shown that simultaneous phosphorylation of these residues increases motility and proliferation in rat schwannoma cells (Ye, 2007). PKA also phosphorylates Merlin at Ser66 which increases the affinity of Ezrin to Merlin's C-terminal domain, facilitating Merlin's association with the plasma membrane (Ye, 2007).

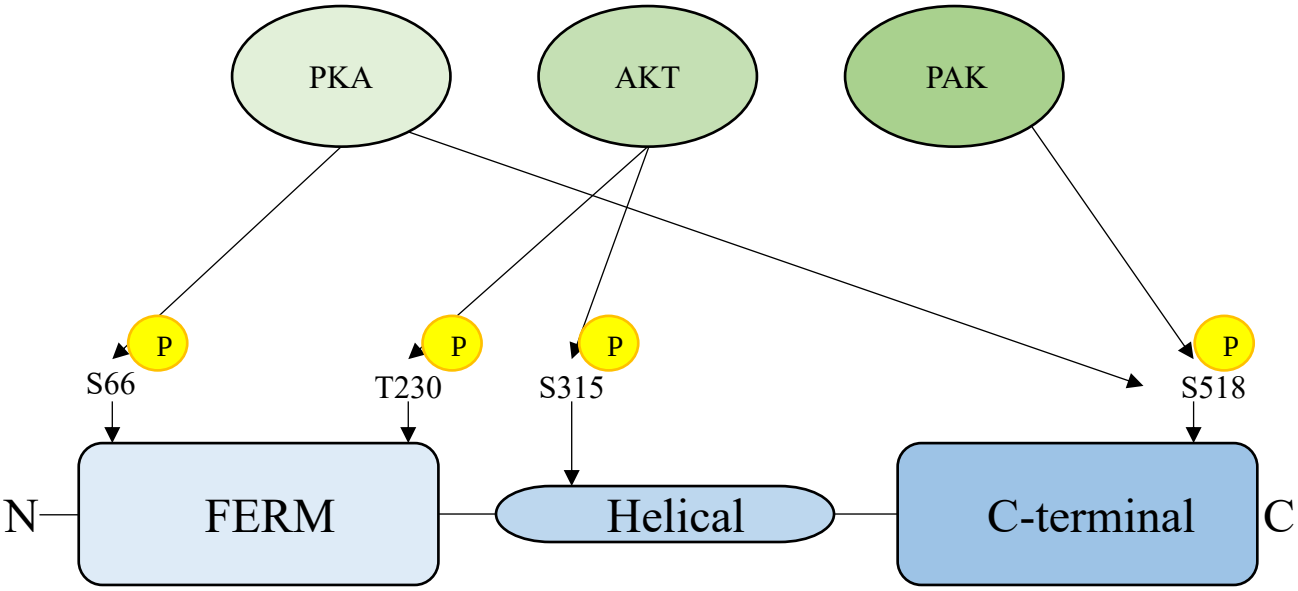

Figure 1.1: The domains of the tumour suppressor Merlin. Merlin contains an N-terminal FERM domain, a helical domain and a C-terminal hydrophobic tail. The specific residues that are phosphorylated by PKA (Ser66 and Ser518), AKT (Thr230 and Ser315) and PAK (Ser518) to regulate Merlin's activity are illustrated.

Since its discovery, studies have well-characterised the way in which Merlin regulates tumour suppression in an effort to identify molecular targets for therapies (Cooper and Giancotti, 2014). Merlin loss activates a range of downstream signalling pathways such as: mitogen-activated protein kinase (MAPK); focal adhesion kinase/Proto-oncogene tyrosine-protein kinase (FAK; Src); phosphoinositide 3-kinase/ Protein Kinase B (PI3K; AKT); Mammalian Target of Rapamycin Complex One (mTORC1) and Wnt/β-catenin (James et al., 2009, Zhou and Hanemann, 2012, Poulikakos et al., 2006). Indeed, Merlin also regulates growth via inhibiting the downstream signals of a variety of receptor tyrosine kinases (RTKs) including erythroblastic oncogene B homologue 2 (erbB2), erythroblastic oncogene B homologue 3 (erbB3), platelet-derived growth factor receptor beta (PDGFRβ) and insulin-like growth factor 1 receptor (IGF1R) (Ammoun et al., 2012) (Haskins et al., 2014, Torres-Martin et al., 2013, Beauchamp et al., 2020). Merlin has

been shown to promote PDGFRβ internalisation and degradation in the schwannoma cell line HEI-193 (Fraenzer et al., 2003). Knockdown of Merlin with RNA interference increases the expression of these RTKs in mouse Schwann cells and they are also elevated in human primary schwannoma cells compared to Schwann cells expressing Merlin (Lallemand et al., 2009).

As well as activating various transmembrane receptors that stimulate mitogenic pathways, Merlin also influences cell growth in the cytoplasm. Merlin inhibits Ras activation, which reduces mitogen-activated protein kinase (MAPK) activity by disrupting the interaction of RAS with growth factor receptor bound protein 2 (GRB2) (Zhou and Hanemann, 2012). More recently it has been shown that Merlin interacts with Ras and p120 Ras GTPase activating protein, however activation of RAS signalling in orthotopic models where primary mouse Schwann cells with Ras knockdown were injected into the sciatic nerve did not lead to tumourigenesis (Cui et al., 2019). This shows that RAS activation driven by loss of Merlin is not sufficient for schwannoma tumorigenesis, and that other mitogenic pathways must be involved. Elevated MAPK activity led to increased phosphorylated ERK in Merlin null primary schwannoma cells that was enhanced by PDGFRβ signalling (Fraenzer et al., 2003). Merlin also inhibits the RAC1/PAK pathway, which ultimately leads to a reduction in c-Jun N-terminal kinase (JNK) signalling by preventing PAK from associating with focal adhesions. (Kissil et al., 2003). Merlin has also been shown to inhibit the activity of the PI3K/AKT/MTORC signalling axis by blocking an interacting between phosphatidylinositol 3-kinase enhancer L (PIKE) and PI3K. Furthermore, Merlin null tumour tissue DNA sequencing of schwannomas and meningiomas both feature increased phosphorylation and expression of AKT (Yesiloz et al., 2017). MTORC1 is also inhibited by Merlin independently of upstream MAPK activity; it has been shown that whilst blocking MAPK activity with chemical inhibitors, MTORC function could still be blocked by knockdown

of Merlin (James et al., 2009). These complex sets of signalling pathways are described in figure 1.1. The importance of Merlin in the context of the Hippo pathway will be discussed in Section 1.3.4.

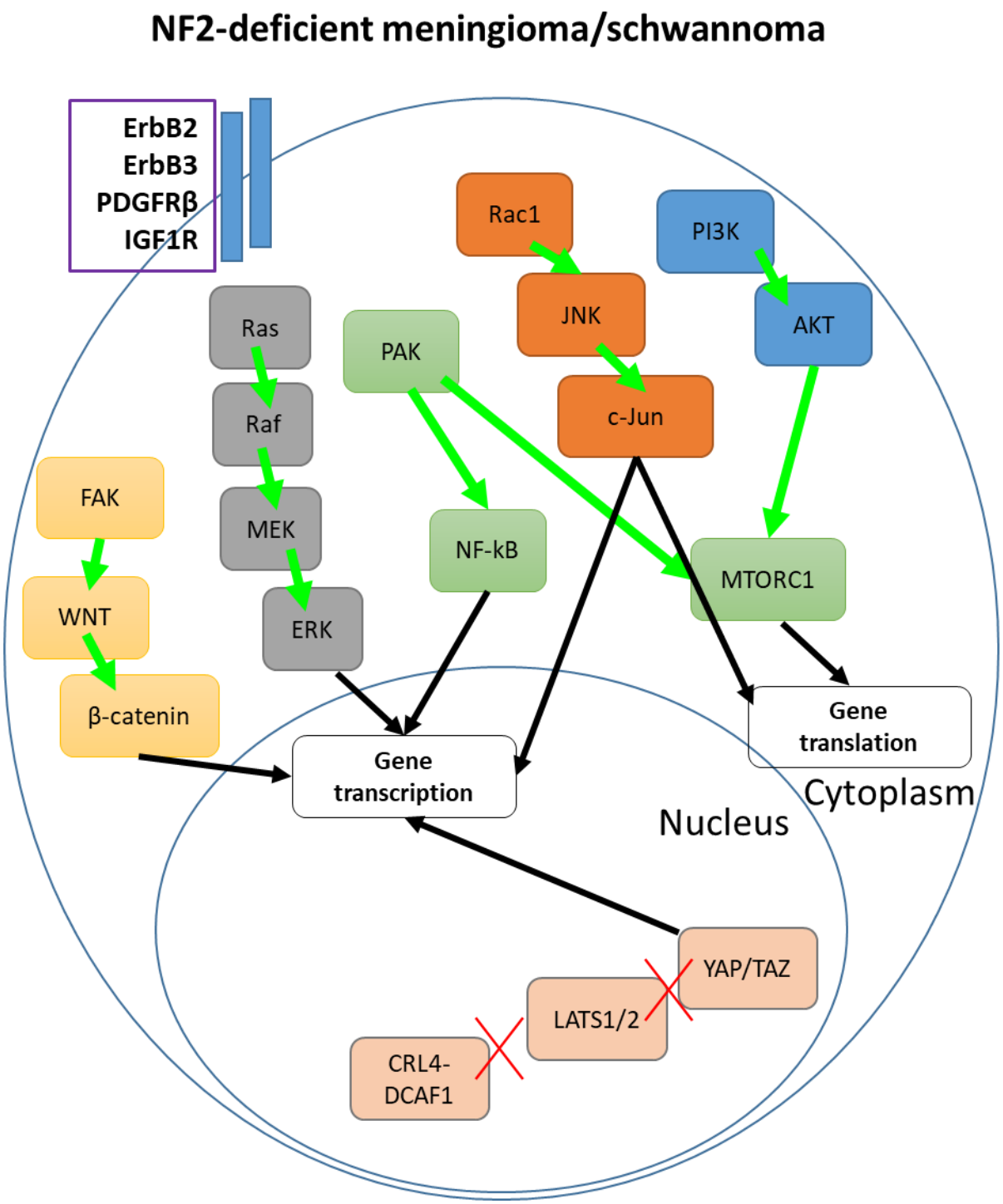

Figure 1.2: Signalling pathways affected by loss of Merlin. Here we show the various pathways that have been identified in the literature as dysregulated following loss of Merlin. Green arrows represent the activation of a pathway, whereas red crosses represent proteins being inhibited following loss of Merlin. Black arrows represent the end result of the pathway that contribute to tumour phenotypes. The growth factor receptors erythroblastic oncogene B homologue 2 (erbB2), erythroblastic oncogene B homologue 3 (erbB3), platelet-derived growth factor receptor beta PDGFRβ and insulin-like growth factor 1 receptor (IGF1R) have all been shown to be activated following loss of Merlin. Growth factor receptors stimulate downstream signalling through pathways such as the phosphoinositide 3-kinase/ Protein Kinase B (PI3K; AKT), which activates Mammalian Target of Rapamycin Complex One (mTORC1). Activation of Ras and downstream signalling in the mitogen-activated protein kinase (MAPK) pathway leads to phosphorylation of MAP3K (RAF), MAP2K (MEK) which phosphorylates MAPK (ERK). In addition, Focal-adhesion kinase (FAK), can activate Wnt signalling and lead to nuclear localisation of β-catenin. Transcription can also be driven by p21-activated kinase activating NF-κB signalling. Loss of Merlin leads to an increase in CRL4/DCAF1-mediated degradation of large tumour suppressor kinase 1/2 (LATS1/2), leading to nuclear accumulation of yes-associated protein (YAP) and Transcriptional coactivator with PDZ-binding motif (TAZ). These pathways have all been shown to be activated following loss of Merlin and subsequently been linked to tumour phenotypes.

The phosphorylation of Ser518 is the main regulatory modification that attenuates Merlin's activity by giving rise to a more closed conformation, the closed conformation leads to deactivation of Merlin and a failure to suppress growth. (Rong et al., 2004, Cooper and Giancotti, 2014). Work done in a rat schwannoma cell line has shown that reintroduction of Merlin suppresses schwannoma cell growth (Morrison et al., 2001a), Merlin was found to form a complex with the cytoplasmic tail of CD44 to facilitate growth-suppressive signalling. Merlin can be phosphorylated by p21-activated kinase (PAK) following a signal by RAC1 (De Maria, 2017). Additionally, PKA can phosphorylate Merlin at S10 which disrupts interactions with the actin-cytoskeleton (Ye, 2007). More recently, protein-protein interaction studies with mutant variants of Merlin has led to identification of novel binding partners such as apoptosis-stimulated p53 protein 2 (Hennigan et al., 2019). The molecular studies with mutant forms of Merlin are continuing to identify the way in which Merlin transduces signals from the various types of cell junctions to regulate cell growth.

Loss of Merlin has been seen reported in subsets of schwannoma, meningioma osteosarcomas, mesothelioma, renal carcinoma and hepatocellular carcinoma (Harvey et al., 2013). For example in mesothelioma, Merlin is inactivated in 21% of tumours and 50% of mesotheliomas were found to have acquired somatic NF2 mutations during or after tumourigenesis (Sekido, 2011). Meningiomas and schwannomas that are the result of neurofibromatosis type 2 all have one germline mutation in NF2 and the consensus of studies is that the other copy of nf2 is mutated in >70% of tumours screened (Ruggieri et al., 2016). The genetics shown in meningioma and schwannoma are consistent with Knudson's two-hit hypothesis which states that genes require two mutations before a phenotype is seen (Knudson, 2001). It is likely that all schwannomas and meningiomas found in neurofibromatosis type 2 patients feature biallelic loss of Merlin. Similarly, nf2 is frequently mutated and biallelic loss occurs in about 50-60% and 70% of in sporadic

meningioma and schwannoma cases respectively (Yuzawa et al., 2016, Havik et al., 2018).

1.3 The Hippo Pathway

The Hippo pathway is an evolutionarily conserved signalling cascade that maintains tissue and organ size in a variety of organisms from drosophila to humans. Although components of the pathway were identified earlier, the Hippo pathway was formally established in 2003 by *Udan et al* and was so called due to the phenotype seen on the heads of Hippo knockout *Drosophila* (Udan et al., 2003). The mammalian orthologues of Hippo are the macrophage stimulating protein kinases 1 and 2 (MST1/2). In the following paragraphs, I will give an in-depth overview of the mammalian Hippo pathway and its role in responding to cell-cell contacts (1.3.1), its role in cancer (1.3.2) and its significance in Merlin null meningioma and schwannoma tumour types (1.3.3).

1.3.1 Pathway Overview

Hippo signalling is active when a tissue has grown to fill its compartment, and acts to prevent aberrant growth once development is complete, although the pathway may be deactivated following injury, allowing for tissue repair to the affected compartment (Maugeri-Sacca and De Maria, 2018). The pathway centres around a core kinase cascade whereby upstream signals will lead to cytoplasmic retention or nuclear translocation of the co-transcriptional activators Yes-associated protein (YAP) and transcriptional co-activator with PDZ-binding motif (TAZ) (Figure 1.2) (Maugeri-Sacca, 2018). When the kinase cascade is active, the pathway is considered “on”, which means that YAP and TAZ are transcriptionally inactive. Mechanistically, an upstream signal causes MST1/2 to phosphorylate large tumour suppressor kinase 1/2 (LATS1/2), which in turn will

phosphorylate the Ser132 residue of YAP and the Ser89 residue of TAZ. Phosphorylation of YAP and TAZ leads to their cytoplasmic sequestration by 14-3-3 proteins and subsequent ubiquitin mediated proteasomal degradation by the E3 ligase SCF complex β-TrCP (Zhao et al., 2007, Shanzer et al., 2017). Nuclear YAP and TAZ do not bind DNA directly. When the kinase cascade is inactive, YAP and TAZ remain unphosphorylated and translocate to the nucleus where they act as transcriptional co-activators and drive transcription of genes associated with proliferation and evasion of apoptosis (Maugeri-Sacca and De Maria, 2018).

Structurally, YAP and TAZ are paralogues, they share 46% amino acid sequence homology (Tang et al., 2018) and feature many conserved domains and motifs (Figure 1.3). Both proteins feature a TEAD binding domain at their N-terminus, which is the binding site for the canonical transcription factors associated to Hippo signalling: TEA-domain family members 1-4 (TEAD1-4). This is followed by a 14-3-3 binding domain in both YAP and TAZ, which is required for cytoplasmic retention. However, YAP and TAZ structure do differ in some elements as the YAP protein contains two conserved WW domains compared to TAZ's one. The WW domain is a site of protein interaction, typically with proline-rich motifs, so called due to the presence of two conserved tryptophan residues. The presence of one or two WW domains results in different affinities to various cytoplasmic interactors or nuclear transcription factors separate from TEAD1-4 (Cooper and Giancotti, 2014). For example YAP's two WW domains facilitates interaction with the PY motif of RUNX1/2 whereas TAZ's one domain allows for interactions with nuclear β-catenin (Cooper and Giancotti, 2014). The WW domains contain the corresponding serine residues, which are phosphorylated by LATS1/2 when the Hippo pathway is active. At the C-terminus of YAP and TAZ there is a transactivation domain which is also the site at which proteasomal degradation of both proteins is initiated (Piccolo et al., 2014).

1.3.2 Hippo Pathway and Contact Inhibition

Contact inhibition is the process by which cell division is inhibited due to contacts with neighbouring cells (Gumbiner and Kim, 2014, Zhao et al., 2007). In the context of both development and tumourigenesis, contact inhibition must be overcome for proliferation and tumour growth to occur. In 2007, *Zhao et al* first showed that the Hippo pathway was implicated in cell-cell contact inhibition; they showed that signals transduced from the cell membrane leads to the phosphorylation of YAP by LATS1/2. They hypothesised that the plasma membrane protein FAT tumour suppressor homolog 4 (FAT4) may dimerise with neighbouring cells to recruit Merlin to the membrane and facilitate activation of the core kinase cascade in the Hippo pathway by recruiting and acting as a scaffold for MST1/2 and LATS1/2 (Zhao et al., 2007). Since then, other studies have shown that cell-cell contacts lead to Hippo pathway activation through adherens junctions and β-catenin interacting with Merlin (McClatchey and Yap, 2012). Merlin is also recruited to tight junctions by angiomotin which again facilitates the Hippo pathway kinase cascade (Yi et al., 2011). *In vitro* studies have shown that Merlin also mediates contact inhibition through the cytoplasmic tail of the transmembrane hyaluronic acid receptor CD44 (Morrison et al., 2001b), association of Merlin to the CD44 cytoplasmic tail was shown to block MAPK pathway signalling in Schwann cells.

In the context of the peripheral nervous system, cell-cell contacts are vital during nerve development and repair. In peripheral nerves, Schwann cells will associate to axons in a 1:1 ratio and begin myelination; alternatively, one Schwann cell will associate with multiple small-diameter axons but will not myelinate, this is known as a Remak bundle (Jessen and Mirsky, 2019). Schwann cells provide trophic support to axons, whilst myelinating Schwann cells allow for rapid saltatory conduction of electrical nerve signals that jump between nodes of Ranvier (Jessen et al., 2015). The stages of Schwann cell development in the peripheral nervous system are described in Figure 1.3. During

development, myelinating Schwann cells form autotypic, intracellular tight junctions with the adjacent lamellae in membrane regions of non-compacted myelin, these tight junctions are required for efficient salutatory conduction as mice lacking claudin -19, a tight junction component, had deficient nerve conduction in myelinated axons (Miyamoto et al., 2005). Additionally, loss of Merlin in mouse Schwann cells was shown to lead to abnormal organisation in the paranodal regions adjacent to the nodes of Ranvier, these nerves also had abnormal Schmidt-Lanterman incisures, which are small pockets of cytoplasm that remain after the Schwann cell has myelinated an axon (Denisenko et al., 2008). Upon nerve crush injury, both non-myelinating and myelinating Schwann cells undergo de-differentiation into repair Schwann cells and disassociate from their associated axons, as axons degenerate in areas distal to the crush site (Jessen et al., 2015). Repair Schwann cells will clear debris, proliferate and migrate towards the distal stump in order to guide regenerating axons growing from the proximal side of the nerve injury. When Merlin is deleted in Schwann cells and a nerve crush injury is performed, Schwann cells become completely unable to effectively adopt the repair phenotype, but instead over-proliferate and show histological hallmarks of schwannoma development (Mindos et al., 2017b); this will be discussed further in 1.5.1. We hypothesised that in the context of nerve injury and in the absence of Merlin, one explanation for the hyper-proliferation and nerve repair failure, leading to hallmarks of schwannoma tumourigenesis, is that Schwann cells are unable to appropriately transduce signals from cell-cell contacts, causing them to remain in a proliferative state and be unable to re-differentiate and support axons again, thus they remain in a mitogenic state.

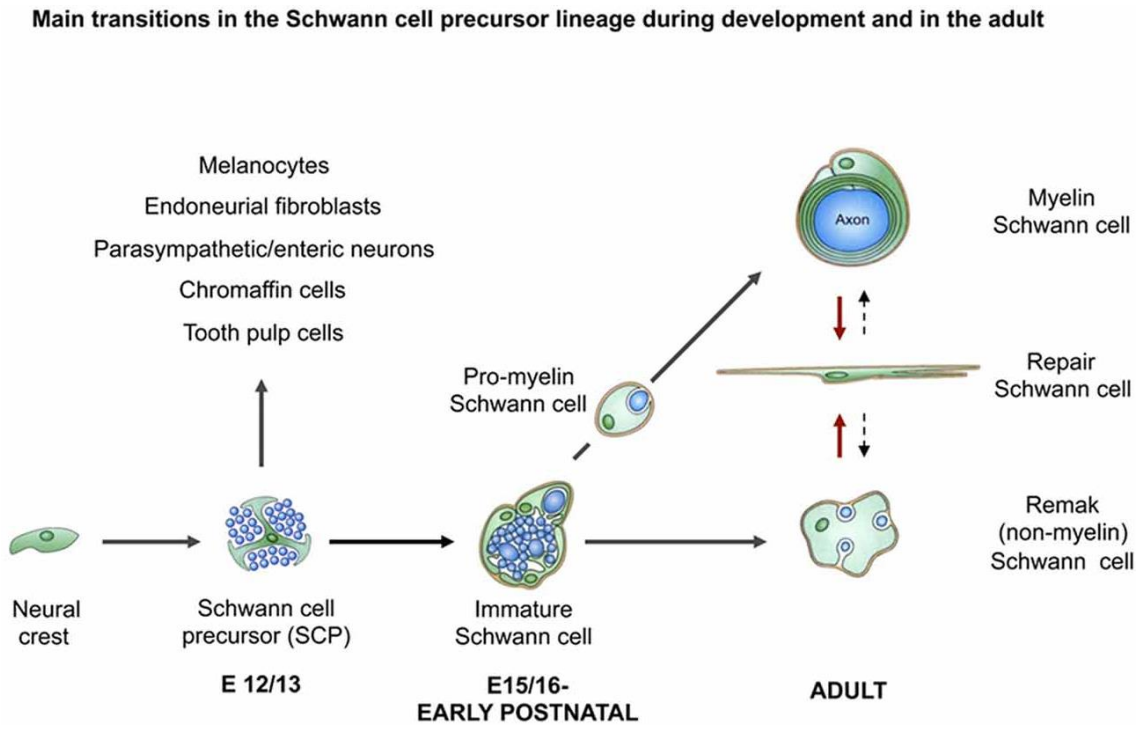

Figure 1.3: Adapted from *Jessen et al, 2015*. Stages of Schwann cell development. During development, Schwann cells will adopt either a non-myelinating phenotype and will associate with multiple axons in a Remak bundle. Alternatively, Schwann cells will myelinate a large diameter axon to allow for saltatory conduction between nodes of Ranvier, allowing for rapid conduction of nerve signals. Upon nerve injury, both non-myelinating Schwann cells and myelinating Schwann cells de-differentiate into a repair Schwann cell in order to clear debris, proliferate and guide regenerating axons back to their distal targets.

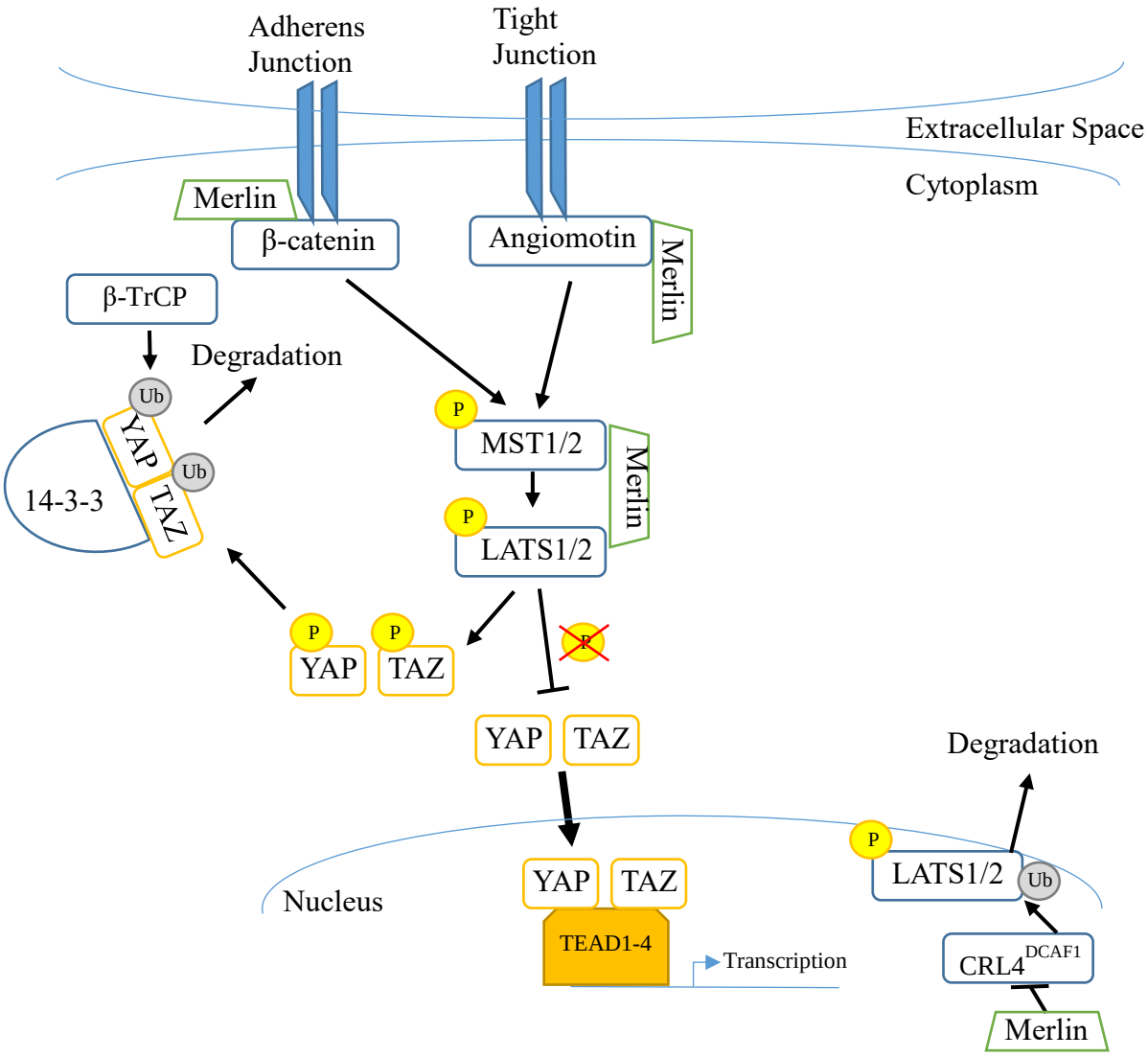

Figure 1.4: Overview of Merlin's influence on the mammalian Hippo Pathway. Merlin is recruited to tight junctions and adherens junctions to facilitate activation of MST1/2. Merlin also acts as a scaffold for the core kinase cascade of the Hippo pathway that results in phosphorylation of YAP and TAZ. In the nucleus, Merlin inhibits $CRL4^{DCAF1}$ which prevents ubiquitination and degradation of LATS1/2. Loss of Merlin results in non-phosphorylated YAP and TAZ translocating to the nucleus and activating transcription through various associated transcription factors (eg TEAD1-4).

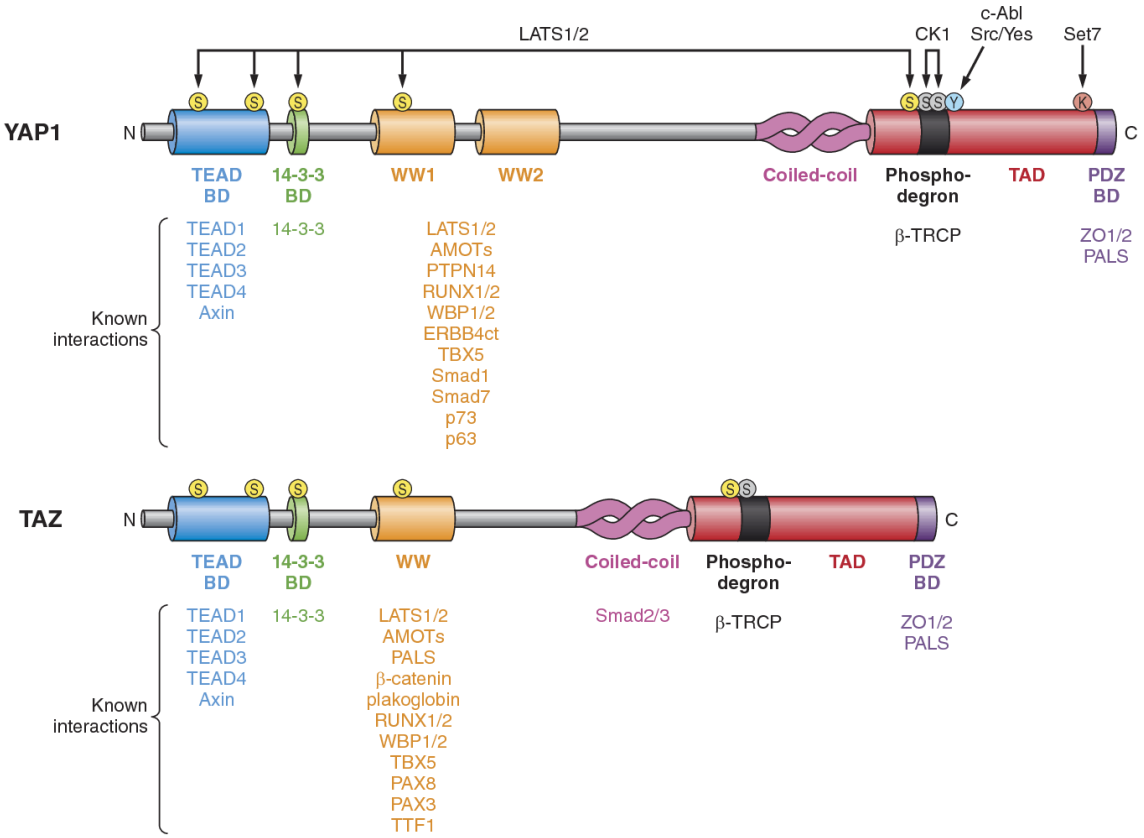

Figure 1.5: The structural features of the Hippo effector paralogues, YAP and TAZ. The second WW domain within the structure of YAP alters the range of transcription factors and regulatory proteins that these paralogues may interact with. Adapted from *Piccolo et al, 2014*.

1.3.3 Upstream Signalling and Merlin

As a regulator of organ and tissue size, the upstream signalling that activates the core kinase cascade of Hippo signalling is primarily regulated by cell density (Maugeri-Sacca and De Maria, 2018). At adherens junctions, which link the E-cadherin transmembrane protein to cells via their actin cytoskeleton, α-catenin interacts with 14-3-3 proteins to allow cytoplasmic sequestration of YAP (Yang et al., 2015). At the impermeable tight junction barriers, CRB3 is the mammalian homologue of Crumbs in Drosophila, and forms a complex which recruits various proteins including angiomotin and Merlin (Mao et al., 2017). Merlin is a cytoskeletal linker that utilises its FERM domain to scaffold Hippo pathway components with various cell junctions, facilitating signal transduction. Merlin is well-characterised as a facilitator of the interaction between angiomotin and MST1/2, which activates MST1/2 to phosphorylate LATS1/2, leading to YAP/TAZ cytoplasmic retention (Cooper and Giancotti, 2014). Another role for Merlin is in the nucleus where it has been shown to inhibit the ubiquitination of LATS1/2 by the E3 ligase $CRL4^{DCAF1}$ (Li et al., 2010). In the absence of Merlin, LATS1/2 becomes ubiquitinated and is subject to degradation, thereby it cannot phosphorylate YAP and TAZ, resulting in an increase in their nuclear activity.

1.3.4 Hippo Signalling in Meningioma and Schwannoma

The somatic mutation theory of cancer states that cancer is a disease of genomic instability and that mutations in DNA give rise to transformed cells that drive tumourigenesis and progression (Fisher, 1958). However, we now know that epigenetic transcriptional inactivation of Merlin along with mutational inactivation are both drivers of tumourigenesis in sporadic meningioma and schwannoma (Lomas et al., 2005, Gonzalez-Gomez et al., 2003).

Recent reviews have shown that aberrations in the Hippo signalling pathway play a role in the tumourigenesis and progression of multiple cancers (Maugeri-Sacca et al., 2018,

Kim and Kim, 2017, Moroishi et al., 2016, Mo et al., 2014, Felley-Bosco and Stahel, 2014, Petrilli and Fernandez-Valle, 2016). Although other mutations within the Hippo pathway exist, loss of the nf2 gene has been well-characterised in multiple tumour types, in particular, mesothelioma, meningioma and schwannoma (Sourbier et al., 2018, Miyanaga et al., 2015, Striedinger et al., 2008, Scherer and Gutmann, 1996). In the wider literature, aberrant Hippo signalling, leading to nuclear YAP and TAZ, have been shown to drive multiple tumour phenotypes (Mo et al., 2014). For example, when undergoing epithelial mesenchymal transition, YAP is required to interact with TEAD to drive expression of N-cadherin and vimentin, which facilitates the metastasis of breast cancer cells (Lamar et al., 2012). YAP and TAZ have also been implicated in conferring drug resistance, for example YAP driven CTGF expression provides resistance to paclitaxel in osteosarcoma cells by activating the expression of micro-RNAs and angiogenic factors such as Angiopoietin 2 (Tsai et al., 2014).

Given that Merlin is a tumour suppressor that has been shown to be important for many processes that converge on the Hippo pathway effectors YAP and TAZ, the wider literature has looked to identify the modulatory effect that nuclear YAP and TAZ have on transcription in order to drive tumour phenotypes. However in meningioma and schwannoma, published studies have focused on the effects which YAP and TAZ have as drivers of proliferation (Striedinger et al., 2008). For the development of targeted therapies one needs to understand the transcriptional changes that elevated nuclear YAP and TAZ proteins are eliciting in these tumours.

Knockdown studies by *Striedinger et al* in cell lines have revealed that loss of NF2 results in elevated proliferation of both meningioma cell lines and their untransformed arachnoidal cell counterparts (Striedinger et al., 2008). Loss of Merlin also resulted in increased nuclear localisation of the downstream effector YAP. Interestingly, when Merlin and YAP were knocked down together, this ameliorated the increased

proliferation phenotype seen when knocking down Merlin alone. This suggests that in Merlin null meningioma, increased activity of the Hippo pathway paralogues YAP and TAZ are important drivers of proliferation. There is also evidence that when analysing the immunohistochemical expression of the proliferation marker Ki-67 in 170 resected meningiomas, Merlin null meningiomas were more proliferative than Merlin positive meningiomas (Pavelin et al., 2014).

In schwannoma, there is evidence that loss of Merlin increases the transcriptional activity of YAP and TAZ is through the inhibition of $CRL4^{DCAF1}$ (Li et al., 2010). Whilst there are limited studies on the effect of Hippo signalling in schwannomas, loss of YAP in NF2-deficient Schwann cells has been shown to lead to apoptosis (Guerrant et al., 2016). The study by Guerrant et al showed that YAP regulates the expression of cyclooxygenase-2 and amphiregulin, resulting in epidermal growth factor receptor (EGFR) signalling that drives cell proliferation. Perhaps the most comprehensive study assessing the Hippo pathway in schwannoma was conducted by *Boin et al* in 2014. This study used a variety of proteomic arrays in 68 human schwannomas to evaluate various signalling pathways such as RTK signalling (Boin et al., 2014). Their study revealed that expression of transcriptionally active YAP was positively correlated with the PDGFRβ receptor and the proliferation marker Ki67. Additionally, ErbB2 and ErbB3 expression levels were also positively correlated to YAP expression. In addition this study was conducted when all schwannomas were assumed to be Merlin-deficient (see 1.4.1), now known not to be the case (Havik et al., 2018), which may have diluted the positive correlation seen between YAP and the RTK driven proliferation in these schwannomas.

1.3.5 Drugs Targeting the Hippo Pathway

Many drugs have been developed to target aberrant Hippo signalling in tumours, drugs being developed or repurposed to target the association of YAP and TAZ with the TEAD family members (Calses et al., 2019). The focus of small molecule disruption of YAP and TAZ are defined into two categories. The drug verteporfin which is marketed as Visudyne has been shown to disrupt the interaction made between YAP or TAZ with TEAD family members. There is evidence in multiple tumour types that verteporfin can reduce the mRNA and protein expression levels of CTGF, a target of both YAP and TAZ (Liu-Chittenden et al., 2012, Felley-Bosco and Stahel, 2014). Verteporfin is a porphyrin ring derivative that until recently has had little competition in the realm of YAP-TEAD inhibition. Conversely, *Wang et al* report that verteporfin's mechanism of action is not by YAP-TEAD inhibition but by upregulation of 14-3-3 which leads to increased sequestration of YAP in the cytoplasm (Wang et al., 2016). Verteporfin is considered a toxic drug that is known to induce damaging oligomerisation of proteins that lead to cellular damage. Another compound named CA3 has been shown to target the YAP-TEAD interaction (Maugeri-Sacca et al., 2018). Another focus in disruption of YAP/TAZ driven transcription is through inhibition of the conserved sites of palmitoylation in the TEAD family members (Chan et al., 2016). Palmitoylation is a post-translational modification that attaches the fatty acid palmitate to threonine, serine or cysteine residues. Typically, palmitoylation influences the trafficking of proteins to subcellular locations, but in the case of TEADs, palmitoylation facilitates the interaction of the TEAD protein with YAP or TAZ. Palmitoylation of TEADs is also required for their protein stability (Noland et al., 2016)(Kim and Gumbiner, 2019).

The pharmaceutical company Vivace Therapeutics Inc. is currently developing small molecules that target TEAD palmitoylation as a method for inhibiting YAP and TAZ driven transcription. These molecules are described as fluorene-oxime compounds but

information is limited as they are under patent (Calses et al., 2019). Other efforts to target YAP/TAZ driven TEAD transcription include development of cyclic peptides such as vgll4 that competitively inhibit YAP's binding interaction with TEAD family members (Jiao et al., 2014). Mechanistically such a cyclic peptide acts as an antagonist for TEAD family activation by competing for TEAD binding. Development of YAP and TAZ inhibitors is ongoing and likely will offer clinical improvements in tumours where the Hippo pathway is dysregulated.

1.3.6 The Biology of Meningioma and Schwannoma

Recent advances in sequencing and profiling techniques are painting an increasingly complex and heterogeneous genomic and epigenetic landscape for schwannomas and especially meningiomas (Lomas et al., 2005, Gonzalez-Gomez et al., 2003, Yuzawa et al., 2016, Havik et al., 2018). Currently, Merlin is still the primary differentiator for stratification of these tumours at the level of gene expression and represents an opportunity for the identification of targeted therapies common to a large proportion of patients. However, it is important to consider the spectrum of known other mutations that these tumours harbour, some of which co-occur with Merlin loss. Data such as site of mutation or methylation status are only just beginning to be correlated with clinical factors such as anatomical location or histological subtype. It is important to be aware of and integrate this data with the clinical picture in order to best stratify treatment.

1.4 Overview of the Clinical Treatment and Biology of Meningiomas and Schwannomas

Meningiomas and schwannomas are tumours which either occur sporadically or as part of the tumour predisposition syndrome neurofibromatosis type 2, in which the individual is also predisposed to ependymomas, which are tumours of the cerebrospinal fluid producing ependymal cells of the spinal cord and brain. Schwannomas also occur in schwannomatosis patients who are deficient in either SMARCB1 or Leucine zipper-like transcriptional regulator 1 (Ruggieri et al., 2016). The following sections in this chapter will focus on the current clinical status of meningiomas and schwannomas of both sporadic and neurofibromatosis type 2 presentation.

1.4.1 Clinical Treatment of Meningiomas

36% of all brain tumours are meningiomas, making them the most common intracranial brain tumour (Willis et al., 2005). Meningiomas arise from the arachnoidal layer of the meninges, which is the middle layer between the exterior dura mater and interior pia mater that encapsulate the brain and spinal cord. The arachnoidal layer is so-called as its web-like protrusions attach to the pia mater. Meningiomas are thought to originate from arachnoidal cap cells which reside within the arachnoid villi which function to absorb cerebrospinal fluid (Marosi et al., 2008). Meningiomas appear in a variety of locations within the meninges but most commonly in the convexity, parasagittal or sphenoid regions (Willis et al., 2005). 64% of all meningiomas are classified as World Health Organisation (WHO) grade I benign tumours and are termed meningiothelial, fibrous or transitional. 34% of meningiomas are WHO grade 2 tumours classified as atypical, clear cell or chordoid. These meningiomas often contain histological features such as increased cellularity and high nucleus to cytoplasm ratio. The remaining 2% of meningiomas are malignant WHO grade 3 anaplastic meningiomas which are either rhabdoid or papillary.

Rhabdoid meningiomas are generally larger, whereas papillary meningiomas tend to grown along blood vessels (Mawrin et al., 2015, Kshettry et al., 2015). The primary care approach to meningiomas is to surgically resect the tumour with post-surgery radiotherapy where appropriate. Complete resection is often unachievable due to the location of the meningioma, such as if a meningioma is located in the posterior fossa which is associated to the brainstem and cerebellum (Gousias et al., 2016). Grade I meningiomas can be asymptomatic and are often found incidentally during other clinical investigations. Often for these tumours, a watch and wait strategy is employed to monitor tumour growth and neurological symptoms before a resection is considered (Gousias et al., 2016).

1.4.2 Clinical Treatment of Schwannomas

The Schwann cell is the cell of origin for schwannomas. Schwannomas occur spontaneously or due to neurofibromatosis type 2. Vestibular schwannomas form on the eighth cranial nerve and are the most common type of schwannoma. Bilateral vestibular schwannomas are a common presentation in neurofibromatosis type 2 patients (Halliday et al., 2019), Spinal and cutaneous schwannomas are less common presentations. Vestibular schwannomas may compress the vestibular nerve which leads to hearing loss, dizziness and imbalance. Similar to meningiomas, surgical resection and radiotherapy are the primary approaches to these tumours. Cochlear implants are also common to mitigate against loss of hearing. Similar to meningiomas, monitoring, resection with adjunct radiotherapy are the primary treatment options for schwannoma (Apicella et al., 2016).

1.4.3 Drug Treatments and Clinical Trials

The MTORC1 inhibitor Everolimus is currently in a phase 2 trial for treatment of vestibular schwannomas and meningiomas (Graillon et al., 2020). Previous phase I trials with Everolimus showed a modest retardation in tumour growth in meningioma and shrinkage of tumours in 3 out of 11 schwannomas, however this did not improve hearing

(Goutagny et al., 2017). A combinatorial phase 2 trial using Everolimus and bevacizumab did not see an increase in efficacy but there were increased toxicity events (Shih et al., 2016)

There have also been various clinical trials testing the efficacy of a variety of RTK inhibitors against Merlin-deficient tumours, including nilotinib, imatinib and sorafenib. Previous phase 2 trials have yielded limited success, imatinib was well tolerated and achieved sufficient plasma levels but was not significantly efficacious (Wen et al., 2009). Clinical trials of the drugs nilotinib and lapatinib, which inhibit platelet-derived growth factor receptor beta (PDGFRβ) in vestibular schwannoma patients have been completed or are still in progress (Paldor et al., 2017). There is also potential for combinatorial therapy with nilotinib and the MEK inhibitor selumetinib (Ammoun et al., 2010). A phase 2 trial with selumetinib alone is currently active.

The EGF receptor (EGFR) has also been targeted in recurrent meningioma by the drugs gefitinib and erlotinib in a phase 2 trial (Norden et al., 2010); again no significant efficacy was seen although the drugs were tolerated well with few adverse side effects reported by patients. Multiple clinical trials of various therapies for meningioma and schwannoma have yielded modest results. More recently, trials have focused on combinatorial treatments that may boost efficacy or bypass resistance mechanisms resulting in better clinical outcomes such as the recent study combining Everolimus and octreotide, conducted by the Kalamarides group (Graillon et al., 2020).

1.4.4 Genetic Alterations in Schwannoma

In Merlin null tumours, the type of genetic alteration in the Merlin gene has been proven to influence the clinical picture. A truncated form of Merlin is the result of a frameshift or nonsense mutation in the coding sequence. This truncated form is associated with a more severe schwannoma that grows faster, leading to patients having a higher tumour

burden, compared to in frame mutations or deletions that result in complete loss of Merlin protein? (Ruggieri et al., 2016)

Until 2016 and the release of a seminal study by *Agnihotri et al*, all schwannomas were believed to be Merlin-deficient. This robust study used whole-exome sequencing in 125 sporadic schwannomas followed by methylation profiling and identified that 77% of schwannomas harboured mutations that led to inactivation of Merlin. The other mutations identified in these schwannomas were those of AT-rich interaction domain (ARID) family members (29%) which are components of the SWI-SNF complex, which is responsible for chromatin remodelling. The receptor tyrosine kinase DDR1 was also mutated in 11.2% of cases, the mutation seen has previously been reported to be hyper activating in KRAS driven lung adenocarcinoma (Ambrogio et al., 2016). The other major genomic rearrangement was a novel protein resulting from the fusion of the serine protease HTRA1 and SH3PXD2A, which was shown to increase levels of phosphorylated ERK and proliferation. The discovery of Merlin positive schwannomas means our view of this putatively homogenous population of sporadic tumours needs to be re-assessed. It also means that retrospective studies that took biallelic inactivation of nf2 for granted may need to be revisited.

1.4.5 Genetic Alterations in Meningioma

Unlike schwannomas, meningiomas were never thought to be exclusively Merlin negative; the consensus in the literature is that 50-60% of sporadic meningiomas feature inactivation of Merlin (Petrilli and Fernandez-Valle, 2016). A genomic analysis of 553 meningiomas by *Yuzawa et al* in 2016 provided important insights into the mutations that drive Merlin positive tumours (Yuzawa et al., 2016). It is of note that in meningioma, some mono-allelic mutations at other loci co-occur with loss of Merlin. The Yuzawa study also catalogued previously identified proteins known to harbour mutations in meningiomas: TNF receptor-associated factor seven (TRAF7); Kruppel-like factor four

(KLF4); AKT1; Smoothened (SMO) and phosphatidylinosityl-4,5-bisphosphate 3-kinase (PIK3CA). TRAF7 is an inflammatory regulator and is mutated in approximately 20% of meningiomas, with >90% of its mutations occurring within its WD40 domain. Unlike KLF4 and AKT1, TRAF7 mutations do not co-occur with loss of both copies of Merlin. Mechanistically, TRAF7 mutations may prevent apoptosis and thus promote meningioma survival by reducing TRAF7-mediated polyubiquitination of lysosomal c-FLIP (Zotti et al., 2017). KLF4 is a transcription factor thought to promote stemness (Tang et al., 2017) and is mutated in approximately 9% of meningiomas, typically on a residue within the zinc finger domain, these mutations are thought to alter the ability of KLF4 to regulate cell stemness (Yuzawa et al., 2016). The canonical AKT1mutation E17K occurs in approximately 9% of meningiomas and has been shown to drive MTOR and ERK activation (Yesiloz et al., 2017). SMO is a G-protein coupled receptor implicated in sonic hedgehog signalling of which putative activating mutations are seen in 3% of meningiomas (Boetto et al., 2018). PI3KCA is the catalytic subunit of PI3K and mutations of this protein are seen in various tumour types (Yuzawa et al., 2016) and occur in approximately 4.5% of meningiomas. Mutations in PI3KCA have been shown to lead to constitutive activation of PI3K (Zadeh et al., 2016). The fact that many of the described mutations can co-occur with or without loss of Merlin means that meningiomas represent a highly heterogeneous population of tumours. This heterogeneity has led to implementation of large-scale epigenetic and ‘omics’ studies to further categorise these diverse tumours.

1.4.6 Epigenetics of Meningioma and Schwannoma

Much of the work in meningioma and schwannoma epigenetics has focused on methylation studies (Torres-Martin et al., 2015, Lomas et al., 2005). Methylation of DNA promoters typically results in repression of transcription. The only major study into methylation of vestibular schwannoma was conducted in 2015 and

generated methylation data on 40 schwannomas (Torres-Martin et al., 2015). Analysis showed that schwannomas trended towards a state of hypomethylation, with several homeobox genes such as HOXD1, HOXD3 and HOXD4 represented in hypomethylated areas. Other studies in methylation in schwannoma are limited and typically focus on the epigenetics of the nf2 gene. Schwannomas did not show aberrant methylation at the nf2 locus in a study by Lomas et al (Lomas et al., 2005), this was confirmed in the later study by Torres-Martin et al who found no differential methylation signatures in vestibular and non-vestibular schwannoma.

Meningiomas have seen much more investigations into their epigenetics, both in terms of methylation and microRNAs (Nassiri et al., 2019, Sahm et al., 2017, Murnyak et al., 2015, Wang et al., 2015, Zhi et al., 2013). Similar to schwannoma, there is no significant differential methylation at the nf2 locus in sporadic meningioma (Hansson et al., 2007). A study of 49 sporadic tumours reported only one aberrantly methylated CpG island in the NF2 promoter. Analysis of meningioma CpG islands by *Bello et al* have identified tissue inhibitor of metalloproteinase three (TIMP3), tumour protein 73 (p73) and CDKN2A as sites that are hypermethylathed in more than 10% of tumours (Bello et al., 2004). Recent reports suggest that hypermethylation in meningioma is more prevalent in grade 2 or grade 3 tumours, for example, TIMP3 is hypermethylated in between 40-60% of grade 3 meningiomas (Murnyak et al., 2015). In recent years, analysis of individual genes associated to hypermethylated or hypomethylated CpG islands has progressed into analysis of global methylation signatures in meningioma. In 2017 *Olar et al* and *Sahm et al* both identified clusters of methylation that sorted meningiomas into two distinct groups with the Sahm study dividing tumours into a further six sub-groups (Olar et al., 2017, Sahm et al., 2017). Interestingly, the study by *Sahm et al* clustered most Merlin positive tumours separately from meningiomas

with loss of Merlin. When correlated with WHO grade and clinical presentation, the methylation signature of meningiomas has shown the potential to be predictive of outcome of survival (Suppiah et al., 2019).

1.5 Meningioma and Schwannoma Mouse Models

The importance of translating in vitro work into appropriate in vivo model systems has long been established as a vital stepping-stone in translational medicine. Drugs tested in vitro do not assess bioavailability or off-target toxicity in the same way that an in vivo model can. Additionally, rare diseases such as neurofibromatosis type 2 often have limited patient numbers that meet selection criteria for a clinical trial. This section will summarise the currently available animal systems used as pre-clinical models for meningioma and schwannoma.

1.5.1 Schwannoma Mouse Models

The approach to making schwannoma mouse models has been through genetic removal of the nf2 gene by deletion of exon two (McClatchey et al., 1997). Global knockout of NF2 in mice is lethal at embryonic day seven, whereas heterozygous mice do not develop schwannomas but instead osteosarcomas in old age (Giovannini et al., 2000). Analysis has shown that the osteosarcomas that form have heterozygous loss of nf2, it is likely that the quiescent nature of Schwann cells and the short lifespan of the mouse prevents schwannomas forming in this system (McClatchey et al., 1998). In 2000, *Giovannini et al* used the Cre recombinase system to generate nf2 mutant alleles that differed by those described by *McClatchey et al* in 1997. The use of the Cre driver used sought to produce a Schwann cell-specific knockout using a short P0 promoter fragment to drive recombination at exon two of the nf2 gene, which was flanked by loxP sites. This ensured that exon two of the nf2 gene was only deleted in Schwann cells in peripheral nerves. Homozygous mice which had Cre and the flanking loxP sites ($NF2^{fl/fl}$) were generated. However the Cre driver in these mice had a longer 1.1 kb promoter fragment than later

P0 Cre mice used in this thesis (Mindos et al., 2017b). The Giovannini group identified through β-galactosidase staining that the larger promoter fragment resulted in earlier recombination at the nf2 locus at embryonic day 9.5 resulting in loss of Merlin in neural crest cells resulting in a knockout that is not Schwann cell-specific. These mice were viable and developed peripheral nerve schwannomas from 10 months of age and older, however penetrance was low at only 36% (n=17). These mice also developed osteosarcomas as the Cre recombination took place as early as embryonic day nine where cells of the neural Crest migrate into bone as osteoblast precursor cells. This model is limited due to the long period of time before tumours are seen in these mice and the poor frequency with which schwannomas present; also, the osteosarcomas are not seen in human patients.

The later P0.NF2$^{fl/fl}$ mice developed by the Feltri lab featured a shorter promoter leading to recombination at embryonic day 13.5 providing a much more specific knockout of Merlin from Schwann cells (Feltri et al., 1999). This model has been widely used to generate Schwann cell conditional knockouts and is standard in the field of Schwann cell research. P0.NF2$^{fl/fl}$ were assessed for their response to sciatic nerve crush injury and interestingly Merlin null Schwann cells show a phenotype where the ability to repair nerve injury is completely ablated (Mindos et al., 2017a). After nerve crush, P0.NF2$^{fl/fl}$ mice do not regenerate axons or remyelinate, but instead Schwann cells proliferate and the nerve fails to regenerate; unlike the Cre negative control, which sees a full functional recovery at 21 days post-injury. This distal sciatic nerve after injury shows clear histopathological hallmarks of schwannoma in terms of the Schwann cell hyperplasia and expansion, however histological features such as Antoni A bodies were not seen. This model may be considered useful in understanding the changes that Schwann cells undergo when transforming into a schwannoma. *Schulz et al* also produced a similar model created by conditional heterozygous removal of the nf2 allele in both Schwann cells and axons

by crossing the Feltri lab's P0.Cre mice with Neurofilament heavy class promoter (Nefh) Cre mice. These mice failed to remyelinate and sustained macrophage recruitment was observed at the injury site (Schulz et al., 2016). This study demonstrated the importance of crosstalk between Schwann cells and axons that was driven by Merlin and mechanistically occurs through a neuregulin-1 and ErbB2/3 signalling axis. Loss of Merlin in neurons and not Schwann cells resulted in a downregulation in neuregulin expression which led to Schwann cells upregulating ErbB2/3, thus making them more sensitive to mitogenic signals (Schulz et al., 2016), this elevated ErbB2 phenotype is also observed in human schwannoma tissue (Lallemand et al., 2009).

Analysis of P0.NF2$^{fl/fl}$ nerves showed elevated expression of YAP and the Hippo readout gene CTGF after injury which was not seen in the Cre negative animals (Mindos et al). Previous studies of conditional NF2 loss in liver carcinomas showed YAP activation drove tumour development (Zhang et al., 2010) and led to the cross of a YAP$^{fl/fl}$ mouse with the P0.NF2$^{fl/fl}$ to generate a Schwann cell specific double knockout P0.NF2$^{fl/fl}$YAP$^{fl/fl}$ mouse to test the phenotype, both to test the effects of YAP loss upon regeneration and tumour growth. YAP$^{fl/fl}$ single knockout mice and NF2$^{fl/fl}$YAP$^{fl/fl}$ and showed no changes in nerve structure or function prior to injury. When sciatic nerve crush was performed, loss of YAP and NF2 reversed the phenotype seen in NF2 single null mice and functional recovery was indistinguishable from Cre^{-} littermate controls. This was the first study that showed the Hippo signalling effector YAP modulating the proliferation of Schwann cells after nerve injury, where loss of YAP in NF2$^{fl/fl}$ Schwann cells led to a decrease in proliferation post-injury.

All mouse models for schwannoma discussed so far have either required a nerve injury, displayed poor genetic penetrance or were not Schwann-cell specific for loss of NF2. This led to attempts to develop a schwannoma mouse model in which spontaneous tumours develop with high penetrance. A different promoter was used by *Gehlhausen et al* in 2015

to create an objectively superior model that more accurately represents the disease phenotype seen in humans (Gehlhausen et al., 2015). The Periostin-Cre.NF2$^{fl/fl}$ (Postn-Cre.NF2$^{fl/fl}$) is driven by the Periostin promoter element which is known to drive Schwann cell gene expression from embryonic day 10 (Lindsley et al., 2007). Analysis of mice at five months of age showed enlarged dorsal root ganglia (DRG) in Postn-Cre.NF2$^{fl/fl}$ mice that was not seen in Cre negative littermate controls. At eight months of age, Postn-Cre.NF2$^{fl/fl}$ had developed distinct schwannomas in their DRGs that shared histological features with the human condition, namely Antoni A bodies within tumours, with cells positive for the Schwann cell marker S100. Cohort analysis of these mice showed that tumours develop with 100% penetrance in the Postn-Cre.NF2$^{fl/fl}$ mice and littermate controls did not develop tumours. Five of 16 Postn-Cre.NF2$^{fl/fl}$ mice in the study did not reach the cohort endpoint and were euthanised due to health reasons, upon examination they were found to have developed malignant peripheral nerve sheath tumours that are not seen in the human NF2 patients. Human schwannomas are not frequently reported in DRGs and primarily develop on the vestibular nerve (Babu et al., 2013). Postn-Cre.NF2$^{fl/fl}$ mice also develop cranial nerve tumours and Schwann cell hyperplasia was observed in Scarpa's ganglion which is where neuronal cell bodies reside that transduce signals from hair cells within the cochlea. When assessed for hearing loss, Postn-Cre.NF2$^{fl/fl}$ mice showed significantly reduced hearing from eight months of age onwards compared to Cre negative controls. Qualitative observation of the Postn-Cre.NF2$^{fl/fl}$ mice suggested that balance was becoming impaired, where mice with schwannomas would frequently tilt their heads or walk in circles repetitively. Behavioural testing revealed that the Postn-Cre.NF2$^{fl/fl}$ mice did indeed have significant impairment of their balance and coordination compared to littermate controls. The Postn-Cre model is superior to the P0.Cre model in terms of penetrance and the development of vestibular tumours that confer hearing loss and balance impairment that mirrors the human condition. It would

be of interest to introduce a Schwann cell specific loss of YAP in these mice as was done by *Mindos et al* in P0-Cre mice to assess whether loss of YAP is sufficient to prevent schwannoma formation. This work is ongoing in our lab along with studies to assess the effect of loss of TAZ and the role of macrophages in the microenvironment of these tumours.

In summary of the approaches to make mouse models of schwannoma, cohorts of the Giovannini P0-Cre.NF2$^{fl/fl}$ mice develop schwannomas after 10 months, but with low penetrance and tumours such as osteosarcomas are also seen in these mice (Giovannini et al., 2000), which are not observed in human patients. The Postn-Cre.NF2$^{fl/fl}$ model developed by Gehlhausen et al offers a much more accurate representation of the human disease and is the current best option for modelling schwannoma in vivo (Gehlhausen et al., 2015). Additionally the P0-Cre.NF2$^{fl/fl}$ injury model may be a more efficient way of modelling the events that Schwann cells undergo when transforming into a schwannoma cell in order to study tumour initiation, however, the necessity of the injury in this model makes the Postn-Cre.NF2$^{fl/fl}$ model the best currently available. There is the opportunity in all of these models to introduce additional knockouts such as YAP or TAZ using the Cre recombinase system that may further elucidate the importance of Hippo signalling in driving the initiation and growth of Merlin null schwannomas. It is of note that all schwannoma mouse models were generated when the consensus was that loss of Merlin is seen in all schwannomas. There are currently no mice that model Merlin positive schwannoma, but these will doubtless be under development at the moment to target ARID family members as well as DDR1 in Schwann cells to see whether this will lead to schwannoma tumours

1.6 **Meningioma Mouse Models**

Approximately 60% of sporadic meningiomas are Merlin-deficient, this led to studies seeking to model meningiomas in mice by removing Merlin expression from the

meninges (Kalamarides et al., 2002). Unlike schwannoma mouse models, early attempts at meningioma mouse models lacked a suitable promoter to drive Cre expression for a tissue-specific knockout for $NF2^{fl/fl}$ mice that leads to tumour formation, so Cre-recombinase was first injected into the meninges of mice to generate loss of Merlin. More recent work by the Kalamarides group used the Prostaglandin D synthase promoter to drive Cre expression in arachnoidal cells (Kalamarides et al., 2011) . There was a poor penetrance of meningioma formation in this Prostaglandin D synthase model, only 38% of mice developed tumours (Kalamarides et al., 2002). As additional mutations are commonplace in Merlin null meningiomas, one allele of the tumour suppressor p53 was also removed in this model but in human meningiomas p53 mutation is rare, in fact only mutations within and not loss of p53 is seen in meningioma (Yuzawa et al., 2016). However cyclin-dependent kinase inhibitor 2A (CDKN2A) is frequently mutated in meningioma with more than 20% of grade 2 meningiomas harbouring mutations (Bostrom et al., 2001), these alterations are more commonly seen in WHO grade 2 and grade 3 meningiomas (Ishii et al., 1999, Bostrom et al., 2001). Even the addition of an activated PDGF receptor in the NF2/CDKN2A model did not increase the penetrance of meningiomas in these mice (Peyre et al., 2015). The current literature is yet to consider the role of SMO, KLF4, TRAF7 or AKT1 mutations in genetic meningioma mouse models. Overall, the genetically modified models of meningioma have provided useful insights into genetic drivers of meningioma, however due to the poor penetrance of these models it is important to consider xenograft models for in vivo drug testing.

Genetically modified mice are generally considered a more robust model for the study of cancer than xenograft models as they can often mirror the human genetic situation, the tumour microenvironment and immune response can also be observed in immunocompetent mice, in contrast with orthotopic tumour models were mice must be immunocompromised to allow cells to establish at the injection site (Richmond and Su,

2008). However, the poor penetrance and long latency of disease seen in genetic models of meningioma has led to the development of xenograft models that do have some benefits. Xenografted cells can be manipulated genetically before they are injected in the host and studies often have shorter latencies than genetic experiments. Meningioma xenografts typically feature the Merlin negative WHO grade I cell line: Benign-meningioma-1 (BM1) cells . WHO grade 3 cell lines: KT21 and IOMM-Lee are also used which are Merlin negative and Merlin positive respectively (Mawrin, 2017). Xenografts were first tested in the subcutaneous flanks of animals which does not represent the human situation, although analysis of patient-derived primary meningioma cells or IOMM-Lee cells into the skull base or cerebral convexity to give rise to meningioma have a penetrance >90% (Friedrich et al., 2012, Mawrin, 2017). The IOMM-Lee xenograft model generated by the *Mawrin* group is the only xenograft model in the literature that has had success with drug treatments. They used sorafenib to inhibit PDGFR and significantly inhibit the growth and invasion of tumour cells by reducing ERK activity (Tuchen et al., 2017) and this data supports an ongoing clinical trial. Patient-derived xenografts are desirable for recapitulating the human situation but the complex genetic background seen in meningioma is likely to make results difficult to reproduce. It is yet to be seen whether a BM1 or other suitable grade I cell line model can be reproducibly injected into the skull convexity of mice to effectively test chemotherapies.

1.7 RNA Sequencing for Differential Expression Analysis

The term ‘Omics’ in biology is an umbrella term for the collective analysis of a particular subset of biological molecules ranging from DNA [genomics] to metabolites [metabolomics]. A wide range of ‘omics’ techniques are now consistently used to help our understanding of cell biology and disease. This thesis uses next generation RNA-sequencing (RNA-seq) to identify the transcriptional changes caused by loss of Merlin and an overview of the technique will be given below. Since the advent of next generation

sequencing, microarray studies have mostly given way to RNA-seq technology which generates orders of magnitudes more data, and is more sensitive to transcripts that are either highly abundant or very low in number (Costa-Silva et al., 2017). In addition, RNA-seq is not restricted to known genomic sequences that have to be programmed into the microarray (Wang et al., 2009). RNA-seq has the potential to detect splice variants and non-coding transcripts and sensitivity of RNA-seq is such that as little as 10 pg of cDNA is required, which has led to the advent of single-cell analysis (Mantione et al., 2014).

Briefly, the workflow of RNA-seq for differential expression will occur over three general steps:

1. Library preparation:

Appropriately isolated RNA will be processed, purified and reverse transcribed into complementary DNA (cDNA) using a poly-A tail primer to distinguish messenger RNA from transfer RNA and ribosomal RNA. Sequences are labelled and broken down into fragments that range in size from 50-500 base. Quality control is performed to assess the concentration and fragment sizes in individual samples. Reads are assembled into transcripts and their abundance is then quantifiable (Mantione et al., 2014).

2. Sequencing:

RNA-seq typically generates millions of reads per sample and aligns reads to generate full length transcripts. For gene expression, reads required are less than that required by total RNA profiling which needs to assign reads to non-coding RNA. In our sequencing experiments, we considered transcripts with Log_{10} counts per million > 0.5.

3. Analysis and validation:

Once differential expression data is generated and statistically assessed, functional annotations or gene ontology terms can be augmented onto the data using various bioinformatic tools and databases (Manzoni et al., 2018). Quantitative PCR at the transcript level and Western blotting are the main techniques used to validate RNA sequencing results.

Over 50 years ago, Francis Crick's central dogma of biology states that once information has been passed from a transcript to a protein, this information cannot be passed back, this highlights one of the key limitations of RNA-seq as an omics tool. There are multiple examples of limitations associated with RNA-seq differential expression studies, foremost being that regulation of RNA may not lead to differential protein expression (Manzoni et al., 2018, Hirsch et al., 2015). Another limitation is that RNA-seq cannot detect post-translational modifications that may occur in the encoded protein, or how that protein will be regulated following translation. This is a problem that is less prevalent in proteomics, especially since the introduction of techniques such as phospho-proteomics that do not just predict proteomic abundance but also activity, however proteomic coverage of an organisms genome is typically much less than in RNA-seq (Manzoni et al., 2018). The situational advantages of each omics technique has led to effort in integrating omics data in what is being called panomics or multiomics to mitigate against the limitations of a single technique such as RNA-seq or proteomics (Manzoni et al., 2018, Charkoftaki et al., 2019).

1.8 Cancer Stem Cells and ALDH1A1

The cancer stem cell theory states that within a tumour, there are stem-cell like populations that possess the capacity to self-renew and give rise to different types of tumour cell (Yu et al., 2012). Cancer stem cell markers may be critical for self-renewal

and chemoresistance. Aldehyde dehydrogenase 1A1 (ALDH1A1) is one such cancer stem cell marker that has been found to be upregulated in Schwann cell derived tumours (Liesche et al., 2019b). There is a large amount of evidence that ALDH1A1 is a cancer stem cell marker in various tumour types (Tomita et al., 2016, Nwani et al., 2019, Kalantari et al., 2017, Hoshino et al., 2015, Ciccone et al., 2019). ALDH1A1 has been implicated in a wide range of cellular processes to elicit its role as a cancer stem cell marker. One such way ALDH1A1 is tumourigenic is by reducing levels of reactive oxygen species which allows for tumour growth. ALDH1A1 has also been shown to convert the chemotherapeutic cyclophosphamide into the inactive carboxyphosphamide which can be harmlessly excreted by tumour cells (Sladek et al., 2002). The biology and therapeutic potential of ALDH1A1 in schwannoma and meningioma will now be discussed.

In humans, ALDH1A1 is part of the 19 member aldehyde dehydrogenase (ALDH) superfamily that catalyses the oxidation of aldehydes in the presence of $NADP^+$ (Tomita et al., 2016). ALDH family members metabolise a range of endogenous and exogenous aldehydes, with ALDH1A1 showing the highest affinity to retinaldehyde, the vitamin A derivative and catalysing its oxidation into retinoic acid, this reaction is also catalysed by the isozymes ALHD1A2 and ALDH1A3. Retinol in the cytoplasm is bound to cellular retinol binding proteins (CRBPs) and converted into retinaldehyde by alcohol dehydrogenases. Retinaldehyde is oxidised into retinoic acid by ALDH1A1 in the cytosol is shuttled to the nucleus by cellular retinoic acid binding protein (CRABPs) where it acts as a ligand for retinoic acid receptors (RARs) and retinoid X receptors (RXRs). Upon activation by retinoic acid, RARs and RXRs drive transcription of genes associated to a wide range of effects (Figure 1.4) (Tomita et al., 2016). ALDH1A1 has been shown to convert retinaldehyde into 9-cis retinoic acid, which is considered to be the most potent retinoic acid stereoisomer for inducing RAR and RXR driven gene transcription (Zhao et

al., 1996). The ALDH1A1 promoter has also been shown to be activated by RARs when retinoic acid levels are low, indicative of a feedback loop that maintains a stasis of retinoic acid levels (Yanagawa et al., 1995). This pathway has been hypothesised as the way in which cancer stem cells self-renew. The idea is that when ALDH1A1 is expressed then cells are proliferative but if ALDH1A1 becomes downregulated, low levels of retinoic acid would lead to stimulation of self-renewal in cancer stem cells (Chute et al., 2006, Vassalli, 2019).

Apart from the biosynthesis of retinoic acid, ALDH1A1 has also been implicated in enabling tumours to confer resistance to chemotherapies (Vassalli, 2019, Tomita et al., 2016, Januchowski et al., 2016). Some studies have highlighted the way in which ALDH1A1 achieves drug resistance. In lung cancer cell lines, ALDH1A1 knockdown restored sensitivity to cisplatin by metabolising reactive oxygen species, and also reduced levels of phosphorylated AKT (Wei et al., 2017). Recent studies have led to the development of potent ALDH1A1 competitive inhibitors that already show therapeutic potential when used in combination with established chemotherapies (Nwani et al., 2019). ALDH1A1 chemical inhibition has been shown to restore sensitivity to chemotherapeutic agents (Kohn et al., 1987, Liu et al., 2019). PARP inhibitors which block DNA repair are used to treat ovarian cancer with BRCA1/2 mutations, upregulation of ALDH1A1 has been shown to boost the DNA repair process in PARP treated cells. Combinatorial therapy with an ALDH1A1 inhibitor restored sensitivity to PARP inhibitors in these tumours (Liu et al., 2019). Interestingly, ALDH1 subtypes were recently identified as potential biomarkers for Schwann cell-derived tumours (Liesche et al., 2019a).

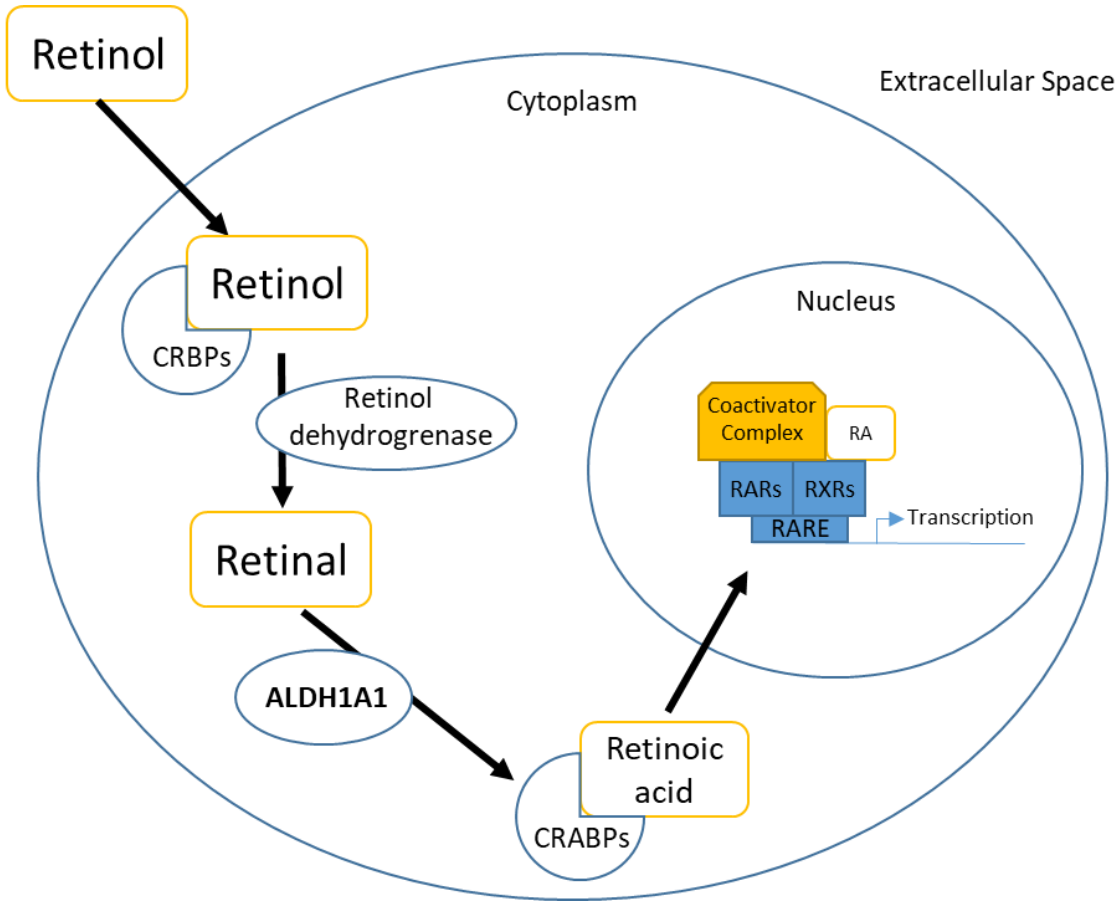

Figure 1.6: Overview of retinoic acid signalling. Retinol diffuses into the cytoplasm from the extracellular space, is metabolised into retinoic acid and then shuttled into the nucleus where it is needed to recruit activator or repressor complexes to retinoic acid response elements (RAREs) by interacting with nuclear retinoid X receptors (RXRs) and retinoic acid receptors (RARs). Upon binding retinoic acid, RARs will homodimerise with a second RAR or heterodimerise with an RXR. The conversion of retinol to retinal is the rate-limiting step in this pathway.

1.9 **Project Aims**

There is a growing body of evidence that tumours which drive transcription through YAP and TAZ are sensitive to Hippo pathway inhibition (Calses et al., 2019). Here we hypothesise that genetic and pharmacological targeting of the aberrant Hippo pathway signalling seen in Merlin null meningioma and schwannoma will reduce tumour proliferation and highlight novel therapeutic targets.

This PhD will examine the role of Hippo signalling in Merlin null meningioma and schwannoma by exploring the following aims:

1. Validate differentially regulated genes previously identified in an RNA sequencing screen using a Merlin-deficient and YAP-deficient mouse model and assess their importance in tumourigenesis and progression in schwannoma and meningioma tumour cells.
2. Stratify meningiomas and schwannomas by Merlin status and compare their expression of Hippo pathway proteins as well as their rate of proliferation.
3. Analyse the effects of YAP and TAZ inhibition on primary human meningioma and schwannoma tumours as well as in mouse tumour models.

These aims will be assessed using both immortalised and primary human meningioma and schwannoma cells, as well as whole human tumour tissue and mouse models.

2 Materials and Methods

2.1 Clinical Samples

Anonymised meningioma and schwannoma tissue samples under the ‘MN’ series were collected during planned surgical procedures and surplus frozen tissue was available after diagnostic testing. Patients were consented to the 'Identifying and validating molecular targets in low grade brain tumours' study and given a unique molecular target identification number (MN). This study was granted full national ethics approval by the South West research ethics committee (REC No: 14/SW/0119; IRAS project ID: 153351) and local research and development approval (Plymouth Hospitals NHS Trust: R&D No: 14/P/056 and North Bristol NHS Trust: R&D No: 3458). Clinical information on meningiomas presented in this project can be found in Tables 2.10.

Merlin Positive	Experiment	Age	Gender	Location	Other Mutations	Grade
MN088	VP/YAP	unknown	Female	Transitional	WT for panel	1
MN147	VP/YAP	62	Female	Left anterior clinoid meningioma	AKT1 E17K heterozygous	1
MN122	VP/YAP	79	male	anterior fossa	WT for panel	1
MN133	VP/YAP			Right fronto-parietal meningioma	WT for panel	1
MN149	VP/YAP	unknown	unknown		AKT1 E17K heterozygous	1
Merlin Negative	Experiment					
MN126	VP/YAP	41	Female	Planum sphenoidale meningioma		1
MN123	VP/YAP	64	Female	Right occipital parafalcine meningioma	TRAF7 N520S hetero	1
MN143	VP/YAP	74	Male	Left cavernous sinus meningioma	TRAF7 N520S hetero	1
MN139	VP/YAP			R frontal meningioma	genotyping not completed	1
MN140	VP/YAP	74	Male	Left recurrent parasagittal meningioma	genotyping not completed	1
Merlin Negative	Experiment					
MN126	YAP/TAZ kd	41	Female	Planum sphenoidale meningioma		1
MN123	YAP/TAZ kd	64	Female	Right occipital parafalcine meningioma	TRAF7 N520S hetero	1
MN143	YAP/TAZ kd	74	Male	Left cavernous sinus meningioma	TRAF7 N520S hetero	1
Merlin Negative						
MN091	Vivace drugs	62	Female	Left spheoid wing	TRAF7 N520S heterozygous	1
MN126	Vivace drugs	41	Female	Planum sphenoidale	WT for panel	1
MN243	Vivace drugs	73	Female	Left frontal convexity	genotyping not completed	1
MN246	Vivace drugs	37	Female	Left petroclival	POLR2A heterozygous	1
MN257	Vivace drugs	34	Female	Left Occipital	WT for panel	1
Merlin Positive						
MN214	Vivace Drugs	59	Female	Olfactory bulb	AKT1 E17K homozygous, TRAF7 N520S heterozygous	1
MN218	Vivace Drugs	Unknown	Male	Left frontal convexity	genotyping not completed	1
MN272	Vivace Drugs	81	Female	Right sphenoid wing	genotyping not completed	1
MN268	Vivace Drugs	67	Female	Bilateral olfactory groove	genotyping not completed	1
MN346	Vivace Drugs	Unknown	Male	T11/T12 Spinal	genotyping not completed	1
Merlin Negative						
MN243	ALDH1A1 inhibitors	73	Female	Left frontal convexity	genotyping not completed	1
MN246	ALDH1A1 inhibitors	37	Female	Left petroclival	POLR2A heterozygous	1
MN257	ALDH1A1 inhibitors	34	Female	Left Occipital	WT for panel	1

Table 2.1: Clinical information for primary meningioma cells used in this thesis.

2.2 Cell Culture

A range of cell lines and primary cells were derived and used as an in vitro cell culture model for meningioma and schwannoma tumours.

2.2.1 Immortalised Human Cell Lines

Human meningioma and schwannoma cell lines were used in this project were received from Dr Emanuela Ercolano (University of Plymouth), and were used between passage 10 and passage 30. Cell lines were cultured at 37ºC in 5% CO_2 in Dulbecco's Modified Eagle's Medium (DMEM; Thermo Fisher Scientific) containing: 10% foetal bovine serum (FBS; Thermo Fisher Scientific); 5.5 g/L D-glucose (Thermo Fisher Scientific); 100 U/mL penicillin/streptomycin (Thermo Fisher Scientific); 2 mM L-glutamine (Thermo Fisher Scientific).

Ben-Men-1 (BM1) cells are a Merlin null grade I meningioma cell line (Puttmann et al., 2005). KT21 cells are a Merlin null grade III meningioma cell line derived from a malignant meningioma after transplantation into nude mice (Tanaka et al., 1989). HEI-193 cells are Merlin null and were derived from a neurofibromatosis type II patient schwannoma (Hung et al., 2002).

2.2.2 Primary meningioma and human meningeal cells

Human meningeal cells (HMC) were obtained from ScienCell and cultured in their Meningeal Cell Medium with Meningeal Cell Growth Supplement (ScienCell): 1% penicillin/streptomycin and 5% FBS (ScienCell). Primary meningiomas were received to the lab at Derriford and the tumours were cut into small pieces with a scalpel. Tumour pieces were then incubated in DMEM with 10% FBS, 100 U/mL penicillin/streptomycin and 20 U/mL Collagenase III (Worthington Biochemical Corp.) for overnight enzymatic digestion at 37^0C in 5% CO_2. Tumour pieces were further mechanically broken up by pipetting up and down until a single cell suspension was obtained, and then pelleted by centrifugation at 250 g. Pelleted cells were resuspended in DMEM with 10% FBS; 100

U/mL penicillin/streptomycin; 1% D-glucose and 2mM L-glutamine at 37°C in 5% CO_2. Adherent cells were passaged into tissue culture flasks.

2.2.3 Primary schwannoma

Primary schwannomas were digested in the same manner as primary meningiomas (see Section 2.2.2), similarly to previous descriptions (Dilwali et al., 2014). Schwannomas were cultured on poly-L-lysine (PLL)/laminin coated plates: 0.1 mg/mL poly-L-lysine (PLL) (Sigma), diluted in PBS (Gibco; pH 7.2) was added to cell culture flasks for 30 minutes at room temperature and washed with PBS. Following PLL coating, 0.004 mg/mL laminin (Sigma), diluted in PBS was added for two hours at room temperature to apply a laminin coating to the flask. A further PBS wash was completed just before cells were plated. Schwannomas were cultured in proliferation medium for Schwann cells and schwannoma (GFM), DMEM containing: 20% FBS; 100 U/mL penicillin/streptomycin; 0.5 µM forskolin (Sigma); 2.5 µg/mL amphotericin B (Sigma); 2.5 µg/mL insulin (Sigma); 10nM β1-heregulin (Sigma) and 0.5mM 3-Isobutyl-1-methylxanthine (IBMX) (Sigma).

2.2.4 Primary human Schwann cells

Schwann cells were isolated from the sural nerves of donors with informed consent. Dr Emanuela Ercolano prepared the nerves after dissection. Withdrawn nerves were stripped of their epineurium and fascicles were separated from the remaining interfascicular epineurium and incubated at 37^0C, 10% CO_2 for 7-14 days in DMEM with 10% FBS; 500 U/mL penicillin/streptomycin and 2.5 mg/mL amphotericin B. Fascicles were then cut into 2mm-long pieces and digested in DMEM with 10% FBS; 500 U/mL penicillin/streptomycin and collagenase type 1A 160 U/mL. The resulting Schwann cells were then amplified on plates coated with 0.1 mg/mL PLL in DMEM with 20% FBS; 100 U/mL penicillin/streptomycin; 0.5 µM forskolin (Sigma); 2.5 mg/mL amphotericin 2.5

mg/mL; 2.5 mg/ml insulin (Sigma); 10 nM β1-heregulin (Sigma) and 0.5 mM IBMX (Sigma).

2.2.5 Primary mouse Schwann cells

Primary mouse Schwann cells were collected from the dissected brachial plexuses and sciatic nerves of P0-Cre^{+} and P0-Cre^{-} $NF2^{fl/fl}$ conditional null mouse pups as previously described (Mindos et al., 2017b), ranging from post-natal ages of 3-7 days. These tissues were incubated at room temperature in Leibowitz's L-15 medium (Gibco) until dissection of all animals were complete. Nerves were then digested in 1.25 mg/mL trypsin and 2 mg/mL collagenase type 1A at 37^{0}C for 30 minutes. Mechanical dissociation was achieved by pipetting up and down with a 1 mL pipette tip followed by a 200 µL pipette tip until a single cell suspension was achieved. Dissociated cells in trypsin/collagenase were neutralised by addition of low glucose DMEM (1g/L glucose; Gibco) containing: 4% FBS and 100 U/mL penicillin/streptomycin and then the preparation - centrifuged at 1000 g for five minutes to pellet the crude Schwann cell preparation. For serum purification of Schwann cells, cells were plated onto PLL and laminin coated flasks (see Section 2.2.3) in low glucose DMEM containing: 4% FBS; 100 U/mL penicillin/streptomycin; 1 g/L D-glucose and 10 µM cytosine arabinoside for 48 hours to kill rapidly dividing fibroblasts. Purified Schwann cells were then expanded in low glucose DMEM containing: 4% FBS; 100 U/mL penicillin/streptomycin; 2µM forskolin and 10 ng/mL neuregulin-1 (NRG-1; R&D Systems) for us in further experiments.

2.2.6 Passaging Cells

Cells were passaged by removing medium, washing with phosphate buffered saline (PBS; Gibco) and incubating with trypsin-ethylenediaminetetraacetic acid (EDTA) (0.05%; Gibco) at 37^{0}C until cells detached. The detached cell suspension was neutralised with the relevant growth medium and transferred to a fresh culture flask.

2.3 Mice

Experiments with mice were conducted in accordance with Home Office regulations under the UK Animals (Scientific Procedures) Act 1986. Experiments were approved by Plymouth University Animal Welfare and Ethical Review Board.

2.3.1 Genotypes of transgenic mouse lines

Mice with a Schwann cell-specific knockout of Merlin were the focus of this project. This was achieved using the Cre recombinase system. A cell-specific promoter drives expression of Cre recombinase, which will recognise loxP sites which flank the gene of interest. A gene which is flanked by two loxP sites is described as floxed (fl) and when recombination occurs, this results in deletion of an exon within the gene of interest (Kim et al., 2018). Using either a P0 (Feltri et al., 1999) or Periostin (Postn) (Gehlhausen et al., 2015) Cre line as described previously, mice with a Schwann cell-specific homozygous deletion of the NF2 gene ($NF2^{fl/fl}$) were generated. These mice were crossed with conditional null YAP (Zhang et al., 2010) and TAZ (Hwang et al., 2019) mice to generate $NF2^{fl/fl}$, $NF2^{fl/fl}YAP^{fl/fl}$ and $NF2^{fl/fl}TAZ^{fl/fl}$ animals. Age matched cre negative littermates were used as controls. ALDH1A1 global null mice (Fan et al., 2003) were gratefully received from Dr Joseph Napoli (University of California, Berkeley) and were crossed with $NF2^{fl/fl}$ mice to generate $NF2^{fl/fl}$ALDH1A1 knockout mice.

Here after, P0.Cre+ and Postn.Cre+ followed by "$gene^{fl/fl}$" (e.g. P0.Cre+$NF2^{fl/fl}$) refer to mice expressing Cre recombinase and have therefore removed the floxed gene, whereas P0.Cre- and Postn.Cre- followed by "$gene^{fl/fl}$" (e.g. P0.Cre-$NF2^{fl/fl}$) are control mice as they do not express Cre recombinase. These groups were compared as age-matched littermates with a single animal represented one biological repeat. Unless otherwise stated, all experiments used n=3 mice for each condition, power calculations were not performed to decide sample size. Mice were bred with homozygous floxed alleles whereas the Cre recombinase was heterozygous. No exclusion criteria was required as all

mice bred were suitable for use in experiments, thus, no data from any animal was excluded after analysis. Randomisation was not formally used to allocate animals into experiments, however both males and females used in similar numbers. For injury experiments, blinding was not possible at the timepoints analysed as the P0.Cre+NF2$^{fl/fl}$ mice showed a clear repair deficit compared to P0.Cre-NF2$^{fl/fl}$ controls. For experiments in results chapter 3.3, Postn.Cre+NF2$^{fl/fl}$ mice were consistently smaller than Postn.Cre-NF2$^{fl/fl}$ littermate controls, additionally for the drug experiments, dissolving the drug into the vehicle solution made a cloudy suspension whereas the vehicle control remained a clear solution, therefore it was impossible to blind the researcher to animal genotype and whether the animal received drug or vehicle. Mice were assessed for protein expression by immunostaining or western blotting and proliferation by EdU proliferation assay. All animals were kept on a C57BL/6 background.

2.3.2 Genotyping

Ear notches and tail snips were used as a source of tissue to identify the genotypes of mice. Crude DNA preparations suitable for genotyping were produced by alkaline lysis using the HotSHOT method (Truett et al., 2000). Ear notches or tail snips were submerged in 75 µL of alkaline lysis buffer (25 mM NaOH and 0.2 mM EDTA in H_2O) and heated to 95^{0}C for 90 minutes. Following heating, the solution was vortexed and 75 µL of neutralisation buffer (40 mM Tris-HCl; Sigma) in H_2O) was added, DNA was stored at 4^{0}C short term or -20^{0}C long term. DNA was genotyped using primers (Table 2.4) (Eurofins) and reagents (Promega), a typical reaction mix and PCR steps are shown in Tables 2.2 and 2.3.

PCR products were resolved on a 1.4% (w/v) agarose gel (Sigma) dissolved in Tris-acetate-EDTA buffer (Sigma). The mix was heated in a microwave to dissolve the agarose and GelRed (Biotium) was added (1:50 000 dilution) to visualise the DNA fragments under UV light. Gels were run in 1 x Tris-acetate-EDTA buffer at 120 volts using a Power

Pac 300 (BioRad) for 60 minutes. Gels were imaged on a SYNGENE PXI 4. A typical agarose gel image can be seen in Figure 2.1.

Reagent	Volume of Stock	Concentration in PCR mix
5x Green GoTaq Buffer (Promega #M891A)	5µL	
ddH_2O (Sigma #W4502)	14.9µL	
DNA	2µL	
Deoxyribonucleotide triphosphates (Promega #U120A-U123A)	0.5µL	200µM
25mM $MgCl_2$ (Promega #A351H)	1.5µL	1.5mM
Primers (Eurofins)	1µL	0.5µM each
Taq Polymerase (Promega #M740B)	0.1µL	1.25U

Table 2.2: Master Mix reagents for PCR genotyping.

Step Number	Condition
1	95˚C 5 minutes
2	95˚C 30 seconds
3	55˚C 45 seconds
4	72˚C 60 seconds
5	Repeat 2-4, 38 times
6	72˚C 5 minutes
7	4˚C (infinite storage)

Table 2.3: Steps for a genotyping PCR reaction. Annealing temperatures varied between primers and can be viewed in Table 2.3

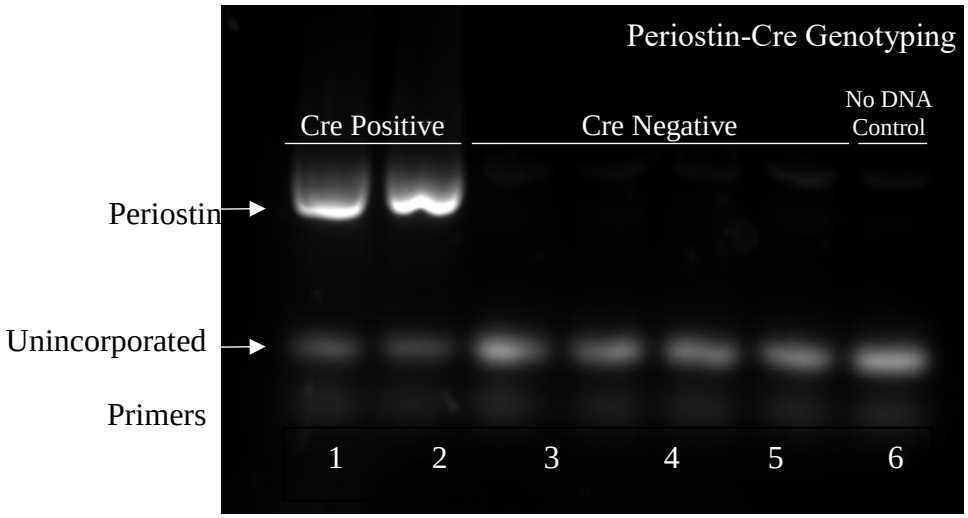

Figure 2.4: Typical PCR gel image for Periostin Cre mice. Lanes 1-2 show Cre positive mice, lanes 3-6 Cre show negative mice, lane 7 show a no DNA control PCR mix. The $NF2^{fl/fl}$ allele was detected at 440 base pairs.

Gene	Forward primer sequence 5’- 3’	Reverse primer sequence 5’- 3'	Anneal temp (˚C)	No. of Cycles	Size (bp)
NF2	GGGGCTT CGGGAAA CCTGG	GTCTGGG AAGTCTG TGGAGG	60	38	574
P0	CCACCAC CTCTCCA TTGCAC	GCTGGCC CAAATGT TGCTGG	57	35	492
Periostin	CATTTGG GCCAGCT AAACAT	CCCGGCA AAACAGG TAGTTA	57	38	444
YAP	CCAGACG ACTTCCT CAACAGT G	GCATCTC CTTCCAG TGTGCCA A	57	38	400
TAZ	CTT CCA AGG TGC TTC AGA GA	GGA GAG GTA AAG CCC ACC AG	60	38	400
ALDH1A1	CAACCCT GAGCAAA	TGGATGT GGAATGT GTGCGAG	60	40	300

	TCCTCCA C				

Table 2.4: Primers used to determine mouse genotypes.

2.3.3 Sciatic Nerve Injury

Sciatic nerve crush was performed under isoflurane anaesthesia as previously described (Mindos et al., 2017b). Adult mice of comparable ages had their sciatic nerves crushed for 30 seconds using forceps, followed by another 30 seconds in a position orthogonal to the first crush. Following crush, animals were given analgesia and monitored daily. Only the right-hand sciatic nerve of each mouse underwent crush injury for 7 or 21 days, the left-hand side was used as a contralateral control. At the experiment endpoint, mice were sacrificed by cervical dislocation. Samples were prepped for immunohistochemistry by submerging sciatic nerves in 4 % PFA for 24 h or for western blot by submerging nerves in RIPA buffer (see Section 2.5).

2.3.4 Vivace Oral Gavage

The Vivace drug VT03989 was administered by oral gavage in Postn.Cre+$NF2^{fl/fl}$ mice to assess the effect on tumour proliferation. Mice were gavaged with a dose of 30 mg/kg for 14 days consecutively using an FTP-20-30 polypropylene tube (Linton Instrumentation) attached to a 1 mL plastic syringe (BD Plastipak). Animals were monitored for weight loss and other clinical signs during gavage experiments and suffered no weight loss or other adverse effects.

2.4 RNA Sequencing

RNA sequencing was used to identify differentially expressed genes following Schwann cell specific loss of NF2 and NF2/YAP in the sciatic nerves of injured and uninjured mice.

2.4.1 Sample Preparation

RNA was prepared by Dr Thomas Mindos and sequenced by Cambridge Genomic Services (CGS). Gene expression profiling was performed on RNA purified from the sciatic nerves of four Schwann cell conditional null $NF2^{-/-}$, $NF2^{-/-}YAP^{-/-}$ and control mice, at the time point of seven days post-injury (see Section 2.3.3), with the uninjured

contralateral nerve taken as control for each animal. For each nerve, the section of the sciatic nerve and distal branches downstream of the injury site were harvested. For contralateral uninjured nerves, the same portion of the nerve was dissected out. Dissected nerves were put into RNAlater (Thermo Fisher) and RNA was isolated using a miRNA easy kit (Qiagen). RNA integrity was assessed by using a nanodrop 2000 machine (Thermo Fisher Scientific) to measure the 28 S: 18 S ratio.

An RNA integrity number > 6 was required for samples sent for sequencing by CGS.
Data Analysis

2.4.2 Data Analysis

Data from CGS was analysed by Prof Matthias Futschik. The data was generated using the Illumina NextSeq 550 system and generated counts which correlated to an Entrez Gene ID. Averaged differential expression between genotypes and injured/control animals was presented as a Log_2 [fold change] (FC). A two-tailed t-test with a false discovery rate (FDR) adjustment was used to determine genes which were differentially regulated in a statistically significant manner. Genes were considered to be differentially regulated if they had a $Log_2FC > 1$ or a Log2FC < -1, with Log_{10} [counts per million] (CPM) > 1.5 to prevent identifying genes which were expressed at insignificant levels. An FDR < 0.05 was considered statistically significant.

2.5 Antibodies

Antibodies used in this thesis are listed in tables 2.6 and 2.7. Antibodies for immunofluorescence were validated by using a no primary antibody control, in the presence of a secondary antibody. Antibodies for western blots, where possible, were validated with a negative control. No primary antibody immunofluorescence images alongside representative examples of the primary antibody immunostaining used in this thesis can be seen in the appendix. Western blot membranes were often cut in order to

visualise antibodies raised in the same species, uncropped membrane sections for western blots can be found in the appendix.

2.6 Western Blotting

Western blotting was used to determine the amount of proteins in various cells and tissues. Briefly: Samples were prepared; resolved using sodium dodecyl sulphate (SDS; Fisher) polyacrylamide gel electrophoresis (PAGE) with reducing conditions; separated proteins were transferred onto a membrane and incubated with antibodies; antibodies were detected using horseradish peroxidase (HRP) and a chemiluminescent substrate, detected by an electronic developer.

2.6.1 Western Blot Sample Preparation

Sciatic nerves were lysed in 150 µL of SDS buffer: 50 mM Tris-HCl; 2% SDS; 10% glycerol; 1% β-mercaptoethanol; 12.5 mM EDTA and 0.02% bromophenol blue. Dissected nerves were added to the buffer and stored at -20^{0}C. Nerves were thawed and sonicated using a Q500 sonicator (Fisher) to fully lyse the sample into the buffer. Care was always taken to dissect the same amount of nerve tissue for each sample and lyse into a set volume of SDS buffer. Typically, 20 µL of lysed nerve sample was loaded for each polyacrylamide gel run.

Cells grown in vitro were lysed in radioimmunoprecipitation assay (RIPA) buffer containing: 10 mM Tris-HCl; 1 mM EDTA; 1% Triton-X-100; 0.1% sodium deoxycholate; 0.1% SDS and 140 mM NaCl in distilled H_2O. Prior to use, a protease inhibitor cocktail (1:100; Sigma) was added which ad broad specificity for serine, cysteine and acid proteases as well as aminopeptidases. Cells were washed with ice-cold PBS, RIPA buffer was added and cells were mechanically scraped off the dish or flask, with the resultant lysate collected and spun at 25 000 x g for 15 minutes. The supernatant from the lysate was transferred to a fresh tube and stored at -20^{0}C short term or -80^{0}C

long term. Protein estimation for cell lysates was conducted using the BCA assay kit (Thermo Fisher) and lysate corresponding to 20 µg total protein of each sample was typically diluted into SDS loading buffer before running on a polyacrylamide gel.

2.6.2 Western Blot Gel Running, Transfer and Detection

SDS-PAGE gels were made to the recipes shown in Table 2.5 and run using the PROTEAN system (BioRad). Gels were run in running buffer containing 192 mM glycine (Sigma), 25 mM Tris Base (Sigma) and 0.1% SDS diluted in 1 L of distilled H_2O. Gels were transferred in transfer buffer containing 192mM glycine, 25 mM Tris Base and 200 mL methanol made up to 1L with 800 mL of distilled H_2O. 8 µL of dual colour protein ladder (BioRad) was run alongside of protein samples to allow estimation of the molecular weight of proteins.

List of steps used:

1. Prior to running, aliquots of samples were denatured by heating to 95^0C for five minutes and stored on ice.
2. Protein ladder and samples were loaded into the gel and run using a Power Pac 300 at 150 volts until appropriately separated and the bromophenol blue dye had reached the bottom of the resolving gel, typically 90 minutes.
3. Separated proteins were transferred onto a polyvinylidene fluoride (PDVF) membrane which had been previously activated by soaking in methanol for 20 seconds. Proteins were transferred from the resolving gel to the PDVF membrane at 300 mA for 90 minutes with an ice pack in the tank to prevent overheating.
4. Following transfer, the PDVF membrane was blocked for 60 minutes at RT in 5% bovine serum albumin (BSA; Thermo Fisher) diluted in 1X Tris-buffered saline containing 0.5% Tween (TBS-T; Fisher).

5. Primary antibody to the protein of interest was added to the blocking solution at the relevant concentration (Table 2.10) and incubated overnight at 4^0C.
6. Next, the membrane was washed three times for 10 minutes in TBS-T to remove unbound primary antibody before being incubated with the species-specific secondary antibody (HRP conjugated) at the relevant concentration (Table 2.X) for 60 minutes at room temperature.
7. The membrane was washed three times for 10 minutes in TBS-T and HRP-dependent chemiluminescence was detected using the Pierce ECL Western Blotting Substrate (Fisher) kit following the manufacturer's instructions.
8. Chemiluminescence present on the membrane was imaged using the SYNGENE PXI 4 and formatted using ImageJ.
9. Western blots were normalised for quantification by comparing the ratio of signal between the protein of interest and the loading control in each individual lane to give a relative expression value. This relative expression of samples were then compared to the relative expression of the control which was defined to be 1.

Reagent	Resolving					4% Stacking
	5%	8%	10%	12%	15%	
10% Ammonium Persulphate	75µL	75µL	75µL	75µL	75µL	75µL
10% Sodium Dodecyl Sulphate	100µL	100µL	100µL	100µL	100µL	100µL
40% Acrylamide	1.25mL	2mL	2.5mL	3mL	3.75mL	1mL
H_2O	5.9mL	5.3mL	4.8mL	4.5mL	3.9mL	7.6mL
TEMED	10µL	10µL	10µL	10µL	10µL	10µL
Tris-HCl 1.5M (pH 8.8)*	2.8mL	2.5mL	2.5mL	2.3mL	2.0mL	1.25mL

Table 2.5: Reagents used for SDS-Page gel electrophoresis. *For stacking gel, Tris-HCl pH was 6.8.

2.7 EdU Proliferation Assay

5-Ethynyl-2'deoxyuridine (EdU; Thermo Fisher Scientific) was used to label proliferating cells in vitro and in vivo. EdU was stored as a 10 mM stock solution in dimethyl sulphoxide (DMSO; Sigma) according to manufacturer's instructions. For mice, a 2 mg of stock solution EdU (diluted with PBS) was administered via intraperitoneal injection (total volume 200 µL) and after three hours/ 24 hours mice were sacrificed, dorsal root ganglia and sciatic nerves were collected and fixed in 4% paraformaldehyde (PFA; Sigma) for analysis. For cultured cells: four hours prior to fixation in 4% PFA for 10 minutes, cells were administered 10 µM EdU diluted into the relevant cell culture medium (see Section 2.2). Proliferation was measured using the Click-iT™ EdU kit (Thermo Fisher Scientific) as per the manufacturer's directions on prepared cells and tissue fixed in PFA:

List of Steps for EdU labelling:

1. Cells/tissue sections were permeabilised in 1% Triton-X-100 (Sigma), diluted in 3% BSA in PBS.
2. Cells/tissue sections were washed twice for five minutes in 3% BSA in PBS.
3. The EdU reaction mix was made using kit components and added to cells/sections for 30 minutes (see Table 2.6 for reaction mix, the molarities of the kit components were not disclosed by the kit manufacturer, so concentrations cannot be used to describe the amount of each reagent used).
4. Cells/sections were washed three times in PBS and counter-stained with 1 µg/mL Hoechst (Invitrogen) for 15 minutes.
5. Cells/sections were washed three times in PBS and mounted onto glass coverslips (VWR) using CitiFluor-AF1 mounting medium (Science Services) before imaging on a Leica IM8 microscope. Images were quantified and formatted using ImageJ.

Reagent	Volume
Reaction buffer	0.86mL
Copper (II) sulphate pentahyrdrate	0.04mL
Alexa Fluor™ 488 5-Carboxamido-(6-Azidohexanyl), Bis (Triethylammonium Salt)), 5-isomer	0.0025mL
Reaction buffer additive	0.1mL
Total volume	1mL

Table 2.6: Reagents used to make 1 mL of EdU reaction mix.

2.8 Immunofluorescence

Immunofluorescence was used to determine the presence, abundance and localisation of various proteins in cells and tissues. Briefly, prepared cells and tissues were labelled with primary antibodies which were detected by fluorescently conjugated secondary antibodies, the latter of which can be detected when excited by certain wavelengths of light and imaged on a microscope. Immunofluorescence images were scanned using a Leica SPE confocal microscope. Images from immunofluorescence experiments were formatted using Adobe Photoshop and quantified using ImageJ. Quantification of the nuclear localisation of protein was completed by measuring the fluorescence intensity within the whole cell, then only within the nucleus, subtracting the nuclear value to get the cytoplasmic fluorescence intensity value, from this, the ratio of cytoplasmic: nuclear protein expression was calculated. Fluorescence intensity was calculated in 50 cells per biological repeat. For EdU and Ki-67 quantification, EdU and Ki-67 positive nuclei were counted and the percentage of positive cells was calculated against the total nuclei counts. EdU and Ki-67 were quantified by assessing 3 fields of view containing at least 200 cells per technical/biological repeat.

2.8.1 Immunofluorescence for Cultured Cells

Cells were analysed for the expression of various proteins using specific primary and secondary antibodies in the following way:

1. An appropriate amount of cells, (typically 5000) were seeded as a 15 µL droplet of media in the centre of a sterile glass coverslip, which had been placed into a 24-well tissue culture plate (Thermo Fisher). After two hours approximately, when all cells had adhered to the coverslip, 485 µL of the relevant medium (see Section 2.2) was added to top up the wells.
2. Following the conclusion of the experimental time course, cells were first washed in PBS and then fixed for 15 minutes in 4% PFA.

3. Coverslips were removed from the 24-well plate and placed onto pedestals in a humid environment.
4. Fixed cells were permeabilised for 45 minutes in 1% Triton-X-100, diluted in 1% BSA in PBS.
5. Permeabilised cells were blocked in 3% BSA/PBS for 90 minutes.
6. Blocked cells were incubated in primary antibody diluted in blocking solution at the relevant concentration (see Table 2.7) overnight.
7. Cells were subjected to three 10 minute PBS washes to remove unbound primary antibody before incubation with secondary conjugated antibodies (see Table 2.8).
8. For the two layer system, cells were incubated with secondary antibody in 3% BSA for 60 minutes and then washed three times for 10 minutes in PBS.
9. For the three layer system, cells were incubated in species specific biotinylated secondary antibody for 60 minutes, washed three times for 10 minutes in PBS and then incubated with a streptavidin conjugated antibody for 60 minutes.
10. Cells/sections were washed three times in PBS and counter-stained with 1 µg/mL Hoechst (Invitrogen) for 15 minutes.
11. Cells were mounted onto glass coverlips (VWR) using Citi-Fluor AF1 mounting medium before imaging on a Leica IM8 or Leica SPE microscope.

2.8.2 Tissue preparation, sectioning and immunofluorescence

1. Mouse sciatic nerve or human meningioma tumour tissue were fixed in 4% PFA and was embedded in Optimal Cutting Temperature compound (OCT; Fisher) before snap freezing in liquid N_2. Tissue was then washed in PBS, cryoprotected for 48 h in 30 % sucrose in w/v in PBS

2. Frozen embedded tissue was sectioned using a Leica CM 1680 cryostat machine, cut as transverse sections, 8 µm thick. Cut sections were collected on SuperFrost Plus slides (VWR), stored at -20^{0}C short term or -80^{0}C long term.
3. Frozen sections were thawed and an outline around the tissue was drawn using an ImmEdge pen (Vector Laboratories) to provide a hydrophobic barrier and contain immunostaining reagents.
4. OCT on the slide was dissolved using two PBS washes for five minutes and tissue was permeabilised in 1% Triton-X-100 for 15 minutes.
5. Slides were blocked in 3% (w/v) BSA in PBS for 90 minutes.
6. Blocked tissue was incubated in primary antibody at the relevant concentration (see Table 2.7) overnight at 4 ^{o}C.
7. Tissue was subjected to three 10 minute PBS washes before incubation with conjugated antibodies (see Table 2.8).
8. For the two layer system, tissue was incubated with secondary antibody in 3% BSA for 60 minutes and then washed three times for 10 minutes in PBS.
9. For the three layer system, tissue was incubated in species specific biotinylated secondary antibody for 60 minutes, washed three times for 10 minutes in PBS, and then incubated with a streptavidin antibody for 60 minutes.
10. Tissue was washed three times in PBS and counter-stained with 1 µg/mL Hoechst for 15 minutes.
11. Tissue was mounted onto with cover glass (VWR) using Citi-Fluor AF1 mounting medium before imaging on a Leica IM8 or Leica SPE microscope.

2.9 Paraffin Embedded Immunohistochemistry (IHC)

Clinical human Merlin negative schwannoma tissue, Merlin positive acoustic neuroma and healthy nerve controls in the present study were selected, cut and stained with the

help of Dr Aditya Shivane and Mr Phillip Edwards. Mouse tumour model tissue was gratefully received from Prof C Mawrin (University of Magdeburg) and Prof Long-Sheng Chang (Ohio State University) these tissues were cut but not stained by Mr Phillip Edwards. Sections were cut to 4 µm in thickness and stored at 37^0C. For staining of paraffin sections, paraffin was melted by incubating slides at 60^0C for 60 minutes.

2.9.1 Staining of Paraffin Sections

Tissue was stained using the VECTASTAIN ABC kit (Vector Laboratories) as per manufacturer's instructions:

1. Tissue was de-waxed and washed in first 100% Xylene (Fisher), then 100% ethanol (Fisher) and finally under running tap water, each for five minutes.
2. Tissue was blocked for 30 minutes in 3% H_2O_2 (Fisher) in 100% methanol and washed under running tap water for 10 minutes.
3. Tissue was pre-treated for 30 minutes in 100mM EDTA dissolved in distilled H_2O to retrieve antigens, heated to boiling in a microwave and then washed under running tap water for 10 minutes.
4. An ImmEdge pen was then used to outline the tissue in the section and contain the liquid reagents for staining. The sections were then blocked for 30 minutes in diluted normal horse serum. One drop of normal horse serum (VECTASTAIN ABC kit) diluted in TBS-T, used in a quantity to ensure the tissue was covered.
5. Primary antibody diluted in TBS-T at the appropriate concentration (Table 2.7) was added to cover the tissue and the slide then incubated at 4^0C overnight.
6. Tissue was washed in TBS-T twice for five minutes and secondary/tertiary antibodies (VECTASTAIN ABC kit) were made up 30 minutes prior to use. Two drops (1:50) of secondary/tertiary antibody from the kit was added to TBS-T and added for 30 minutes in turn, with two five minute TBS-T washes in-between.

7. 3,3'-Diaminobenzidine (DAB; Sigma) was diluted to 0.66 mg/mL in H_2O as per the manufacturer's instructions and filtered using a 0.22 µm filter (Merck Millipore). The glass slide was drained of remaining TBS-T post-washing and DAB was added for five minutes. Tissue was then washed for 10 minutes under running water.
8. Mayer's Haematoxylin (Sigma) was added for two minutes at RT and washed under running water for 10 minutes once.
9. Tissue was washed twice for five minutes in 100 % ethanol, followed by 100% Xylene in the same manner.
10. Tissue was mounted using DPX mountant (Sigma) and covered with cover glass.
11. Staining was imaged using a Leica IM8 microscope and captured images formatted using Adobe Photoshop.

Antigen	Antibody	Type	[WB]	[ICC/ IHC-F]	[IHC-P]
ALDH1A1	ab52492 Abcam	Rabbit Monoclonal Antibody	1/1000	1/200	1/100
CTGF	Ab6992		1:500		
Cyclin D1	sc-718 Santa Cruz Biotechnology	Rabbit Polyclonal Antibody	1/250		
GAPDH	AB2302 Merck	Mouse Monoclonal Antibody	1/10 000		
Ki-67	ab15580 Abcam	Rabbit Polyclonal Antibody		1/100	
LATS1	#3477 Cell Signalling Technology	Rabbit Monoclonal Antibody	1/1000		
LATS2	#5888 Cell Signalling Technology	Rabbit Monoclonal Antibody	1/1000		

MBP	sc-13914 Santa Cruz Biotechnology	Goat Polyclonal Antibody		1/100	
Neurofilament	ab4680 Abcam	Chicken Polyclonal Antibody		1/10 000	
Pan-TEAD	#13295 Cell Signalling Technology	Rabbit Monoclonal Antibody	1/1000		
P-YAP (S127)	#4911 Cell Signalling Technology	Rabbit Monoclonal Antibody	1/1000		
TAZ	sc-48805 Santa Cruz Biotechnology	Rabbit Polyclonal Antibody	1/500	1/100	
TEAD1	#12292 Cell Signalling Technology	Rabbit Monoclonal Antibody	1/1000		
TEAD2	#SAB2501231	Goat Polyclonal Antibody	1/1000		
TEAD3	#13224 Cell Signalling Technology	Rabbit Monoclonal antibody	1/1000		

TEAD4	Ab58310	Mouse Monoclonal Antibody	1/1000		
YAP	#14074 Cell Signalling Technology	Rabbit Monoclonal Antibody	1/1000	1/200	
YAP/TAZ	#8418 Cell Signalling Technology	Rabbit Monoclonal Antibody	1/1000		

Table 2.7: Primary antibody usage, for Western Blot (WB); immunocytochemistry on cells (ICC); immunohistochemistry on frozen sections (IHC-F) and immunohistochemistry on paraffin sections (IHC-P).

Species/Conjugate	Antibody	Dilution	Application
Chicken Alexa Fluor 488nm	#A-11039 Invitrogen	1/200	ICC/IHC-F
Chicken Alexa Fluor 568nm	#A-11041 Invitrogen	1/200	ICC/IHC-F
Goat Alexa Fluor 488nm	#A-11055 Invitrogen	1/200	ICC/IHC-F
Goat Alexa Fluor 568nm	#A-11957 Invitrogen	1/200	ICC/IHC-F
Mouse Alexa Fluor 488nm	#A-11001 Invitrogen	1/200	ICC/IHC-F
Mouse Alexa Fluor 568nm	#A-11004 Invitrogen	1/200	ICC/IHC-F
Mouse HRP	#1706516 Bio-Rad	1/5000	WB
Rabbit Alexa Fluor 488nm	#A-11008 Invitrogen	1/200	ICC/IHC-F
Rabbit Alexa Fluor 568nm	#A-11011 Invitrogen	1/200	ICC/IHC-F
Rabbit Biotinylated	BA-1000 Vector Laboratories	1/500	ICC/IHC-F
Rabbit HRP	#1706515 Bio-Rad	1/5000	WB
Streptavidin Alexa Fluor 488nm	#S11223 Invitrogen	1/1000	ICC/IHC-F
Streptavidin Alexa Fluor 568nm	#S11226 Invitrogen	1/1000	ICC/IHC-F

Table 2.8: Secondary/tertiary antibodies used in this study and conjugate usage.

2.10 Lentivirus

Recombinant Lentiviral vectors were used to achieve shRNA-mediated knockdown of ALDH1A1, YAP and TAZ in various cell lines and primary cells.

2.10.1 Lentiviral Plasmid Preparation

Mission® shRNA (Sigma) glycerol bacterial stocks were used to obtain purified transfection grade plasmid DNA for lentiviral knockdown. Sequences for knockdown were inserted into the pLKO.1-puro vector. This vector is under the control of a U6 promoter and contains ampicillin and puromycin resistance cassettes for selection. Knockdown and scramble sequences for ALDH1A1, YAP and TAZ can be seen in Table 2.8. Plasmids were packaged using the pCMV-VSV-G envelope and the pCMV-dr8.2 packaging plasmids (Addgene).

For plasmid generation: bacterial glycerol stocks were streaked onto Luria-Bertani (LB) agar (Sigma) plates containing 100 µg/mL ampicillin (Sigma) over a flame using aseptic technique. Overnight culture with agitation at 30^0C yielded single colonies that were used to inoculate starter cultures of 1500 µL of LB broth (Sigma) containing 100 µg/mL ampicillin. Bacteria were then further amplified by adding 200 µL of bacteria to 150 mL of LB broth containing 100 µg/mL ampicillin and culturing overnight with shaking at 30^0C. Cultures were then centrifuged at 12 000 x g for 45 minutes to pellet bacteria. The supernatant was removed and plasmid DNA prepared from the bacterial pellets using the QIAGEN Plasmid Midi Kit following manufacturer's instructions. Purified plasmid DNA was stored at -20^0C.

2.10.2 Lentiviral Transfection and Production

293FT cells were transfected with lentiviral constructs and packaging plasmids in order to produce lentiviral particles. 293FT cells are commonly used to produce lentivirus (Ansorge et al., 2009). 293FT cells were taken from University of Plymouth stocks and

were used at low passage (passage <10), cultured in DMEM containing 10% FBS and 1% penicillin/streptomycin.

The following steps were used:

1. 293FT cells were seeded in a 10 cm tissue culture dish at a density of 7 x 10^5 cell/mL in DMEM containing 10% FBS and incubated at 5 % CO_2 and 37^0C overnight.
2. 18 µL of Fugene6 (Promega) was diluted in 72 µL of Opti-MEM (Gibco) and incubated for five minutes at room temperature.
3. 3 µg, 3 µg and 0.3 µg of the relevant hairpin construct, pCMV-dr8.2 packaging plasmid and pCMV-VSV-G envelope respectively were diluted in 225 µL of Opti-MEM.
4. The plasmid mix was added to the diluted Fugene6 and incubated for 30 minutes at room temperature.
5. 315 µL of the resultant transfection mix was added to the 293FT cells which were incubated at 37^0C overnight.
6. The following day, 293FT cells were medium changed into DMEM containing 20% FBS and 1% penicillin/streptomycin, and incubated at 37^0C overnight.
7. The following day, the resultant media (now containing lentiviral particles) was collected and centrifuged at 40 x g for 5 minutes to remove cell debris.
8. Steps 6 and 7 were repeated to allow for 2 days of lentiviral production and collection of viral media.
9. Pooled viral media was stored in aliquots at -80^0C.

2.10.3 Lentiviral Transduction

Lentiviral particles were transduced into the relevant cell type in the following way:

1. Viral media containing 16 µg/mL protamine sulphate (Sigma) to increase viral particle permeation, was added to cells which were 70% confluent, for 48 hours.
2. Cells were allowed to recover for 24 hours in their standard cell culture medium (See Section 2.2), before addition of 4 µg/mL puromycin (Gibco) to select transduced cells and kill cells that were not transduced.
3. Cells were maintained in media containing puromycin until non-transduced cells were all dead and drug selection for lentiviral transduced cells was complete. After this, transduced cells were used in the relevant experiments as described.

	Target	Region	Sequence 5'-3'
SHC002	Scramble	Not applicable	CCGGCAACAAGATGAAGAGCACCAA CTCGAGTTGGTGCTCTTCATCTTGTTG TTTTT
SHCLNG-NM_000689-1	ALDH1A1	Coding Region	CCGGGCTGATTTAATCGAAAGAGATC TCGAGATCTCTTTCGATTAAATCAGC TTTTT
SHCLNG-NM_000689-2	ALDH1A1	Coding Region	CCGGGCCAAATCATTCCTTGGAATTC TCGAGAATTCCAAGGAATGATTTGGC TTTTT
SHCLNG-NM_015472-1	TAZ	Coding Region	CCGGGCGATGAATCAGCCTCTGAATC TCGAGATTCAGAGGCTGATTCATCGC TTTTT
SHCLNG-NM_015472-2	TAZ	Coding Region	CCGGGCGATGAATCAGCCTCTGAATC TCGAGATTCAGAGGCTGATTCATCGC TTTTTG
SHCLNG-NM_006106-1	YAP	Coding Region	CCGGGCCACCAAGCTAGATAAAGAA CTCGAGTTCTTTATCTAGCTTGGTGG CTTTTTG
SHCLNG-NM_006106-2	YAP	3'-Untranslated Region	CCGGCCCAGTTAAATGTTCACCAATC TCGAGATTGGTGAACATTTAACTGGG TTTTTG

Table 2.9: Sequences of lentiviral constructs used for shRNA knockdown of target mRNAs.

2.11 Drug Treatments

The drugs used for treatments of cell lines and primary cells are listed in table 2.9. For controls, the solvent for each drug was given equivalent to the maximum volume to that of cells treated with varying concentrations of drugs.

Drug	Target	Solvent	Working Concentration
Verteporfin (Sigma)	YAP-TEAD interaction	100% DMSO	1-2 µM
Vivace compounds (Vivace Therapeutics)	TEADs	100% DMSO	10-2000 nM
ALDH1A1 Inhibitors (NCATS)	ALDH1A1	100% DMSO	10 µM
Cisplatin (Cayman Chemicals)	DNA replication	100% DMSO	25-100 µM
TTNPB (Cayman Chemicals)	Pan-RAR agonist	100% DMSO	10 µM

Table 2.10: Drugs used in this thesis to measure their effects upon cell lines, primary cells and mice.

2.12 Statistical Analysis

Data was analysed using GraphPad Prism 8 and is presented as mean ± SEM. Experiments were completed with at least three technical or biological repeats with P-values < 0.05 taken to be statistically significant (except where FDR is used). Technical repeats were used for immortalised cell lines and were carried out separately from each other. Biological repeats were used for primary tumour cultures or mouse samples where each repeat represented a separate sample from a unique patient/animal. For quantification of proliferation measured by Ki-67 antibody staining or EdU, at least 3 fields of view and 200 cells per repeat were analysed in for at least three technical (cell lines) or biological (primary cells/mice) repeats. Results were assessed using a one-way analysis of variance (ANOVA) with Bonferroni's correction. For quantification of levels of nuclear and cytoplasmic YAP, the pixel density of the cell which co-localised with a Hoechst nuclear stain was subtracted from the pixel density of the total area of the cell using ImageJ. This gave rise to a cytoplasmic: nuclear ratio of YAP in each cell. For each repeat, 50 cells were assessed this manner.

3 Results

3.1 RNA Sequencing of Schwann cell conditional knockout nerves before and after injury identifies novel targets for human meningioma and schwannoma.

3.1.1 Introduction

After sciatic nerve injury, P0-Cre+.NF2$^{fl/fl}$ mice undergo an almost complete failure to remyelinate and repair (Mindos et al., 2017b). Instead, Schwann cells in the nerve stump distal to the injury site proliferate, maintain an inflammatory environment and begin to show histopathological features similar to that of human schwannoma as discussed in Section 1.5.1. Following the additional knockout of YAP in NF2-deficient Schwann cells, the proliferative and inflammatory phenotype in the distal stumps of injured mice is almost completely reversed; mice that are P0.Cre+NF2$^{fl/fl}$YAP$^{fl/fl}$ show a functional recovery after injury which is indistinguishable from P0.Cre-NF2$^{fl/fl}$YAP$^{fl/fl}$ littermate controls (Mindos et al., 2017b). Mice with heterozygous loss of Merlin in Schwann cells and axons also showed a similar phenotype after sciatic nerve injury (Schulz et al., 2014).

Because of this phenotype that showed hallmarks of schwannoma tumourigenesis that was reversed by removal of the Hippo effector YAP, our lab decided to conduct an RNA sequencing screen to determine the expression profiles of Schwann cells before and 7-days after sciatic nerve crush injury in P0-Cre+.NF2$^{fl/fl}$ mice, P0-Cre+.NF2$^{fl/fl}$YAP$^{fl/fl}$ mice and P0.Cre-NF2$^{fl/fl}$ littermate controls. The rationale of this study was to identify RNA transcripts with an expression profile where a gene was differentially regulated in P0.Cre+NF2$^{fl/fl}$ compared to P0.Cre-NF2$^{fl/fl}$ littermate controls, that is abolished when YAP is removed in the, P0-Cre+.NF2$^{fl/fl}$YAP$^{fl/fl}$ mice. RNA transcripts following this expression profile would be indicative of genes which are dysregulated following loss of NF2 whose transcription is dependent on the nuclear activity of YAP in Schwann cells.

The relevance of this nerve injury model with respect to tumourigenesis has been previously described (Mindos et al., 2017b) and was discussed in 1.5.1. In this model the injury is the key stimulus to trigger Schwann cell proliferation and inflammation, which, when on an NF2-deficient background, leads to tumourigenesis. In the absence of injury, P0.Cre+NF2$^{fl/fl}$ peripheral nerves develop normally and tumours do not form.

Prof David Parkinson and Dr Thomas Mindos conducted the sciatic nerve injury, dissected and purified RNA from sciatic nerves, which were sent for sequencing by Cambridge Genomic Services. Data from RNA sequencing was annotated with the help of Dr Matthias Futschik and Dr Vasilis Lenis. Liyam Laraba then analysed the annotated transcripts, and developed a selection criteria based on relative abundance of RNA transcript and the level of dysregulation.

The hypothesis in this chapter is that comparison of differentially expressed RNA transcripts in P0.Cre+NF2$^{fl/fl}$ compared with P0.Cre-NF2$^{fl/fl}$ controls in intact and 7 days post-injury mice will yield novel targets that become dysregulated following loss of Merlin in Schwann cells. These dysregulated transcripts can then be assessed within the current literature for links to their roles in tumour development and Hippo signalling.

3.1.2 Conditional deletion of NF2 and YAP in Schwann cells causes differential expression of genes before and after sciatic nerve crush injury.

RNA transcripts were annotated using the *mus musculus* Ensembl gene ID database. Sequencing of control or injured P0-CRE^{+}.NF2$^{fl/fl}$ mice, P0-CRE^{+}.NF2$^{fl/fl}$YAP$^{fl/fl}$ mice and CRE^{-} littermate controls nerve mRNAs was performed (n=4 per genotype) and Ensembl IDs were given as raw counts per million; a false discovery rate correction was applied to p-values, the false discovery rate was used to adjust for the number of false positives that arise from multiple statistical tests. RNA transcripts were filtered according to the following inclusion criteria: false discovery rates < 0.05 were considered significant

and differential regulation was defined as a Log_2 (fold change) > 1 or Log_2 (fold change) < -1 meaning that transcript number had at least doubled or halved respectively. There was also a minimum thresholds where Log_{10} (counts per million) > 0.5 in order to only analyse transcripts with a relevant abundance that would have the potential to elicit a change in protein expression. Transcripts with Log_{10} (counts per million) < 0.5 may appear as significantly differentially regulated between genotypes however this would likely not result in any changes at the cellular level. The bioinformatics tool Venny 2.1 was used to identify overlaps between genotypes before and seven days after sciatic nerve injury in P0-CRE^+.$NF2^{fl/fl}$ mice and CRE^- littermate controls.

There were 521 upregulated transcripts that met inclusion criteria, of which 110 were exclusive to intact nerves between genotypes, 330 were exclusive to injured nerves and 81 were upregulated in both conditions (Figure 3.1.1A). There were 482 downregulated transcripts that met inclusion criteria, of which 147 were exclusive to intact nerves, 249 were exclusive to injured nerves and 86 were downregulated in both conditions (Figure 3.1.1B). Overlap of these diagrams showed that differentially regulated transcripts did not move from upregulated to downregulated or vice versa before and after injury (Figure 3.1.1C). The top 10 upregulated and downregulated transcripts ranked by fold change for P0-CRE^+.$NF2^{fl/fl}$ mice and CRE^- littermate controls are shown in Table 3.1. In the NF2-deficient mice post-injury, Neurofilament RNA was significantly downregulated which was a good indicator that the inclusion criteria was capturing the repair phenotype seen in these mice. NF2 transcripts did not reach the inclusion criteria of Log_{10} (counts per million) < 0.5 in the P0-CRE^+.$NF2^{fl/fl}$ mice which is the reason that NF2 itself did not show in the data as a dysregulated transcript based on the inclusion criteria. The following section will focus on our validation of a top upregulated transcript ALDH1A1. ALDH1A1 was selected due to it being found to be regulated by the Hippo pathway transcriptional coactivator TAZ in lung cancer (Yu et al., 2017), additionally, ALDH1

has been shown to be a potential diagnostic marker of Schwann cell-derived tumours based on human histological studies (Liesche et al., 2019a). Other candidates are also being followed up in our lab, outside of the work done in this thesis.

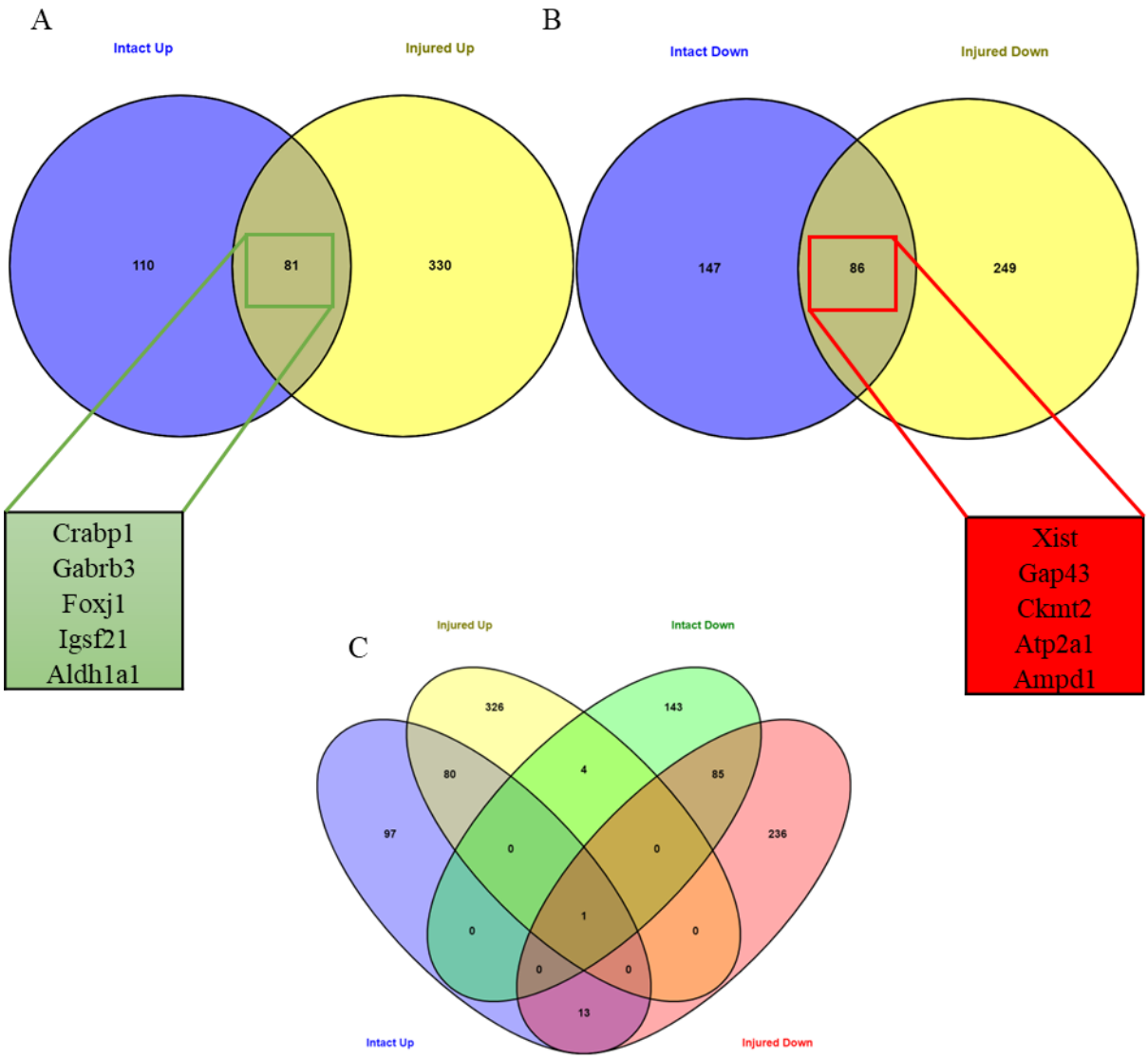

Figure 3.1.1: Venn diagrams denoting the RNA transcript overlap between intact and seven day post-injury sciatic nerves in (**A**) upregulated, (**B**) downregulated and (**C**) Combined P0-CRE^{+}.NF2$^{fl/fl}$ mice compared to CRE^{-} littermate controls. Transcripts shown in green and red represent examples of top upregulated and downregulated genes respectively. There is very little overlap between significantly upregulated and downregulated transcripts in CRE^{+} vs CRE^{-} mice in both injured and intact settings.

A Top 10 Upregulated Genes in P0.Cre+NF2$^{fl/fl}$ Mice Intact Sciatic Nerve

Gene	EntrezGene	Log_2 (Fold Change)	Log_2 (Counts Per Million)	False Discovery Rate
Crabp1	12903	3.65	4.42	7.75E-164
C1s2	317677	3.58	3.36	4.71E-15
Gabrb3	14402	3.42	3.98	1.11E-53
Foxj1	15223	3.23	2.30	2.07E-19
Htr1b	15551	3.16	4.21	3.48E-122
Igsf21	230868	3.12	1.78	7.38E-41
Ucn2	171530	2.89	2.30	8.18E-11
Aldh1a1	11668	2.82	9.44	8.30E-227
Col11a1	12814	2.80	8.61	4.95E-291
D430036J16Rik	319405	2.49	2.53	1.23E-37

B Top 10 Downregulated Genes in P0.Cre+NF2$^{fl/fl}$ Mice in Intact Sciatic Nerve

Gene	EntrezGene	Log_2 (Fold Change)	Log_2 (Counts Per Million)	False Discovery Rate
Actc1	11464	-5.44	5.41	1.85E-20
Myh1	17879	-4.65	5.75	4.76E-08
Ampd1	229665	-4.18	4.27	2.67E-06
Trdn	76757	-4.06	4.08	5.22E-10
Ano5	233246	-4.01	1.88	2.47E-06
Mylpf	17907	-3.78	7.70	1.01E-07
Pvalb	19293	-3.72	7.26	2.80E-07
Myl1	17901	-3.69	6.98	3.25E-09
Ckm	12715	-3.65	8.70	7.97E-06
Atp2a1	11937	-3.64	8.32	8.72E-07

C Top 10 Upregulated Genes in P0.Cre+NF2$^{fl/fl}$ Mice in 7 Day Post-Injury Sciatic Nerve

Gene	EntrezGene	Log_2 (Fold Change)	Log_2 (Counts Per Million)	False Discovery Rate
Npy6r	18169	5.55	1.70	1.94E-54
1110015O18Rik	100503859	4.86	2.18	1.86E-45
Cntn6	53870	4.83	2.64	2.64E-151
Igsf21	230868	4.64	1.78	1.55E-66
Aldh1a1	11668	4.46	9.44	1.55E-67
Foxj1	15223	4.23	2.30	3.46E-137
Lrtm2	211187	4.23	2.93	1.72E-149
Il17b	56069	4.15	2.94	8.75E-180
Gabrb3	14402	4.10	3.98	8.00E-218
Crabp1	12903	3.95	4.42	3.35E-279

D Top 10 Downregulated Genes in P0.Cre+NF2$^{fl/fl}$ Mice in 7 Day Post-Injury Sciatic Nerve

Gene	EntrezGene	Log_2 (Fold Change)	Log_2 (Counts Per Million)	False Discovery Rate
Xist	213742	-9.19	6.90	2.12E-20
Tyrp1	22178	-6.00	3.81	2.46E-33
Gap43	14432	-4.97	2.66	1.63E-246
Ckmt2	76722	-4.95	4.36	2.44E-65
Nefh	380684	-4.74	2.25	4.18E-33
Slc17a8	216227	-4.52	4.12	4.66E-59
Rph3a	19894	-4.29	2.71	3.06E-29
Ucn2	171530	-4.21	2.30	3.38E-202
Dlk1	13386	-4.16	2.79	1.78E-117
Ntm	235106	-4.05	3.87	2.19E-273

Table 3.1: The top candidates from RNA sequencing of Schwann cell conditional NF2 null mouse sciatic nerve, intact (**A**,**B**) and seven days post-injury **(C**,**D**) P0.Cre+NF2$^{fl/fl}$ mice were compared to P0.Cre-NF2$^{fl/fl}$ intact and injured controls respectively (n=4 per condition). Genes with Log_2 (Counts Per Million) > 1.5 were considered. GeneID is taken from the Ensembl mouse reference genome.

3.1.3 Discussion

This chapter has briefly shown the top upregulated and downregulated transcript in intact and 7 dpi P0.Cre+NF2$^{fl/fl}$ sciatic nerves compared to P0.Cre-NF2$^{fl/fl}$ littermate controls. We will now discuss the decision made to focus on ALDH1A1 and also contextualise some of the other candidates from table 3.1.

All of the top candidates were subjected to a literature search in order to find putative links to Merlin null tumour biology or the Hippo pathway. From the upregulated targets ALDH1A1 was selected for validation as it was well-characterised as a cancer stem cell marker in multiple tumour types (Nwani et al., 2019; Namekawa et al., 2019; Yu et al., 2017; Hoshino et al,. 2015). Additionally, ALDH1A1 had previously been linked to the Hippo pathway and specifically TAZ, where it was shown that TAZ drives ALDH1A1 expression to induce cancer stem cell properties in lung cancer (Yu et al., 2017). This literature provided a direct link between transcriptional changes due to loss of Merlin and the Hippo pathway. In section 3.2.3 this was validated by confirming ALDH1A1 upregulation in P0.Cre+NF2$^{fl/fl}$ and Postn.Cre+NF2$^{fl/fl}$ sciatic nerve. CRABP1 was also in the top 10 upregulated transcripts in both intact and 7 dpi P0.Cre+NF2$^{fl/fl}$ sciatic nerves. CRABP1 binds cytosolic retinoic acid and shuttles it into the nucleus and a literature search only revealed that its expression is associated with poor prognosis in breast cancer (Liu et al., 2015). As ALDH1A1 is directly upstream of CRABP1 in the retinoic acid signalling pathway (Figure 1.4) it would be of interest to explore the role of CRABP1 in Merlin null meningioma and schwannoma further.

Other top upregulated candidates in both injured and intact P0.Cre+NF2$^{fl/fl}$ sciatic nerve included Immunoglobulin superfamily member 21 (Igsf21). Immunoglobulin superfamily members are typically involved in cell-cell recognition (Li et al., 2017), however literature searches did not reveal a link to Merlin or the Hippo pathway. Forkhead box protein J1 (Foxj1) is part of the forkhead family of transcription factors,

primarily shown to be important for ciliogenesis in tissues such as the lungs or kidney (Yu et al., 2008). Foxj1 has been shown to be overexpressed in colorectal cancer where it promotes nuclear localisation of β-catenin (Liu et al., 2017). Merlin has previously been shown to inhibit β-catenin signalling(Kim et al., 2016), so loss of Merlin and FoxJ1 upregulation may be having a synergistic effect although due to the lack of a link to the Hippo pathway this was not explored further. Contactin 6 (Cntn6) was exclusively upregulated in the 7 dpi P0.Cre+NF2$^{fl/fl}$ sciatic nerves compared to P0.Cre-NF2$^{fl/fl}$ controls. Contactin 6 is another immunoglobulin superfamily member which functions as a cell adhesion molecule, it is reported to be expressed on the cell membranes of axons and neurons in peripheral nerves (Zuko et al., 2016). No literature was found linking Cntn6 to the Hippo pathway or Merlin null tumours.

In terms of downregulated transcripts from the RNA sequencing, the non-coding RNA X-inactive specific transcript (Xist) was the most downregulated transcript in 7 dpi P0.Cre+NF2$^{fl/fl}$ sciatic nerves compared to P0.Cre-NF2$^{fl/fl}$ controls. No literature links Xist to the Hippo pathway or Merlin null tumours, also, Xist was found to be upregulated in cervical and oesophageal cancers (Chen et al., 2019, Wu et al., 2017). Adenosine monophosphate deaminase 1 (Ampd1) was exclusively downregulated in intact P0.Cre+NF2$^{fl/fl}$ sciatic nerves compared to P0.Cre-NF2$^{fl/fl}$ controls. AMPD1 converts adenosine monophosphate into inosine monophosphate, liberating a molecule of ammonia. No literature was found to link AMPD1 to the Hippo pathway or Merlin null tumours.

In summary, ALDH1A1 was an upregulated transcript in 7 dpi P0.Cre+NF2$^{fl/fl}$ sciatic nerves compared to P0.Cre-NF2$^{fl/fl}$ controls. Upon literature review, ALDH1A1 was deemed the most promising candidate for validation due to the links with the Hippo pathway co-transcriptional activator TAZ (Yu et al., 2017) and the link to ALDH1 being a potential histological marker for Schwannoma (Liesche et al., 2019a). The role of

ALDH1A1 in Merlin null schwannoma and meningioma will now be explored in chapter 3.2.

3.2 The Cancer Stem Cell Marker ALDH1A1 is Upregulated in Merlin Null Meningioma and Schwannoma Tumours

3.2.1 Introduction

This chapter will discuss the role of ALDH1A1 in meningioma and schwannoma. ALDH1A1 is a subtype within the aldehyde dehydrogenase superfamily and its primary enzymatic substrate is retinal (Tomita et al., 2016). ALDH1A1 catalyses the oxidation of retinal into retinoic acid and thus is an integral component of retinoic acid (RA) signalling. In summary, lipid soluble retinol enters cells by passive diffusion and is sequestered by cellular retinol binding proteins (CRBPs) in the cytoplasm. Retinol dehydrogenase then converts retinol into retinal, with ALDH1A1 then oxidising retinal further to generate retinoic acid. RA is then shuttled to the nucleus by cellular retinoic acid-binding proteins (CRABPs), where it then activates nuclear retinoic acid receptors (RARs) and retinoid X receptors (RXRs) by recruiting a co-activator or co-repressor complex which modulates gene expression at various loci. RARs and RXRs drive transcription of genes which feature a retinoic acid response element (RARE) within their promoter (Figure 1.4) (Janesick et al., 2015). ALDH1A1 has been reported as a cancer stem cell marker in various malignancies. These include gastric, colon, ovarian, bladder, breast, lung and brain tumours. (Namekawa et al., 2019, Li et al., 2014b, Januchowski et al., 2016, Gao et al., 2015, Hoshino et al., 2015, Zhao et al., 2018). ALDH1A1 has been shown to have potential roles in detoxification of reactive oxygen species to protect tumour cells, as well as metabolising chemotherapeutics such as cyclophosphamide to confer chemoresistance (Januchowski et al., 2016, Tomita et al., 2016).

ALDH1A1 was significantly upregulated in NF2-deficient nerves before and after injury with Log_2 fold changes of 2.82 and 4.46 respectively (see 3.1.2). Additionally, CRABP1 was also the first and 10^{th} upregulated transcript in intact and injured nerves with Log_2 fold changes of 3.65 and 3.95 respectively (see 3.1.2). CRABPs have previously been implicated in promoting retinoic acid signalling in breast cancer (Liu et al., 2015). This results chapter will assess the role of ALDH1A1 in schwannoma mouse models, primary meningioma and schwannoma. We hypothesised that if we can validate the overexpression of ALDH1A1 and identify its role, chemical inhibition or knockdown may lead to a reduction in tumour phenotypes in Merlin-null schwannoma and meningioma.

3.2.2 ALDH1A1 is upregulated in NF2-Deficient Mouse Models

The RNA sequencing screen discussed in section 3.1 showed that ALDH1A1 was the 8th and 5th most significantly upregulated gene before and after sciatic nerve crush injury respectively, in P0.Cre+NF2$^{fl/fl}$ mice compared to P0.Cre-NF2$^{fl/fl}$ mice (Table 3.1). This screen was used to identify differentially regulated genes in P0.Cre+NF2$^{fl/fl}$ adult mice compared to P0.Cre-NF2$^{fl/fl}$ littermate controls both before and seven days after sciatic nerve crush injury.

This regulation of Aldh1a1 was validated in P0.CreNF2$^{fl/fl}$ and Postn.CreNF2$^{fl/fl}$ mice, by assessing ALDH1A1 protein expression by western blot of sciatic nerve lysates and immunofluorescence of sciatic nerve sections, compared to age-matched Cre^{-} littermate controls (Figure 3.2.1). ALDH1A1 was significantly upregulated in intact P0.Cre+NF2$^{fl/fl}$ sciatic nerve (Figure 3.2.1a), with expression increasing at least two-fold (Figure 3.2.1b). Likewise, at both seven and 21 days post injury (dpi), upregulation of ALDH1A1 was seen in injured P0.Cre+NF2$^{fl/fl}$ sciatic nerve transverse sections compared to P0.Cre-NF2$^{fl/fl}$ injured littermate controls (Figure 3.2.2c). Interestingly, in intact NF2-deficient mice, ALDH1A1 upregulation was almost exclusively seen in non-myelinating Schwann cells within the sciatic nerve (white arrows, Figure 3.2.2). ALDH1A1 positive cells did not localise with the MBP positive myelinating Schwann cells in transverse sections of NF2-deficient sciatic nerve (Figure 3.2.2a). ALDH1A1 positive cells also did not associate with large diameter Neurofilament positive axons, but were only found close to smaller axons which are likely to be unmyelinated and reside in a Remak bundle (Figure 3.2.2b). These results indicate that non-myelinating P0.Cre+NF2$^{fl/fl}$ Schwann cells upregulate ALDH1A1 prior to nerve injury. Post-injury, all de-differentiated Schwann cells also upregulate ALDH1A1 and this is maintained to at least 21 dpi when compared to P0.Cre-NF2$^{fl/fl}$ injured controls.

Adult Mice Sciatic Nerve

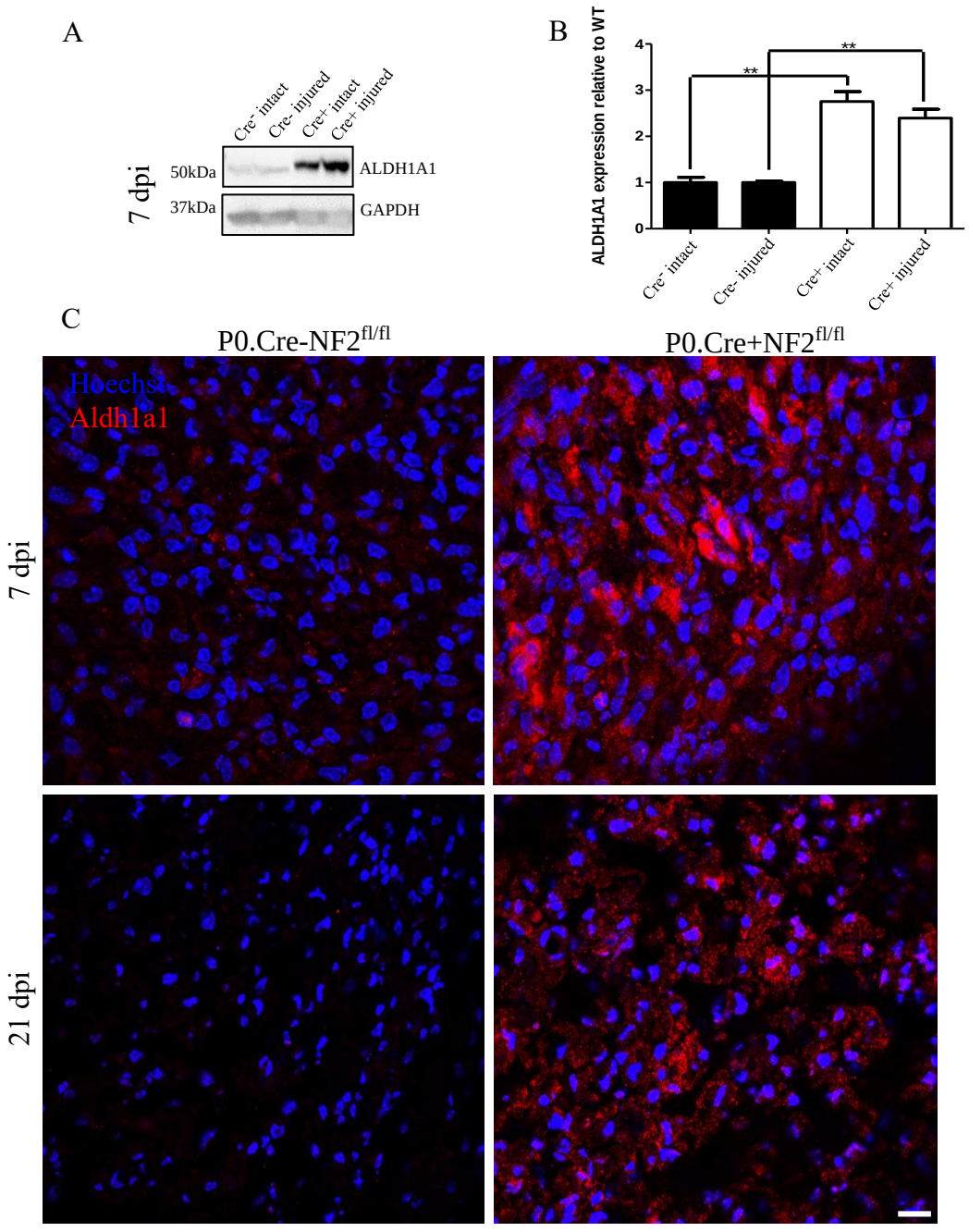

Figure 3.2.1: ALDH1A1 is upregulated in vivo in mouse sciatic nerve following loss of Merlin in Schwann cells. (**A**) Western blot showing ALDH1A1 expression in P0.Cre-$NF2^{fl/fl}$ (Cre-) and P0.Cre+$NF2^{fl/fl}$ (Cre+) sciatic nerve lysates from adult mice at 7 days post-sciatic nerve crush injury (dpi), as well as the intact contralateral control, GAPDH was used as loading control. (**B**) Quantification of A, One way ANOVA with Bonferroni's correction, $p < 0.01$ = **. (**C**) Representative Immunofluorescence of (n=3) sciatic nerve transverse sections showing ALDH1A1 expression (red) at seven (top) and 21 dpi (bottom) in P0.Cre-$NF2^{fl/fl}$ (left) and P0.Cre+$NF2^{fl/fl}$ (right) adult mice; nuclei were counterstained with Hoechst (blue), scale bar = 10 µm.

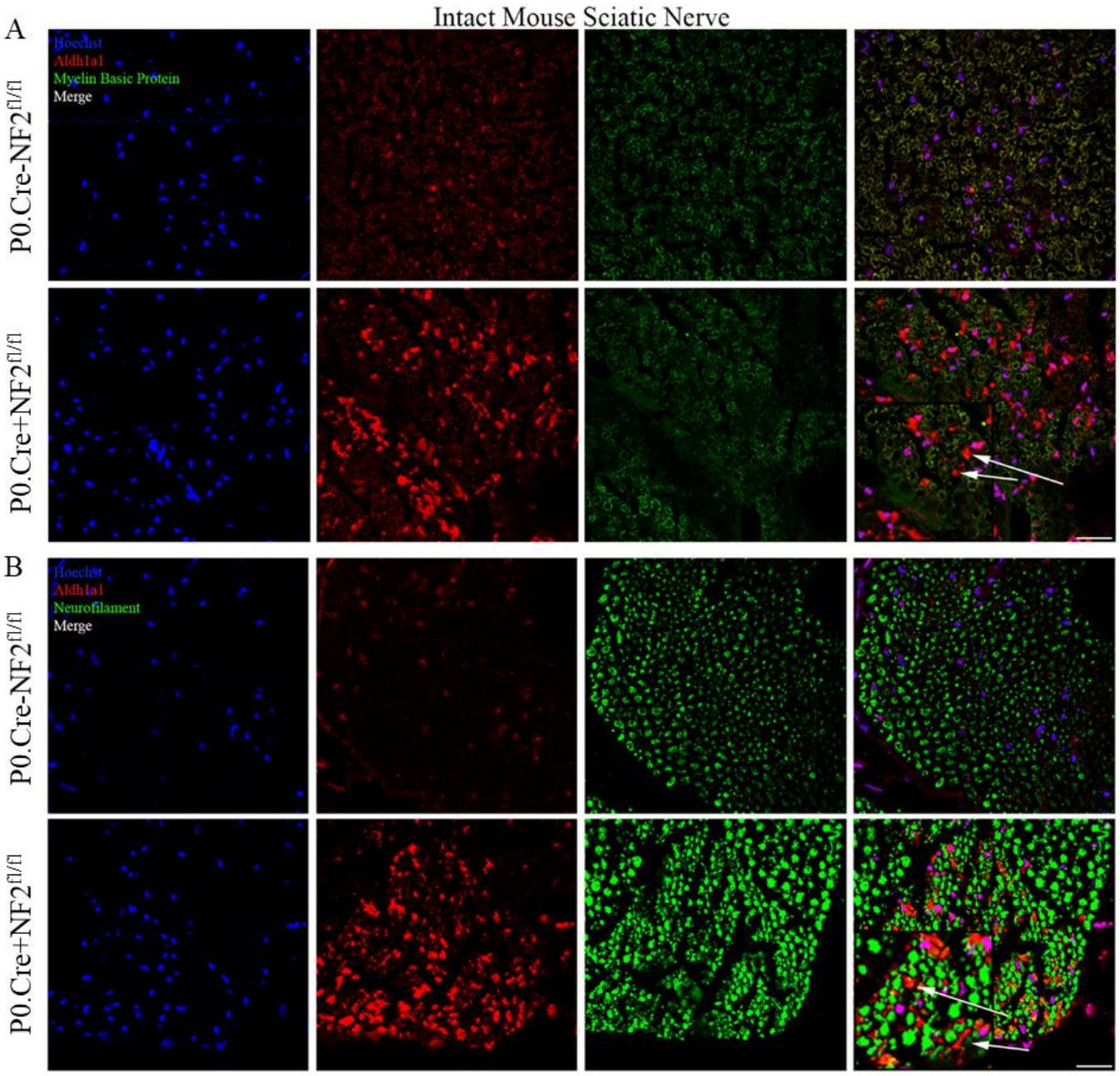
Intact Mouse Sciatic Nerve
A
Hoechst
Aldh1a1
Myelin Basic Protein
Merge
P0.Cre-NF2fl/fl
P0.Cre+NF2fl/fl
B
Hoechst
Aldh1a1
Neurofilament
Merge
P0.Cre-NF2fl/fl
P0.Cre+NF2fl/fl

Figure 3.2.2: ALDH1A1 is exclusively upregulated by non-myelinating Schwann cells in NF2-deficient intact sciatic nerve. The following is representative immunofluorescence of n=3 repeats. (**A**) P0.Cre-NF2$^{fl/fl}$ (top) and P0.Cre+NF2$^{fl/fl}$ (bottom) transverse sciatic nerve sections showing ALDH1A1 (red) and myelin basic protein (green). Arrows show no apparent co-localisation between myelinating (MBP+) Schwann cells and cells upregulating ALDH1A1. (**B**) P0.Cre-NF2$^{fl/fl}$ (top) and P0.Cre+NF2$^{fl/fl}$ (bottom) transverse sciatic nerve sections showing ALDH1A1 (red) and Neurofilament (green). Arrows show ALDH1A1-positive Schwann cells are not associated with large diameter axons stained with Neurofilament. Bottom right image in **A** and **B** feature enlarged insets. Hoechst counter-stained nuclei. Scale bar = 10 µm.

3.2.3 The Hippo Pathway Effector TAZ is Required for ALDH1A1 Expression in Mouse Schwann Cells

We next assessed was whether the Hippo pathway effectors YAP and TAZ affect ALDH1A1 expression in a Merlin null background. This was done because previous work in our lab had shown that YAP and TAZ contribute towards the proliferative phenotype seen in NF2-deficient Schwann cells following sciatic nerve injury (Mindos et al., 2017b). Additionally, YAP and TAZ have been identified as regulators of ALDH1A1 in two different cancer types (Zhao et al., 2018, Yu et al., 2017). These mice were generated by crossing $YAP^{fl/fl}$ or $TAZ^{fl/fl}$ mice with P0 or Postn.Cre-$NF2^{fl/fl}$ mice to maintain the conditional knockout in Schwann cells.

Interestingly, loss of TAZ but not loss of YAP resulted in a significant reduction in ALDH1A1 expression in P0.Cre+$NF2^{fl/fl}$ mouse sciatic nerve (Figure 3.2.3). Western blots of sciatic nerve showed loss of Merlin together with TAZ in Schwann cells saw ALDH1A1 levels return to those levels seen in P0.Cre-$NF2^{fl/fl}$ mice (Figure 3.2.3a). Concomitant loss of NF2 and YAP appeared to further increase ALDH1A1 levels, however this result was not significant (Figure 3.2.3b) The same result was seen when assessed by immunofluorescence (Figure 3.2.3c). Additionally, P0.Cre+$TAZ^{fl/fl}$ sciatic nerves that are $NF2^{WT/WT}$ show even lower level of ALDH1A1, relative to both P0.Cre-$NF2^{fl/fl}$ and P0.Cre+$NF2^{fl/fl}$ nerves (Figure 3.2.3c). Taken together, these results show that TAZ is required for the expression of ALDH1A1 in sciatic nerve mouse Schwann cells in vivo.

To further confirm this result, we decided to look at the same combinations of genotypes, but using the Postn.Cre driver where schwannoma tumour development within the DRGs and vestibulocochlear nerves occur spontaneously without the need for nerve injury, to remove NF2, together with either TAZ or YAP. The results seen in P0.Cre+$NF2^{fl/fl}$ mice sciatic nerves were consistent with those seen in the sciatic nerves of Postn.Cre+$NF2^{fl/fl}$

mice (Figure 3.2.4), as well as in Postn.Cre+NF2$^{fl/fl}$ DRGs where tumours form (not shown). Firstly, in the DRG of Postn.Cre+NF2$^{fl/fl}$ mice, we saw a clear upregulation of ALDH1A1 at three and five months, timepoints at which there is schwannoma tumour development (Gehlhausen et al., 2015) and (Grimm de Guibert, unpublished observations). Western blots of sciatic nerve showed at three months and five months (Figure 3.2.4a) ALDH1A1 was upregulated in Postn.Cre+NF2$^{fl/fl}$ mice compared to Postn.Cre-NF2$^{fl/fl}$ controls and that concomitant knockout of TAZ returned ALDH1A1 expression to Postn.Cre-NF2$^{fl/fl}$ levels.

Similarly, when looking by immunofluorescence of either sciatic nerve, ALDH1A1 is upregulated in Postn.Cre+NF2$^{fl/fl}$ compared to Postn.Cre-NF2$^{fl/fl}$ controls (Figure 3.2.4b). Interestingly, the morphology of the Schwann cells in intact nerve appear similar to those seen in P0.Cre+NF2$^{fl/fl}$ mice, however there appear to be long protrusions on the Schwann cells which are upregulating ALDH1A1 in Postn.Cre +NF2$^{fl/fl}$ mice. Taken together, these results demonstrate that ALDH1A1 is upregulated in two NF2-deficient mouse models in the sciatic nerve.

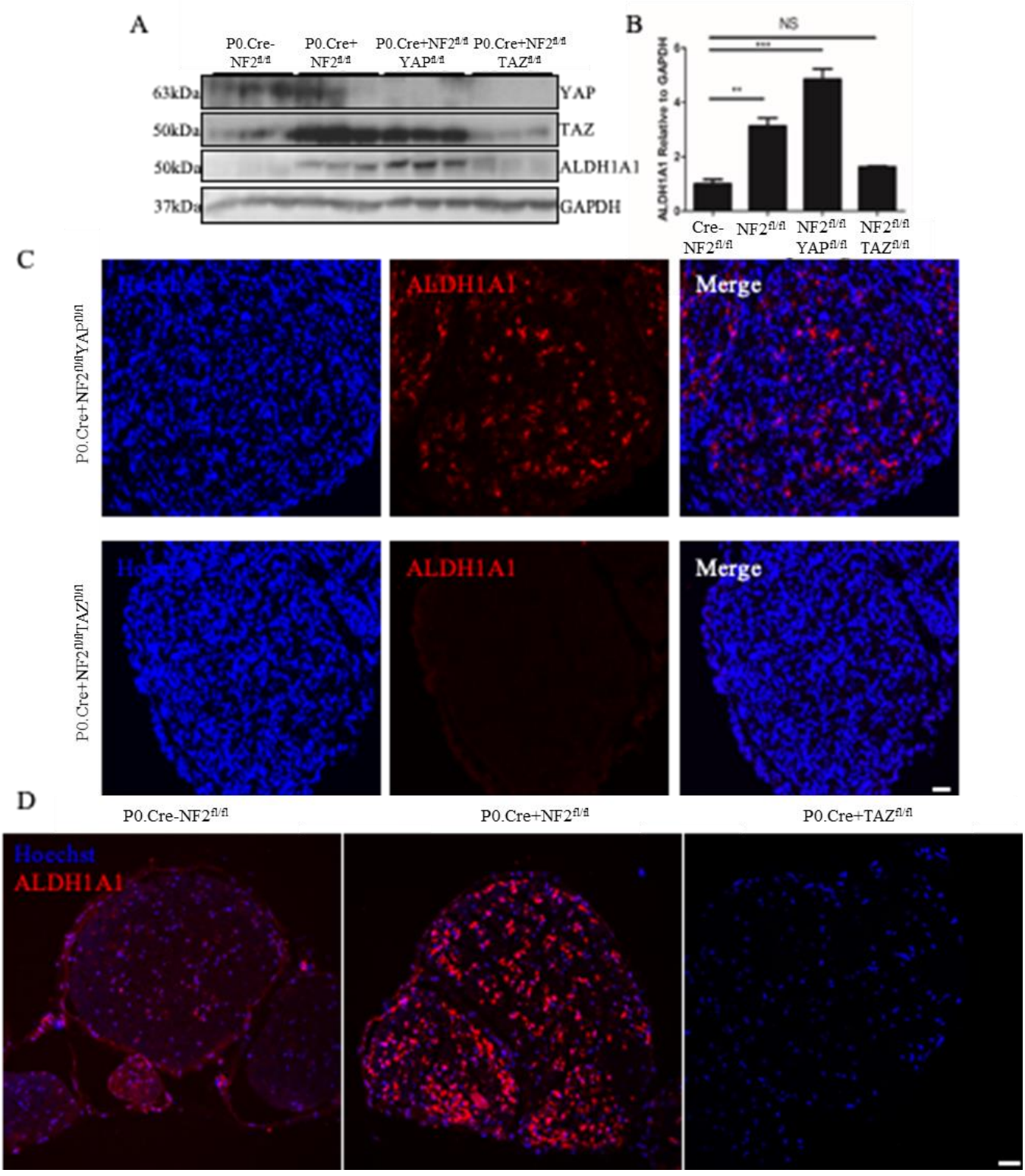
A
P0.Cre-NF2fl/fl
P0.Cre+NF2fl/fl
P0.Cre+NF2fl/fl YAPfl/fl
P0.Cre+NF2fl/fl TAZfl/fl
63kDa
YAP
50kDa
TAZ
50kDa
ALDH1A1
37kDa
GAPDH
B
NS
***
**
ALDH1A1 Relative to GAPDH
Cre-NF2fl/fl
NF2fl/fl
NF2fl/fl YAPfl/fl
NF2fl/fl TAZfl/fl
C
P0.Cre+NF2fl/flYAPfl/fl
ALDH1A1
Merge
P0.Cre+NF2fl/flTAZfl/fl
ALDH1A1
Merge
D
P0.Cre-NF2fl/fl
P0.Cre+NF2fl/fl
P0.Cre+TAZfl/fl
Hoechst
ALDH1A1

Figure 3.2.3: TAZ is required for ALDH1A1 expression in mouse sciatic nerve. (**A**) Western blot showing YAP, TAZ and ALDH1A1 levels in: P0.Cre-NF2$^{fl/fl}$ (lanes 1-3), P0.Cre+NF2$^{fl/fl}$ (lanes 4-6), P0-Cre+NF2$^{fl/fl}$YAP$^{fl/fl}$ (lanes 7-9) and P0-Cre+NF2$^{fl/fl}$ TAZ$^{fl/fl}$ (lanes 10-12) sciatic nerve lysates, GAPDH was used as loading control. (**B**) Quantification of Panel A, results were normalised to GAPDH and the P0.Cre-NF2$^{fl/fl}$, data plotted as mean +/- SEM, one-way ANOVA with Bonferroni's correction, $P<0.01$ = **, $P<0.001$ = ***. (**C**) Representative Immunofluorescence from (n=3) mice showing ALDH1A1 (red) in P0.Cre+NF2$^{fl/fl}$YAP$^{fl/fl}$ and P0.Cre+NF2$^{fl/fl}$TAZ$^{fl/fl}$ sciatic nerve, Hoechst counter stained nuclei (blue), scale bar = 10 μm. (**D**) Immunofluorescence showing ALDH1A1 (red) in P0.Cre-NF2$^{fl/fl}$, P0.Cre+NF2$^{fl/fl}$ and P0.Cre+TAZ$^{fl/fl}$ sciatic nerves. Hoechst counter stained nuclei (blue), scale bar = 10 μm.

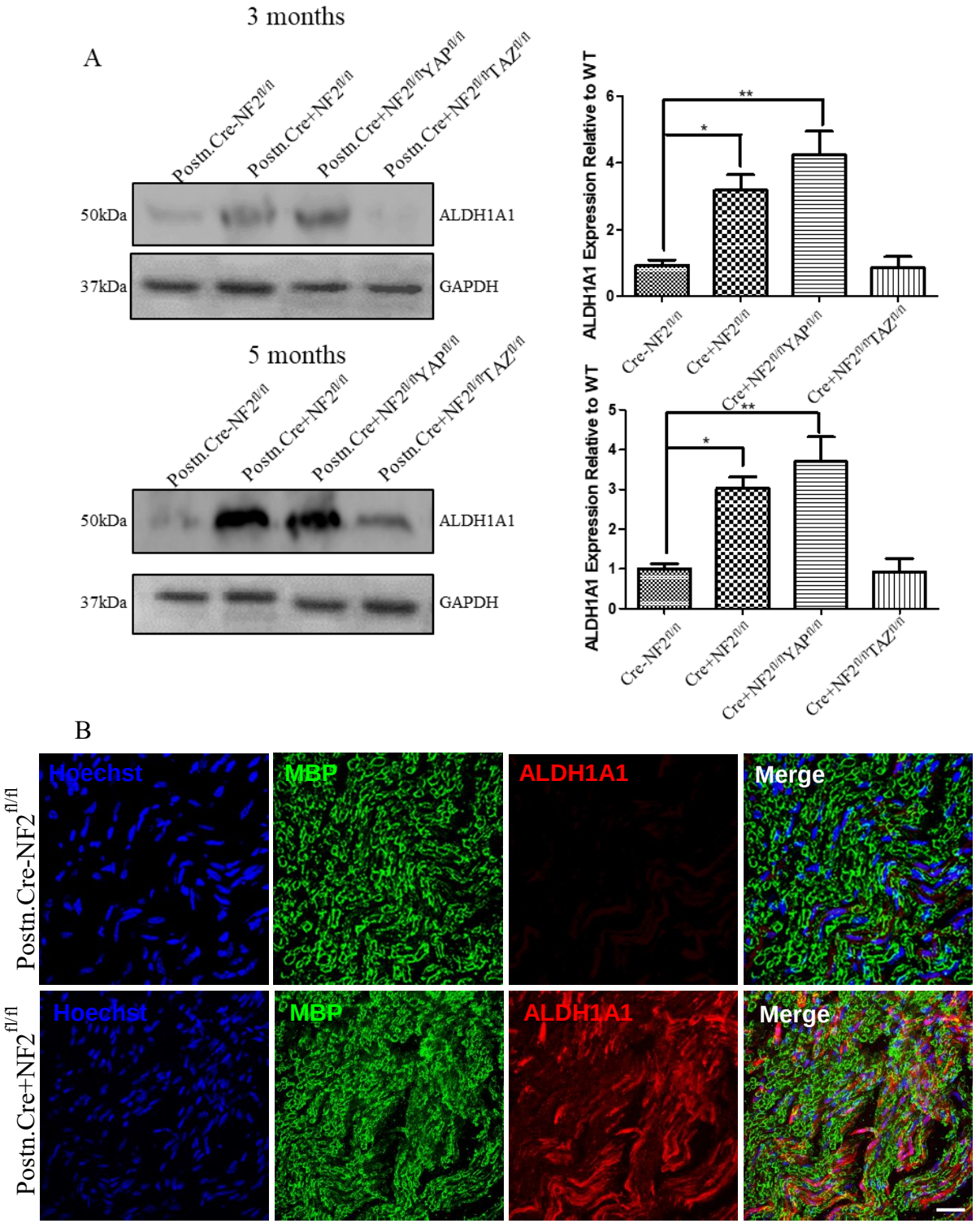
A
3 months
Postn.Cre-NF2fl/fl
Postn.Cre+NF2fl/fl
Postn.Cre+NF2fl/flYAPfl/fl
Postn.Cre+NF2fl/flTAZfl/fl
50kDa
ALDH1A1
37kDa
GAPDH
5 months
ALDH1A1 Expression Relative to WT
Cre-NF2fl/fl
Cre+NF2fl/fl
Cre+NF2fl/flYAPfl/fl
Cre+NF2fl/flTAZfl/fl
B
Postn.Cre-NF2fl/fl
Postn.Cre+NF2fl/fl
Hoechst
MBP
ALDH1A1
Merge

Figure 3.2.4: ALDH1A1 is upregulated in Postn.Cre+NF2$^{fl/fl}$ mouse sciatic nerve. (**A**) Representative (n=3) western blot (left) and quantification (right) of three-month old (top) and five-month old (bottom) mouse sciatic nerve. GAPDH was the loading control, data plotted as MEAN +/- SEM (n=3), one way ANOVA with Bonferroni's correction, $P<0.05$ = *, $P<0.01$ = **. (**B**) Representative immunofluorescence of (n=3) ALDH1A1 (red), myelin basic protein (green) in transverse sections of sciatic nerve in Postn.Cre-NF2$^{fl/fl}$ controls (top) and Postn.Cre+NF2$^{fl/fl}$ 5-month old mice. The endogenous background staining of ALDH1A1 in neuronal cell bodies was qualitatively similar in Cre^{-} and Cre^{+} mice. Hoechst counter stained nuclei (blue), scale bar = 10 μm.

3.2.4 ALDH1A1 is upregulated in human meningioma and schwannoma

Having seen Aldh1a1 upregulation in the sciatic nerve and DRGS in our mouse models, we next tested whether the TAZ-dependent ALDH1A1 expression was seen in human Merlin null schwannomas and meningiomas. Firstly, expression of ALDH1A1 was confirmed in meningioma and schwannoma cell lines, primary cells and tissue. Expression was determined by Western blot and, where possible, IHC. ALDH1A1 was upregulated in grade I BM1 and grade III KT21 cell lines (both Merlin null according to previous publications (Puttmann et al., 2005, Tanaka et al., 1989)), and also in grade III Merlin positive IOMM-Lee meningioma cell lines compared with HMC controls, a human meningeal cell line (Figure 3.2.5a). Immunofluorescence of cells showed that ALDH1A1 had a cytoplasmic expression and was upregulated in BM1 compared to HMC (Figure 3.2.5b). A panel of four Merlin positive and four Merlin negative grade I primary meningiomas cell lysates were assessed for ALDH1A1 expression (Figure 3.2.6a). ALDH1A1 was expressed in three out of four tumours within each Merlin status group. IHC of frozen sections of grade I meningioma whole tumour tissue also revealed a cytoplasmic expression of ALDH1A1 (Figure 3.2.6). The findings of the primary tissue western blots were not consistent with the hypothesis that ALDH1A1 expression is increased following loss of Merlin, however these differences could be due to the presence of other cell types in the tumour tissue lysates such as tumour-associated macrophages or fibroblasts which could express varying levels of ALDH1A1.

ALDH1A1 expression in Merlin null human schwannoma tissue was assessed by IHC of paraffin-embedded sections. Sections were cut and stained by Dr Aditya Shivane and Dr Phillip Edwards in the neuropathology labs at Plymouth University Hospital. Aditya Shivane provided clinical information and assessed scores for the strength of ALDH1A1 staining (Figure 3.2.7, Table 3.2.1). Nine schwannomas were analysed for ALDH1A1 expression of which six (66.6%) received a clinical score of three (strong

stain), two (22.2%) received a clinical score of two (moderate) and one (11.1%) received a clinical score of one (mild). Normal vestibular nerve and traumatic neuroma tissue (Merlin positive) also scored one. ALDH1A1 expression appeared to be homogenous throughout the tissue in all samples; it is not restricted to a sub-population of cells as is seen in other tumour types (Nwani et al., 2019). These data show ALDH1A1 is strongly upregulated in Merlin null schwannoma tissue with 8/9 tumours showing increased staining compared to both healthy and neuroma controls.

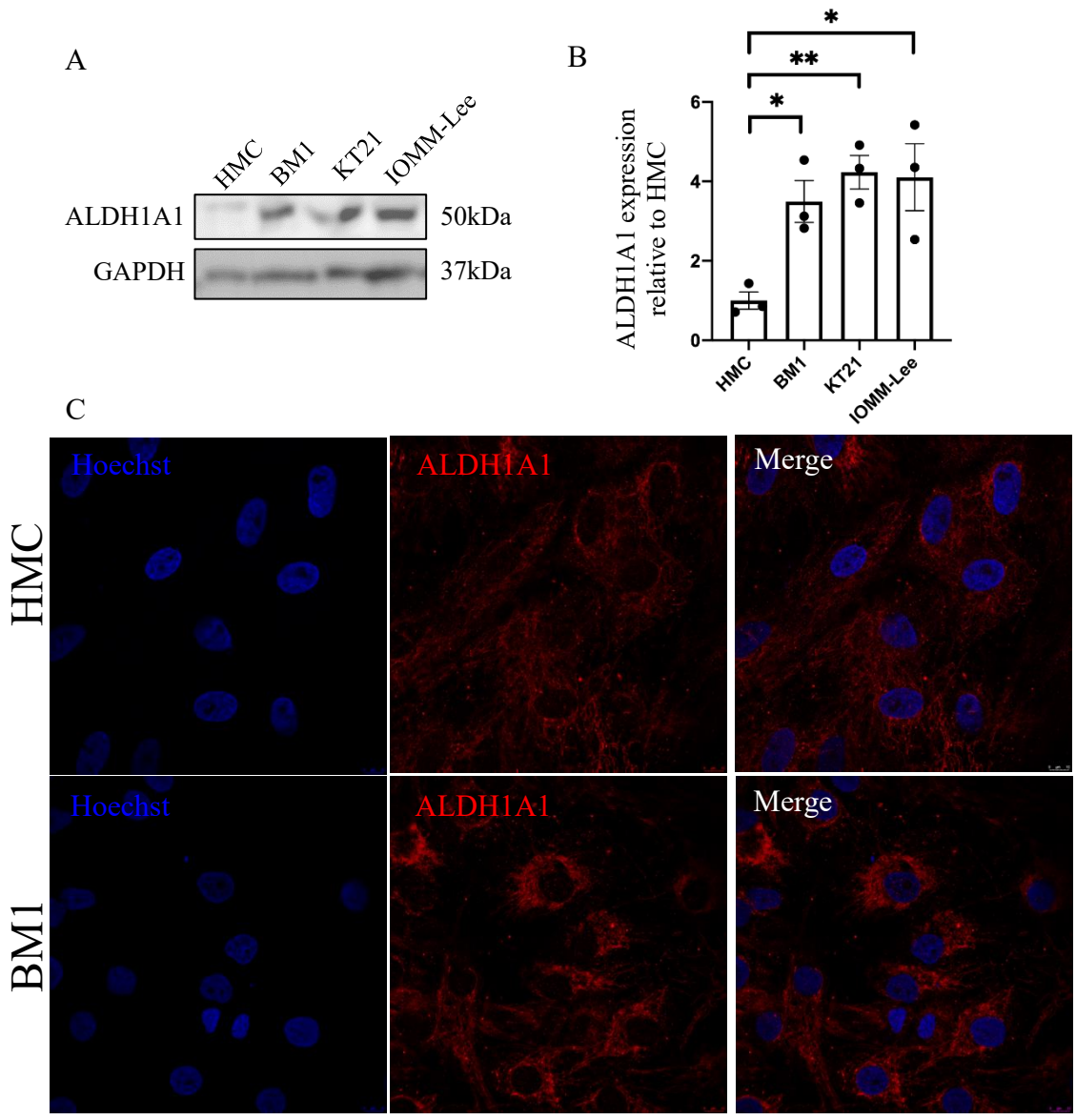

Figure 3.2.5: ALDH1A1 is upregulated in meningioma cell lines. (**A**) Representative image of n=3 western blots showing ALDH1A1 expression in human meningeal cells (HMC), BM1, KT21 and IOMM-Lee cells (lanes 1-4 respectively), GAPDH was the loading control. (**B**) Quantification of (A) showing ALDH1A1 expression in meningioma cell lines relative to HMC, one-way ANOVA with Bonferroni's correction, *P < 0.05, **P < 0.01. (**C**) Representative immunofluorescence (n=3) of ALDH1A1 protein expression (red) in HMC and BM1 cells, Hoechst (blue) counter-stained nuclei, scale bar = 5 μm.

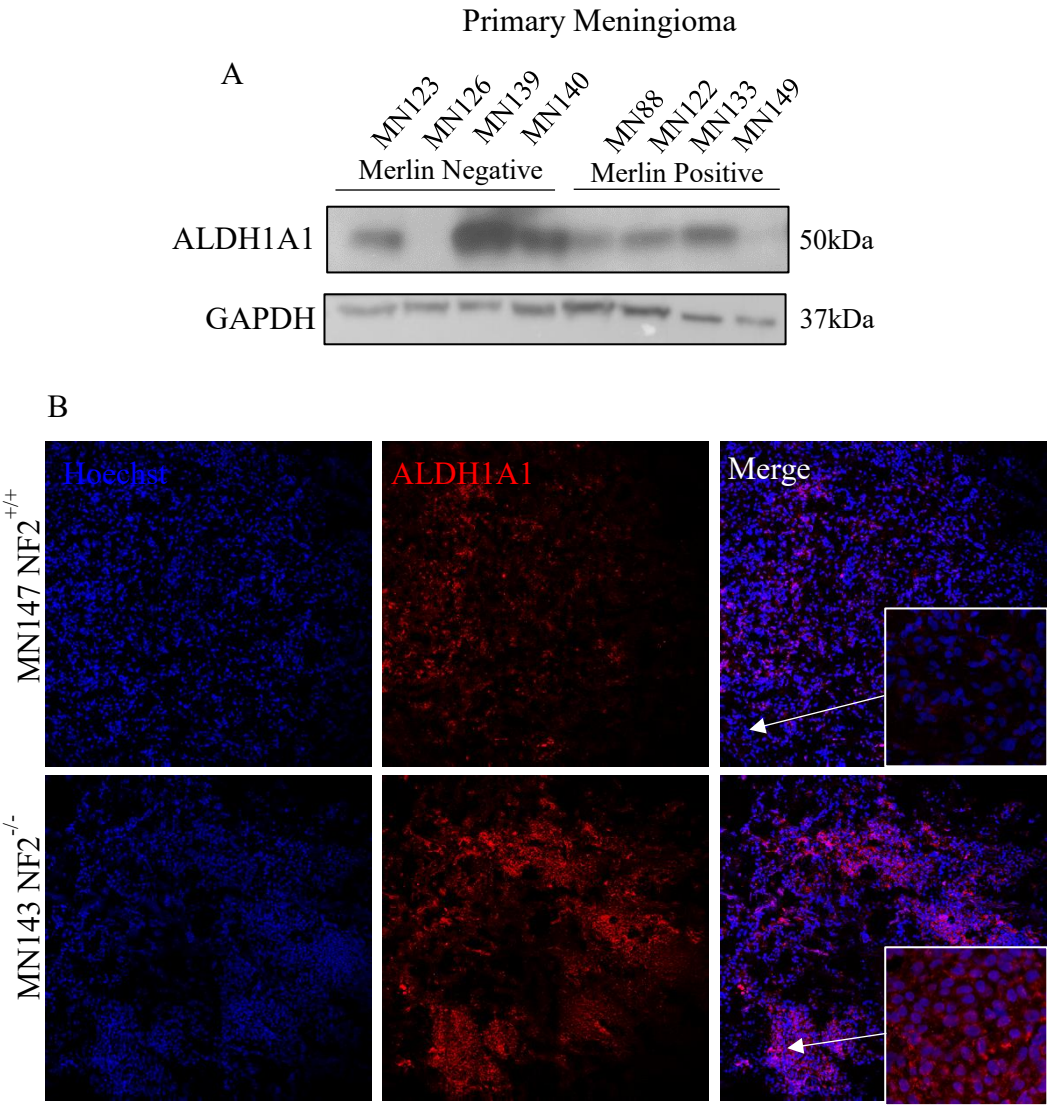

Figure 3.2.6: ALDH1A1 expression in primary meningioma cells and whole tumour tissue. (**A**) Western blot showing ALDH1A1 expression in Merlin negative and Merlin positive primary tumour cell lysates, GAPDH was used as loading control. (**B**) Representative immunofluorescence of (n=3) Merlin negative and Merlin positive meningioma (n=3), frozen tissue sections showing ALDH1A1 (red). Inset image is a zoom of the right panel. Hoechst (blue) counter-stained nuclei, scale bar = 50 µm.

Case number	Clinical Information	Histology	ALDH1A1	Follow-up (as per lab records)
28929/10	Left CP angle tumour	Schwannoma	2	No recurrence
32973/11	Acoustic neuroma, recent rapid growth	Cellular schwannoma	1	Rapid growth prior to surgery, no recurrence
7533/16	Multiple intradural spinal lesions	Schwannoma	3	Symptomatic lesion excised, no recurrence
24218/15	Thoracic intradural tumour	Schwannoma	2	No recurrence
30315/14	Left CP angle tumour, ? NF2	Schwannoma	3	Large size, re-excision in 2015
34687/14	Intradural L3 tumour	Cellular schwannoma	3	No recurrence
30454/13	Right CP angle tumour	Schwannoma	3	No recurrence
6584/09	Left acoustic neuroma. Bilaterallesions, L>R. NF2	Schwannoma	3	No recurrence
22375/06	NF2. Neuroma on left arm andaxilla	Schwannoma	3	No recurrence, Also has multiple meningiomas, schwannomas at other sites.

0= negative staining
1= mild, occasional cells staining
2= moderate staining
3= strong staining

Table 3.2.1: Clinical information and scores for paraffin-embedded schwannomas that were assessed for ALDH1A1 expression.

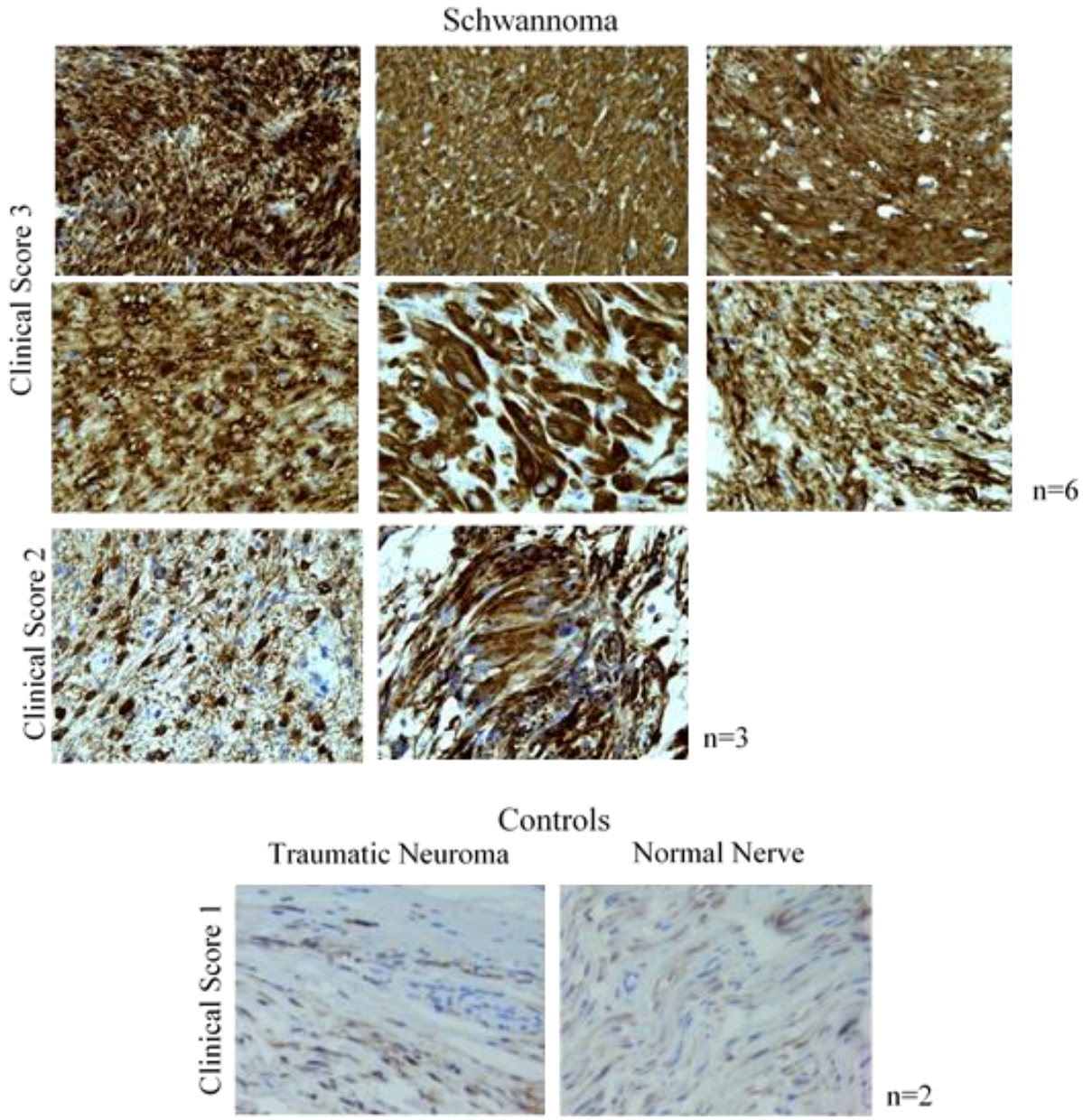

Figure 3.2.7: IHC of Merlin null schwannomas (n=9) stained for ALDH1A1. Schwannomas are grouped by their clinical score. Merlin positive normal nerve tissue and Merlin positive traumatic neuroma tissue were used as controls.

In summary, ALDH1A1 expression is upregulated in meningioma cell lines compared with HMCs however this was seen in both Merlin negative human cell lines (BM1 and KT21), as well as Merlin positive cell lines (IOMM-Lee). In primary meningioma, ALDH1A1 could be detected in cell lysates and in sections of frozen tissue however there was not a clear correlation between Merlin status and expression.

Following this, the importance of ALDH1A1 for the proliferation of meningioma and schwannoma cells was assessed. ALDH1A1 activity was modulated in three ways: Firstly, we used chemical inhibition using newly-derived compounds from a collaboration with the National Center for Advancing Translational Sciences (NCATS) group, MD, USA, led by Dr Adam Yasgar (Yang et al., 2018); Secondly we used lentiviral shRNA-mediated direct knockdown of ALDH1A1 and thirdly or knockdown of TAZ in cells. Based on our observations in the mouse model Figures 3.2.3 and 3.2.4.), we would predict that loss of TAZ would also reduce Aldh1a1 in tumour cells.

3.2.5 ALDH1A1 drives proliferation in Merlin Null meningioma and schwannoma cells in vitro.

Given that in mouse sciatic nerve the expression of ALDH1A1 TAZ-dependent, we next sought to assess whether the same was true in human meningioma and schwannoma cells. Lentiviral mediated shRNA knockdown of YAP and TAZ was performed to assess whether ALDH1A1 expression is dependent on either of the Hippo pathway co-transcriptional activators in human meningioma and schwannoma. ALDH1A1 knockdown was also performed using lentiviral mediated shRNA.

This was first performed in the BM1 cell line before moving on to primary meningioma cells which are more heterogeneous (Figure 3.2.8a). Sequences targeting YAP and TAZ (Table 2.9) were used alongside scramble controls to induce knockdown. Western blotting showed that knockdown of TAZ but not YAP reduced ALDH1A1 expression

compared to scramble controls (Figure 3.2.8). This result is consistent with that seen in mouse sciatic nerve, and suggests that TAZ drives increased ALDH1A1 expression in a Merlin null background in these tumour cells. Since YAP did not reduce ALDH1A1 expression in BM1 cells, only TAZ was knocked down in primary schwannomas to view any effects upon ALDH1A1 (Figure 3.2.8b). As expected, knockdown of TAZ reduced ALDH1A1 protein expression in primary schwannoma cells compared with scramble controls.

Initially, a set of six ALDH1A1 inhibitors from NCATS were screened in BM1 and HEI-193 cells, which are grade I Merlin null meningioma and schwannoma cell lines respectively. Cells were incubated with 10 μM of each inhibitor for 48h and assessed for CyclinD1 levels (Figure 3.2.9,b) and Ki67 (Figure 3.2.9c). Inhibitors 1-6 failed to reduce CyclinD1 expression in HEI-193 cells. Inhibitors one and two were the only compounds effective in reducing CyclinD1 in BM1 cells and these compounds also significantly reduced the number of Ki67 positive cells following 48h treatment.

Following this, inhibitors were titrated down in concentration to assess efficacy of the compounds. Using inhibitor one at concentrations ranging from 1 μM to 10 μM there was a significant reduction in Ki67 positive cells at 2 μM and maximum inhibition achieved at 5 μM (Figure 3.2.10a). Next these compounds were tested in Merlin null primary meningioma. ALDH1A1 significantly decreased Ki67 cells In Merlin null primary meningiomas after treatment with inhibitors 1 and 2 for 48h (Figure 3.2.10b).

It has previously been established that ALDH1A1 inhibition or knockdown can restore sensitivity to some chemotherapeutics (Januchowski et al., 2016, Sladek et al., 2002). This was tested in BM1 cells by combining ALDH1A1 inhibition with the chemotherapeutic agent Cisplatin Figure 3.2.11a). BM1 cells were incubated for 48h with either, vehicle, 10 μM inhibitor one, 25 μM Cisplatin or 10 μM inhibitor one and 25 μM

Cisplatin. The combination treatment had an additive effective compared to Cisplatin alone, resulting in a significant decrease in EdU positive cells. To resolve any off target effects of the ALDH1A1 inhibitors, BM1 cells transduced with shALDH1A1 or shTAZ lentivirus were compared with scramble controls for proliferation assessed by EdU incorporation (Figure 3.2.11b). BM1 cells transduced with shTAZ and shALDH1A1 constructs had significantly less EdU positive cells.

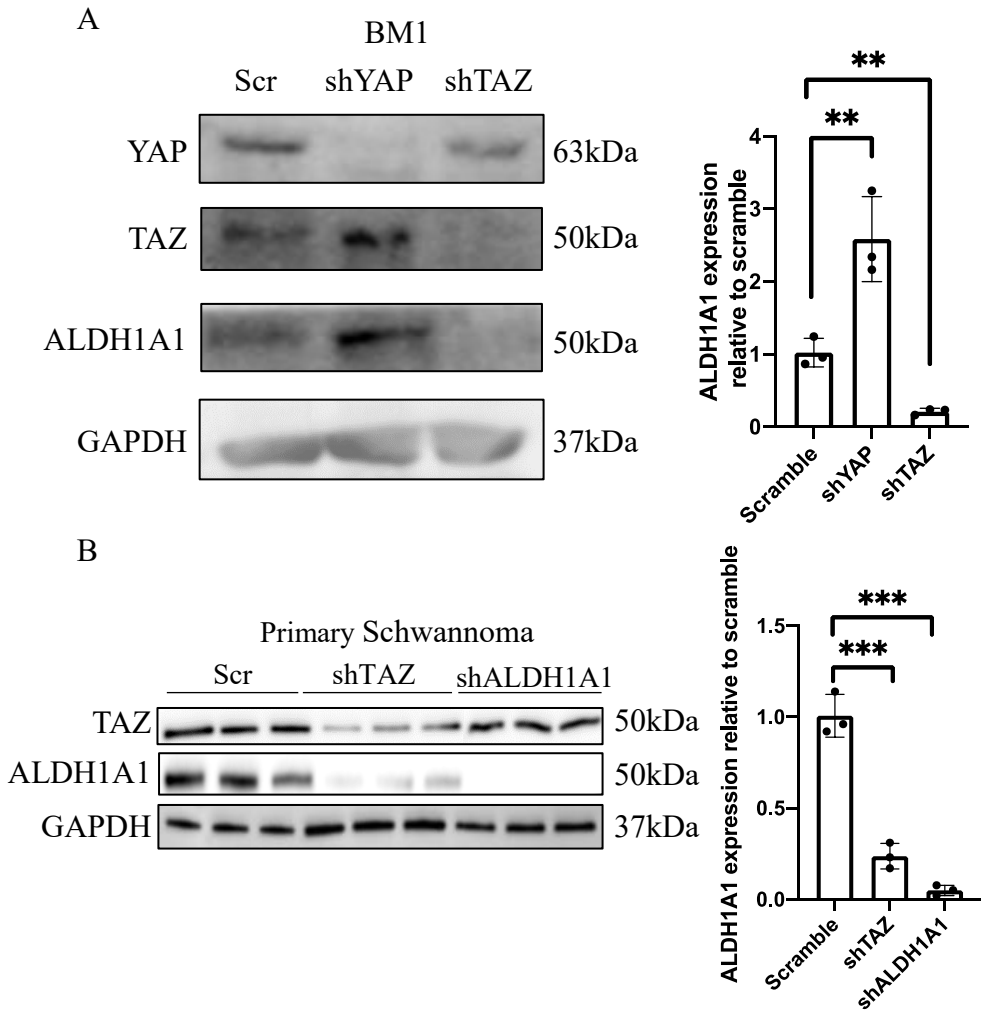

Figure 3.2.8: Knockdown of TAZ but not YAP reduces ALDH1A1 expression. Lentiviral-mediated short-hairpin knockdown of YAP, TAZ and ALDH1A1. (**A**) Representative western blot (n=3) and quantification of BM1 cells transduced with scramble control, shYAP and shTAZ constructs (left to right respectively), GAPDH was the loading control. (**B**) Western blot and quantification of primary schwannoma cells transduced with scramble, shTAZ and shALDH1A1 lentiviral constructs (left to right respectively). GAPDH was used as a loading control. One-way ANOVA with Bonferroni's correction, ** P<0.01, ***P<0.001.

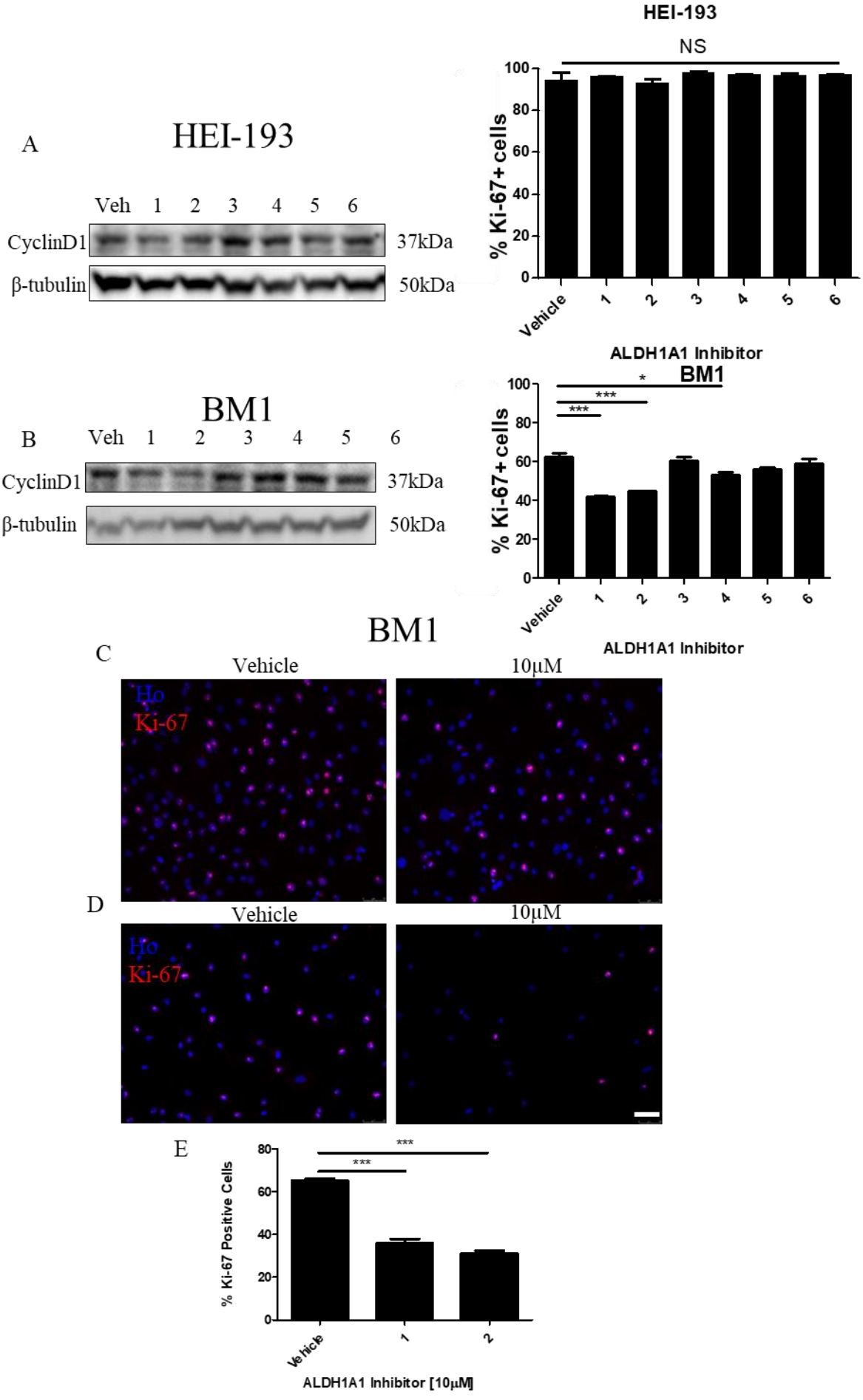
A
HEI-193
Veh 1 2 3 4 5 6
CyclinD1
37kDa
β-tubulin
50kDa
HEI-193
NS
% Ki-67+ cells
Vehicle 1 2 3 4 5 6
ALDH1A1 Inhibitor
B
BM1
Veh 1 2 3 4 5 6
CyclinD1
37kDa
β-tubulin
50kDa
BM1
*
***
***
% Ki-67+ cells
Vehicle 1 2 3 4 5 6
ALDH1A1 Inhibitor
C
BM1
Vehicle
10μM
Ho
Ki-67
D
Vehicle
10μM
Ho
Ki-67
E
***
***
% Ki-67 Positive Cells
Vehicle 1 2
ALDH1A1 Inhibitor [10μM]

Figure 3.2.9: Chemical inhibition of ALDH1A1 enzymatic activity in meningioma and schwannoma cell lines for 48h at 10 μM influences CyclinD1 expression and proliferation. (**A**) Representative (n=3) western blot (left) and quantification (right) for CyclinD1 in HEI-193 human schwannoma cells, β-tubulin was used as loading control, NS = non-significant. (**B**) Representative (n=3) western blot (left) and quantification (right) for CyclinD1 in BM1 cells, β-tubulin was the loading control, $P<0.05$ = *, $P<0.001$ = ***. (**C, D**) Representative immunofluorescence of Ki67 (red) in BM1 cells with incubated with either vehicle or 10 μM of inhibitor 1 (C) or 2 (D). Hoechst (blue) counter-stained nuclei. (**E**) Quantification of C and D, data plotted as mean +/- SEM (n=3), one-way ANOVA with Bonferroni's correction, $P<0.001$ = ***.

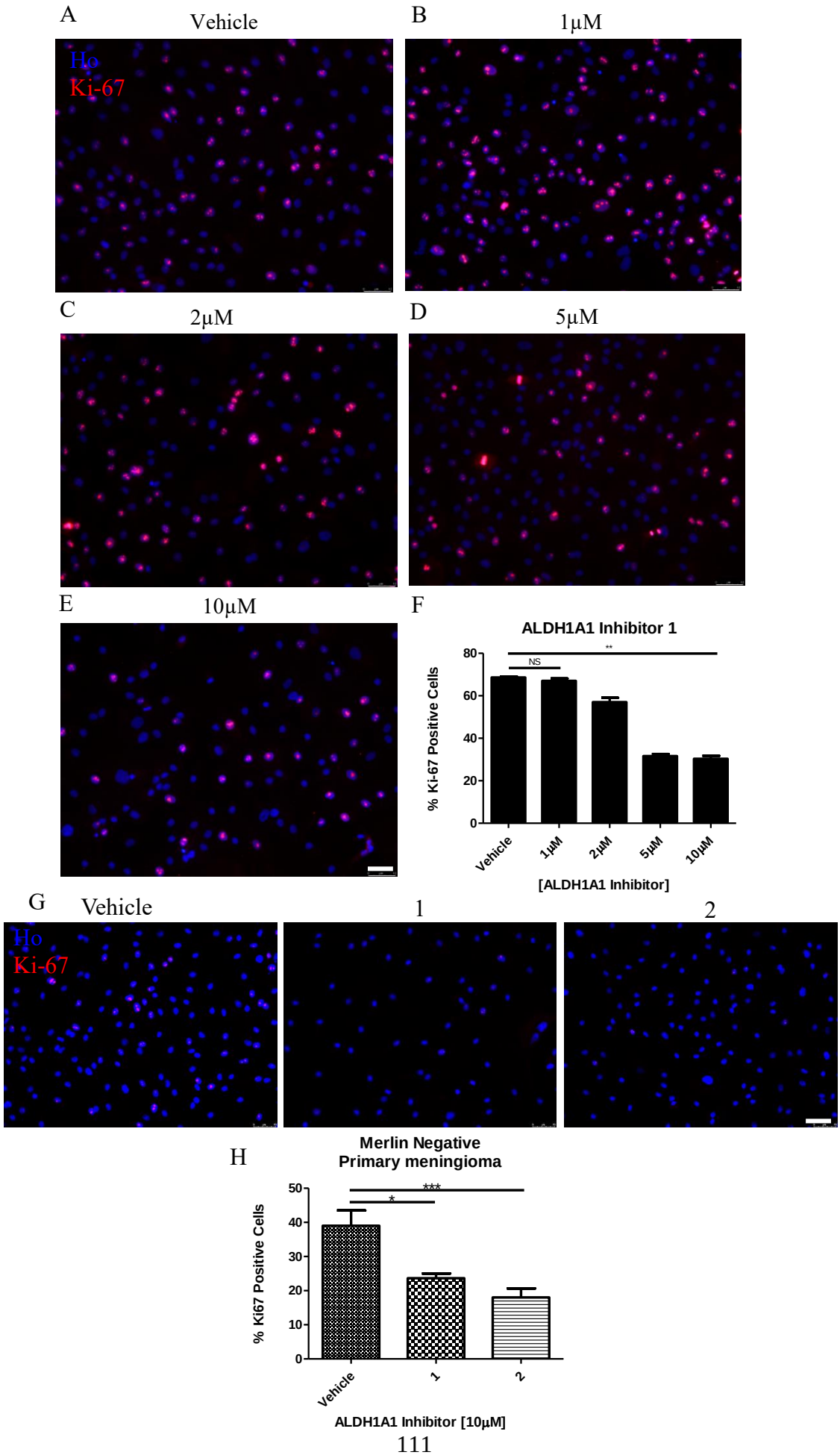
A
Vehicle
Ho
Ki-67
B
1μM
C
2μM
D
5μM
E
10μM
F
ALDH1A1 Inhibitor 1
% Ki-67 Positive Cells
NS
**
80
60
40
20
0
Vehicle
1μM
2μM
5μM
10μM
[ALDH1A1 Inhibitor]
G
Vehicle
1
2
Ho
Ki-67
H
Merlin Negative
Primary meningioma
% Ki67 Positive Cells
***
*
50
40
30
20
10
0
Vehicle
1
2
ALDH1A1 Inhibitor [10μM]

Figure 3.2.10: Chemical inhibition of ALDH1A1 activity in BM1 cells and primary meningioma cells significantly reduces proliferation. (**A-E**) Representative immunofluorescence images of Ki67 (red) treated with ALDH1A1 inhibitor 1 in BM1 cells, Hoechst (blue) counter-stained nuclei. (**F**) Quantification of % Ki-67 positive cells in (A-E), data plotted as mean +/- SEM (n=3), one-way ANOVA with Bonferroni's correction, NS = non-significant, P<0.01 = **. (**G**) Representative immunofluorescence images of Ki67 (red) treated with 10 μM of ALDH1A1 inhibitor 1 or 2. (**H**) Quantification of % Ki-67 positive cells in primary meningioma following incubation for 48h with either 10 μM of inhibitor 1 or 2. Hoechst (blue) counter-stained nuclei. Data plotted as mean +/- SEM (n=3), one-way ANOVA with Bonferroni's correction, P<0.05 = *, P<0.001 = ***. Scale bars = 10 μm.

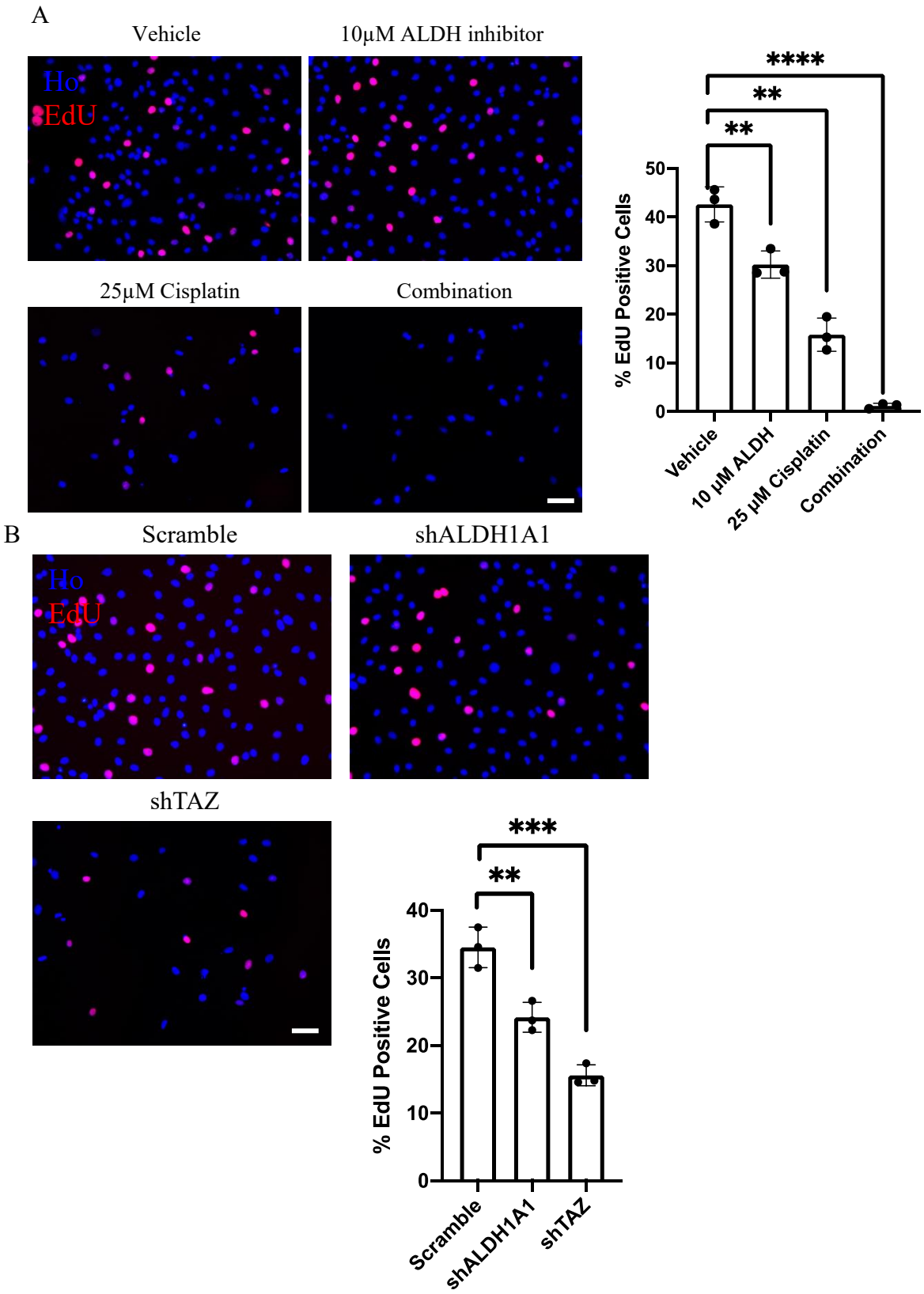
A
Vehicle
10μM ALDH inhibitor
Ho
EdU
25μM Cisplatin
Combination
% EdU Positive Cells
Vehicle
10 μM ALDH
25 μM Cisplatin
Combination
B
Scramble
shALDH1A1
shTAZ
% EdU Positive Cells
Scramble
shALDH1A1
shTAZ

Figure 3.2.11: ALDH1A1 inhibitors increase Cisplatin sensitivity in BM1 cells (**A**) Representative immunofluorescence images (left) of EdU positive cells (red) and quantification (right) of BM1 cells incubated for 48 h with ALDH1A1 inhibitor one, Cisplatin, or combined. Hoechst (blue) counter-stained nuclei. Data plotted as mean +/- SEM (n=3), one-way ANOVA with Bonferroni's correction, $P<0.05$ = *. (**B**) Representative immunofluorescence images (left) of EdU positive cells (red) and quantification (right) of EdU-positive BM1 cells transduced with Scramble, shALDH1A1 or shTAZ lentiviral constructs. Hoechst (blue) counter-stained nuclei. Data plotted as mean +/- SEM (n=3), one-way ANOVA with Bonferroni's correction, $P<0.05$ = *$P<0.01$ = **.

The effect of ALDH1A1 inhibition on proliferation was also assessed in primary schwannoma (n=3). Incubation with concentrations of inhibitor one ranging from 2 μM to 10 μM for 48h resulted in a significant dose-dependent reduction in Ki67 positive cells (Figure 3.2.13). Taken together, the results summarised here show that meningioma and schwannomas express ALDH1A1. Chemical inhibition or lentiviral knockdown of ALDH1A1 protein levels reduces proliferation in BM1 cells and Merlin null primary meningioma. ALDH1A1 inhibition was also shown to have an additive effect when combined with the chemotherapeutic agent Cisplatin in BM1 cells. The following discussion will contextualise these results.

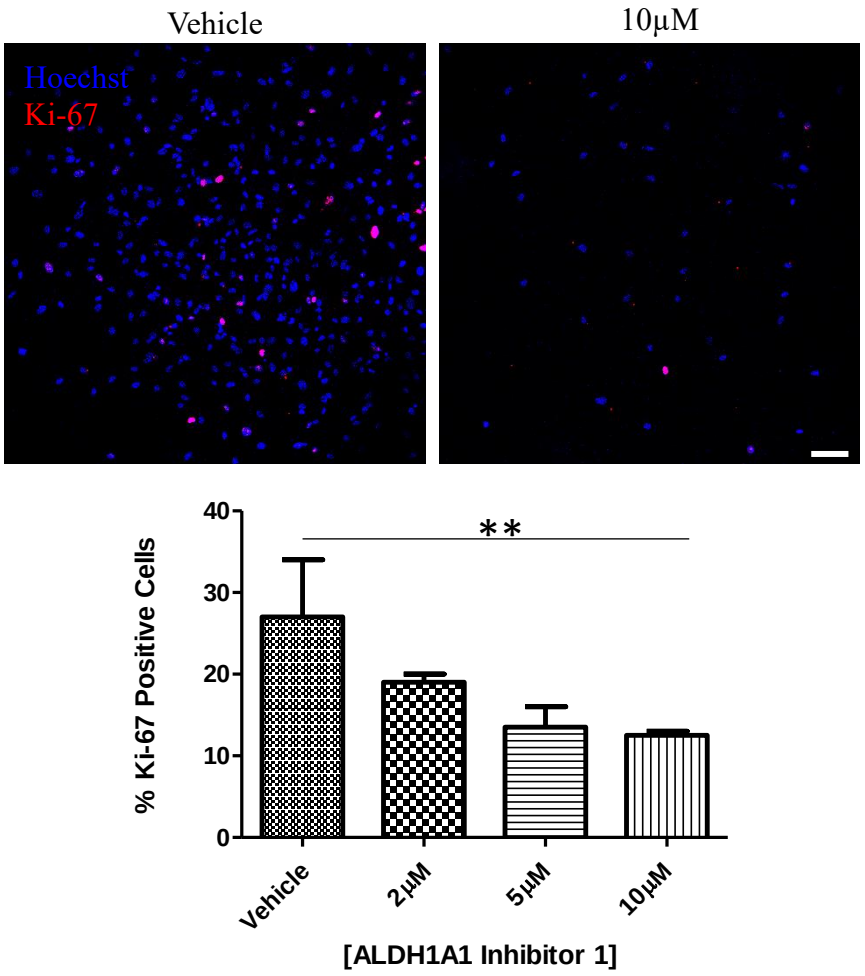

Figure 3.2.12 Representative immunofluorescence (n=3) and quantification of Ki67 (red) in primary schwannoma following ALDH1A1 inhibition. Hoechst (blue) counter-stained nuclei. Data plotted as mean +/- SEM (n=3), one-way ANOVA with Bonferroni's correction, $P<0.01$ = **, scale bar = 5 μm.

3.2.6 Discussion

ALDH1A1 has been identified as a cancer stem cell marker in multiple different tumour types including bladder, ovarian, lung and colon cancers (Namekawa et al., 2019, Nwani et al., 2019, Yu et al., 2017, Januchowski et al., 2016, Li et al., 2014b). One recent study, published in 2019, has used FFPE schwannoma tissue and identified that ALDH1 staining could be used as a prognostic marker for schwannoma, however this study did not use any subtype specific antibody nor did they confirm that these schwannomas were Merlin positive or negative (Liesche et al., 2019b). This study also used meningioma and spindle-cell tumours for control tissue whereas normal nerve tissue would be a better control. In our study, ALDH1A1 is significantly upregulated in two different NF2-deficient Schwann cell mouse models of tumour formation. When this was translated to human schwannoma, ALDH1A1 was highly upregulated by immunohistochemistry of Merlin null schwannoma tissue compared to both Merlin positive normal nerve and traumatic neuroma. However, in terms of meningioma, western blotting and immunofluorescence did not establish a clear correlation between loss of Merlin and an increase in ALDH1A1 expression, however ALDH1A1 inhibitors were still efficacious at reducing proliferation in primary Merlin null meningioma cells (Figure 3.2.10g).

Upregulation of ALDH1A1 was seen before sciatic nerve injury and was still seen at 7 and 21 dpi. In intact sciatic nerve in both the P0 and Postn-Cre mice, upregulation appears to be exclusive to non-myelinating Schwann cells, this is interesting as there is evidence that the cell of origin for malignant peripheral nerve sheath tumours seen in neurofibromatosis type I patients originate from non-myelinating Schwann cells (Joseph et al., 2008). As far as we are aware there is no way to lineage-trace non-myelinating Schwann cells after injury to measure if the proliferation seen in P0-CreNF2$^{fl/fl}$ mice is exclusively that of non-myelinating Schwann cells. Additionally, any non-myelinating Schwann cell markers such as L1 would be downregulated following injury. In

Postn.CreNF2$^{fl/fl}$ mice, ALDH1A1 is also upregulated within the non-myelinating Schwann cells of the sciatic nerves and DRGs compared to Cre^{-} littermate controls at early and late timepoints in tumour development (three and five months). It would be of interest to cross Postn.CreNF2$^{fl/fl}$ mice with an ALDH1A1$^{fl/fl}$ mice with our schwannoma mouse model. Currently, the ALDH1A1$^{fl/fl}$ mouse has not been developed however a global ALDH1A1 knockout mice exists and is viable. ALDH1A1 knockout mice were gratefully received from Dr Joseph Napoli (Berkeley, California) and have been crossed with our NF2-deficient mice to elucidate the role of ALDH1A1 upregulation in this schwannoma mouse model. ALDH1A1 knockout mice show increased energy dispensation (they are a lot more active in the cage compared to ALDH1A1$^{+/+}$ or ALDH1A1$^{+/-}$ littermates) and no other phenotype, our preliminary data (not shown) suggests that their peripheral nervous system develops and functions normally.

Our group has previously identified that the phenotype seen in NF2-deficient Schwann cells following sciatic nerve injury can be successfully rescued by loss of the Hippo pathway effectors YAP or TAZ (Mindos et al., 2017b). The Hippo effector TAZ was found to be required for ALDH1A1 expression in both P0 and Postn NF2-deficient mice, this concurs with the study in lung cancer which showed that TAZ interacts with the ALDH1A1 promoter to drive TAZ expression (Yu et al., 2017). We did not see a change in ALDH1A1 expression in NF2-deficient Schwann cells following knockout of YAP, although this has been seen in bladder cancer (Zhao et al., 2018).

ALDH1A1 was identified to be upregulated in Merlin negative meningioma cell lines and primary cells when compared to HMC controls and Merlin positive meningiomas. No studies have implicated ALDH1A1 as important for meningiomas however we have shown that inhibition of ALDH1A1 significantly decreases the proliferation of both the Merlin negative meningioma cell line BM1 and, more importantly, also human primary

meningioma tumour cells in vitro . The BM1 cell line, in line with our NF2-deficient mouse models, also requires TAZ for expression of ALDH1A1.

In human Merlin negative schwannoma, ALDH1A1 was strongly expressed compared to Merlin positive normal nerve and traumatic neuroma controls. Primary schwannoma cells also require TAZ for expression of ALDH1A1. These findings concur with previously published Affymetrix data in schwannoma and also other studies assessing ALDH1 expression in FFPE schwannoma tissue (Liesche et al., 2019b, Torres-Martin et al., 2013), but this study is the first to link the Hippo pathway co-transcriptional activator to ALDH1A1 expression on a Merlin-null background.

Given our evidence of the importance of Aldh1a1 in driving tumour growth, we then targeted ALDH1A1 activity in tumour cells to measure effects upon cell proliferation and phenotype. ALDH1A1 competitive inhibitors from NCATS and lentiviral-mediated knockdown of ALDH1A1 was used to assess the efficacy of inhibition in meningioma cell lines and primary cells, as well as primary schwannoma. In all these settings, ALDH1A1 inhibition or knockdown significantly reduced proliferation. These data show promise and following development of the PostnCre.NF2$^{fl/fl}$ALDH1A1^{ko} mice, could be moved into in vivo use in both schwannoma and meningioma mouse models. The mechanism by which ALDH1A1 supports cancer stem cells varies by cell type but recent reports have begun to elucidate some of the roles of ALDH1A1 in tumours. Firstly, ALDH1A1 acts through modulating levels of retinoic acid signalling which results in recruitment of RARE elements an can lead to modulation of protein expression (Namekawa et al., 2019). Another mechanism of action for ALDH1A1 is through detoxification of reactive oxygen species or chemotherapeutics (Liu et al., 2019, Wei et al., 2017). In line with the study in Cisplatin-resistant lung cancer, our data shows that ALDH1A1 inhibition increases sensitivity to Cisplatin in BM1 cells. More experiments

need to be conducted to determine the role of ALDH1A1 in NF2-deficient meningioma and schwannoma.

Interestingly, another top upregulated candidate in the RNAseq analysis in Chapter 3.1 was CRABP1, a protein which shuttles retinoic acid from the cytoplasm into the nucleus. This adds weight to the hypothesis that ALDH1A1 upregulation is increasing the bioavailability of nuclear retinoic acid in NF2-deficient Schwann cells and that this leads to increased retinoic acid signalling through nuclear receptors. Future studies in this area should seek to identify the mechanism by which ALDH1A1 is driving proliferation in Merlin negative meningioma and schwannoma and also determine the phenotype in the Postn.Cre schwannoma mouse model following ALDH1A1 knockout. Figure 3.2.14 outlines a summary of the NF2-TAZ dependent upregulation of ALDH1A1 upregulation seen in Merlin-deficient schwannoma and meningioma.

In summary, this chapter identifies that the cancer stem cell marker ALDH1A1 is upregulated in NF2-deficient meningioma and schwannoma. The Hippo pathway effector TAZ is required for upregulation of ALDH1A1 and ALDH1A1 inhibition or knockdown reduces proliferation in meningioma and schwannoma primary cell lines. Further work on this cancer stem cell marker may yield new therapeutic opportunities.

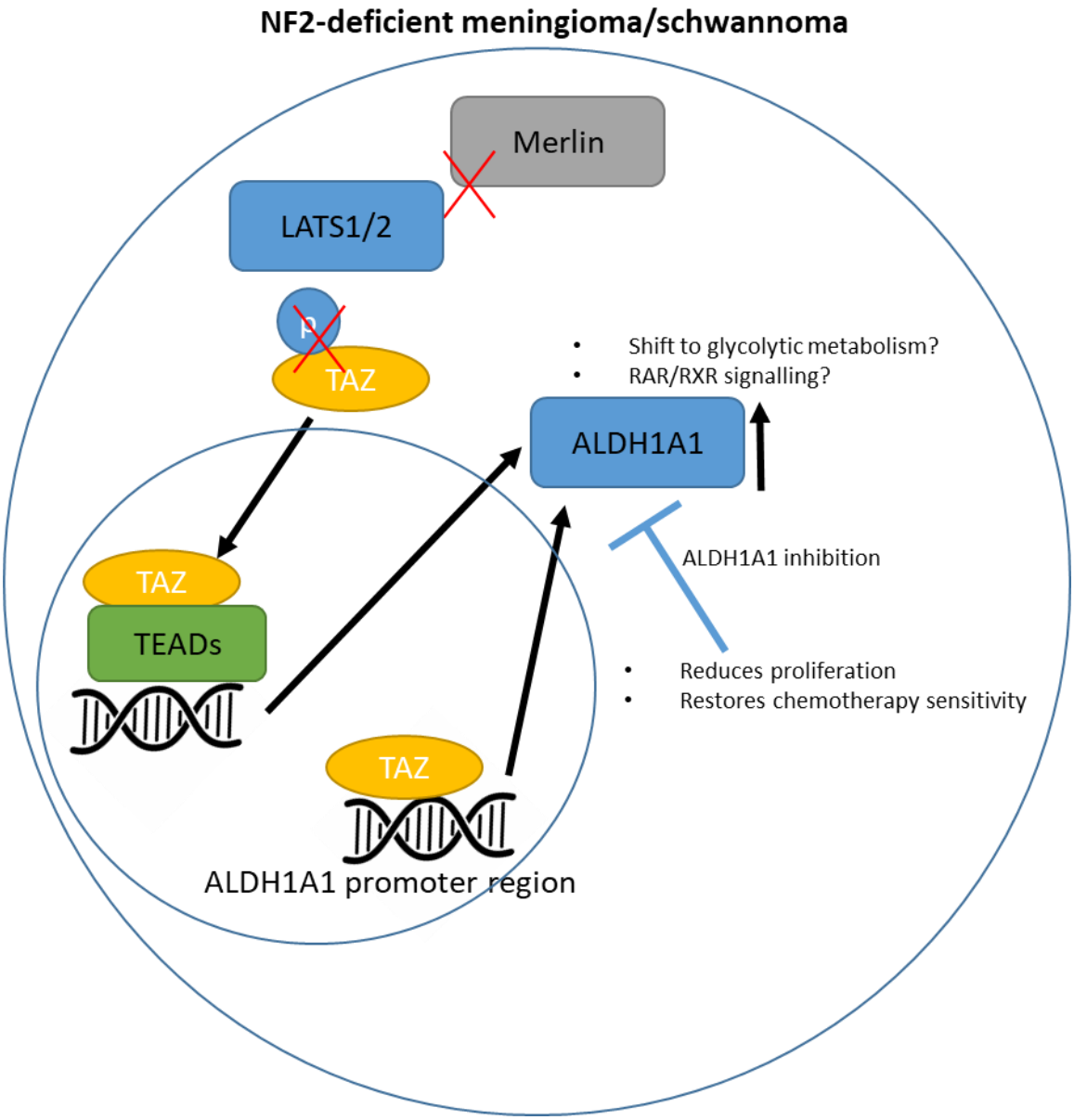

Figure 3.2.14: Aldehyde dehydrogenase 1A1 (ALDH1A1) is upregulated in NF2-deficient schwannoma and meningioma through a Transcriptional coactivator with PDZ-binding motif (TAZ)-dependent mechanism. We propose that nuclear accumulation of TAZ due to lack of phosphorylation by large tumour suppressor kinase 1/2 (LATS1/2) drives expression of ALDH1A1 through either activation of the TEAD transcription factors or a direct interaction with the ALDH1A1 promoter region. ALDH1A1/TAZ knockdown or ALDH1A1 inhibition reduces proliferation in primary human meningioma and schwannoma cells and restores sensitivity to the chemotherapeutic cisplatin.

3.3 Hippo Pathway regulation in meningioma and schwannoma and the use of novel inhibitors to target YAP/TEAD activity.

3.3.1 Introduction

Loss of Merlin occurs in 50-60% of sporadic meningiomas and in more than 70% of sporadic schwannomas (Yuzawa et al., 2016, Havik et al., 2018). Previous data in meningioma and schwannoma cells have shown that loss of Merlin dysregulates Hippo signalling, resulting in increased nuclear YAP and TAZ localisation (Striedinger et al., 2008, Li et al., 2010). The first aim of this thesis was to identify and characterise the differences in the Hippo pathway signalling displayed by Merlin positive and Merlin negative tumours. To examine this, the expression of Hippo pathway components in primary meningioma needed to be assessed first to determine if there is differential expression and/or activation of YAP, TAZ or upstream pathway components. Following this, we next asked whether Merlin negative tumours require Hippo signalling to be tumourigenic, in terms of proliferation, survival or other tumour phenotypes. To approach these aims we first used lentiviral-mediated knockdown and chemical inhibition of YAP and TAZ activity. Primary meningiomas stratified by Merlin status are hugely diverse in their genetics and epigenetics. There are various mutational hotspots that either co-occur with loss of Merlin but are also present in Merlin positive meningioma tumours, either alone or in combination with other mutations. These include proteins such as TRAF7, KLF4 or AKT1 (Suppiah et al., 2019, Yuzawa et al., 2016). Although in this project the only selection criteria for primary cells was Merlin status, other factors were kept record of in order to make subsequent correlations if necessary. These include clinical factors such as age gender and tumour location. Merlin negative and positive tumours can vary by mutations of well-characterised proteins such as TRAF7, AKT1, SMO or SMARCB1. Typically, Merlin negative tumours do not feature homozygous mutations in these

proteins, however following sequencing of tumour DNA by Dr Claire Adams in the Hanemann group in Plymouth, some were found to be heterozygous for certain screened proteins such as TRAF7.

Data in this chapter will show an analysis of the expression of Hippo pathway components in Merlin null tumours compared to both controls and Merlin positive meningioma tumours. It will also assess the correlation between nuclear localisation of YAP and TAZ with respect to proliferation in these tumours. The work in this chapter will also assess the effect of chemical inhibition of the YAP and TAZ interaction with TEAD family members and knockdown of YAP and TAZ in these tumours. We hypothesise that inhibition of YAP/TAZ driven transcription will lead to a decrease in proliferation in Merlin null meningioma and schwannoma.

3.3.2 Expression of Hippo Pathway Proteins in Meningioma Cell Lines and Primary Meningioma cells

As an initial investigation of Hippo signalling in meningioma cells, the effects of Merlin status on Hippo pathway protein level and activation was examined by western blot (Figure 3.3.1). The Hippo pathway centres around a core kinase cascade in which LATS1/2 phosphorylate YAP and TAZ to sequester them in the cytoplasm. When the pathway is active, YAP and TAZ do not activate transcription factors such as TEAD family members (Figure 1.2). HMC and BM1 cells were used, which are human meningeal control cells and a grade 1 Merlin negative immortalised cell line respectively. HMC cells, BM1 cells as well as three Merlin positive and three Merlin negative primary meningioma cell lysates were western blotted for: LATS1; LATS2; YAP; phosphorylated YAP (p-YAP); and TAZ. In schwannomas, Merlin has been shown to inhibit the degradation of LATS1/2 (Li et al., 2010), leading to stabilisation and activation of YAP and TAZ, however there was no apparent differential expression of LATS1 or LATS2 proteins in Merlin negative compared to Merlin positive primary meningioma cells.

LATS1 protein levels were downregulated in BM1 cells compared to HMC cells but LATS2 levels were unchanged. HMC cells have limited use as a control cell as they were derived from foetal tissue and therefore do not represent meningeal cells that have been fully developed in an adult human, that being said, HMC cells were also the best available source of non-tumourous meningeal cells that can be cultured. This data suggests Merlin does not modulate LATS1/2 protein expression levels in primary meningioma. Similarly, there was no change in levels of YAP, p-YAP or TAZ when comparing Merlin negative and Merlin positive tumour cell lysates. This suggests that loss of Merlin does not modulate the overall expression of YAP or TAZ. Loss of Merlin also does not affect the expression of LATS1 or LATS2 proteins in primary meningioma cells in vitro (Figure 3.3.1). Due to this, an important next step in this thesis was deducing whether Hippo signalling is more active in Merlin negative primary meningioma.

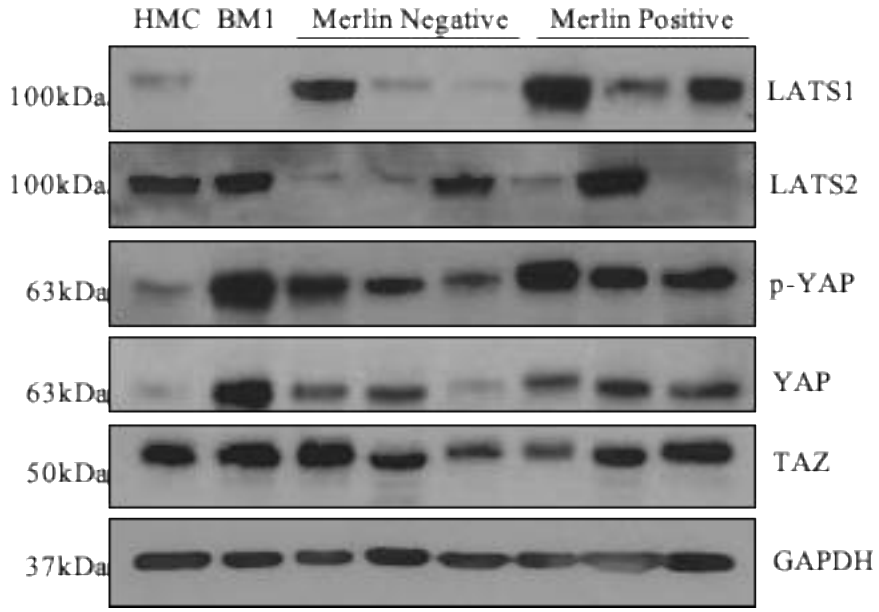

Figure 3.3.1: Merlin status does not regulate expression of Hippo pathway components in cultured primary meningioma cells. Western blot showing expression of Hippo pathway components in HMC cells, BM1 cells (n=3 technical repeats) and three Merlin negative/positive primary meningioma cell lysates (n=3 biological repeats). GAPDH was the loading control. In line with previous reports, protein expression in meningiomas is highly heterogeneous.

3.3.3 The YAP-TEAD Inhibitor Verteporfin Reduces Proliferation in Primary Meningioma Cells

Verteporfin (VP) is a porphyrin derivative compound used in photodynamic eye therapy that has seen recent repurposing as a potent inhibitor of the YAP-TEAD interaction (Felley-Bosco and Stahel, 2014). VP's role as a YAP-TEAD inhibitor is independent from its established role as a photosensitiser, where it is combined with infrared laser light to treat vascular issues in the retina (Felley-Bosco and Stahel, 2014), indeed it has been shown that VP elicits its effect on the YAP-TEAD interaction in the absence of light (Feng et al., 2016). At the start of the work in this thesis, VP was the only well characterised commercially available inhibitor of the Hippo pathway downstream effectors YAP and TAZ. VP was used to determine how critical YAP and TAZ are for driving proliferation in primary meningioma. Five Merlin negative and five Merlin positive primary meningioma cell cultures were treated with either: vehicle, 1 μM or 2μM VP for 48 h. The tumour cells were then assessed for proliferation by Ki-67 staining (Figure 3.3.2a). In Merlin negative tumours, average proliferation in the vehicle treated cells was 68% ± 6% whereas in Merlin positive tumours it was 36% ± 4% (Figure 3.3.2b). Merlin positive tumours were not only less proliferative than Merlin negative tumours but they were also less affected by VP treatment. VP only significantly ($p < 0.001$) reduced proliferation in Merlin positive tumours at the 2 μM concentration, whereas in Merlin negative tumours, 1 μM VP significantly ($p < 0.01$) reduced proliferation and the reduction of proliferation was much more marked (Figure 3.3.2b).

Given that YAP and TAZ are not significantly differentially expressed in primary meningioma in our experiments, the nuclear localisation of YAP and TAZ were investigated to see if this could reveal both differences in Hippo signalling and the differential effects of VP on Merlin negative and Merlin positive tumours. A study

looking at endometrial cancer demonstrated that VP influenced the subcellular localisation of YAP and TAZ (Wang et al., 2016).

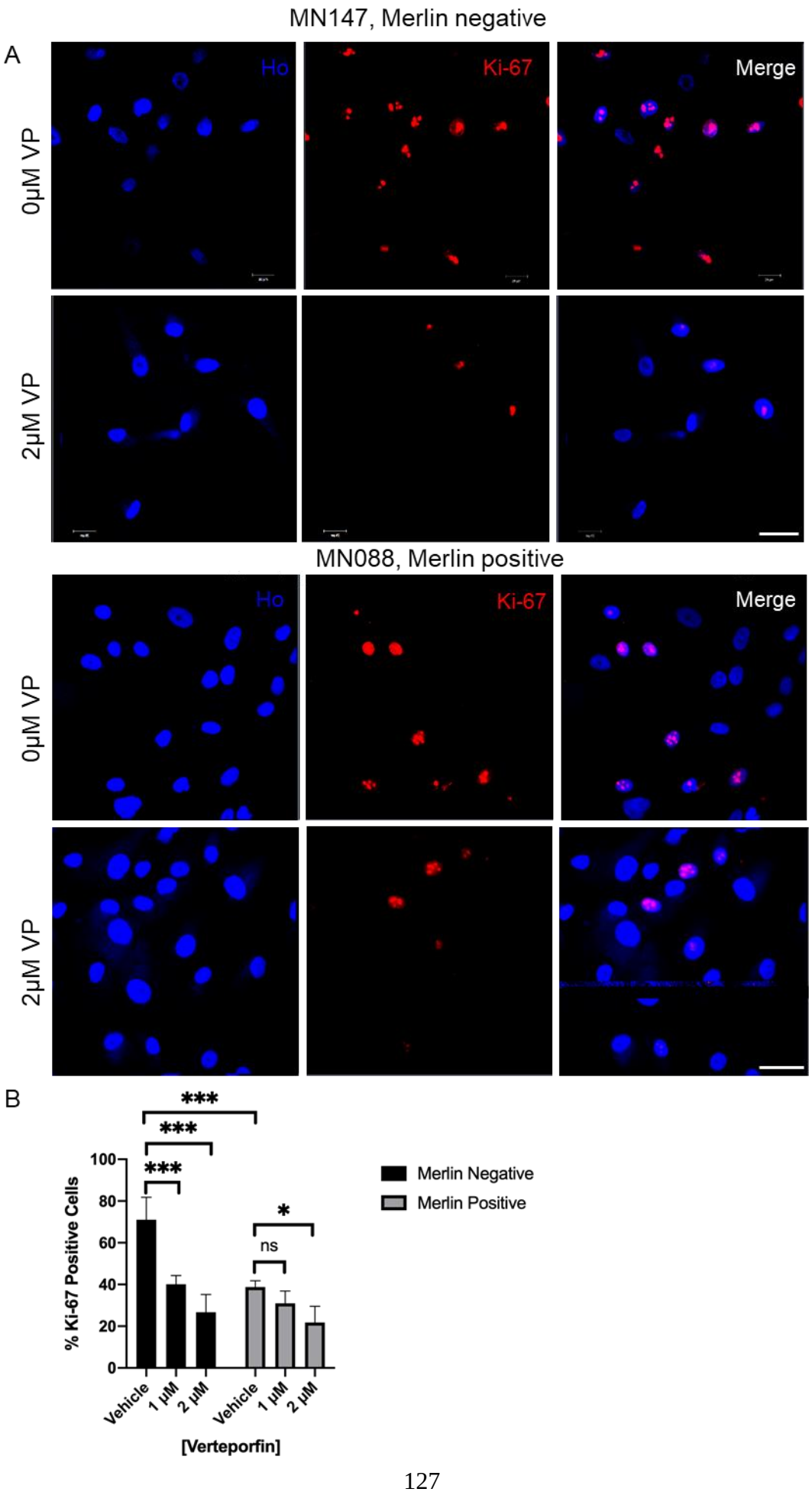
MN147, Merlin negative
A
Ho
Ki-67
Merge
0μM VP
2μM VP
MN088, Merlin positive
Ho
Ki-67
Merge
0μM VP
2μM VP
B
***
***
***
*
ns
100
80
60
40
20
0
% Ki-67 Positive Cells
Vehicle
1 μM
2 μM
Vehicle
1 μM
2 μM
[Verteporfin]
Merlin Negative
Merlin Positive

Figure 3.3.2: Verteporfin reduces proliferation in Merlin negative and Merlin positive primary meningioma cells. (A) Representative immunofluorescence of (n=5) Merlin negative (top panel) and Merlin positive (bottom panel) cultured primary meningioma. Ki-67 positive staining (red) in the nucleus shows proliferating cells, nuclei were counter-stained with Hoechst, scale bar = 10 µm. (B) Quantification of Ki-67 positive nuclei in (A), n = 5, two-way ANOVA with Bonferroni's correction, *P<0.05, ***P<0.001 NS = non-significant.

3.3.4 Loss of Merlin Causes Translocation of YAP into the Nucleus in Meningioma

We then next investigated whether loss of Merlin resulted in increased nuclear localisation of YAP. Increased nuclear YAP was seen in human Merlin-depleted arachnoidal cells and a Merlin negative meningioma cell line by *Striedinger et al,* but has not been investigated in primary cells. Nuclear localisation of YAP was assessed in Merlin negative and Merlin positive primary meningioma (n=3 biological repeats) by immunofluorescence (Figure 3.3.3a) and quantified (Figure 3.3.3b). Quantification was completed by subtracting the fluorescence intensity of YAP antibody signal from the total fluorescence intensity per cell. As expected, there was significantly higher nuclear localisation of YAP in the Merlin negative meningiomas. Average nuclear YAP in Merlin negative tumours was 72% compared to 34% in Merlin positive tumours. The nuclear localisation of YAP was also assessed following 2 μM VP inhibition as previous reports have suggested that VP upregulates 14-3-3 proteins resulting in increased cytoplasmic sequestration of YAP (Wang et al., 2016). In both Merlin negative and Merlin positive primary meningioma there was no significant difference in YAP localisation following VP treatment (Figure 3.1.3b), suggesting that in these tumours, VP is acting through inhibition of the YAP-TEAD interaction in the nucleus of meningioma cells and not by altering YAP localisation.

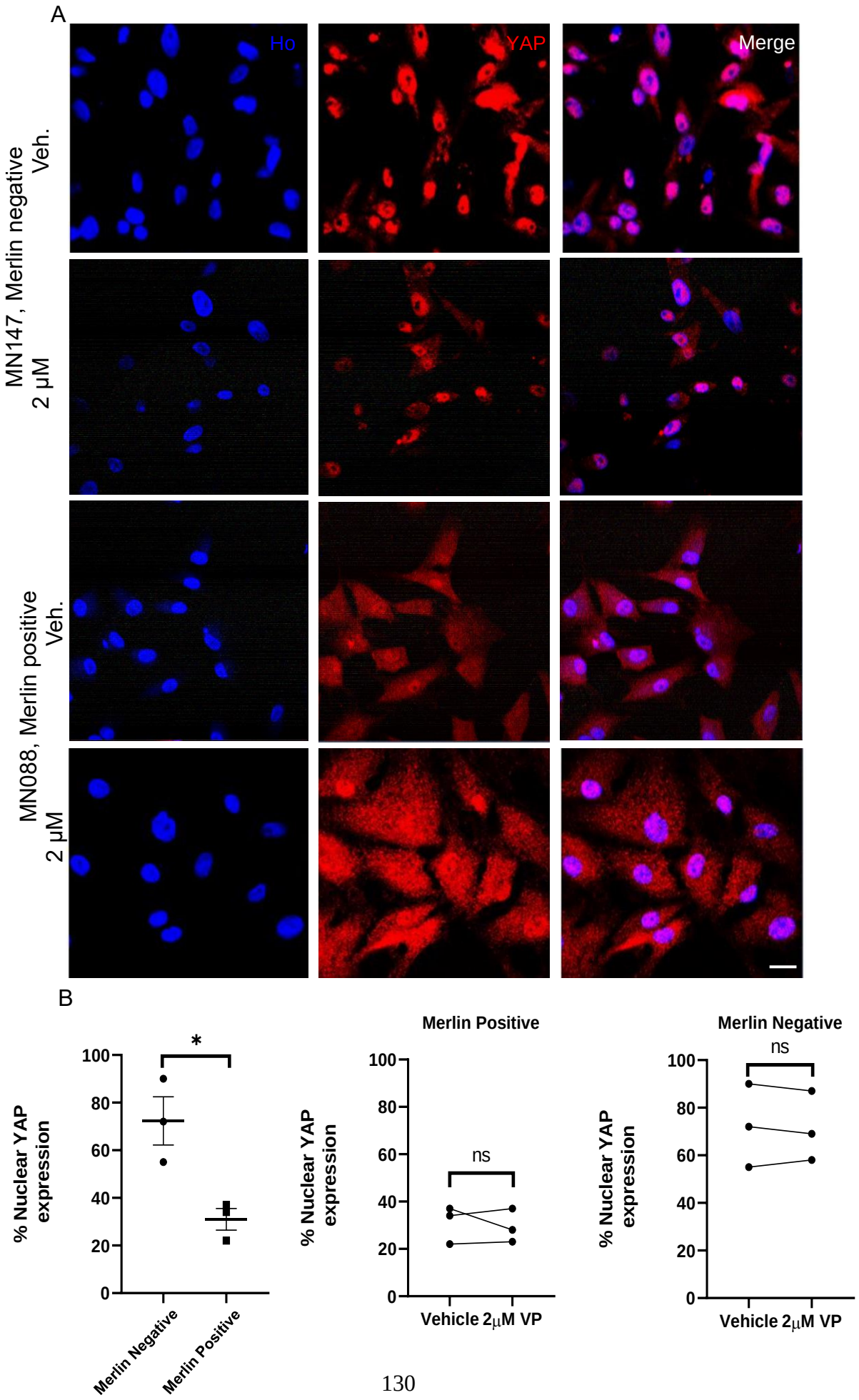
A
Ho
YAP
Merge
MN147, Merlin negative
Veh.
2 µM
MN088, Merlin positive
Veh.
2 µM
B
% Nuclear YAP expression
100
80
60
40
20
0
*
Merlin Negative
Merlin Positive
Merlin Positive
ns
Vehicle 2µM VP
Merlin Negative
ns
Vehicle 2µM VP

Figure 3.3.3: Verteporfin does not affect the nuclear localisation of YAP in primary meningioma cells. (**A**) Representative YAP (red) immunofluorescence of (n=3) Merlin negative (top two panels) and Merlin positive (bottom two panels) cultured primary meningioma, nuclei were counter-stained with Hoechst, scale bar = 10 μm. (**B**) Quantification of the amount of nuclear YAP in primary meningioma treated with either vehicle or 2 μM verteporfin, n = 3, unpaired t-test, *P<0.05, NS = non-significant.

3.3.5 Knockdown of YAP or TAZ Proteins Reduces Proliferation of both the Meningioma cell line BM1 and Primary Human Meningioma Cells

Having seen a strong effect of VP upon meningioma cell proliferation, we next performed experiments using lentiviral shRNA constructs to knockdown either YAP or TAZ in cells and measure the effects upon cell proliferation. As with other inhibitors, VP may have other targets so a knockdown approach was used. YAP or TAZ were knocked down in meningioma and schwannoma cells in order to determine if the effect of VP inhibition on proliferation was due to the drug blocking YAP and TAZ nuclear activity. VP has been shown to block the TEAD interaction with both YAP and TAZ (Liu-Chittenden et al., 2012), knockdown experiments will demonstrate whether VP is also having off target effects as well as whether YAP and TAZ exert different effect in Merlin null tumours (Felley-Bosco and Stahel, 2014). We hypothesised that if VP inhibition leads to a stronger reduction in proliferation compared with YAP and TAZ knockdown, then VP was eliciting off target effects. Knockdown of YAP or TAZ was first performed in the Merlin negative BM1 immortalised cell-line. Lentiviral-mediated knockdown of YAP and TAZ was achieved using two shRNA constructs for each, targeted towards YAP (YAP^{281}, YAP^{282}) and TAZ (TAZ149 and TAZ^{150}). Following lentiviral infection and puromycin selection of BM1 cells, cells were assessed for knockdown by first western blot and then cell proliferation using Ki-67 immunofluorescence. YAP expression was reduced to less than 10% seen in control BM1 cells following transduction with both YAP shRNA constructs, whereas TAZ expression was reduced to approximately 24% for TAZ^{149} and 18% for TAZ^{150}. This knockdown of YAP and TAZ proteins was confirmed by western blot (Figure 3.3.4.A, B, C, and D); all lentiviral shRNA constructs significantly reduced their respective target protein compared to scramble control expressing vectors.

In the following experiments YAP^{282} and TAZ^{150} were used as they displayed the highest mean knockdown in BM1 cells (Figure 3.3.4) In BM1 cells, knockdown of both YAP and TAZ significantly reduced the proportion of Ki-67 positive proliferating cells compared to scramble control infected cells (Figure 3.3.4.E,F). When compared to VP treatment, knockdown of YAP or TAZ resulted in a lesser reduction in proliferation, this may be due to off target effects of VP or the incomplete knockdown of YAP and TAZ we observed, or that YAP and TAZ would need to be knocked down simultaneously. Following this, knockdown of YAP or TAZ proteins was assessed in three Merlin negative primary meningiomas. Knockdown in primary meningioma was also verified by western blot (Figure 3.3.5C). Primary human meningioma cell proliferation was significantly reduced following knockdown of either YAP or TAZ compared to scramble controls (Figure 3.3.5A, B). Once again, the reduction of proliferation seen by knockdown was less than that following VP treatment.

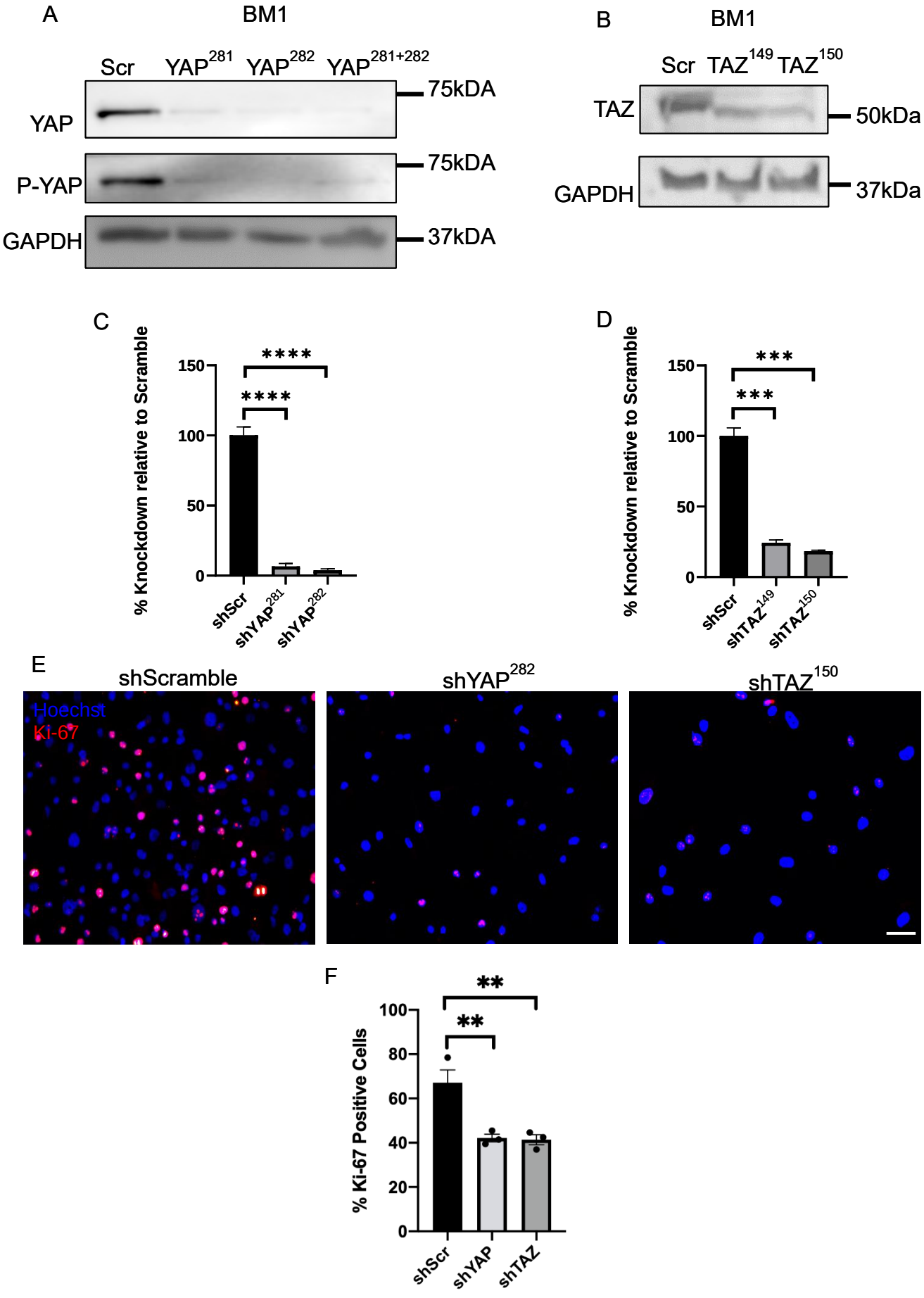
A
BM1
Scr
YAP281
YAP282
YAP281+282
YAP
75kDA
P-YAP
75kDA
GAPDH
37kDA
B
BM1
Scr
TAZ149
TAZ150
TAZ
50kDa
GAPDH
37kDa
C
% Knockdown relative to Scramble
****
****
150
100
50
0
shScr
shYAP281
shYAP282
D
% Knockdown relative to Scramble
***
***
150
100
50
0
shScr
shTAZ149
shTAZ150
E
shScramble
shYAP282
shTAZ150
Hoechst
Ki-67
F
% Ki-67 Positive Cells
**
**
100
80
60
40
20
0
shScr
shYAP
shTAZ

Figure 3.3.4: Knockdown of YAP or TAZ significantly reduces proliferation in BM1 cells. Representative Western blots (n=3) showing (**A**) YAP and (**B**) TAZ knockdown compared to scramble controls, GAPDH was the loading control. In BM1 cells, both YAP and TAZ expression is decreased following transduction with lentiviral constructs. Quantification of (**C**) YAP and (**D**) TAZ expression following knockdown relative to scramble controls. (**E**) Representative immunofluorescence images showing Ki-67 (red) following YAP and TAZ knockdown relative to scramble controls, scale bar = 10 μm. (**F**) Quantification of (E) displayed as the percentage of Ki-67^{+} nuclei; knockdown of YAP or TAZ significantly reduces proliferation in BM1 cells, n = 3, one-way ANOVA, *P<0.05.

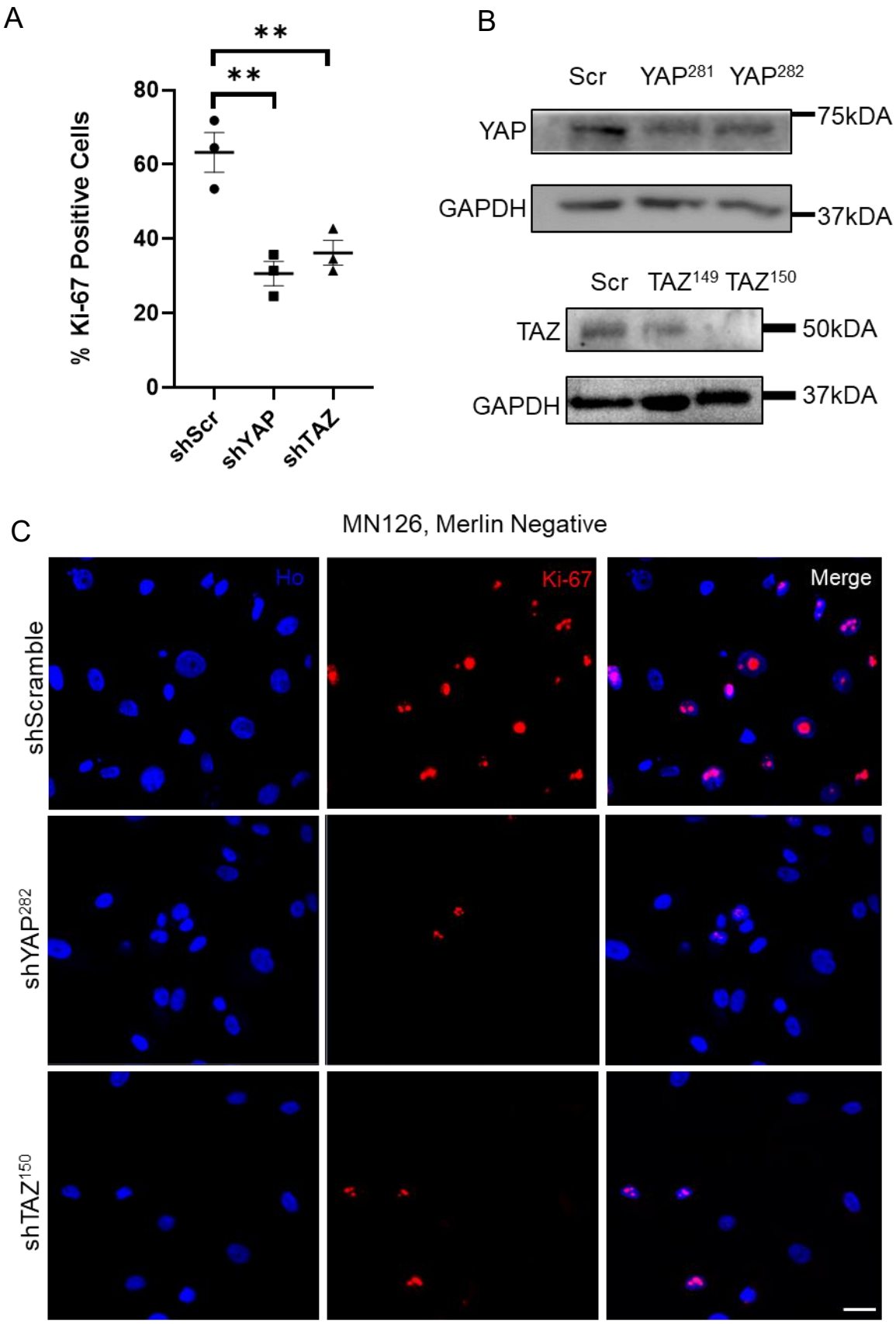
A
**
**
% Ki-67 Positive Cells
80
60
40
20
0
shScr
shYAP
shTAZ
B
Scr
YAP281
YAP282
YAP
75kDA
GAPDH
37kDA
Scr
TAZ149
TAZ150
TAZ
50kDA
GAPDH
37kDA
C
MN126, Merlin Negative
Ho
Ki-67
Merge
shScramble
shYAP282
shTAZ150

Figure 3.3.5: Knockdown of YAP or TAZ in primary Merlin-null meningioma cells reduces proliferation. (**A**) Quantification of (C) displayed as the percentage of Ki-67^{+} nuclei, n = 3, one-way ANOVA, **P<0.01. (**B**) Western blot confirming knockdown of YAP and TAZ in primary meningioma MN126, GAPDH was used as loading control. (**C**) Representative immunofluorescence of Ki-67 (red) following YAP or TAZ knockdown compared to scramble controls, scale bar = 10 μm. Cellular proliferation measured by Ki-67 expression is significantly reduced following knockdown of either YAP or TAZ in Merlin negative primary meningioma compared to scramble transduced controls.

3.3.7 Vivace Inhibitors are a Novel Selective Inhibitor of YAP and TAZ Mediated TEAD Transcriptional Activity

Vivace Therapeutics have developed a library of small molecule inhibitors that inhibit TEAD autopalmitoylation (Calses et al., 2019). Palmitoylation is a necessary post-translational modification for TEAD protein stability as well as for YAP and TAZ to bind and drive transcription (Kim and Gumbiner, 2019). A collaboration with Vivace allowed for screening of six inhibitors with varying specificities for TEADs 1-4, with some that selectively inhibiting one isoform and others that inhibit all TEAD proteins. The structure and composition of the Vivace inhibitors are currently under patent and protected by a material transfer agreement, so cannot be discussed in this thesis.

The six Vivace inhibitors were first screened for activity using an EdU proliferation assay in BM1 cells as a preliminary experiment before primary human meningioma cells were tested. EdU is incorporated into the nucleic DNA of proliferating cells during S-phase in the cell cycle and can be detected by a Click chemistry reaction, providing a cleaner more efficient signal than with Ki-67 immunostaining following a four hour EdU pulse. EdU was adopted at this point in the thesis as attempts to immunostain for Ki-67 in mouse DRG did not provide a specific punctate-nuclear signal as we were seeing in immunocytochemistry experiments (see EdU staining in Figure 3.3.13). 1 μM or 2 μM of each of the six different inhibitor compounds was administered to BM1 cells for 48 h; DMSO (the compound vehicle) was used as a control, these starting concentrations for the compounds were recommended to us by Vivace Therapeutics (private communication). All six Vivace compounds significantly reduced the number of EdU^+ nuclei compared to vehicle controls (Figure 3.3.6A) with compounds 3 (VT03697) and 5 (VT04153) causing the biggest reduction in proliferation from 22% in the DMSO vehicle to 3% and 2% respectively at 1 μM (Figure 3.1.6B). As these inhibitors should be efficacious in tumours that rely on aberrant YAP activation, the grade 3 Merlin negative

meningioma cell-line KT21 and the Merlin negative schwannoma cell-line HEI-193 were also screened with the six different Vivace compounds for their effects on proliferation. In both HEI-193 schwannoma and KT21 meningioma cells, proliferation was significantly inhibited by Vivace compounds at concentrations of 2 μM, with VT04153 providing the strongest inhibition of proliferation (Figure 3.3.7).

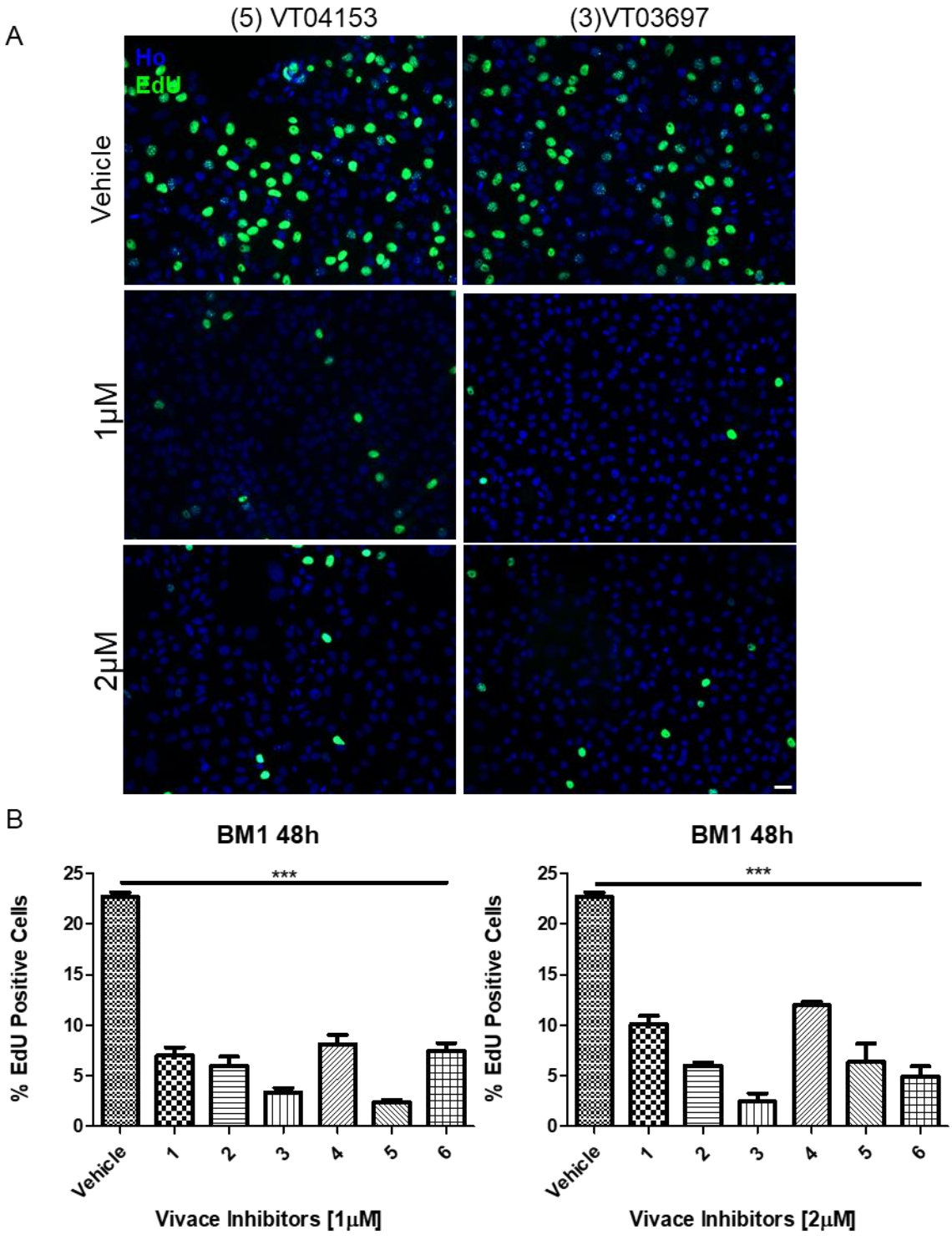
A
(5) VT04153
(3)VT03697
Ho
EdU
Vehicle
1μM
2μM
B
BM1 48h
% EdU Positive Cells
***
Vehicle
1
2
3
4
5
6
Vivace Inhibitors [1μM]
BM1 48h
% EdU Positive Cells
***
Vehicle
1
2
3
4
5
6
Vivace Inhibitors [2μM]

Figure 3.3.6: Vivace compounds significantly reduce proliferation in BM1 cells. (**A**) Representative immunofluorescence of EdU (green) in BM1 cells following inhibition with two Vivace inhibitors: VT04153 (compound 5) and VT03697 (compound 3), scale bar = 10 μm. (**B**) Quantification of all six Vivace inhibitors that were screened in BM1 cells at concentrations of 1 μM (left) and 2 μM (right), displayed as the percentage of EdU^+ nuclei, n = 3, one-way ANOVA, ***P<0.001.

(5) VT04153

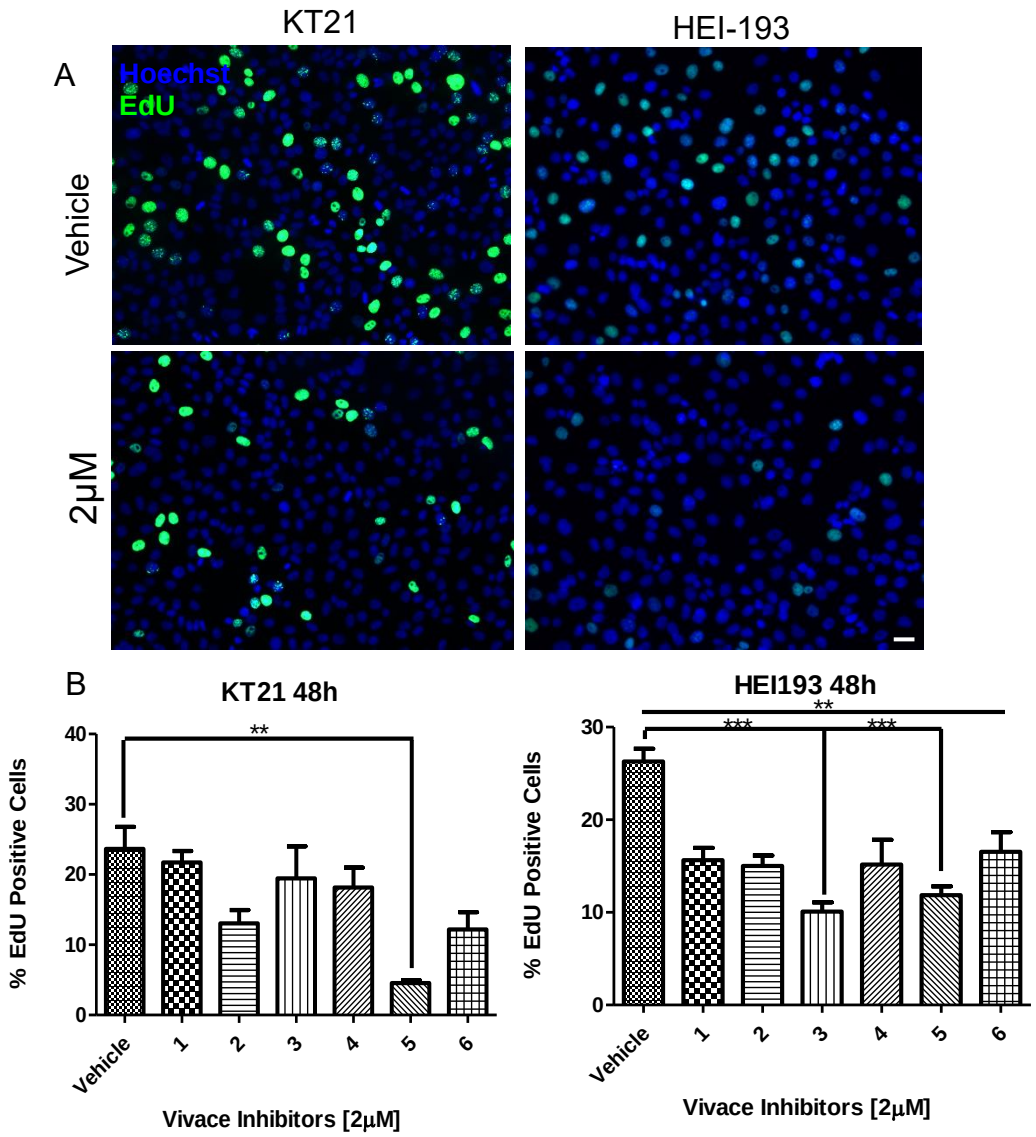
KT21
HEI-193
A
Hoechst
EdU
Vehicle
2μM
B
KT21 48h
HEI193 48h
% EdU Positive Cells
Vivace Inhibitors [2μM]
Vehicle
1
2
3
4
5
6
**
***

Figure 3.3.7: The proliferation of the Merlin negative grade 3 meningioma cell line KT21 and the Merlin negative schwannoma cell line HEI-193 is inhibited by VT04153 (compound 5) (**A**) Representative immunofluorescence of EdU (green) in KT21 cells (left) and HEI-193 cells (right) following inhibition with Vivace inhibitors, scale bar = 10 μm. (**B**) Quantification of all six Vivace inhibitors that were screened in KT21 and HEI-193 cells at concentrations of 1 μM (left) and 2 μM (right), displayed as the percentage of cells with EdU^+ nuclei, n = 3, one-way ANOVA, **P<0.01 ***P<0.001.

Given that inhibition of palmitoylation in TEAD family members has been shown to lead to decreased protein stability (Kim and Gumbiner, 2019), we next tested if the Vivace inhibitors were causing a reduction in total TEAD levels in BM1, KT21 and HEI-193 cells. Cells were incubated with either vehicle or 2 μM of each inhibitor for 7 days. This long incubation was chosen to ensure that all existing palmitoylated TEADs would likely be turned over within 7 days and that any TEAD expression detected would have been transcribed and translated in the presence of inhibitor. This timeline was based on previous studies in HEK293 cells where the protein translation inhibitor cycloheximide was used to show mutant TEAD4 that cannot undergo palmitoylation is degraded within 24 hours, whereas WT TEAD4 is stable for > 24 hours (Kim and Gumbiner, 2019). All four TEAD protein family members were detected by Western blot using a Pan-TEAD antibody. In BM1 cells, five out of six compounds significantly reduced TEAD1-4 expression by more than 50% compared to the vehicle (Figure 3.3.8A, B). In KT21 cells (Figure 3.3.8C) and HEI-193 cells (Figure 3.3.8D), there was no significant change in TEAD expression in treated cells compared to vehicle, suggesting that in these cells Vivace compounds do not modulate TEAD expression.

Overall, the efficacy of these inhibitors in a low and high grade meningioma cell line and a schwannoma cell line provided a foundation to move on to testing in both human primary meningioma and schwannoma tumour cells. A limitation of these results is that cell death was not assessed, however during these experiments, we did not see any examples of pyknotic nuclei that may have been indicative of apoptosis or necrosis.

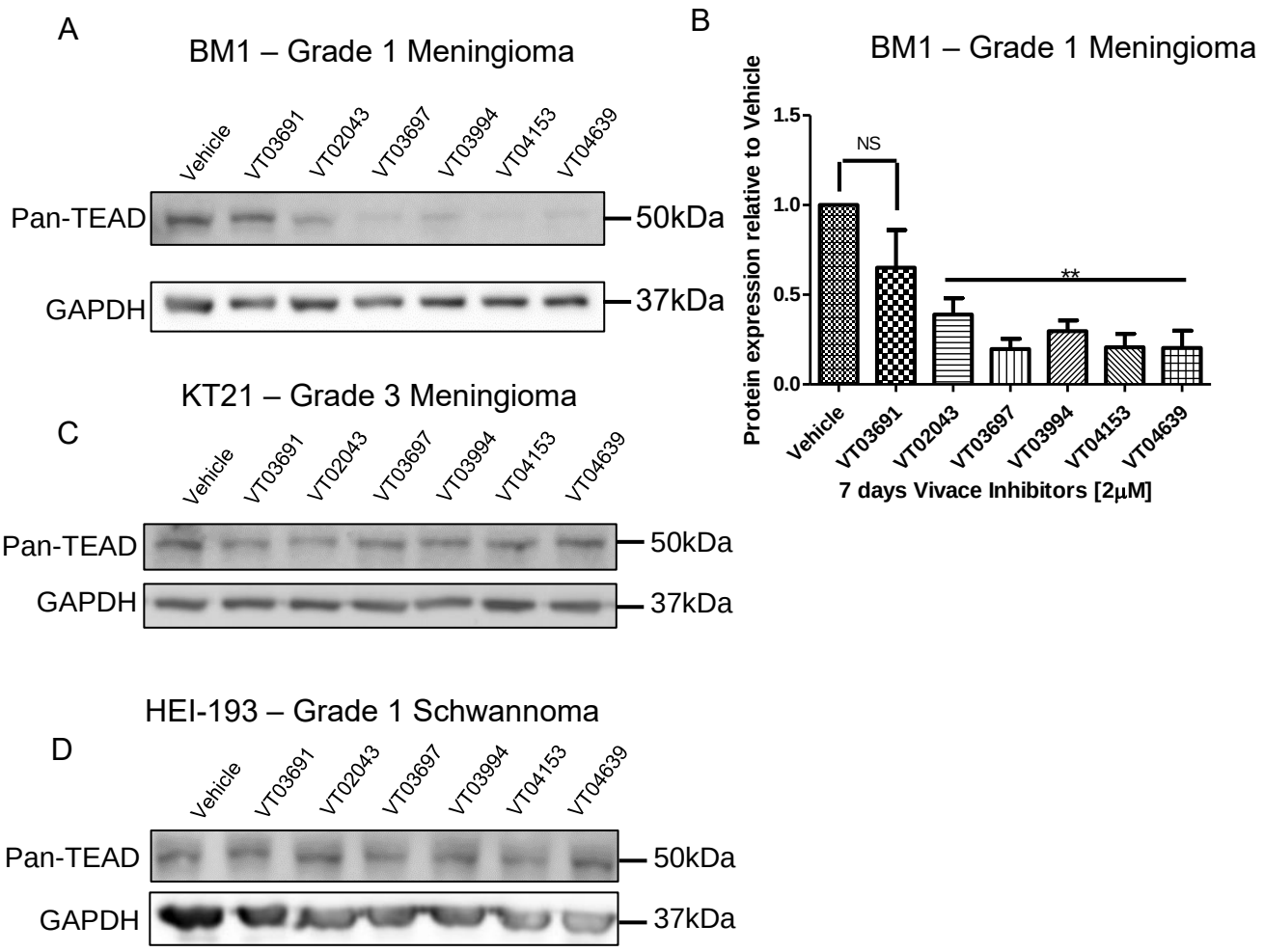

Figure 3.3.8: TEAD family expression is reduced in BM1 cells following treatment with Vivace inhibitors (**A**) Representative Western blot showing TEAD expression in BM1 cells incubated with vehicle or 2 μM Vivace inhibitor for 7 d.(**B**) Quantification of TEAD expression relative to vehicle seen in (A), n = 3, one-way ANOVA, **P<0.01. (**C**) Representative Western blot showing TEAD expression in KT21 cells incubated with vehicle or Vivace inhibitor for 7 d. (**D**) Representative Western blot showing TEAD expression in HEI-193 cells incubated with vehicle or 2 μM Vivace inhibitor for 7 d. GAPDH was the loading control.

3.3.8 Vivace Compounds Inhibit Primary Meningioma and Schwannoma in Vitro

Next, we determined the efficacy of Vivace compounds in primary meningioma cells. We hypothesised that the Merlin negative primary meningiomas would be more susceptible to inhibition that Merlin positive tumours. We performed EdU proliferation assays on Merlin negative primary meningiomas (n=3) treated for 48 h with either: vehicle, 10 nM; 100 nM or 1 µM of VT04153, the most efficacious inhibitor based on inhibition of BM1 cells. This concentration range was chosen as our previous results testing VP had revealed that primary meningioma cells were more sensitive to YAP and TAZ knockdown than cell lines in terms of reducing proliferation (see Figures 3.3.4 and 3.3.5), additionally we wanted to use a log-range of concentrations in order to determine IC_{50} values. Merlin negative primary meningioma cell proliferation was significantly reduced with VT04153 at concentrations of 100 nM and above compared to vehicle (Figure 3.3.9A, B), where cell proliferation decreased 3-fold with an IC_{50} of 34.6 nM. Following this, VT04153 was used at 100 nM for subsequent experiments. Next, the efficacy of VT04153 was tested in five Merlin positive meningiomas alongside five Merlin negative meningiomas. Surprisingly, Merlin positive meningiomas saw a greater decrease in proliferation following 48 h treatment, where in two cases, no EdU positive cells were observed. (Figure 3.3.9C), although their baseline proliferation was significantly less than in Merlin negative meningiomas. When both Merlin negative and Merlin positive tumours are grouped together, mean proliferation is significantly reduced from 28.6% to 9.4% (Figure 3.3.9D). Subsequently, the expression of the four TEAD family members was assessed by western blot to see if in primary meningiomas, an isoform specific inhibitor could be used which would be favourable for clinical use as it would only inhibit TEAD family members expressed in meningioma and schwannoma and not target different isoforms that may be expressed in healthy tissue. Three Merlin negative and three Merlin positive

grade 1 meningioma cells were western blotted and showed variable expression of all four family members, there was no trend between Merlin status and isoform expression (Figure 3.3.10). However, western blot quantification of all TEAD isoforms detected by a Pan-TEAD antibody showed that total TEAD expression was significantly higher in Merlin positive tumours compared with Merlin negative tumours (Figure 3.3.10), this may provide an explanation as to why Merlin positive tumours are also susceptible to VT inhibition (see Figure 3.3.9c) . Clinical and genotype information for these tumours were collected and compiled by Dr Claire Adams and are shown in table 3.3.1. For Merlin negative tumours, MN122 was heterozygous for TRAF7 N520S whilst MN139 and MN140 did not have any mutations at tested hotspots. For Merlin positive tumours, MN088 did not have any mutations at tested hotspots, MN147 was heterozygous for TRAF7 N520S and MN149 was heterozygous for AKT1 E17K. This panel would need to be expanded to ascertain whether common mutations seen in Merlin negative and Merlin positive meningiomas lead to differential expression of TEAD family members.

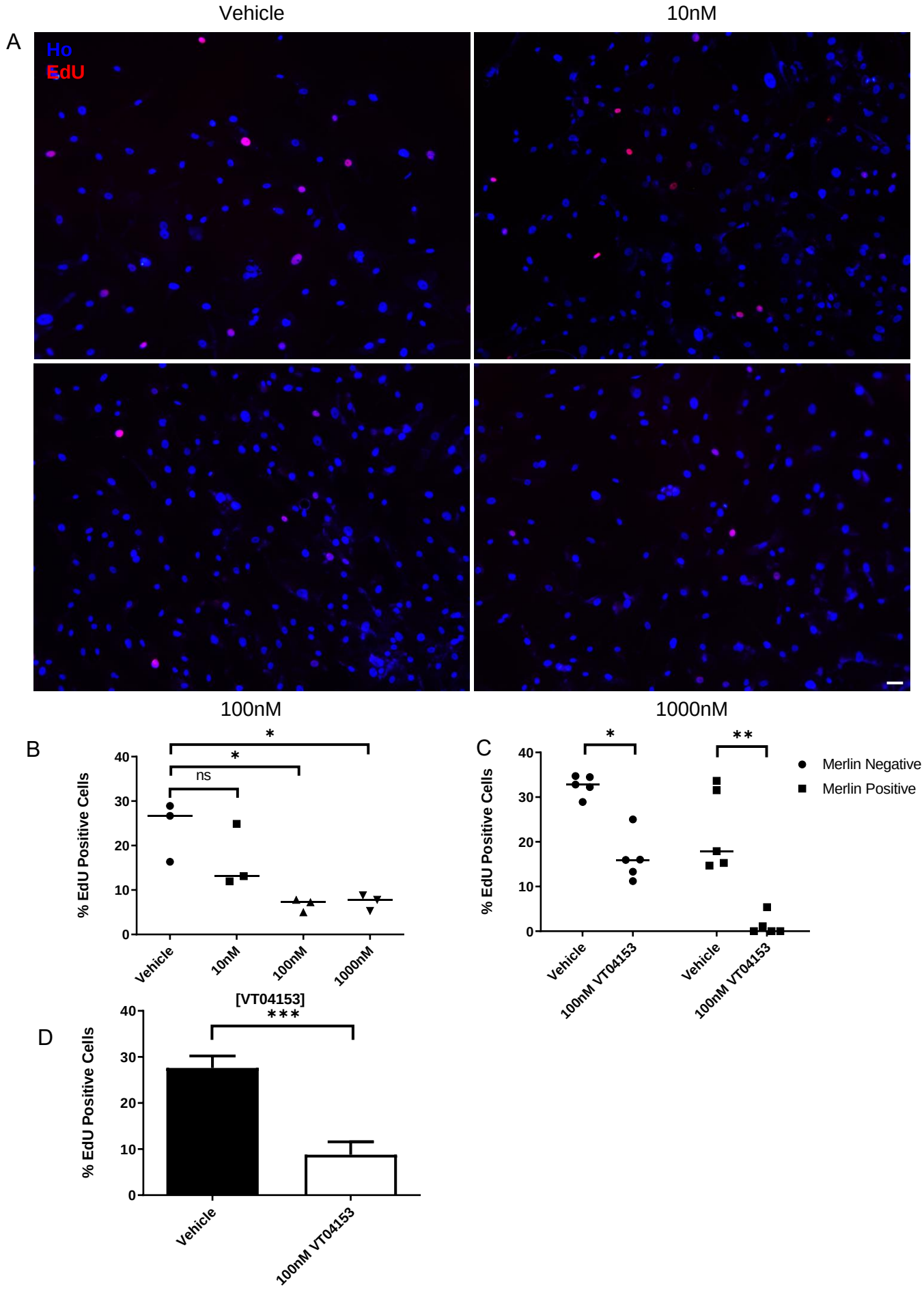
Vehicle
10nM
A
Ho
EdU
100nM
1000nM
B
% EdU Positive Cells
ns
*
*
Vehicle
10nM
100nM
1000nM
C
% EdU Positive Cells
*
**
Merlin Negative
Merlin Positive
Vehicle
100nM VT04153
Vehicle
100nM VT04153
D
[VT04153]
***
% EdU Positive Cells
Vehicle
100nM VT04153

Figure 3.3.9: Vivace compounds reduce proliferation in Merlin null primary meningioma cells (**A**) Representative immunofluorescence showing EdU positive cells (red), Hoechst counter-stains nuclei (blue). (**B**) Quantification of EdU positive cells following inhibition with VT04153 seen in (A), n = 3, one-way ANOVA, *P<0.05. (**C**) Comparison of Merlin negative and Merlin positive primary meningiomas treated with vehicle or VT04153, n = 5, two-way ANOVA with Bonferroni's correction, *P<0.05, **P<0.01 (**D**) Combined quantification of all meningiomas regardless of Merlin status (n = 10), one-way ANOVA, *P<0.001.

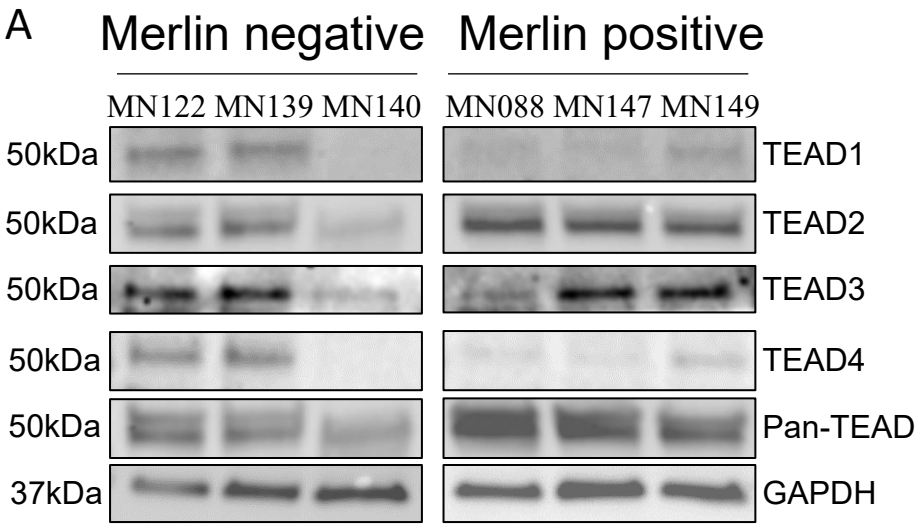
A
Merlin negative
Merlin positive
MN122 MN139 MN140
MN088 MN147 MN149
50kDa
TEAD1
50kDa
TEAD2
50kDa
TEAD3
50kDa
TEAD4
50kDa
Pan-TEAD
37kDa
GAPDH

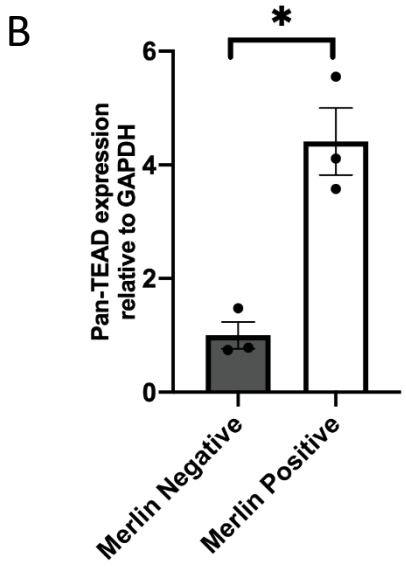
B
*
Pan-TEAD expression relative to GAPDH
6
4
2
0
Merlin Negative
Merlin Positive

Figure 3.3.10: TEAD expression in heterogeneous in primary meningioma cells but Merlin positive meningiomas express higher levels of TEAD overall. **(A)**Western blot of n=3 Merlin negative and Merlin positive primary meningioma cells for TEAD family members, GAPDH was the loading control. Expression of the various TEAD family members is heterogeneous between Merlin negative and Merlin positive tumours with no apparent correlation between expression and Merlin status. (**B**) Quantification of (A), Merlin-positive primary tumour cells express significantly higher Pan-TEAD when compared to Merlin negative primary tumour cells, Student's t-test with Welch's correction, *P <0.05.

Merlin negative primary schwannoma cells were also dosed with VT04153 to determine the effect of TEAD inhibition on their proliferation as well as to assess TEAD expression. Personal communication with Vivace led us to investigate whether VT04153 could also cause dysregulation of TEAD family member expression as previously reported (Kim and Gumbiner, 2019). Three primary schwannomas were treated for 48 h and 7 d with VT04153 and assessed for proliferation by an EdU incorporation assay (Figure 3.3.11) and western blot to determine expression of TEAD levels and the Hippo pathway readout gene CTGF (Figure 3.3.12). Following treatment, primary schwannoma cell proliferation was significantly reduced at concentrations of 100 nM and above (Figure 3.3.11A, B), with mean proliferation decreasing from 14.2% ± 0.4% to 5.2% ± 1.6%. Following this, the same primary schwannomas were treated for 7 d with 2 μM VT04153 to assess TEAD and CTGF expression. As seen in primary meningioma, primary schwannoma cells showed variable expression of TEAD family members between replicates. The hippo readout gene CTGF was downregulated following treatment with VT04153 indicating that the drug is blocking TEAD-dependent transcription (Figure 3.3.12). Taken together these results suggest that inhibition of Hippo pathway driven TEAD transcription can effectively reduce proliferation in both primary meningioma and schwannoma cells.

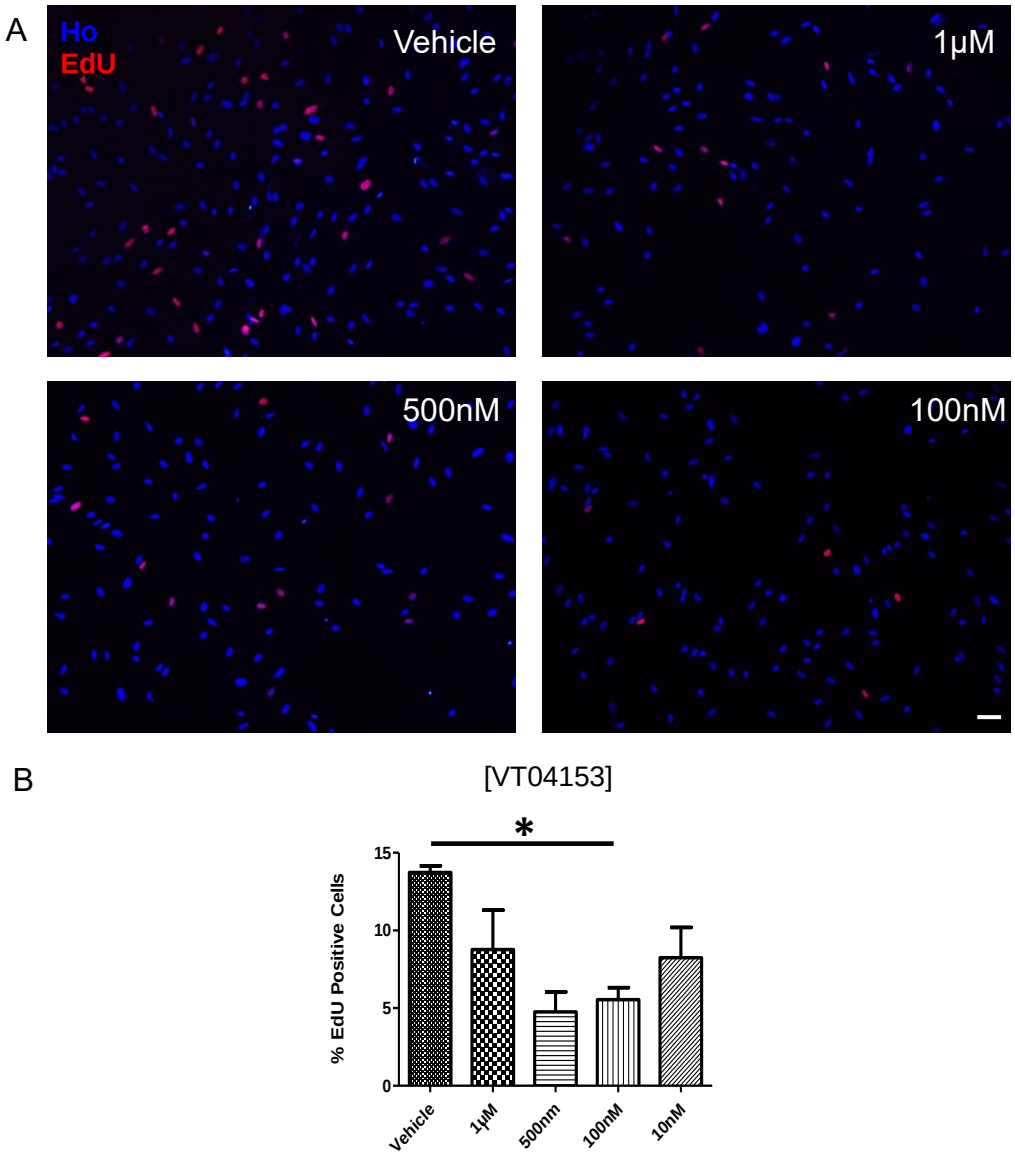

Figure 3.3.11: Vivace compounds reduce proliferation in primary schwannoma cells (**A**) Representative immunofluorescence showing EdU positive cells (red), Hoechst counter-stains nuclei (blue). (**B**) Quantification of EdU positive cells following inhibition with VT04153 seen in (A), n = 3, one-way ANOVA, *P<0.05.

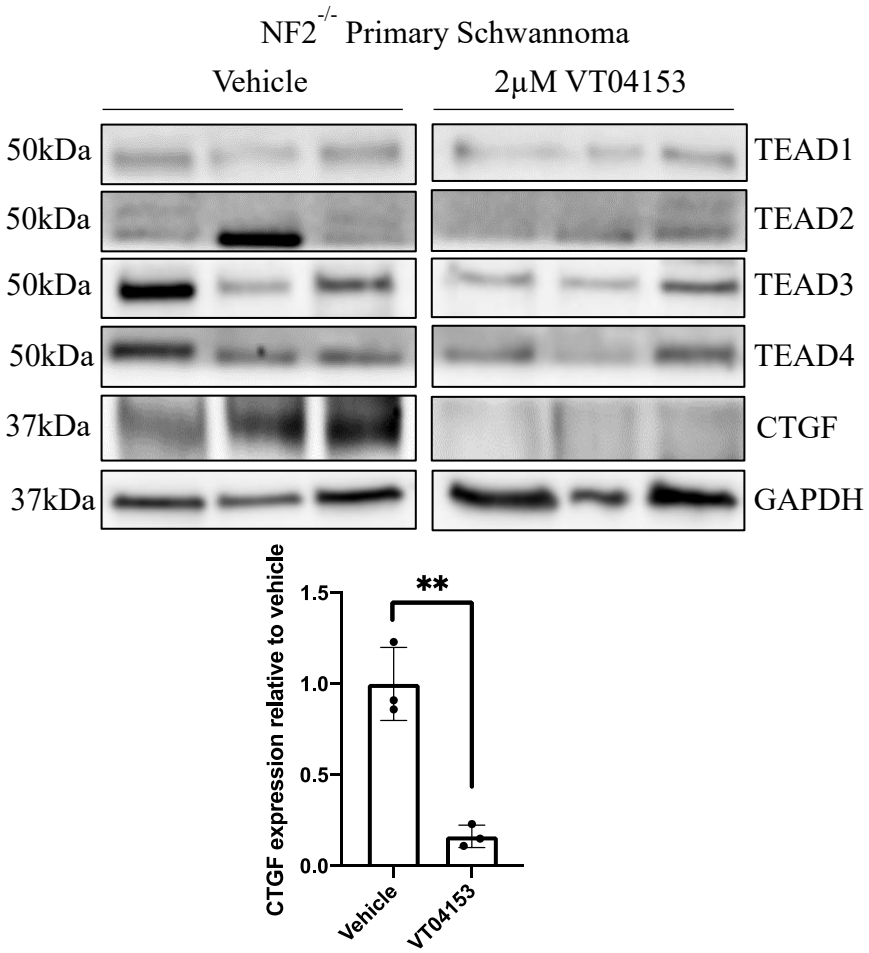

Figure 3.3.12: Vivace compounds decrease CTGF expression in primary schwannoma. Western blot and quantification of CTGF expression in n=3 Merlin negative primary schwannoma cells for TEAD family members and CTGF following 7 d treatment with 2 µM VT04153, GAPDH was the loading control. CTGF expression was significantly reduced following treatment with VT04153. Student's T-test, ** $p < 0.01$.

3.3.9 Preliminary Assessment of Vivace Inhibitors in the Postn-Cre Schwannoma Mouse Model

Vivace compounds which inhibited all TEAD members significantly reduced proliferation in primary meningioma and schwannoma. In primary schwannoma we also demonstrated that CTGF, a protein whose expression is driven by TEADs, was significantly downregulated at the protein level following inhibition with Vivace drugs. Following this, we looked to test the compounds *in vivo* using the Postn-Cre schwannoma mouse model. In these mice, *NF2* is removed by Cre recombinase specifically in Schwann cells of the PNS. These mice develop schwannomas in their DRGs and vestibulocochlear apparatus at 5-months of age although Schwann cell proliferation and hyperplasia can be seen in 3-month old mice. In order to label the Schwann cell and Schwann cell-derived satellite glial cell population within the DRG, these mice also carried the PLP-GFP transgene which tags these cells with GFP.

Following personal communication with Vivace, we decided to carry out a preliminary experiment in 3-month old mice to assess the efficacy of inhibiting Hippo pathway driven TEAD transcription. For this experiment, Vivace directed us to use VT03989, a pan-TEAD inhibitor approved for *in vivo* use that they reported was well-tolerated for up to 60 days given via daily oral gavage with no adverse effects (unpublished data). 30 mg/kg VT03989 was administered daily for 14 days to Postn.Cre+NF2$^{fl/fl}$GFP^{+} 3-month old mice by oral gavage, with Postn.Cre-NF2$^{fl/fl}$GFP^{+} mice serving as age-matched littermate controls. 24 h before tissue collection mice were pulsed with 100 mg/kg EdU in order to assess proliferation in the DRGs. Sciatic nerves were also analysed by western blot in order to establish whether VT03989 was reducing TEAD and CTGF expression in Schwann cells.

Treatment with VT03989 significantly reduced proliferation of Postn.Cre+NF2$^{fl/fl}$GFP^{+} Schwann cells and satellite glial cells which were associated with neuronal cell bodies

within the DRG compared to Postn.Cre+NF2$^{fl/fl}$GFP^{+} vehicle controls (Figure 3.3.13). Schwann cell proliferation in mice treated with VT03989 was 30% ± 6.4% less than in vehicle controls (Figure 3.3.13A, D). Western blotting in sciatic nerve showed that CTGF was only highly expressed in Postn-Cre^{+}NF2$^{fl/fl}$ mice (Figure 3.3.13C). Treatment with VT03989 significantly reduced CTGF expression in Postn.Cre+NF2$^{fl/fl}$ to levels seen in Postn-Cre-NF2$^{fl/fl}$ control mice, suggesting that the drug is blocking TEAD transcriptional activity (3.3.13D). Additionally, the reduction in total TEAD levels in treated Postn-Cre^{+}NF2$^{fl/fl}$ approached significance (P=0.0529), suggesting that inhibition of TEAD palmitoylation may be reducing TEAD stability, leading to increased degradation of the protein (Figure 3.3.13E). These results demonstrate that inhibition of Hippo-mediated TEAD-driven transcription *in vivo* reduces proliferation of Schwann cells and satellite glial cells in Postn.Cre+NF2$^{fl/fl}$ DRGs. There was no adverse effects or weight gain/loss during the oral gavage treatment period, there was also no observable difference in phenotype between vehicle and treated mice at this time point (Table 3.3.1). Subsequently, 5-month old mice will be tested as this preliminary data is expanded upon.

Mouse	Gender	Genotype	Weight			Adverse Effects		
			day 1	day 7	day 14	day 1	day 7	day 14
n452	Male	Postn.Cre+NF2fl/fl	23g	22g	21g	n/a	n/a	n/a
n453	Female	Postn.Cre+NF2fl/fl	19g	21g	20g	n/a	n/a	n/a
n455	Female	Postn.Cre+NF2fl/fl	16g	17g	16g	n/a	n/a	n/a
n475	Female	Postn.Cre-NF2fl/fl	31g	32g	32g	n/a	n/a	n/a
n476	Female	Postn.Cre-NF2fl/fl	34g	32g	34g	n/a	n/a	n/a
n454	Male	Postn.Cre-NF2fl/fl	28g	27g	27g	n/a	n/a	n/a

Table 3.3.1: Table to show the weight and any adverse effects of mice who received 30 mg / kg of VT03989 by oral gavage for 14 consecutive days. N/A = not applicable.

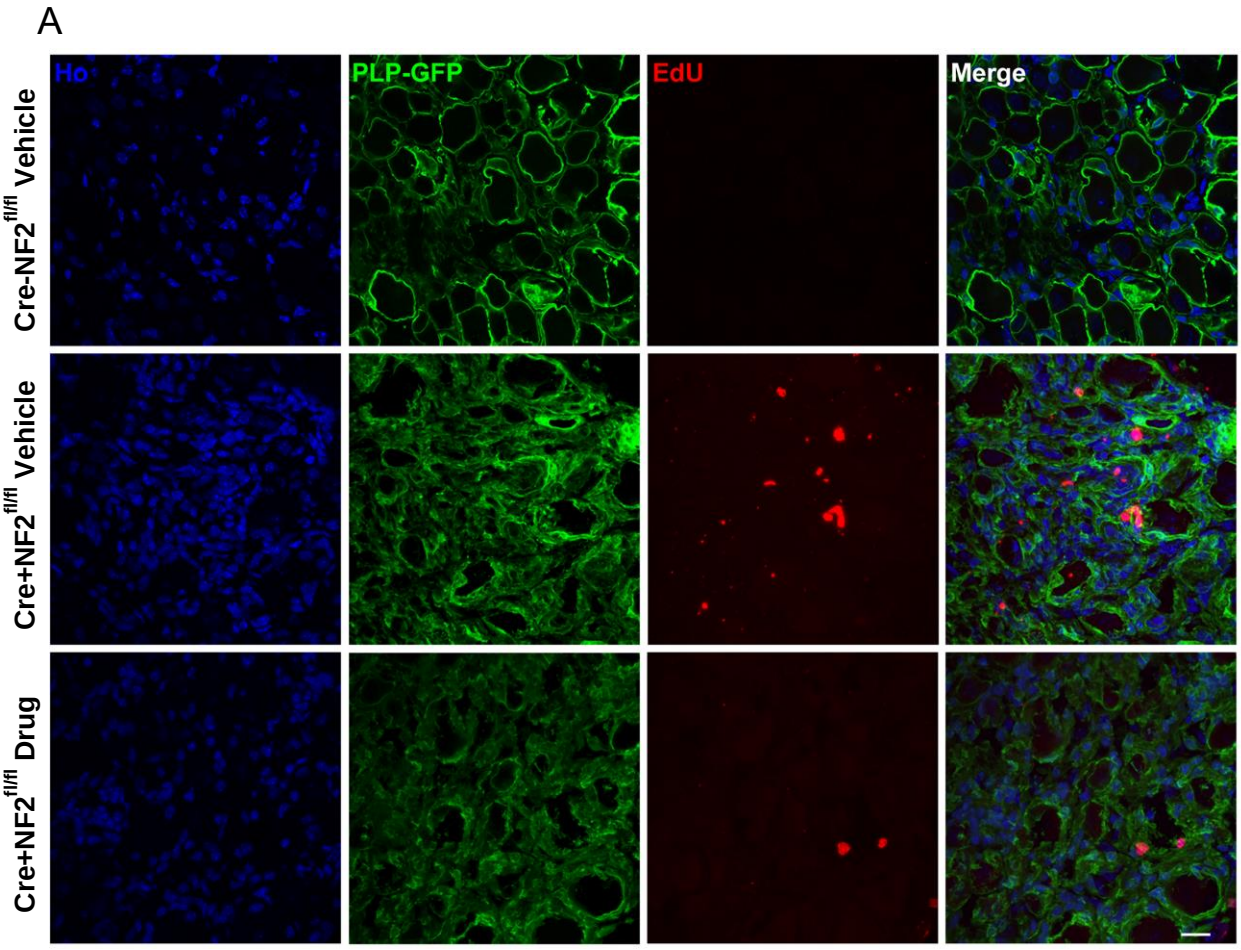
A
Ho
PLP-GFP
EdU
Merge
Cre-NF2fl/fl Vehicle
Cre+NF2fl/fl Vehicle
Cre+NF2fl/fl Drug

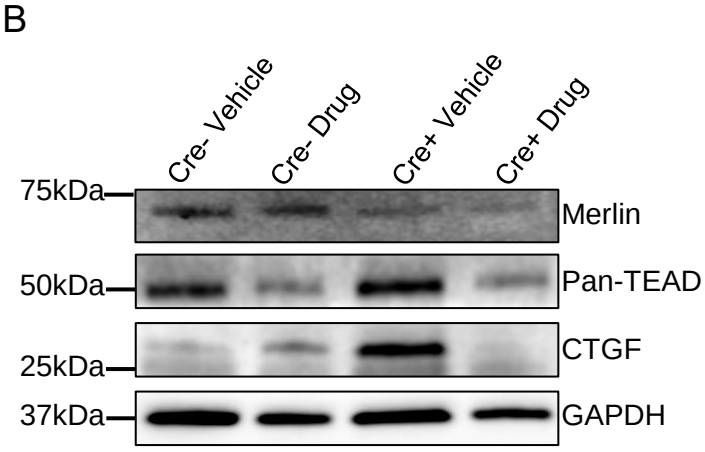
B
Cre- Vehicle
Cre- Drug
Cre+ Vehicle
Cre+ Drug
75kDa
Merlin
50kDa
Pan-TEAD
25kDa
CTGF
37kDa
GAPDH

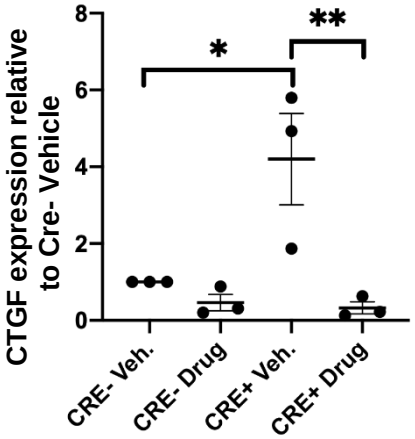
C
CTGF expression relative to Cre- Vehicle
*
**
CRE- Veh.
CRE- Drug
CRE+ Veh.
CRE+ Drug

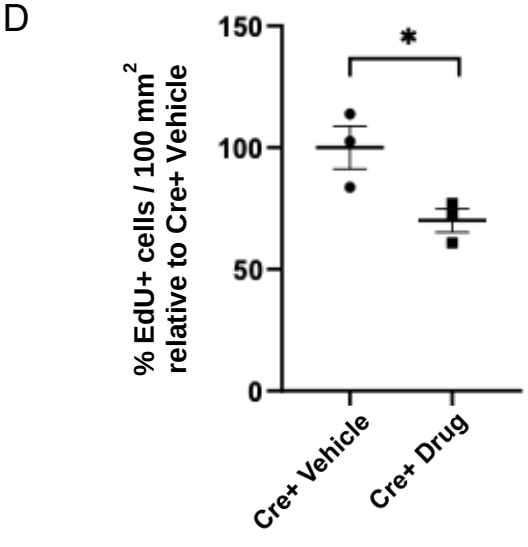
D
% EdU+ cells / 100 mm2 relative to Cre+ Vehicle
*
Cre+ Vehicle
Cre+ Drug

Figure 3.3.13 Oral gavage with VT03989 reduces proliferation in NF2 null dorsal root ganglia (DRGs) (**A**) Representative immunofluorescence images of (n=3) 3-month old Postn-Cre.NF2$^{fl/fl}$ mouse dorsal root ganglia treated with either vehicle or 30 mg/kg daily of VT03989 (drug) for 14 d by oral gavage. Top panel is the Postn.Cre-NF2$^{fl/fl}$ vehicle control, middle panel is the Postn.Cre+NF2$^{fl/fl}$ vehicle and the bottom panel is the Postn.Cre+NF2$^{fl/fl}$ drug. PLP-GFP (green) labels Schwann cells (SCs) and satellite glial cells (SGCs). In all images, EdU (red) depicts proliferating cells and Hoechst (blue) counter-stains nuclei. Proliferation is seen in the GFP^{+} SCs and SGCs which surround neuronal bodies. Scale bars = 10 μm. (**B**) Representative western blot of (n=3) biological repeats of mouse sciatic nerve lysate for connective tissue growth factor (CTGF) and Pan-TEAD, (GAPDH was the loading control) in a Postn.Cre-NF2$^{fl/fl}$ vehicle mouse (lane 1), a Postn.Cre-NF2$^{fl/fl}$ drug treated mouse (lane 2), a Postn.Cre+NF2$^{fl/fl}$ vehicle treated mouse (lane 3), and a Postn.Cre+NF2$^{fl/fl}$ drug treated mouse (lane 4). (**C**) Quantification of (B), CTGF expression was significantly upregulated in Postn.Cre+NF2$^{fl/fl}$ vehicle treated mice and treatment with drug in Postn.Cre+NF2$^{fl/fl}$ mice returned expression to levels seen in Postn.Cre-NF2$^{fl/fl}$ controls. One-way ANOVA with Bonferroni's correction, *P < 0.05, **P < 0.01. (**D**) Quantification of EdU-positive cells in Postn.Cre+NF2$^{fl/fl}$ vehicle and Postn.Cre+NF2$^{fl/fl}$ drug treated DRGs (n=3 mice). Only SCs and SGCs associated to neuronal cell bodies were counted from. EdU counts were normalised to DRG area by counting EdU+ cells within 3, 10 μm DRG cryosections per mouse and calculating the area of each section using ImageJ. Data plotted as Mean ± SEM, unpaired T-test, * = P<0.05.

3.3.10 Discussion

The work in this Chapter first characterised the protein expression of the Hippo pathway proteins LATS1, LATS2, YAP, p-YAP and TAZ in Merlin negative and Merlin positive primary meningioma cultures, compared to control human meningeal cell controls. Studies have shown that primary meningioma expression of various Hippo pathway proteins is highly variable based on tumour grade and other mutations such as KLF4 and TRAF7, independent of Merlin status (Dunn et al., 2019). Our initial study of Hippo pathway protein expression showed that there is no obvious differential expression based on Merlin status alone. This provided a useful insight into protein expression in Merlin negative and Merlin positive meningiomas and the decision was made to focus on the downstream Hippo effectors YAP and TAZ. We believe that a large panel of stratified groups is needed to identify if a correlation exists between Hippo pathway protein expression and Merlin status. Such stratification would include tumour location, mutational status of other proteins such as SMO, KLF4 and TRAF7 (Suppiah et al., 2019, Yuzawa et al., 2016), as well looking at epigenetic factors such as methylation status (Murnyak et al., 2015, Lomas et al., 2005). Tumours would need to be stratified by the various mutational hotspots with enough in each group for suitable power. The more important readout of Hippo pathway activity in previous reports were changes in the nuclear localisation of the co-transcriptional activators YAP and TAZ (Haskins et al., 2014, Hong, 2013, Striedinger et al., 2008). It would also be of interest to see if Merlin negative meningiomas have increased activity of the E3 ligase CRL4 which has been shown to degrade nuclear LATS1 in schwannoma, resulting in reduced YAP phosphorylation (Figure 1.2) (Li et al., 2014a)

The first link between the Hippo pathway and Merlin was established in 2008 by Striedinger et al (Striedinger et al., 2008). They reported that immortalised meningeal cell lines treated with siRNA for NF2 led to nuclear localisation of YAP. Additionally, when

Merlin was reintroduced into the KT21-MG1 meningioma cell line, this resulted in nuclear exclusion of YAP and was dependent on the phosphorylation of Merlin at residue Ser518. The nuclear localisation seen in our data in primary meningioma is consistent with Striedinger's findings; Merlin negative primary tumour cells contain a higher proportion of nuclear YAP compared to Merlin positive cells. Additionally, the nuclear activity of YAP and TAZ leads to transcription of genes that drive proliferation and in line with previous studies on paraffin-embedded meningioma tumour tissue (Pavelin et al., 2014), Merlin negative tumour cells were seen to have a higher $Ki67^{+}$ index of proliferation compared to Merlin positive tumours. Following this, chemical inhibition of the YAP-TEAD interaction with verteporfin and lentiviral mediated shRNA knockdown of YAP and TAZ were both used to assess if the difference seen in proliferation of Merlin negative and Merlin positive tumours was due to alterations in Hippo signalling. Verteporfin has been shown to block the YAP-TEAD interaction which prevents transcription of TEAD target genes; as expected and in line with other tumour types (Feng et al., 2016, Pan et al., 2016), Merlin negative tumour cells experienced a greater reduction in proliferation compared to Merlin positive cells. A study by *Wang et al* reported that in endometrial cancer, verteporfin acts through upregulating 14-3-3 protein resulting in increased cytoplasmic sequestration of YAP in the cytoplasm (Wang et al., 2016). When we analysed the subcellular localisation following treatment with vehicle or verteporfin, no significant difference was seen between nuclear and cytoplasmic YAP expression. This suggests that in meningiomas, the mechanism of verteporfin inhibition is through disruption of the YAP-TEAD interaction inside the nucleus.

Following this work, shRNA knockdown of YAP and TAZ in Merlin negative primary meningioma cells showed that any off target effects of verteporfin appeared minimal as proliferation rates after either knockdown or treatment with verteporfin resulted in similar

decreases in proliferation compared to scramble or vehicle controls. These results have established that inhibition of YAP/TAZ activated TEAD driven transcription can effectively reduce proliferation in primary Merlin negative meningioma tumour cells. Verteporfin is not a suitable candidate for therapy as it has shown to have off-target toxicity, such as redox reactions with intracellular metal ions to produce reactive oxygen species (Eales et al., 2018). The development of novel TEAD inhibitors by Vivace Therapeutics gave us an unique opportunity to explore a number of orally bioavailable inhibitors that have the potential to be tested in vivo (Calses et al., 2019). These compounds showed efficacy in BM1 and KT21-MG1 Merlin negative meningioma cell lines as well as the HEI-193 Merlin negative schwannoma cell line. In cell lines and primary meningioma cells, the pan-TEAD Vivace inhibitors were consistently more efficacious than compounds which targeted individual TEAD isoforms. This was confirmed when western blotting of primary meningiomas revealed variable TEAD isoform expression between primary meningioma cell lysates and no observable correlation between TEAD expression and Merlin status. The pan-TEAD inhibitor VT04153 was efficacious in primary meningioma at concentrations of 100 nM and above and showed an IC_{50} of 34.6 nM. Surprisingly, Merlin positive tumour cells were also highly susceptible to inhibition, although their basal EdU^{+} index of proliferation is lower than Merlin negative tumour cells. There were not enough tumours tested to be able to effectively stratify Merlin positive tumours by other mutations such as TRAF7 or AKT1 status, but this would clearly be an interesting path to follow in the future. In order to further understand the efficacy of VT04153 seen in Merlin positive primary meningioma we would need to correlate TEAD expression to drug efficacy in terms of reducing proliferation and their mutational status. In Figure 3.3.10 we showed that total TEAD expression was higher in Merlin positive primary meningioma cells compared to Merlin

negative primary meningioma cells, this could be compensating the increased nuclear localisation of YAP that we saw in Figure 3.3.3.

In schwannoma, VT04153 was also efficacious at concentrations of 100 nM and above. Again, primary schwannoma cells showed variable TEAD expression however drug treatment significantly reduced expression of the TEAD-driven Hippo readout gene CTGF. Currently, there are multiple clinical trials ongoing in schwannoma and meningioma that target various cellular processes, such as MTORC1 or ERK inhibitors, that are linked to established mutational hotspots, canonical tumour pathways or immunotherapies (Killeen et al., 2019, Goutagny et al., 2017). An example of a clinical trial targeting an established mutational hotspot is the trial involving Vismodegib which inhibits SMO (trial identifier: NCT02523014) (Nigim et al., 2018). No such clinical trials currently exist in meningioma or schwannoma which target the Hippo pathway.

In vivo testing of compounds is a necessary step which precedes human clinical trials. Communication with Vivace Therapeutics led us to test the *in vivo* approved pan-TEAD inhibitor VT03989 by oral gavage in the Postn-$Cre^{+}NF2^{fl/fl}$ mouse model which is currently the most suitable genetic model of Merlin null schwannoma available (Gehlhausen et al., 2015). This model has been used previously to test the cox-2 inhibitor celecoxib but failed to produce a significant effect (Wahle et al., 2018). The results presented here show that VT03989 reduced DRG proliferation by approximately 33% following daily oral gavage of 30 mg/kg for 14 days. No adverse phenotype or weight loss was seen in either Cre+ Merlin-deficient mice or Cre^{-} littermate controls treated with the compound (data not shown). Personal communication with Vivace Therapeutics has told us that their drug has been used in other tumours with Merlin deficiencies and is well tolerated when orally administered daily for 60 days, with good pharmacokinetics and pharmacodynamics. This information gives us the scope to increase the treatment time course in future experiments. It would also be desirable to assess plasma levels of

VT03989 to determine the bioavailability of a given dose. Analysis of sciatic nerve showed that VT03989 significantly reduced expression of the Hippo readout gene CTGF in Postn-Cre^{+}NF2$^{fl/fl}$ whilst TEAD levels approached a significant reduction. This measure of Schwann cell rich sciatic nerve is a good surrogate for DRG or vestibulocochlear tissue however moving forward it will be important to determine the expression levels of these proteins at the site of tumour formation. These experiments were conducted at an early time point for this mouse model, before there is an established tumour-burden. It will be important to carry out further experiments with mice at five and nine months of age where there is a moderate and severe tumour-burden respectively according to previously published work on the model (Gehlhausen et al., 2015), this work is currently ongoing in our lab. As mice with this model age past nine months when tumour burden leads to mortality, certain vestibulocochlear abnormalities are seen and can be tested by behavioural testing or auditory brainstem response testing. These tests could be used in older mice treated with VT03989 to see if there is a functional hearing benefit. Taken together, the Postn-Cre^{+}NF2$^{fl/fl}$ mouse model is a robust tool for assessing the efficacy of the promising TEAD inhibitors developed by Vivace Therapeutics.

Translation of this drug into a meningioma mouse model has yet to be done. Currently, the most appropriate mouse models for this purpose have been developed by the Mawrin lab. There are currently no suitable Cre drivers that would result in selective genetic deletion of Merlin in meningeal cells (Kalamarides et al., 2002). The prostaglandin D synthase Cre mouse was developed by the Kalamarides lab in 2015 however tumours are only seen in 27% of mice and take 8 months to develop, limiting its use as a meningioma model (Peyre et al., 2015). Orthotopic meningioma models have been developed for injection and establishment of human tumour cells within the mouse brain at either the convexity or the skull base (Mawrin, 2017).

In summary, this Chapter has shown that inhibition of the Hippo pathway in Merlin null tumours is a viable route for reducing tumour proliferation. Figure 3.3.14 shows the mechanisms by which both verteporfin and Vivace therapeutics drugs prevent YAP and TAZ mediated transcription in Merlin-null schwannoma. Vivace therapeutics have developed drugs that are potent at nanomolar concentrations and can be safely used in a pre-clinical *in vivo* mouse models. This work should be expanded across different ages in Postn-Cre^{+}NF2$^{fl/fl}$ and into the orthotopic meningioma mouse models in order to generate a mandate for early-phase human clinical trials.

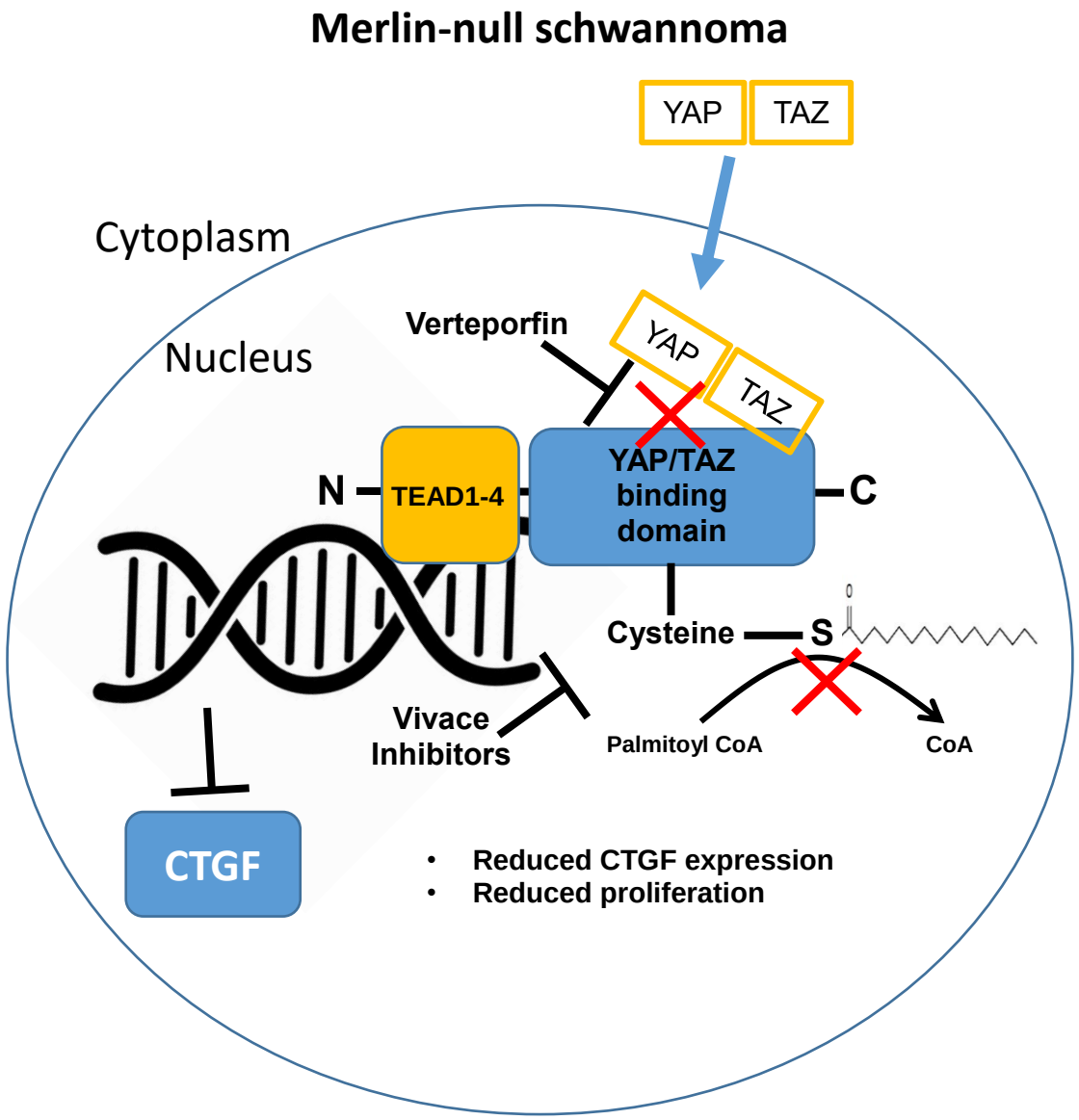

Figure 3.3.14: Proposed mechanisms of verteporfin and Vivace therapeutics drugs inhibition in Merlin-null schwannoma. Verteporfin inhibits yes-associated protein (YAP)/ Transcriptional coactivator with PDZ-binding motif (TAZ) driven transcription by preventing the interaction with TEAD transcription factors. Vivace therapeutics drugs block the autopalmitoylation of a conserved cysteine residue in the YAP/TAZ binding domain of TEAD proteins, which prevents YAP/TAZ binding. In the absence of YAP/TAZ binding, TEADs are less transcriptionally active, leading to reduction in schwannoma proliferation.

4 Discussion

This thesis has sought to establish the role of Hippo signalling in Merlin negative meningioma and schwannoma. In terms of the project aims outlined in section 1.9, firstly, this thesis has validated the upregulation seen by RNA sequencing of the cancer stem cell marker ALDH1A1. ALDH1A1 expression was revealed to be driven by the nuclear activity of the Hippo pathway co-transcriptional activator TAZ, but not YAP (section 3.2). Knockdown or inhibition of ALDH1A1 led to reduction in meningioma and schwannoma proliferation and this work should be continued to identify a mechanism by which ALDH1A1 is influencing proliferation as well as using in vivo models to delete ALDH1A1 in a Merlin-null tumour model. Secondly, we sought to stratify meningiomas by Merlin status, comparing their proliferation rate and expression of Hippo pathway proteins such as LATS1/2, YAP and TAZ. Although there was no clear trend between protein expression, Merlin negative primary meningioma cells were consistently more proliferative than Merlin positive primary meningioma cells (section 3.3.3). Lastly, we showed that chemical inhibition of YAP/TAZ driven TEAD transcriptional activity is efficacious in Merlin null meningioma and schwannoma (section 3.3.3-3.3.10). Overall, we propose the findings of this thesis in figure 4.1.

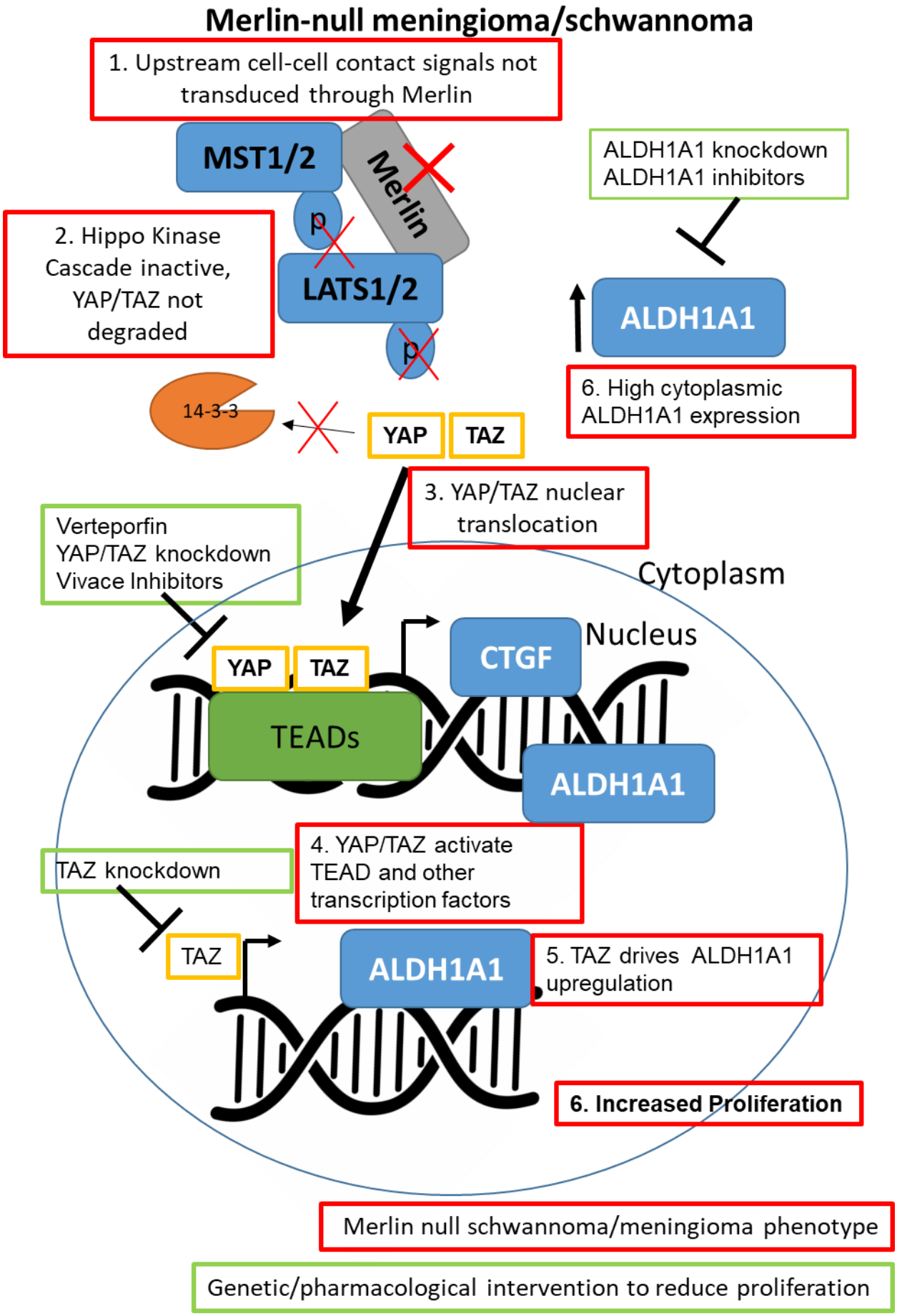
Merlin-null meningioma/schwannoma
1. Upstream cell-cell contact signals not transduced through Merlin
MST1/2
Merlin
P
LATS1/2
P
2. Hippo Kinase Cascade inactive, YAP/TAZ not degraded
14-3-3
YAP
TAZ
ALDH1A1 knockdown
ALDH1A1 inhibitors
ALDH1A1
6. High cytoplasmic ALDH1A1 expression
3. YAP/TAZ nuclear translocation
Verteporfin
YAP/TAZ knockdown
Vivace Inhibitors
Cytoplasm
Nucleus
YAP
TAZ
TEADs
CTGF
ALDH1A1
4. YAP/TAZ activate TEAD and other transcription factors
TAZ knockdown
TAZ
ALDH1A1
5. TAZ drives ALDH1A1 upregulation
6. Increased Proliferation
Merlin null schwannoma/meningioma phenotype
Genetic/pharmacological intervention to reduce proliferation

Figure 4.1: Aberrant Hippo pathway activity in Moesin-ezrin-radixin-like protein (Merlin) null schwannoma and meningioma lead to increased proliferation and aldehyde dehydrogenase 1 A1 (ALDH1A1) upregulation which can be targeted genetically or pharmacologically: Red boxes show the sequence of steps that lead to increased proliferation in Merlin null meningioma and schwannoma. Due to loss of Merlin, upstream contact inhibition signals are not transduced, therefore macrophage stimulating protein 1/2 (MST1/2) does not phosphorylate large tumour suppressor kinase 1/2 (LATS1/2). Unphosphorylated LATS1/2 will not phosphorylate yes-associated protein (YAP) or Transcriptional coactivator with PDZ-binding motif (TAZ), YAP and TAZ translocate into the nucleus and activate transcription factors such as TEAD family members, leading to upregulation of proteins such as connective tissue growth factor (CTGF) which drive proliferation. TAZ is also required for expression of ALDH1A1 in Merlin null schwannoma and meningioma. Green boxes show the various points in the proposed mechanism where genetic or pharmacological interventions have been used to ameliorate aberrant Hippo pathway activity and reduce proliferation.

There are currently no clinically available chemotherapeutics available for these tumours, which highlights the need to develop targeted therapies for those tumours which are inoperable or recur. In line with previous reports in immortalised cell lines (Striedinger et al., 2008), quantification of fluorescence intensity in Merlin negative and Merlin positive meningioma cells showed a significantly higher proportion of YAP localised within the nucleus in Merlin negative meningiomas. VP was initially developed as a sensitizer for photodynamic therapy but has been shown to inhibit the transcriptional activity of YAP and TAZ. VP has been shown to inhibit YAP and TAZ dependent transcription in multiple different tumour types (Feng et al., 2016, Pan et al., 2016, Felley-Bosco and Stahel, 2014, Liu-Chittenden et al., 2012). We have shown for the first time in primary meningioma cells and cell lines, that VP significantly reduces proliferation when compared to vehicle controls. Merlin negative primary meningiomas undergo a significantly larger reduction in proliferation than Merlin positive primary meningioma cells, suggesting that Merlin negative tumours are more dependent on YAP/TAZ transcriptional activity for proliferation. Despite this, VP remains a rather toxic drug with many off target effects and is thus is not suitable for clinical applications with respect to tumour therapy. Our collaboration with Vivace therapeutics has allowed us to test their orally bioavailable inhibitors of TEAD palmitoylation, a post-translational modification of the TEAD family of proteins which is required for transcriptional activation by YAP or TAZ (Chan et al., 2016). These inhibitors significantly reduce proliferation driven by YAP and TAZ at nanomolar concentrations in primary meningioma and schwannoma cells. Our preliminary data also shows that these compounds are efficacious in the PostnCre-NF2 mouse model and these experiments are currently ongoing. In addition, the conditional NF2/YAP and NF2/TAZ Schwann cell conditional double knockout mice previously developed in our lab driven by the P0 promoter (Mindos et al., 2017b), are currently being bred to the Periostin promoter. Based on what we see with the Vivace

drugs and in the work done by Mindos et al, we would expect that in mice that are PostnCre-NF2$^{fl/fl}$YAP$^{fl/fl}$ and PostnCre-NF2$^{fl/fl}$TAZ$^{fl/fl}$ would have a reduced tumour burden compared to PostnCre-NF2$^{fl/fl}$ single knockout mice. This hypothesis is based on the knockdown experiments we conducted in Merlin null primary meningioma and schwannoma where lentiviral mediated knockdown of YAP and TAZ resulted in significant reductions in proliferation compared to scramble controls. The Vivace compounds tested in this thesis show promise as a therapeutic option for treatment of schwannoma that after further in vivo testing could be moved into early phase clinical trials. In addition, the meningioma mouse models developed by the Mawrin lab (Mawrin, 2017) would be the most suitable mouse model for testing the Vivace compounds in vivo using Merlin negative BM1 cells injected into the skull base or skull convexity.

The RNA sequencing screen conducted in this thesis revealed that the cancer stem cell marker ALDH1A1 is significantly and strongly upregulated at the transcript level in Merlin null mouse Schwann cells, validation confirmed the same result at the protein level in two different Merlin conditional null schwannoma mouse models. Additionally, we see that ALDH1A1 is upregulated in Merlin negative vs Merlin positive meningioma and in human schwannoma biopsies compared to neuromas caused by trauma or healthy vestibular nerve. When we tested orally bioavailable ALDH1A1 inhibitors on primary Merlin negative meningioma and schwannoma cells these drugs significantly reduced proliferation. In a recent study the clinically approved antibiotic nifuroxazide has been shown to selectively bind to the ALDH1 subtype of aldehyde dehydrogenases, which leads to inhibition of enzymatic activity but also leads to oxidation of active site residues leading to cell toxicity (Sarvi et al., 2018). Both the ALDH1A1 inhibitors tested in chapter 3.2 and nifuroxazide warrant in vivo testing in our mouse models to further explore their chemotherapeutic potential in schwannoma and meningioma. The ALDH1A1$^{-/-}$ mouse is viable and displays no peripheral nervous system phenotype compared to ALDH1A1$^{+/+}$

mice (data not shown). We are currently conducting breeding to introduce the ALDH1A1 knockout onto the PostnCre-NF2$^{fl/fl}$ background to assess the importance of ALDH1A1 upregulation in this schwannoma model.

5 Future Work

In vivo work with the Vivace compounds needs to be expanded across multiple timepoints in the Postn-CreNF2 schwannoma mouse model to look at intermediate and later stages of tumour development, this work is currently ongoing in our lab. In addition, testing these compounds in the Mawrin lab's established xenograft meningioma models would allow us to progress from our promising in vitro results. In addition, characterisation of proliferation rates in NF2/YAP and NF2/TAZ double knockout Postn-Cre mice will allow us to further evaluate how important Hippo pathway-driven transcription is in this model of schwannoma. We also plan to develop methodologies to reliably quantify proliferation seen in the vestibular nerves and ganglia of the Postn-Cre mouse. Gehlhausen et al show loss of hearing as a phenotype in Postn-Cre Merlin null mice, detected by click-evoked auditory brainstem response analysis (Gehlhausen et al., 2015). Preliminary work in this area has begun in collaboration with Dr Dan Jagger by adapting the sciatic nerve whole-mount protocol developed by Dun et al (Dun and Parkinson, 2018) in order to detect EdU positive cells within the vestibular apparatus (data not shown). Given that in humans the vestibular nerve is the most common site for schwannoma formation (Guan, 2014), developing a methodology for vestibular nerve analysis in Postn-Cre mice will be important for improving the translational potential of studies using both Vivace and ALDH1A1 inhibitors.

The recent study which identified nifuroxazide as a potent inhibitor of ALDH1 subtypes in melanoma cancer stem cell populations shows exciting potential if validated in models of Merlin null meningioma and schwannoma. Nifuroxazide is already approved clinically at efficacious concentrations and not only inhibits ALDH1 proteins but also appears to give rise to significant cell-specific toxicity in cells which express high levels of ALDH1 (Sarvi et al., 2018). In the Periostin-Cre mouse model ALDH1A1 is strongly upregulated in all Schwann cells and satellite glial cells within the DRG whilst IHC analysis of human schwannoma paraffin sections showed ALDH1A1 was present in all tumour cells compared to controls. Given this, nifuroxazide may be able to specifically cause toxicity within ALDH1A1 overexpressing tumour cells without eliciting an effect on surrounding tissues. Investigating the efficacy of nifuroxazide in terms of proliferation and induction of apoptosis in primary meningioma and schwannoma as well as the Postn-Cre schwannoma mouse model may yield promising results.

6 Conclusion

There is a need to develop targeted therapies as an alternative to surgical resection, which is currently the only clinically available treatment for meningioma and schwannoma tumours. This thesis demonstrates that targeting aberrant Hippo pathway in Merlin negative meningioma and schwannoma tumours may yield promising new therapeutic options. Our RNA sequencing screen identified differentially regulated genes following loss of Merlin in mouse Schwann cells, this led to validation work which identified that the cancer-stem cell marker ALDH1A1 is strongly upregulated following loss of Merlin in multiple models of these tumours as well as in primary patient meningioma and schwannoma tissue. Upregulation of ALDH1A1 is driven by the Hippo effector TAZ in primary meningioma and schwannoma cell lines as well as in the P0-Cre and Postn-Cre mouse models. ALDH1A1 inhibitors show good efficacy in reducing proliferation and

repurposing of the clinically approved drug nifuroxazide could accelerate future in vivo studies, to assess whether targeting ALDH1A1 can reduce tumour burden in meningioma and schwannoma mouse models. TEAD palmitoylation inhibitors produced by Vivace Therapeutics have been used to reduce proliferation in primary meningioma and schwannoma cells, they are efficacious at low concentrations and our preliminary in vivo data should be expanded upon in order to create a mandate for an early-phase clinical trial for treatment of Merlin null meningiomas and schwannomas.

7 References

AMBROGIO, C., GOMEZ-LOPEZ, G., FALCONE, M., VIDAL, A., NADAL, E., CROSETTO, N., BLASCO, R. B., FERNANDEZ-MARCOS, P. J., SANCHEZ-CESPEDES, M., REN, X., WANG, Z., DING, K., HIDALGO, M., SERRANO, M., VILLANUEVA, A., SANTAMARIA, D. & BARBACID, M. 2016. Combined inhibition of DDR1 and Notch signaling is a therapeutic strategy for KRAS-driven lung adenocarcinoma. *Nat Med,* 22**,** 270-7.

AMMOUN, S., CUNLIFFE, C. H., ALLEN, J. C., CHIRIBOGA, L., GIANCOTTI, F. G., ZAGZAG, D., HANEMANN, C. O. & KARAJANNIS, M. A. 2010. ErbB/HER receptor activation and preclinical efficacy of lapatinib in vestibular schwannoma. *Neuro Oncol,* 12**,** 834-43.

AMMOUN, S., SCHMID, M. C., RISTIC, N., ZHOU, L., HILTON, D., ERCOLANO, E., CARROLL, C. & HANEMANN, C. O. 2012. The role of insulin-like growth factors signaling in merlin-deficient human schwannomas. *Glia,* 60**,** 1721-33.

ANSORGE, S., LANTHIER, S., TRANSFIGURACION, J., DUROCHER, Y., HENRY, O. & KAMEN, A. 2009. Development of a scalable process for high-yield lentiviral vector production by transient transfection of HEK293 suspension cultures. *J Gene Med,* 11**,** 868-76.

APICELLA, G., PAOLINI, M., DEANTONIO, L., MASINI, L. & KRENGLI, M. 2016. Radiotherapy for vestibular schwannoma: Review of recent literature results. *Rep Pract Oncol Radiother,* 21**,** 399-406.

BABU, R., SHARMA, R., BAGLEY, J. H., HATEF, J., FRIEDMAN, A. H. & ADAMSON, C. 2013. Vestibular schwannomas in the modern era: epidemiology, treatment trends, and disparities in management. *J Neurosurg,* 119**,** 121-30.

BEAUCHAMP, R. L., ERDIN, S., WITT, L., JORDAN, J. T., PLOTKIN, S. R., GUSELLA, J. F. & RAMESH, V. 2020. mTOR kinase inhibition disrupts neuregulin 1-ERBB3 autocrine signaling and sensitizes NF2-deficient meningioma cellular models to IGF1R inhibition. *J Biol Chem*.

BELLO, M. J., AMINOSO, C., LOPEZ-MARIN, I., ARJONA, D., GONZALEZ-GOMEZ, P., ALONSO, M. E., LOMAS, J., DE CAMPOS, J. M., KUSAK, M. E., VAQUERO, J., ISLA, A., GUTIERREZ, M., SARASA, J. L. & REY, J. A. 2004. DNA methylation of multiple promoter-associated CpG islands in meningiomas: relationship with the allelic status at 1p and 22q. *Acta Neuropathol,* 108**,** 413-21.

BOETTO, J., APRA, C., BIELLE, F., PEYRE, M. & KALAMARIDES, M. 2018. Selective vulnerability of the primitive meningeal layer to prenatal Smo activation for skull base meningothelial meningioma formation. *Oncogene,* 37**,** 4955-4963.

BOIN, A., COUVELARD, A., COUDERC, C., BRITO, I., FILIPESCU, D., KALAMARIDES, M., BEDOSSA, P., DE KONING, L., DANELSKY, C., DUBOIS, T., HUPE, P., LOUVARD, D. & LALLEMAND, D. 2014. Proteomic screening identifies a YAP-driven signaling network linked to tumor cell proliferation in human schwannomas. *Neuro Oncol,* 16**,** 1196-209.

BOSTROM, J., MEYER-PUTTLITZ, B., WOLTER, M., BLASCHKE, B., WEBER, R. G., LICHTER, P., ICHIMURA, K., COLLINS, V. P. & REIFENBERGER, G. 2001. Alterations of the tumor suppressor genes CDKN2A (p16(INK4a)), p14(ARF), CDKN2B (p15(INK4b)), and CDKN2C (p18(INK4c)) in atypical and anaplastic meningiomas. *Am J Pathol,* 159**,** 661-9.

CALSES, P. C., CRAWFORD, J. J., LILL, J. R. & DEY, A. 2019. Hippo Pathway in Cancer: Aberrant Regulation and Therapeutic Opportunities. *Trends Cancer,* 5**,** 297-307.

CEA-SORIANO, L., WALLANDER, M. A. & GARCIA RODRIGUEZ, L. A. 2012. Epidemiology of meningioma in the United Kingdom. *Neuroepidemiology,* 39**,** 27-34.

CHAN, P., HAN, X., ZHENG, B., DERAN, M., YU, J., JARUGUMILLI, G. K., DENG, H., PAN, D., LUO, X. & WU, X. 2016. Autopalmitoylation of TEAD proteins regulates transcriptional output of the Hippo pathway. *Nat Chem Biol,* 12**,** 282-9.

CHARKOFTAKI, G., THOMPSON, D. C., GOLLA, J. P., GARCIA-MILIAN, R., LAM, T. T., ENGEL, J. & VASILIOU, V. 2019. Integrated multi-omics approach reveals a role of ALDH1A1 in lipid metabolism in human colon cancer cells. *Chem Biol Interact,* 304**,** 88-96.

CHEN, M. C., TSENG, T. M., HUNG, S. H. & CHEN, P. Y. 2014. Facial nerve schwannoma: A case report and review of the literature. *Oncol Lett,* 8**,** 2787-2789.

CHEN, X., XIONG, D., YE, L., WANG, K., HUANG, L., MEI, S., WU, J., CHEN, S., LAI, X., ZHENG, L. & WANG, M. 2019. Up-regulated lncRNA XIST contributes to progression of cervical cancer via regulating miR-140-5p and ORC1. *Cancer Cell Int,* 19**,** 45.

CHUTE, J. P., MURAMOTO, G. G., WHITESIDES, J., COLVIN, M., SAFI, R., CHAO, N. J. & MCDONNELL, D. P. 2006. Inhibition of aldehyde dehydrogenase and retinoid signaling induces the expansion of human hematopoietic stem cells. *Proc Natl Acad Sci U S A,* 103**,** 11707-12.

CICCONE, V., TERZUOLI, E., DONNINI, S., GIACHETTI, A., MORBIDELLI, L. & ZICHE, M. 2019. Correction to: Stemness marker ALDH1A1 promotes tumor angiogenesis via retinoic acid/HIF-1alpha/VEGF signalling in MCF-7 breast cancer cells. *J Exp Clin Cancer Res,* 38**,** 45.

COOPER, J. & GIANCOTTI, F. G. 2014. Molecular insights into NF2/Merlin tumor suppressor function. *FEBS Lett,* 588**,** 2743-52.

COSTA-SILVA, J., DOMINGUES, D. & LOPES, F. M. 2017. RNA-Seq differential expression analysis: An extended review and a software tool. *PLoS One,* 12**,** e0190152.

CUI, Y., GROTH, S., TROUTMAN, S., CARLSTEDT, A., SPERKA, T., RIECKEN, L. B., KISSIL, J. L., JIN, H. & MORRISON, H. 2019. The NF2 tumor suppressor merlin interacts with Ras and RasGAP, which may modulate Ras signaling. *Oncogene,* 38**,** 6370-6381.

DE MARIA, R. 2017. beta1 integrin-dependent Rac/group I PAK signaling mediates YAP activation of Yes-associated protein 1 (YAP1) via NF2/merlin. *Pharmacol Ther,* 292**,** 19179-19197.

DENISENKO, N., CIFUENTES-DIAZ, C., IRINOPOULOU, T., CARNAUD, M., BENOIT, E., NIWA-KAWAKITA, M., CHAREYRE, F., GIOVANNINI, M., GIRAULT, J. A. & GOUTEBROZE, L. 2008. Tumor Suppressor Schwannomin/Merlin Is Critical for the Organization of Schwann Cell Contacts in Peripheral Nerves. *Journal of Neuroscience,* 28**,** 10472-10481.

DILWALI, S., PATEL, P. B., ROBERTS, D. S., BASINSKY, G. M., HARRIS, G. J., EMERICK, K. S. & STANKOVIC, K. M. 2014. Primary culture of human Schwann and schwannoma cells: improved and simplified protocol. *Hear Res,* 315**,** 25-33.

DUN, X. P. & PARKINSON, D. B. 2018. Whole Mount Immunostaining on Mouse Sciatic Nerves to Visualize Events of Peripheral Nerve Regeneration. *Methods Mol Biol,* 1739**,** 339-348.

DUNN, J., FERLUGA, S., SHARMA, V., FUTSCHIK, M., HILTON, D. A., ADAMS, C. L., LASONDER, E. & HANEMANN, C. O. 2019. Proteomic analysis discovers the differential expression of novel proteins and phosphoproteins in meningioma including NEK9, HK2 and SET and deregulation of RNA metabolism. *EBioMedicine,* 40**,** 77-91.

EALES, K. L., WILKINSON, E. A., CRUICKSHANK, G., TUCKER, J. H. R. & TENNANT, D. A. 2018. Verteporfin selectively kills hypoxic glioma cells through iron-binding and increased production of reactive oxygen species. *Sci Rep,* 8**,** 14358.

EVANS, D. G. R., MORAN, T., KING, A., SAEED, S., GURUSINGHE, J. & RAMSDEN, R. 2005. Incidence of vestibular schwannoma and neurofibromatosis 2 in the North West of England over a 10-year period: Higher incidence than previously thought. *Otology & Neurotology,* 26**,** 93-97.

FAN, X., MOLOTKOV, A., MANABE, S., DONMOYER, C. M., DELTOUR, L., FOGLIO, M. H., CUENCA, A. E., BLANER, W. S., LIPTON, S. A. & DUESTER, G. 2003. Targeted disruption of Aldh1a1 (Raldh1) provides evidence for a complex mechanism of retinoic acid synthesis in the developing retina. *Mol Cell Biol,* 23**,** 4637-48.

FELLEY-BOSCO, E. & STAHEL, R. 2014. Hippo/YAP pathway for targeted therapy. *Transl Lung Cancer Res,* 3**,** 75-83.

FELTRI, M. L., D'ANTONIO, M., PREVITALI, S., FASOLINI, M., MESSING, A. & WRABETZ, L. 1999. P0-Cre Transgenic Mice for Inactivation of Adhesion Molecules in Schwann Cells. *Ann N Y Acad Sci,* 883**,** 116-123.

FENG, J., GOU, J., JIA, J., YI, T., CUI, T. & LI, Z. 2016. Verteporfin, a suppressor of YAP-TEAD complex, presents promising antitumor properties on ovarian cancer. *Onco Targets Ther,* 9**,** 5371-81.

FISHER, J. C. 1958. Multiple-mutation theory of carcinogenesis. *Nature,* 181**,** 651-2.

FRAENZER, J. T., PAN, H., MINIMO, L., JR., SMITH, G. M., KNAUER, D. & HUNG, G. 2003. Overexpression of the NF2 gene inhibits schwannoma cell proliferation through promoting PDGFR degradation. *Int J Oncol,* 23**,** 1493-500.

FRIEDRICH, S., SCHWABE, K., KLEIN, R., KRUSCHE, C. A., KRAUSS, J. K. & NAKAMURA, M. 2012. Comparative morphological and immunohistochemical study of human meningioma after intracranial transplantation into nude mice. *J Neurosci Methods,* 205**,** 1-9.

GAO, F., ZHOU, B., XU, J. C., GAO, X., LI, S. X., ZHU, G. C., ZHANG, X. G. & YANG, C. 2015. The role of LGR5 and ALDH1A1 in non-small cell lung cancer: Cancer progression and prognosis. *Biochem Biophys Res Commun,* 462**,** 91-8.

GEHLHAUSEN, J. R., PARK, S. J., HICKOX, A. E., SHEW, M., STASER, K., RHODES, S. D., MENON, K., LAJINESS, J. D., MWANTHI, M., YANG, X., YUAN, J., TERRITO, P., HUTCHINS, G., NALEPA, G., YANG, F. C., CONWAY, S. J., HEINZ, M. G., STEMMER-RACHAMIMOV, A., YATES, C. W. & WADE CLAPP, D. 2015. A murine model of neurofibromatosis type 2 that accurately phenocopies human schwannoma formation. *Hum Mol Genet,* 24**,** 1-8.

GIOVANNINI, M., ROBANUS-MAANDAG, E., VAN DER VALK, M., NIWA-KAWAKITA, M., ABRAMOWSKI, V., GOUTEBROZE, L., WOODRUFF, J. M., BERNS, A. & THOMAS, G. 2000. Conditional biallelic Nf2 mutation in the

mouse promotes manifestations of human neurofibromatosis type 2. *Genes Dev,* 14**,** 1617-30.
GONZALEZ-GOMEZ, P., BELLO, M. J., ALONSO, M. E., LOMAS, J., ARJONA, D., CAMPOS, J. M., VAQUERO, J., ISLA, A., LASSALETTA, L., GUTIERREZ, M., SARASA, J. L. & REY, J. A. 2003. CpG island methylation in sporadic and neurofibromatis type 2-associated schwannomas. *Clin Cancer Res,* 9**,** 5601-6.
GOUSIAS, K., SCHRAMM, J. & SIMON, M. 2016. The Simpson grading revisited: aggressive surgery and its place in modern meningioma management. *J Neurosurg,* 125**,** 551-60.
GOUTAGNY, S., GIOVANNINI, M. & KALAMARIDES, M. 2017. A 4-year phase II study of everolimus in NF2 patients with growing vestibular schwannomas. *J Neurooncol,* 133**,** 443-445.
GRAILLON, T., SANSON, M., CAMPELLO, C., IDBAIH, A., PEYRE, M., PEYRIERE, H., BASSET, N., AUTRAN, D., ROCHE, C., KALAMARIDES, M., ROCHE, P. H., FUENTES, S., TABOURET, E., BARRIE, M., COHEN, A., HONORE, S., BOUCEKINE, M., BAUMSTARCK, K., FIGARELLA-BRANGER, D., BARLIER, A., DUFOUR, H. & CHINOT, O. L. 2020. Everolimus and Octreotide for Patients with Recurrent Meningioma: Results from the Phase II CEVOREM Trial. *Clin Cancer Res,* 26**,** 552-557.
GUAN, K. L. 2014. Schwannomas and their pathogenesis. *EMBO Rep,* 24**,** 205-20.
GUERRANT, W., KOTA, S., TROUTMAN, S., MANDATI, V., FALLAHI, M., STEMMER-RACHAMIMOV, A. & KISSIL, J. L. 2016. YAP mediates tumorigenesis in neurofibromatosis type 2 by promoting cell survival and proliferation through a COX-2-EGFR signaling axis. *Cancer Res,* 76**,** 3507-19.
GUMBINER, B. M. & KIM, N. G. 2014. The Hippo-YAP signaling pathway and contact inhibition of growth. *J Cell Sci,* 127**,** 709-17.
HALLIDAY, D., PARRY, A. & EVANS, D. G. 2019. Neurofibromatosis type 2 and related disorders. *Curr Opin Oncol,* 31**,** 562-567.
HANAHAN, D. & WEINBERG, R. A. 2000. The hallmarks of cancer. *Cell,* 100**,** 57-70.
HANAHAN, D. & WEINBERG, R. A. 2011. Hallmarks of cancer: the next generation. *Cell,* 144**,** 646-74.
HANEMANN, C. O. 2008. Magic but treatable? Tumours due to loss of merlin. *Brain,* 131**,** 606-15.
HANSSON, C. M., BUCKLEY, P. G., GRIGELIONIENE, G., PIOTROWSKI, A., HELLSTROM, A. R., MANTRIPRAGADA, K., JARBO, C., MATHIESEN, T. & DUMANSKI, J. P. 2007. Comprehensive genetic and epigenetic analysis of sporadic meningioma for macro-mutations on 22q and micro-mutations within the NF2 locus. *BMC Genomics,* 8**,** 16.
HARVEY, K. F., ZHANG, X. & THOMAS, D. M. 2013. The Hippo pathway and human cancer. *Nat Rev Cancer,* 13**,** 246-57.
HASKINS, J. W., NGUYEN, D. X. & STERN, D. F. 2014. Neuregulin 1-activated ERBB4 interacts with YAP to induce Hippo pathway target genes and promote cell migration. *Sci Signal,* 7**,** ra116.
HAVIK, A. L., BRULAND, O., MYRSETH, E., MILETIC, H., AARHUS, M., KNAPPSKOG, P. M. & LUND-JOHANSEN, M. 2018. Genetic landscape of sporadic vestibular schwannoma. *J Neurosurg,* 128**,** 911-922.
HENNIGAN, R. F., FLETCHER, J. S., GUARD, S. & RATNER, N. 2019. Proximity biotinylation identifies a set of conformation-specific interactions between Merlin and cell junction proteins. *Sci Signal,* 12.
HIRSCH, C. D., SPRINGER, N. M. & HIRSCH, C. N. 2015. Genomic limitations to RNA sequencing expression profiling. *Plant J,* 84**,** 491-503.

HONG, W. 2013. Angiomotin'g YAP into the nucleus for cell proliferation and cancer development. *Sci Signal,* 6**,** pe27.
HOSHINO, Y., NISHIDA, J., KATSUNO, Y., KOINUMA, D., AOKI, T., KOKUDO, N., MIYAZONO, K. & EHATA, S. 2015. Smad4 Decreases the Population of Pancreatic Cancer-Initiating Cells through Transcriptional Repression of ALDH1A1. *Am J Pathol,* 185**,** 1457-70.
HUNG, G., LI, X., FAUDOA, R., XEU, Z., KLUWE, L., RHIM, J. S., SLATTERY, W. & LIM, D. 2002. Establishment and characterization of a schwannoma cell line from a patient with neurofibromatosis 2. *Int J Oncol,* 20**,** 475-82.
HWANG, J. H., KIM, A. R., KIM, K. M., IL PARK, J., OH, H. T., MOON, S. A., BYUN, M. R., JEONG, H., KIM, H. K., YAFFE, M. B., HWANG, E. S. & HONG, J. H. 2019. TAZ couples Hippo/Wnt signalling and insulin sensitivity through Irs1 expression. *Nat Commun,* 10**,** 421.
ISHII, N., MAIER, D., MERLO, A., TADA, M., SAWAMURA, Y., DISERENS, A. C. & VAN MEIR, E. G. 1999. Frequent co-alterations of TP53, p16/CDKN2A, p14ARF, PTEN tumor suppressor genes in human glioma cell lines. *Brain Pathol,* 9**,** 469-79.
JAMES, M. F., HAN, S., POLIZZANO, C., PLOTKIN, S. R., MANNING, B. D., STEMMER-RACHAMIMOV, A. O., GUSELLA, J. F. & RAMESH, V. 2009. NF2/merlin is a novel negative regulator of mTOR complex 1, and activation of mTORC1 is associated with meningioma and schwannoma growth. *Mol Cell Biol,* 29**,** 4250-61.
JANESICK, A., WU, S. C. & BLUMBERG, B. 2015. Retinoic acid signaling and neuronal differentiation. *Cell Mol Life Sci,* 72**,** 1559-76.
JANUCHOWSKI, R., WOJTOWICZ, K., STERZYSKA, K., SOSISKA, P., ANDRZEJEWSKA, M., ZAWIERUCHA, P., NOWICKI, M. & ZABEL, M. 2016. Inhibition of ALDH1A1 activity decreases expression of drug transporters and reduces chemotherapy resistance in ovarian cancer cell lines. *Int J Biochem Cell Biol,* 78**,** 248-259.
JESSEN, K. R. & MIRSKY, R. 2019. The Success and Failure of the Schwann Cell Response to Nerve Injury. *Front Cell Neurosci,* 13**,** 33.
JESSEN, K. R., MIRSKY, R. & LLOYD, A. C. 2015. Schwann Cells: Development and Role in Nerve Repair. *Cold Spring Harb Perspect Biol,* 7**,** a020487.
JIAO, S., WANG, H., SHI, Z., DONG, A., ZHANG, W., SONG, X., HE, F., WANG, Y., ZHANG, Z., WANG, W., WANG, X., GUO, T., LI, P., ZHAO, Y., JI, H., ZHANG, L. & ZHOU, Z. 2014. A peptide mimicking VGLL4 function acts as a YAP antagonist therapy against gastric cancer. *Cancer Cell,* 25**,** 166-80.
JOSEPH, N. M., MOSHER, J. T., BUCHSTALLER, J., SNIDER, P., MCKEEVER, P. E., LIM, M., CONWAY, S. J., PARADA, L. F., ZHU, Y. & MORRISON, S. J. 2008. The loss of Nf1 transiently promotes self-renewal but not tumorigenesis by neural crest stem cells. *Cancer Cell,* 13**,** 129-40.
KALAMARIDES, M., NIWA-KAWAKITA, M., LEBLOIS, H., ABRAMOWSKI, V., PERRICAUDET, M., JANIN, A., THOMAS, G., GUTMANN, D. H. & GIOVANNINI, M. 2002. Nf2 gene inactivation in arachnoidal cells is rate-limiting for meningioma development in the mouse. *Genes Dev,* 16**,** 1060-5.
KALAMARIDES, M., STEMMER-RACHAMIMOV, A. O., NIWA-KAWAKITA, M., CHAREYRE, F., TARANCHON, E., HAN, Z. Y., MARTINELLI, C., LUSIS, E. A., HEGEDUS, B., GUTMANN, D. H. & GIOVANNINI, M. 2011. Identification of a progenitor cell of origin capable of generating diverse meningioma histological subtypes. *Oncogene,* 30**,** 2333-44.
KALANTARI, E., SAADI, F. H., ASGARI, M., SHARIFTABRIZI, A., ROUDI, R. & MADJD, Z. 2017. Increased Expression of ALDH1A1 in Prostate Cancer is

Correlated With Tumor Aggressiveness: A Tissue Microarray Study of Iranian Patients. *Appl Immunohistochem Mol Morphol,* 25**,** 592-598.
KILLEEN, D. E., KLESSE, L., TOLISANO, A. M., HUNTER, J. B. & KUTZ, J. W., JR. 2019. Long-Term Effects of Bevacizumab on Vestibular Schwannoma Volume in Neurofibromatosis Type 2 Patients. *J Neurol Surg B Skull Base,* 80**,** 540-546.
KIM, H., KIM, M., IM, S. K. & FANG, S. 2018. Mouse Cre-LoxP system: general principles to determine tissue-specific roles of target genes. *Lab Anim Res,* 34**,** 147-159.
KIM, M., KIM, S., LEE, S. H., KIM, W., SOHN, M. J., KIM, H. S., KIM, J. & JHO, E. H. 2016. Merlin inhibits Wnt/beta-catenin signaling by blocking LRP6 phosphorylation. *Cell Death Differ,* 23**,** 1638-47.
KIM, M. H. & KIM, J. 2017. Role of YAP/TAZ transcriptional regulators in resistance to anti-cancer therapies. *Cell Mol Life Sci,* 74**,** 1457-1474.
KIM, N. G. & GUMBINER, B. M. 2019. Cell contact and Nf2/Merlin-dependent regulation of TEAD palmitoylation and activity. *Proc Natl Acad Sci U S A,* 116**,** 9877-9882.
KISSIL, J. L., WILKER, E. W., JOHNSON, K. C., ECKMAN, M. S., YAFFE, M. B. & JACKS, T. 2003. Merlin, the product of the Nf2 tumor suppressor gene, is an inhibitor of the p21-activated kinase, Pak1. *Mol Cell,* 12**,** 841-9.
KNUDSON, A. 2001. Alfred Knudson and his two-hit hypothesis. (Interview by Ezzie Hutchinson). *Lancet Oncol,* 2**,** 642-5.
KOHN, F. R., LANDKAMER, G. J., MANTHEY, C. L., RAMSAY, N. K. & SLADEK, N. E. 1987. Effect of aldehyde dehydrogenase inhibitors on the ex vivo sensitivity of human multipotent and committed hematopoietic progenitor cells and malignant blood cells to oxazaphosphorines. *Cancer Res,* 47**,** 3180-5.
KSHETTRY, V. R., OSTROM, Q. T., KRUCHKO, C., AL-MEFTY, O., BARNETT, G. H. & BARNHOLTZ-SLOAN, J. S. 2015. Descriptive epidemiology of World Health Organization grades II and III intracranial meningiomas in the United States. *Neuro Oncol,* 17**,** 1166-73.
LALLEMAND, D., MANENT, J., COUVELARD, A., WATILLIAUX, A., SIENA, M., CHAREYRE, F., LAMPIN, A., NIWA-KAWAKITA, M., KALAMARIDES, M. & GIOVANNINI, M. 2009. Merlin regulates transmembrane receptor accumulation and signaling at the plasma membrane in primary mouse Schwann cells and in human schwannomas. *Oncogene,* 28**,** 854-65.
LAMAR, J. M., STERN, P., LIU, H., SCHINDLER, J. W., JIANG, Z. G. & HYNES, R. O. 2012. The Hippo pathway target, YAP, promotes metastasis through its TEAD-interaction domain. *Proc Natl Acad Sci U S A,* 109**,** E2441-50.
LI, W., COOPER, J., ZHOU, L., YANG, C., ERDJUMENT-BROMAGE, H., ZAGZAG, D., SNUDERL, M., LADANYI, M., HANEMANN, C. O., ZHOU, P., KARAJANNIS, M. A. & GIANCOTTI, F. G. 2014a. Merlin/NF2 loss-driven tumorigenesis linked to CRL4(DCAF1)-mediated inhibition of the hippo pathway kinases Lats1 and 2 in the nucleus. *Cancer Cell,* 26**,** 48-60.
LI, W., YOU, L., COOPER, J., SCHIAVON, G., PEPE-CAPRIO, A., ZHOU, L., ISHII, R., GIOVANNINI, M., HANEMANN, C. O., LONG, S. B., ERDJUMENT-BROMAGE, H., ZHOU, P., TEMPST, P. & GIANCOTTI, F. G. 2010. Merlin/NF2 suppresses tumorigenesis by inhibiting the E3 ubiquitin ligase CRL4(DCAF1) in the nucleus. *Cell,* 140**,** 477-90.
LI, X. S., XU, Q., FU, X. Y. & LUO, W. S. 2014b. ALDH1A1 overexpression is associated with the progression and prognosis in gastric cancer. *BMC Cancer,* 14**,** 705.

LI, Y., GUO, M., FU, Z., WANG, P., ZHANG, Y., GAO, Y., YUE, M., NING, S. & LI, D. 2017. Immunoglobulin superfamily genes are novel prognostic biomarkers for breast cancer. *Oncotarget,* 8**,** 2444-2456.

LIESCHE, F., GRIESSMAIR, M., BARZ, M., GEMPT, J. & SCHLEGEL, J. 2019a. ALDH1-A new immunohistochemical diagnostic marker for Schwann cell-derived tumors. *Clinical Neuropathology,* 38**,** 168-173.

LIESCHE, F., GRIESSMAIR, M., BARZ, M., GEMPT, J. & SCHLEGEL, J. 2019b. ALDH1 - A new immunohistochemical diagnostic marker for Schwann cell-derived tumors. *Clin Neuropathol,* 38**,** 168-173.

LINDSLEY, A., SNIDER, P., ZHOU, H., ROGERS, R., WANG, J., OLAOPA, M., KRUZYNSKA-FREJTAG, A., KOUSHIK, S. V., LILLY, B., BURCH, J. B., FIRULLI, A. B. & CONWAY, S. J. 2007. Identification and characterization of a novel Schwann and outflow tract endocardial cushion lineage-restricted periostin enhancer. *Dev Biol,* 307**,** 340-55.

LIU-CHITTENDEN, Y., HUANG, B., SHIM, J. S., CHEN, Q., LEE, S. J., ANDERS, R. A., LIU, J. O. & PAN, D. 2012. Genetic and pharmacological disruption of the TEAD-YAP complex suppresses the oncogenic activity of YAP. *Genes Dev,* 26**,** 1300-5.

LIU, K. L., FAN, J. H. & WU, J. 2017. Forkhead Box Protein J1 (FOXJ1) is Overexpressed in Colorectal Cancer and Promotes Nuclear Translocation of beta-Catenin in SW620 Cells. *Medical Science Monitor,* 23**,** 856-866.

LIU, L., CAI, S., HAN, C., BANERJEE, A., WU, D., CUI, T., XIE, G., ZHANG, J., ZHANG, X., MCLAUGHLIN, E., YIN, M., BACKES, F. J., CHAKRAVARTI, A., ZHENG, Y. & WANG, Q. E. 2019. ALDH1A1 contributes to PARP inhibitor resistance via enhancing DNA repair in BRCA2-/- ovarian cancer cells. *Mol Cancer Ther*.

LIU, R. Z., GARCIA, E., GLUBRECHT, D. D., POON, H. Y., MACKEY, J. R. & GODBOUT, R. 2015. CRABP1 is associated with a poor prognosis in breast cancer: adding to the complexity of breast cancer cell response to retinoic acid. *Mol Cancer,* 14**,** 129.

LOMAS, J., BELLO, M. J., ARJONA, D., ALONSO, M. E., MARTINEZ-GLEZ, V., LOPEZ-MARIN, I., AMINOSO, C., DE CAMPOS, J. M., ISLA, A., VAQUERO, J. & REY, J. A. 2005. Genetic and epigenetic alteration of the NF2 gene in sporadic meningiomas. *Genes Chromosomes Cancer,* 42**,** 314-9.

MANTIONE, K. J., KREAM, R. M., KUZELOVA, H., PTACEK, R., RABOCH, J., SAMUEL, J. M. & STEFANO, G. B. 2014. Comparing bioinformatic gene expression profiling methods: microarray and RNA-Seq. *Med Sci Monit Basic Res,* 20**,** 138-42.

MANZONI, C., KIA, D. A., VANDROVCOVA, J., HARDY, J., WOOD, N. W., LEWIS, P. A. & FERRARI, R. 2018. Genome, transcriptome and proteome: the rise of omics data and their integration in biomedical sciences. *Brief Bioinform,* 19**,** 286-302.

MAO, X., LI, P., WANG, Y., LIANG, Z., LIU, J., LI, J., JIANG, Y., BAO, G., LI, L., ZHU, B., REN, Y., ZHAO, X., ZHANG, J., LIU, Y., YANG, J. & LIU, P. 2017. CRB3 regulates contact inhibition by activating the Hippo pathway in mammary epithelial cells. *Cell Death Dis,* 8**,** e2546.

MAROSI, C., HASSLER, M., ROESSLER, K., RENI, M., SANT, M., MAZZA, E. & VECHT, C. 2008. Meningioma. *Crit Rev Oncol Hematol,* 67**,** 153-71.

MAUGERI-SACCA, M. 2018. The Hippo pathway in normal development and cancer.

MAUGERI-SACCA, M. & DE MARIA, R. 2018. The Hippo pathway in normal development and cancer. *Pharmacol Ther*.

MAUGERI-SACCA, M., DE MARIA, R., SABRA, H., BRUNNER, M., MANDATI, V., WEHRLE-HALLER, B., LALLEMAND, D., RIBBA, A. S., CHEVALIER, G., GUARDIOLA, P., BLOCK, M. R., BOUVARD, D., YESILOZ, U., KIRCHES, E., HARTMANN, C., SCHOLZ, J., KROPF, S., SAHM, F., NAKAMURA, M., MAWRIN, C., TANG, H., ZHU, H., WANG, X., HUA, L., LI, J., XIE, Q., CHEN, X., ZHANG, T., GONG, Y., MEI, Y., BI, W. L., GREENWALD, N. F., AGAR, N. Y., BEROUKHIM, R., DUNN, G. P., DUNN, I. F., SANTUCCI, M., VIGNUDELLI, T., FERRARI, S., MOR, M., SCALVINI, L., BOLOGNESI, M. L., ULIASSI, E., COSTI, M. P., MO, J. S., PARK, H. W., GUAN, K. L., HILTON, D. A., HANEMANN, C. O., FREEMAN, A. K., MORRISON, D. K. & HANEMANN, C. O. 2018. The Hippo pathway in normal development and cancer

beta1 integrin-dependent Rac/group I PAK signaling mediates YAP activation of Yes-associated protein 1 (YAP1) via NF2/merlin

Frequent AKT1E17K mutations in skull base meningiomas are associated with mTOR and ERK1/2 activation and reduced time to tumor recurrence

KLF4 is a tumor suppressor in anaplastic meningioma stem-like cells and human meningiomas

Genomic profile of human meningioma cell lines

The Hippo Pathway and YAP/TAZ-TEAD Protein-Protein Interaction as Targets for Regenerative Medicine and Cancer Treatment

The Hippo signaling pathway in stem cell biology and cancer

Schwannomas and their pathogenesis

14-3-3 Proteins: diverse functions in cell proliferation and cancer progression

Magic but treatable? Tumours due to loss of merlin. *Pharmacol Ther,* 292**,** 19179-19197.

MAWRIN, C. 2017. Animal models of meningiomas. *Chin Clin Oncol,* 6**,** S6.

MAWRIN, C., CHUNG, C. & PREUSSER, M. 2015. Biology and clinical management challenges in meningioma. *Am Soc Clin Oncol Educ Book***,** e106-15.

MCCLATCHEY, A. I. & FEHON, R. G. 2009. Merlin and the ERM proteins--regulators of receptor distribution and signaling at the cell cortex. *Trends Cell Biol,* 19**,** 198-206.

MCCLATCHEY, A. I., SAOTOME, I., MERCER, K., CROWLEY, D., GUSELLA, J. F., BRONSON, R. T. & JACKS, T. 1998. Mice heterozygous for a mutation at the Nf2 tumor suppressor locus develop a range of highly metastatic tumors. *Genes Dev,* 12**,** 1121-33.

MCCLATCHEY, A. I., SAOTOME, I., RAMESH, V., GUSELLA, J. F. & JACKS, T. 1997. The Nf2 tumor suppressor gene product is essential for extraembryonic development immediately prior to gastrulation. *Genes Dev,* 11**,** 1253-65.

MCCLATCHEY, A. I. & YAP, A. S. 2012. Contact inhibition (of proliferation) redux. *Curr Opin Cell Biol,* 24**,** 685-94.

MINDOS, T., DUN, X., NORTH, K., DODDRELL, R. D. S., SCHULZ, A., EDWARDS, P., RUSSELL, J., GRAY, B., ROBERTS, S. L., SHIVANE, A., MORTIMER, G., PIRIE, M., ZHANG, N., PAN, D., MORRISON, H. & PARKINSON, D. B. 2017a. Merlin controls the repair capacity of Schwann cells after injury by regulating Hippo/YAP activity. *J Cell Biol,* 216**,** 495-510.

MINDOS, T., DUN, X. P., NORTH, K., DODDRELL, R. D., SCHULZ, A., EDWARDS, P., RUSSELL, J., GRAY, B., ROBERTS, S. L., SHIVANE, A., MORTIMER, G., PIRIE, M., ZHANG, N., PAN, D., MORRISON, H. & PARKINSON, D. B. 2017b. Merlin controls the repair capacity of Schwann cells after injury by regulating Hippo/YAP activity. *J Cell Biol,* 216**,** 495-510.
MIYAMOTO, T., MORITA, K., TAKEMOTO, D., TAKEUCHI, K., KITANO, Y., MIYAKAWA, T., NAKAYAMA, K., OKAMURA, Y., SASAKI, H., MIYACHI, Y., FURUSE, M. & TSUKITA, S. 2005. Tight junctions in Schwann cells of peripheral myelinated axons: a lesson from claudin-19-deficient mice. *J Cell Biol,* 169**,** 527-38.
MIYANAGA, A., MASUDA, M., TSUTA, K., KAWASAKI, K., NAKAMURA, Y., SAKUMA, T., ASAMURA, H., GEMMA, A. & YAMADA, T. 2015. Hippo pathway gene mutations in malignant mesothelioma: revealed by RNA and targeted exon sequencing. *J Thorac Oncol,* 10**,** 844-51.
MO, J. S., PARK, H. W. & GUAN, K. L. 2014. The Hippo signaling pathway in stem cell biology and cancer. *EMBO Rep,* 15**,** 642-56.
MOROISHI, T., HAYASHI, T., PAN, W. W., FUJITA, Y., HOLT, M. V., QIN, J., CARSON, D. A. & GUAN, K. L. 2016. The Hippo Pathway Kinases LATS1/2 Suppress Cancer Immunity. *Cell,* 167**,** 1525-1539.e17.
MORRISON, H., SHERMAN, L. S., LEGG, J., BANINE, F., ISACKE, C., HAIPEK, C. A., GUTMANN, D. H., PONTA, H. & HERRLICH, P. 2001a. The NF2 tumor suppressor gene product, merlin, mediates contact inhibition of growth through interactions with CD44. *Genes Dev,* 15**,** 968-80.
MORRISON, H., SHERMAN, L. S., LEGG, J., BANINE, F., ISACKE, G., HAIPEK, C. A., GUTMANN, D. H., PONTA, H. & HERRLICH, P. 2001b. The NF2 tumor suppressor gene product, merlin, mediates contact inhibition of growth through interactions with CD44. *Genes & Development,* 15**,** 968-980.
MURNYAK, B., BOGNAR, L., KLEKNER, A. & HORTOBAGYI, T. 2015. Epigenetics of Meningiomas. *Biomed Res Int,* 2015**,** 532451.
NAMEKAWA, T., IKEDA, K., HORIE-INOUE, K., SUZUKI, T., OKAMOTO, K., ICHIKAWA, T., YANO, A., KAWAKAMI, S. & INOUE, S. 2019. ALDH1A1 in patient-derived bladder cancer spheroids activates retinoic acid signaling leading to TUBB3 overexpression and tumor progression. *Int J Cancer*.
NASSIRI, F., MAMATJAN, Y., SUPPIAH, S., BADHIWALA, J. H., MANSOURI, S., KARIMI, S., SAARELA, O., POISSON, L., GEPFNER-TUMA, I., SCHITTENHELM, J., NG, H. K., NOUSHMEHR, H., HARTER, P., BAUMGARTEN, P., WELLER, M., PREUSSER, M., HEROLD-MENDE, C., TATAGIBA, M., TABATABAI, G., SAHM, F., VON DEIMLING, A., ZADEH, G., ALDAPE, K. D. & INTERNATIONAL CONSORTIUM ON, M. 2019. DNA methylation profiling to predict recurrence risk in meningioma: development and validation of a nomogram to optimize clinical management. *Neuro Oncol*.
NIGIM, F., WAKIMOTO, H., KASPER, E. M., ACKERMANS, L. & TEMEL, Y. 2018. Emerging Medical Treatments for Meningioma in the Molecular Era. *Biomedicines,* 6.
NOLAND, C. L., GIERKE, S., SCHNIER, P. D., MURRAY, J., SANDOVAL, W. N., SAGOLLA, M., DEY, A., HANNOUSH, R. N., FAIRBROTHER, W. J. & CUNNINGHAM, C. N. 2016. Palmitoylation of TEAD Transcription Factors Is Required for Their Stability and Function in Hippo Pathway Signaling. *Structure,* 24**,** 179-186.
NORDEN, A. D., RAIZER, J. J., ABREY, L. E., LAMBORN, K. R., LASSMAN, A. B., CHANG, S. M., YUNG, W. K., GILBERT, M. R., FINE, H. A., MEHTA,

M., DEANGELIS, L. M., CLOUGHESY, T. F., ROBINS, H. I., ALDAPE, K., DANCEY, J., PRADOS, M. D., LIEBERMAN, F. & WEN, P. Y. 2010. Phase II trials of erlotinib or gefitinib in patients with recurrent meningioma. *J Neurooncol,* 96**,** 211-7.

NWANI, N. G., CONDELLO, S., WANG, Y., SWETZIG, W. M., BARBER, E., HURLEY, T. & MATEI, D. 2019. A Novel ALDH1A1 Inhibitor Targets Cells with Stem Cell Characteristics in Ovarian Cancer. *Cancers (Basel),* 11.

OLAR, A., WANI, K. M., WILSON, C. D., ZADEH, G., DEMONTE, F., JONES, D. T., PFISTER, S. M., SULMAN, E. P. & ALDAPE, K. D. 2017. Global epigenetic profiling identifies methylation subgroups associated with recurrence-free survival in meningioma. *Acta Neuropathol,* 133**,** 431-444.

PALDOR, I., ABBADI, S., BONNE, N., YE, X., RODRIGUEZ, F. J., ROWSHANSHAD, D., ITZOE, M., VIGILAR, V., GIOVANNINI, M., BREM, H., BLAKELEY, J. O. & TYLER, B. M. 2017. The efficacy of lapatinib and nilotinib in combination with radiation therapy in a model of NF2 associated peripheral schwannoma. *J Neurooncol,* 135**,** 47-56.

PAN, W., WANG, Q., ZHANG, Y., ZHANG, N., QIN, J., LI, W., WANG, J., WU, F., CAO, L. & XU, G. 2016. Verteporfin can Reverse the Paclitaxel Resistance Induced by YAP Over-Expression in HCT-8/T Cells without Photoactivation through Inhibiting YAP Expression. *Cell Physiol Biochem,* 39**,** 481-90.

PAVELIN, S., BECIC, K., FOREMPOHER, G., TOMIC, S., CAPKUN, V., DRMIC-HOFMAN, I., MRKLIC, I., LUSIC, I. & POGORELIC, Z. 2014. The significance of immunohistochemical expression of merlin, Ki-67, and p53 in meningiomas. *Appl Immunohistochem Mol Morphol,* 22**,** 46-9.

PETRILLI, A. M. & FERNANDEZ-VALLE, C. 2016. Role of Merlin/NF2 inactivation in tumor biology. *Oncogene,* 35**,** 537-48.

PEYRE, M., SALAUD, C., CLERMONT-TARANCHON, E., NIWA-KAWAKITA, M., GOUTAGNY, S., MAWRIN, C., GIOVANNINI, M. & KALAMARIDES, M. 2015. PDGF activation in PGDS-positive arachnoid cells induces meningioma formation in mice promoting tumor progression in combination with Nf2 and Cdkn2ab loss. *Oncotarget,* 6**,** 32713-22.

PICCOLO, S., DUPONT, S. & CORDENONSI, M. 2014. The biology of YAP/TAZ: hippo signaling and beyond. *Physiol Rev,* 94**,** 1287-312.

POULIKAKOS, P. I., XIAO, G. H., GALLAGHER, R., JABLONSKI, S., JHANWAR, S. C. & TESTA, J. R. 2006. Re-expression of the tumor suppressor NF2/merlin inhibits invasiveness in mesothelioma cells and negatively regulates FAK. *Oncogene,* 25**,** 5960-8.

PUTTMANN, S., SENNER, V., BRAUNE, S., HILLMANN, B., EXELER, R., RICKERT, C. H. & PAULUS, W. 2005. Establishment of a benign meningioma cell line by hTERT-mediated immortalization. *Lab Invest,* 85**,** 1163-71.

RICHMOND, A. & SU, Y. 2008. Mouse xenograft models vs GEM models for human cancer therapeutics. *Dis Model Mech,* 1**,** 78-82.

RONG, R., SURACE, E. I., HAIPEK, C. A., GUTMANN, D. H. & YE, K. 2004. Serine 518 phosphorylation modulates merlin intramolecular association and binding to critical effectors important for NF2 growth suppression. *Oncogene,* 23**,** 8447-54.

ROULEAU, G. A., MEREL, P., LUTCHMAN, M., SANSON, M., ZUCMAN, J., MARINEAU, C., HOANG-XUAN, K., DEMCZUK, S., DESMAZE, C., PLOUGASTEL, B. & ET AL. 1993. Alteration in a new gene encoding a putative membrane-organizing protein causes neuro-fibromatosis type 2. *Nature,* 363**,** 515-21.

RUGGIERI, M., PRATICO, A. D., SERRA, A., MAIOLINO, L., COCUZZA, S., DI MAURO, P., LICCIARDELLO, L., MILONE, P., PRIVITERA, G.,

BELFIORE, G., DI PIETRO, M., DI RAIMONDO, F., ROMANO, A., CHIARENZA, A., MUGLIA, M., POLIZZI, A. & EVANS, D. G. 2016. Childhood neurofibromatosis type 2 (NF2) and related disorders: from bench to bedside and biologically targeted therapies. *Acta Otorhinolaryngol Ital,* 36**,** 345-367.

SAHM, F., SCHRIMPF, D., STICHEL, D., JONES, D. T. W., HIELSCHER, T., SCHEFZYK, S., OKONECHNIKOV, K., KOELSCHE, C., REUSS, D. E., CAPPER, D., STURM, D., WIRSCHING, H. G., BERGHOFF, A. S., BAUMGARTEN, P., KRATZ, A., HUANG, K., WEFERS, A. K., HOVESTADT, V., SILL, M., ELLIS, H. P., KURIAN, K. M., OKUDUCU, A. F., JUNGK, C., DRUESCHLER, K., SCHICK, M., BEWERUNGE-HUDLER, M., MAWRIN, C., SEIZ-ROSENHAGEN, M., KETTER, R., SIMON, M., WESTPHAL, M., LAMSZUS, K., BECKER, A., KOCH, A., SCHITTENHELM, J., RUSHING, E. J., COLLINS, V. P., BREHMER, S., CHAVEZ, L., PLATTEN, M., HANGGI, D., UNTERBERG, A., PAULUS, W., WICK, W., PFISTER, S. M., MITTELBRONN, M., PREUSSER, M., HEROLD-MENDE, C., WELLER, M. & VON DEIMLING, A. 2017. DNA methylation-based classification and grading system for meningioma: a multicentre, retrospective analysis. *Lancet Oncol,* 18**,** 682-694.

SARVI, S., CRISPIN, R., LU, Y., ZENG, L., HURLEY, T. D., HOUSTON, D. R., VON KRIEGSHEIM, A., CHEN, C. H., MOCHLY-ROSEN, D., RANZANI, M., MATHERS, M. E., XU, X., XU, W., ADAMS, D. J., CARRAGHER, N. O., FUJITA, M., SCHUCHTER, L., UNCITI-BROCETA, A., BRUNTON, V. G. & PATTON, E. E. 2018. ALDH1 Bio-activates Nifuroxazide to Eradicate ALDH(High) Melanoma-Initiating Cells. *Cell Chem Biol,* 25**,** 1456-1469 e6.

SCHERER, S. S. & GUTMANN, D. H. 1996. Expression of the neurofibromatosis 2 tumor suppressor gene product, merlin, in Schwann cells. *J Neurosci Res,* 46**,** 595-605.

SCHULZ, A., ZOCH, A. & MORRISON, H. 2014. A neuronal function of the tumor suppressor protein merlin. *Acta Neuropathol Commun,* 2**,** 82.

SEKIDO, Y. 2011. Inactivation of Merlin in malignant mesothelioma cells and the Hippo signaling cascade dysregulation. *Pathol Int,* 61**,** 331-44.

SHANZER, M., ADLER, J., RICARDO-LAX, I., REUVEN, N. & SHAUL, Y. 2017. The nonreceptor tyrosine kinase c-Src attenuates SCF(beta-TrCP) E3-ligase activity abrogating Taz proteasomal degradation. *Proc Natl Acad Sci U S A,* 114**,** 1678-1683.

SHIH, K. C., CHOWDHARY, S., ROSENBLATT, P., WEIR, A. B., 3RD, SHEPARD, G. C., WILLIAMS, J. T., SHASTRY, M., BURRIS, H. A., 3RD & HAINSWORTH, J. D. 2016. A phase II trial of bevacizumab and everolimus as treatment for patients with refractory, progressive intracranial meningioma. *J Neurooncol,* 129**,** 281-8.

SHIMIZU, T., SETO, A., MAITA, N., HAMADA, K., TSUKITA, S., TSUKITA, S. & HAKOSHIMA, T. 2002. Structural basis for neurofibromatosis type 2. Crystal structure of the merlin FERM domain. *J Biol Chem,* 277**,** 10332-6.

SLADEK, N. E., KOLLANDER, R., SREERAMA, L. & KIANG, D. T. 2002. Cellular levels of aldehyde dehydrogenases (ALDH1A1 and ALDH3A1) as predictors of therapeutic responses to cyclophosphamide-based chemotherapy of breast cancer: a retrospective study. Rational individualization of oxazaphosphorine-based cancer chemotherapeutic regimens. *Cancer Chemother Pharmacol,* 49**,** 309-21.

SOURBIER, C., LIAO, P. J., RICKETTS, C. J., WEI, D., YANG, Y., BARANES, S. M., GIBBS, B. K., OHANJANIAN, L., SPENCER KRANE, L., SCROGGINS,

B. T., KEITH KILLIAN, J., WEI, M. H., KIJIMA, T., MELTZER, P. S., CITRIN, D. E., NECKERS, L., VOCKE, C. D. & MARSTON LINEHAN, W. 2018. Targeting loss of the Hippo signaling pathway in NF2-deficient papillary kidney cancers. *Oncotarget,* 9**,** 10723-10733.

STRIEDINGER, K., VANDENBERG, S. R., BAIA, G. S., MCDERMOTT, M. W., GUTMANN, D. H. & LAL, A. 2008. The Neurofibromatosis 2 Tumor Suppressor Gene Product, Merlin, Regulates Human Meningioma Cell Growth by Signaling through YAP. *Neoplasia,* 10**,** 1204-12.

SUPPIAH, S., NASSIRI, F., BI, W. L., DUNN, I. F., HANEMANN, C. O., HORBINSKI, C. M., HASHIZUME, R., JAMES, C. D., MAWRIN, C., NOUSHMEHR, H., PERRY, A., SAHM, F., SLOAN, A., VON DEIMLING, A., WEN, P. Y., ALDAPE, K., ZADEH, G. & INTERNATIONAL CONSORTIUM ON, M. 2019. Molecular and translational advances in meningiomas. *Neuro Oncol,* 21**,** i4-i17.

TANAKA, K., SATO, C., MAEDA, Y., KOIKE, M., MATSUTANI, M., YAMADA, K. & MIYAKI, M. 1989. Establishment of a human malignant meningioma cell line with amplified c-myc oncogene. *Cancer,* 64**,** 2243-9.

TANG, C., TAKAHASHI-KANEMITSU, A., KIKUCHI, I., BEN, C. & HATAKEYAMA, M. 2018. Transcriptional Co-activator Functions of YAP and TAZ Are Inversely Regulated by Tyrosine Phosphorylation Status of Parafibromin. *iScience,* 2**,** 103.

TANG, H., ZHU, H., WANG, X., HUA, L., LI, J., XIE, Q., CHEN, X., ZHANG, T. & GONG, Y. 2017. KLF4 is a tumor suppressor in anaplastic meningioma stem-like cells and human meningiomas. *J Mol Cell Biol,* 9**,** 315-324.

TOMITA, H., TANAKA, K., TANAKA, T. & HARA, A. 2016. Aldehyde dehydrogenase 1A1 in stem cells and cancer. *Oncotarget,* 7**,** 11018-32.

TORRES-MARTIN, M., LASSALETTA, L., DE CAMPOS, J. M., ISLA, A., PINTO, G. R., BURBANO, R. R., MELENDEZ, B., CASTRESANA, J. S. & REY, J. A. 2015. Genome-wide methylation analysis in vestibular schwannomas shows putative mechanisms of gene expression modulation and global hypomethylation at the HOX gene cluster. *Genes Chromosomes Cancer,* 54**,** 197-209.

TORRES-MARTIN, M., LASSALETTA, L., SAN-ROMAN-MONTERO, J., DE CAMPOS, J. M., ISLA, A., GAVILAN, J., MELENDEZ, B., PINTO, G. R., BURBANO, R. R., CASTRESANA, J. S. & REY, J. A. 2013. Microarray analysis of gene expression in vestibular schwannomas reveals SPP1/MET signaling pathway and androgen receptor deregulation. *Int J Oncol,* 42**,** 848-62.

TROFATTER, J. A., MACCOLLIN, M. M., RUTTER, J. L., MURRELL, J. R., DUYAO, M. P., PARRY, D. M., ELDRIDGE, R., KLEY, N., MENON, A. G., PULASKI, K. & ET AL. 1993. A novel moesin-, ezrin-, radixin-like gene is a candidate for the neurofibromatosis 2 tumor suppressor. *Cell,* 75**,** 826.

TRUETT, G. E., HEEGER, P., MYNATT, R. L., TRUETT, A. A., WALKER, J. A. & WARMAN, M. L. 2000. Preparation of PCR-quality mouse genomic DNA with hot sodium hydroxide and tris (HotSHOT). *Biotechniques,* 29**,** 52, 54.

TSAI, H. C., HUANG, C. Y., SU, H. L. & TANG, C. H. 2014. CTGF increases drug resistance to paclitaxel by upregulating survivin expression in human osteosarcoma cells. *Biochim Biophys Acta,* 1843**,** 846-54.

TUCHEN, M., WILISCH-NEUMANN, A., DANIEL, E. A., BALDAUF, L., PACHOW, D., SCHOLZ, J., ANGENSTEIN, F., STORK, O., KIRCHES, E. & MAWRIN, C. 2017. Receptor tyrosine kinase inhibition by regorafenib/sorafenib inhibits growth and invasion of meningioma cells. *Eur J Cancer,* 73**,** 9-21.

UDAN, R. S., KANGO-SINGH, M., NOLO, R., TAO, C. & HALDER, G. 2003. Hippo promotes proliferation arrest and apoptosis in the Salvador/Warts pathway. *Nat Cell Biol,* 5**,** 914-20.

VASSALLI, G. 2019. Aldehyde Dehydrogenases: Not Just Markers, but Functional Regulators of Stem Cells. *Stem Cells Int,* 2019**,** 3904645.

WAHLE, B. M., HAWLEY, E. T., HE, Y., SMITH, A. E., YUAN, J., MASTERS, A. R., JONES, D. R., GEHLHAUSEN, J. R., PARK, S. J., CONWAY, S. J., CLAPP, D. W. & YATES, C. W. 2018. Chemopreventative celecoxib fails to prevent schwannoma formation or sensorineural hearing loss in genetically engineered murine model of neurofibromatosis type 2. *Oncotarget,* 9**,** 718-25.

WANG, C., ZHU, X., FENG, W., YU, Y., JEONG, K., GUO, W., LU, Y. & MILLS, G. B. 2016. Verteporfin inhibits YAP function through up-regulating 14-3-3σ sequestering YAP in the cytoplasm. *Am J Cancer Res,* 6**,** 27-37.

WANG, M., DENG, X., YING, Q., JIN, T., LI, M. & LIANG, C. 2015. MicroRNA-224 targets ERG2 and contributes to malignant progressions of meningioma. *Biochem Biophys Res Commun,* 460**,** 354-61.

WANG, Z., GERSTEIN, M. & SNYDER, M. 2009. RNA-Seq: a revolutionary tool for transcriptomics. *Nat Rev Genet,* 10**,** 57-63.

WEI, Y., WU, S., XU, W., LIANG, Y., LI, Y., ZHAO, W. & WU, J. 2017. Depleted aldehyde dehydrogenase 1A1 (ALDH1A1) reverses cisplatin resistance of human lung adenocarcinoma cell A549/DDP. *Thorac Cancer,* 8**,** 26-32.

WEN, P. Y., YUNG, W. K., LAMBORN, K. R., NORDEN, A. D., CLOUGHESY, T. F., ABREY, L. E., FINE, H. A., CHANG, S. M., ROBINS, H. I., FINK, K., DEANGELIS, L. M., MEHTA, M., DI TOMASO, E., DRAPPATZ, J., KESARI, S., LIGON, K. L., ALDAPE, K., JAIN, R. K., STILES, C. D., EGORIN, M. J. & PRADOS, M. D. 2009. Phase II study of imatinib mesylate for recurrent meningiomas (North American Brain Tumor Consortium study 01-08). *Neuro Oncol,* 11**,** 853-60.

WIEMELS, J., WRENSCH, M. & CLAUS, E. B. 2010. Epidemiology and etiology of meningioma. *J Neurooncol,* 99**,** 307-14.

WILLIS, J., SMITH, C., IRONSIDE, J. W., ERRIDGE, S., WHITTLE, I. R. & EVERINGTON, D. 2005. The accuracy of meningioma grading: a 10-year retrospective audit. *Neuropathol Appl Neurobiol,* 31**,** 141-9.

WU, X., DINGLIN, X., WANG, X., LUO, W., SHEN, Q., LI, Y., GU, L., ZHOU, Q., ZHU, H., LI, Y., TAN, C., YANG, X. & ZHANG, Z. 2017. Long noncoding RNA XIST promotes malignancies of esophageal squamous cell carcinoma via regulation of miR-101/EZH2. *Oncotarget,* 8**,** 76015-28.

XU, H. M. & GUTMANN, D. H. 1998. Merlin differentially associates with the microtubule and actin cytoskeleton. *J Neurosci Res,* 51**,** 403-15.

YANAGAWA, Y., CHEN, J. C., HSU, L. C. & YOSHIDA, A. 1995. The transcriptional regulation of human aldehyde dehydrogenase I gene. The structural and functional analysis of the promoter. *J Biol Chem,* 270**,** 17521-7.

YANG, C. C., GRAVES, H. K., MOYA, I. M., TAO, C., HAMARATOGLU, F., GLADDEN, A. B. & HALDER, G. 2015. Differential regulation of the Hippo pathway by adherens junctions and apical-basal cell polarity modules. *Proc Natl Acad Sci U S A,* 112**,** 1785-90.

YANG, S. M., MARTINEZ, N. J., YASGAR, A., DANCHIK, C., JOHANSSON, C., WANG, Y., BALJINNYAM, B., WANG, A. Q., XU, X., SHAH, P., CHEFF, D., WANG, X. S., ROTH, J., LAL-NAG, M., DUNFORD, J. E., OPPERMANN, U., VASILIOU, V., SIMEONOV, A., JADHAV, A. & MALONEY, D. J. 2018. Discovery of Orally Bioavailable, Quinoline-Based

Aldehyde Dehydrogenase 1A1 (ALDH1A1) Inhibitors with Potent Cellular Activity. *J Med Chem,* 61**,** 4883-4903.
YE, K. 2007. Phosphorylation of merlin regulates its stability and tumor suppressive activity. *Cell Adh Migr,* 1**,** 196-8.
YESILOZ, U., KIRCHES, E., HARTMANN, C., SCHOLZ, J., KROPF, S., SAHM, F., NAKAMURA, M. & MAWRIN, C. 2017. Frequent AKT1E17K mutations in skull base meningiomas are associated with mTOR and ERK1/2 activation and reduced time to tumor recurrence. *Neuro Oncol,* 19**,** 1088-1096.
YI, C., TROUTMAN, S., FERA, D., STEMMER-RACHAMIMOV, A., AVILA, J. L., CHRISTIAN, N., PERSSON, N. L., SHIMONO, A., SPEICHER, D. W., MARMORSTEIN, R., HOLMGREN, L. & KISSIL, J. L. 2011. A tight junction-associated Merlin-angiomotin complex mediates Merlin's regulation of mitogenic signaling and tumor suppressive functions. *Cancer Cell,* 19**,** 527-40.
YU, J., ALHARBI, A., SHAN, H., HAO, Y., SNETSINGER, B., RAUH, M. J. & YANG, X. 2017. TAZ induces lung cancer stem cell properties and tumorigenesis by up-regulating ALDH1A1. *Oncotarget,* 8**,** 38426-38443.
YU, X., NG, C. P., HABACHER, H. & ROY, S. 2008. Foxj1 transcription factors are master regulators of the motile ciliogenic program. *Nat Genet,* 40**,** 1445-53.
YU, Z., PESTELL, T. G., LISANTI, M. P. & PESTELL, R. G. 2012. Cancer stem cells. *Int J Biochem Cell Biol,* 44**,** 2144-51.
YUZAWA, S., NISHIHARA, H. & TANAKA, S. 2016. Genetic landscape of meningioma. *Brain Tumor Pathol,* 33**,** 237-247.
ZADEH, G., KARIMI, S. & ALDAPE, K. D. 2016. PIK3CA mutations in meningioma. *Neuro Oncol,* 18**,** 603-4.
ZHANG, N., BAI, H., DAVID, K. K., DONG, J., ZHENG, Y., CAI, J., GIOVANNINI, M., LIU, P., ANDERS, R. A. & PAN, D. 2010. The Merlin/NF2 tumor suppressor functions through the YAP oncoprotein to regulate tissue homeostasis in mammals. *Dev Cell,* 19**,** 27-38.
ZHAO, A. Y., DAI, Y. J., LIAN, J. F., HUANG, Y., LIN, J. G., DAI, Y. B. & XU, T. W. 2018. YAP regulates ALDH1A1 expression and stem cell property of bladder cancer cells. *Onco Targets Ther,* 11**,** 6657-6663.
ZHAO, B., WEI, X., LI, W., UDAN, R. S., YANG, Q., KIM, J., XIE, J., IKENOUE, T., YU, J., LI, L., ZHENG, P., YE, K., CHINNAIYAN, A., HALDER, G., LAI, Z. C. & GUAN, K. L. 2007. Inactivation of YAP oncoprotein by the Hippo pathway is involved in cell contact inhibition and tissue growth control. *Genes Dev,* 21**,** 2747-61.
ZHAO, D., MCCAFFERY, P., IVINS, K. J., NEVE, R. L., HOGAN, P., CHIN, W. W. & DRAGER, U. C. 1996. Molecular identification of a major retinoic-acid-synthesizing enzyme, a retinaldehyde-specific dehydrogenase. *Eur J Biochem,* 240**,** 15-22.
ZHI, F., ZHOU, G., WANG, S., SHI, Y., PENG, Y., SHAO, N., GUAN, W., QU, H., ZHANG, Y., WANG, Q., YANG, C., WANG, R., WU, S., XIA, X. & YANG, Y. 2013. A microRNA expression signature predicts meningioma recurrence. *Int J Cancer,* 132**,** 128-36.
ZHOU, L. & HANEMANN, C. O. 2012. Merlin, a multi-suppressor from cell membrane to the nucleus. *FEBS Lett,* 586**,** 1403-8.
ZOTTI, T., SCUDIERO, I., VITO, P. & STILO, R. 2017. The Emerging Role of TRAF7 in Tumor Development. *J Cell Physiol,* 232**,** 1233-1238.
ZUKO, A., OGURO-ANDO, A., POST, H., TAGGENBROCK, R. L., VAN DIJK, R. E., ALTELAAR, A. F., HECK, A. J., PETRENKO, A. G., VAN DER ZWAAG, B., SHIMODA, Y., PASTERKAMP, R. J. & BURBACH, J. P. 2016.

Association of Cell Adhesion Molecules Contactin-6 and Latrophilin-1 Regulates Neuronal Apoptosis. *Front Mol Neurosci*, 9**,** 143.

8 Appendix:

This appendix demonstrates the specificity of antibodies used for immunofluorescence and western blotting in this thesis.

The specificity of fluorophore-conjugated antibodies can be determined by comparing the signal seen in a no primary antibody control (secondary only), with the signal seen in tissue/cells that have been appropriately incubated with both primary and secondary antibodies. All permeabilisation and blocking steps were identical to those used when primary antibodies were included (see Methods section 2.8). Any signal seen in the secondary only control is assumed to be non-specific as it cannot be associated to the primary antibody. The secondary only controls were incubated with the relevant species of their corresponding primary antibody (see Table 2.7), the fluorophore-conjugated secondary antibodies used in this thesis are listed in Table 2.8.

Immunofluorescence antibody validation with no primary antibody controls:

ALDH1A1:

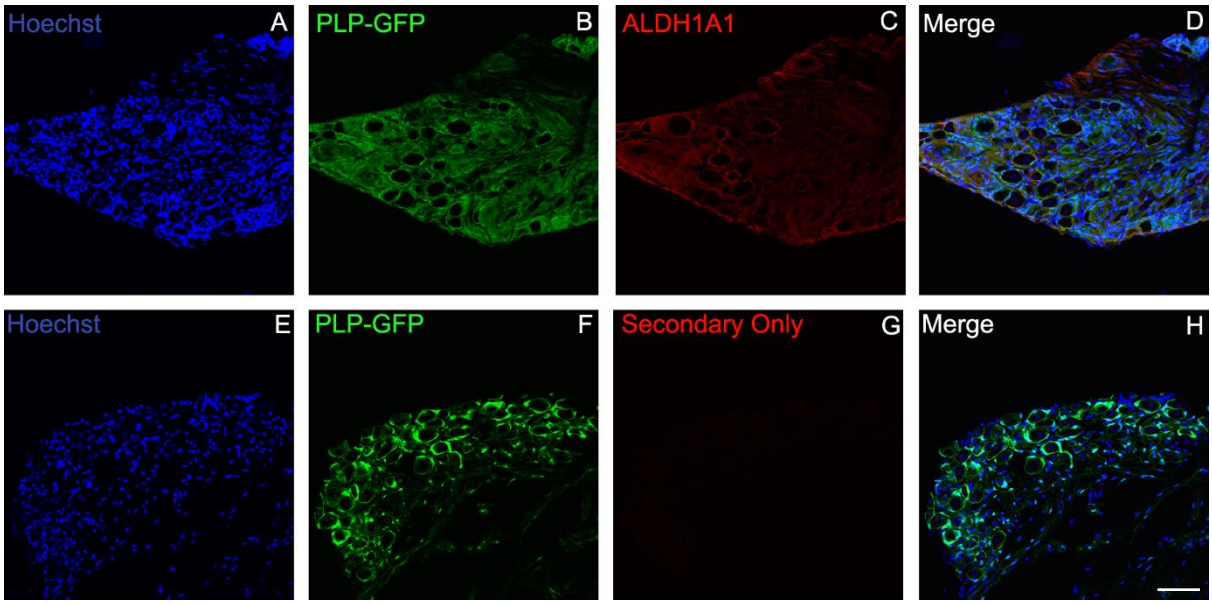

Figure 8.1: Immunofluorescence showing the specificity of the ALDH1A1 antibody in sections from mouse dorsal root ganglia tissue. Panels A-D show primary and secondary antibody whilst panels E-H shows the secondary antibody only control. Hoechst (panels A and E) shows counter-stained nuclei, a proteolipid protein promoter drives green fluorescent protein (PLP-GFP) expression in satellite glial cells and Schwann cells (PLP-GFP; panels B and F). ALDH1A1 primary antibody raised in rabbit, in combination with secondary anti-rabbit antibody reveals ALDH1A1 expression in satellite glial cells and Schwann cells (panel C), whereas in the secondary anti-rabbit antibody control (panel G), no ALDH1A1 signal is seen. Panels D and H show a composite image of all channels (Merge); scale bar = 50 μm.

Ki-67

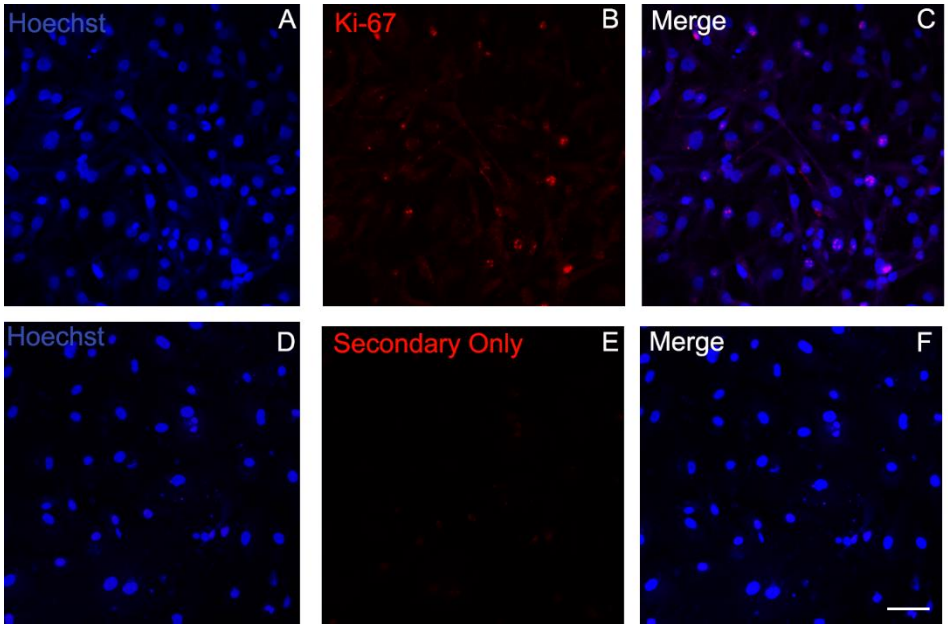

Figure 8.2: Immunofluorescence showing the specificity of the Ki-67 antibody in cultured human primary meningioma cells. Panels A-C shows the primary and secondary antibody whilst panels D-F shows the secondary only control. Hoechst (A and D) shows counter-stained nuclei. Ki-67 primary antibody raised in rabbit, in combination with secondary anti-rabbit antibody reveals nuclear Ki-67 expression (panel B), whereas in the secondary anti-rabbit antibody control (panel E), no Ki-67 signal is seen. Panels C and F show a composite image of both channels (Merge); scale bar = 20 µm.

MBP

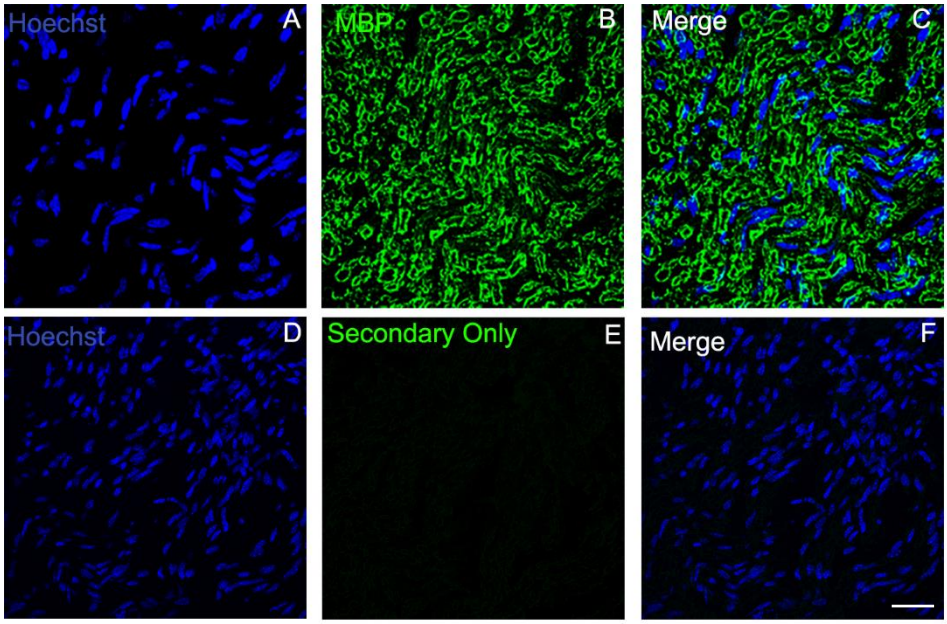

Figure 8.3: Immunofluorescence showing the specificity of the myelin basic protein (MBP) antibody in mouse sciatic nerve. Panels A-C shows the primary and secondary antibody whilst panels D-F shows the secondary only control. Hoechst (A and D) shows counter-stained nuclei. MBP primary antibody raised in rabbit, in combination with secondary anti-rabbit antibody reveals MBP expression (panel B), whereas in the secondary anti-rabbit antibody control (panel E), no MBP signal is seen. Panels C and F show a composite image of both channels (Merge); scale bar = 50 µm.

Neurofilament

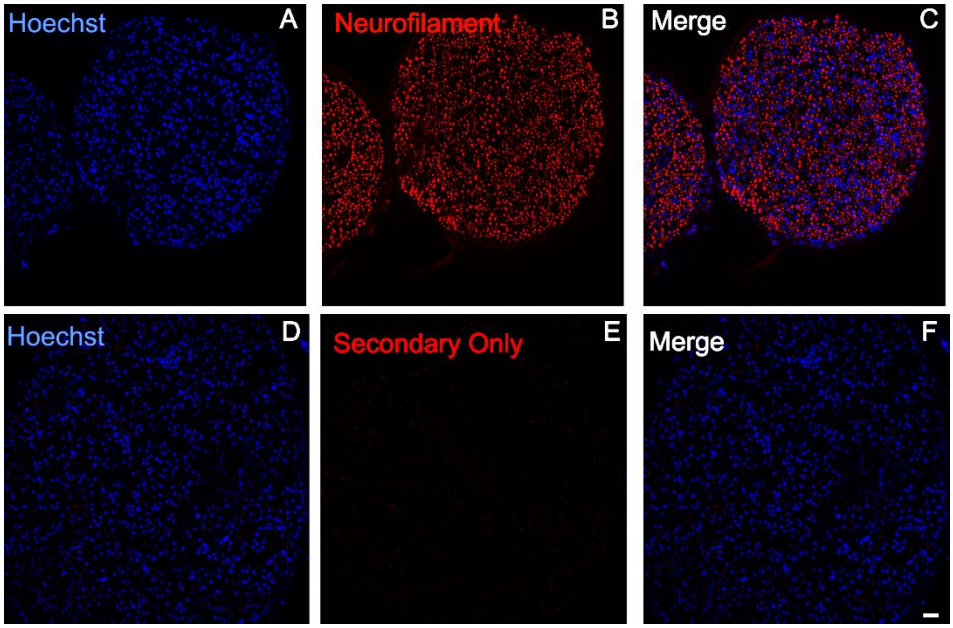

Figure 8.4: Immunofluorescence showing the specificity of the neurofilament antibody in mouse sciatic nerve. Panels A-C shows the primary and secondary antibody whilst panels D-F shows the secondary only control. Hoechst (A and D) shows counter-stained nuclei. Neurofilament primary antibody raised in chicken, in combination with secondary anti-chicken antibody reveals neurofilament expression (panel B), whereas in the secondary anti-chicken antibody control (panel E), no neurofilament signal is seen. Panels C and F show a composite image of both channels (Merge); scale bar = 50 µm.

TAZ

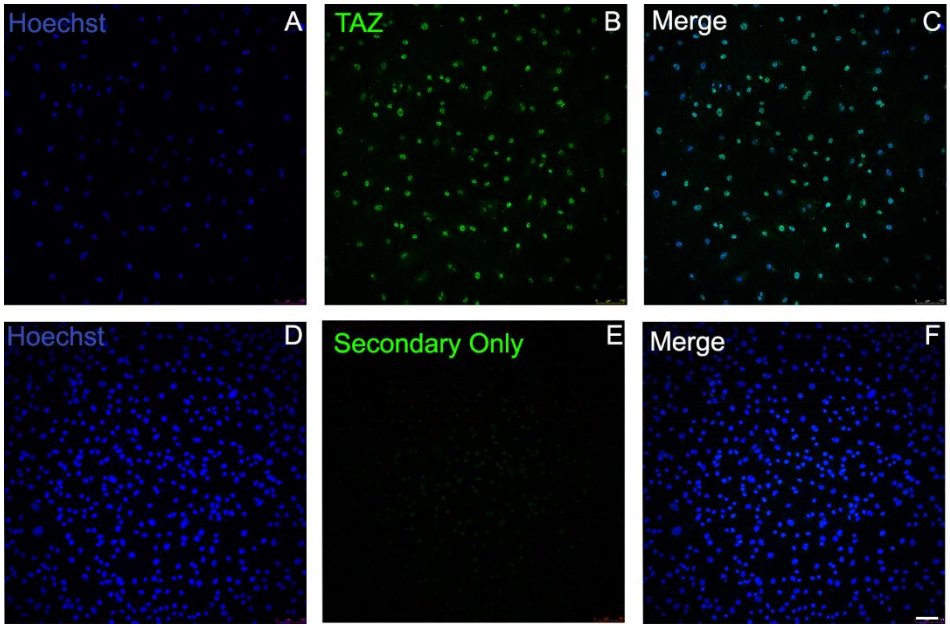

Figure 8.5: Immunofluorescence showing the specificity of the TAZ antibody in cultured human primary meningioma cells. Panels A-C shows the primary and secondary antibody whilst panels D-F shows the secondary only control. Hoechst (A and D) shows counter-stained nuclei. TAZ primary antibody raised in rabbit, in combination with secondary anti-rabbit antibody reveals TAZ expression (panel B), whereas in the secondary anti-rabbit antibody control (panel E), no TAZ signal is seen. Panels C and F show a composite image of both channels (Merge); scale bar = 50 µm.

YAP

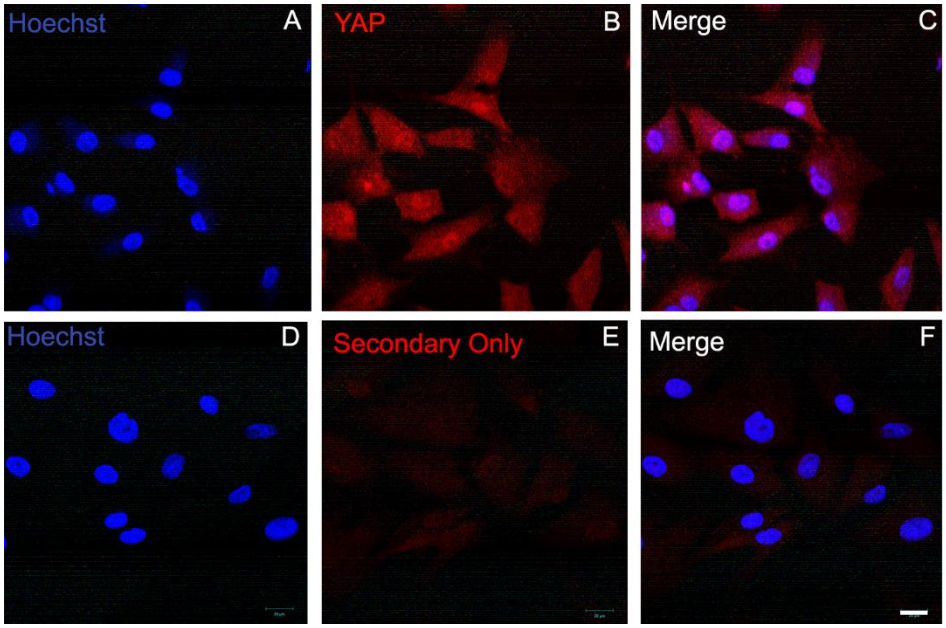

Figure 8.6: Immunofluorescence showing the specificity of the YAP antibody in cultured human primary meningioma cells. Panels A-C shows the primary and secondary antibody whilst panels D-F shows the secondary only control. Hoechst (A and D) shows counter-stained nuclei. YAP primary antibody raised in rabbit, in combination with secondary anti-rabbit antibody reveals YAP expression (panel B), whereas in the secondary anti-rabbit antibody control (panel E), no YAP signal is seen. Panels C and F show a composite image of both channels (Merge); scale bar = 20 µm.

Western blot antibody specificity is demonstrated by showing images of uncropped scans of each antibody used in this thesis. Whilst images are uncropped, membranes may have been cut in order to probe for multiple antibodies raised in the same host species on the same membrane. The datasheets for each antibody are based on the catalogue numbers listed in Table 2.7; images obtained in this thesis were compared with antibody datasheets to ensure that antibody signal was at the correct molecular weight.

Examples of western blot for each antibody:

TEAD1; TEAD2; TEAD3; TEAD4; Pan-TEAD and GAPDH:

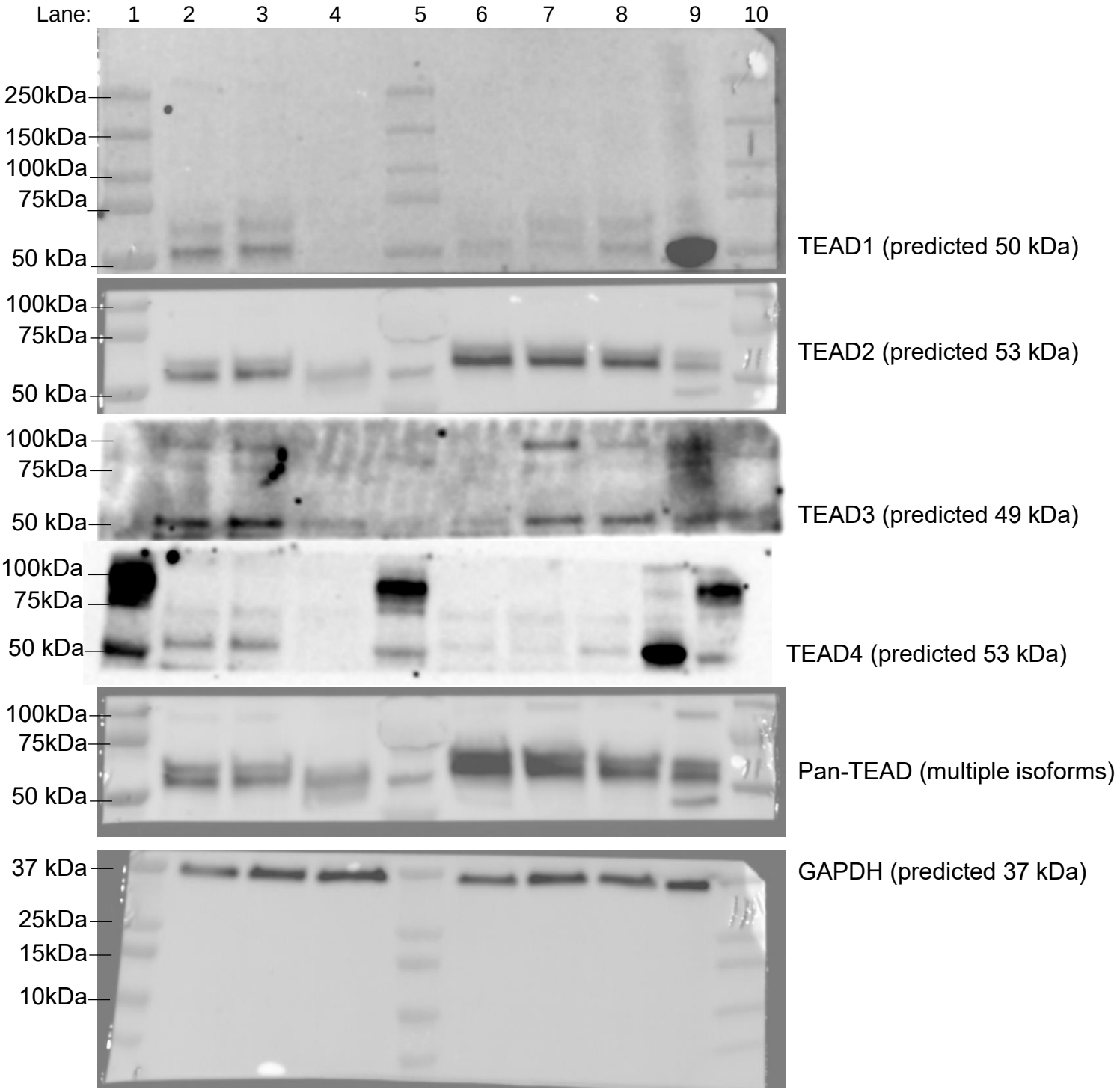

Figure 8.7: Uncropped scan of western blot membrane pieces to show antibody specificity for: TEAD1; TEAD2; TEAD3; TEAD4; Pan-TEAD and GAPDH. This western blot consisted of 10 lanes (1-10, reading from left to right). Lanes 1, 5 and 10 contained a protein size ladder which is labelled with known molecular weights in kilodaltons (kDa) marked on the left of each image. All antibodies showed binding at the relevant molecular weight in lanes 2-4 and 6-9, which contained protein lysate.

ALDH1A1:

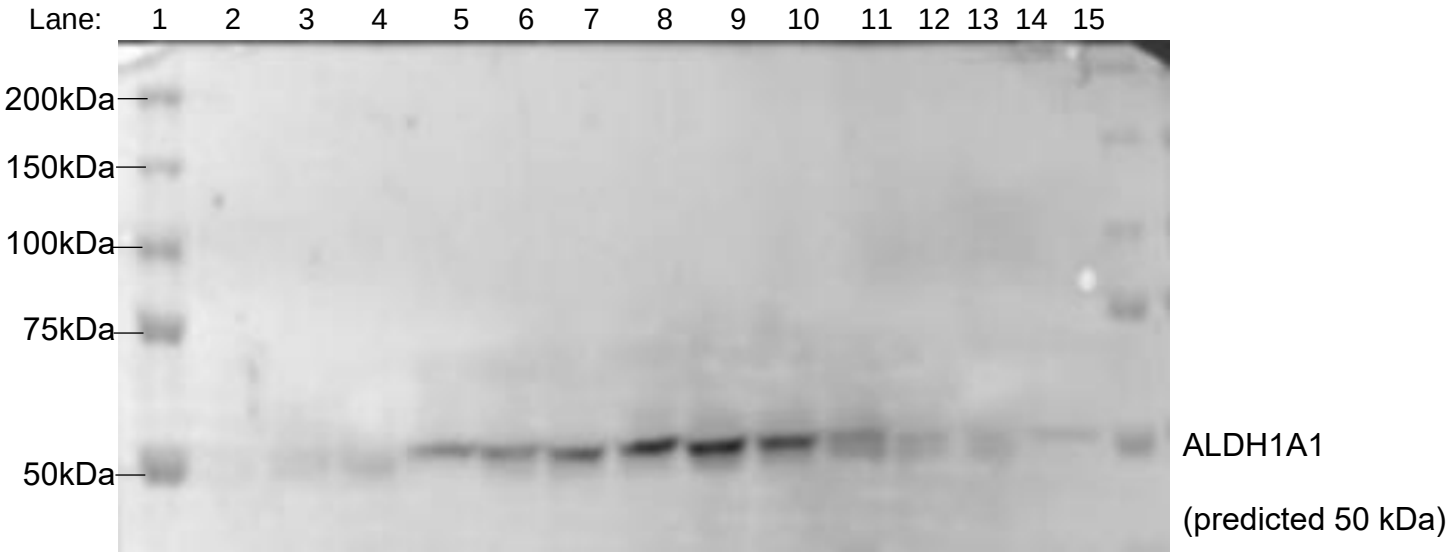

Figure 8.8: Uncropped scan of western blot membrane pieces to show antibody specificity for ALDH1A1. This western blot consisted of 15 lanes (1-15, reading from left to right, the right side of the 15th lane has been slightly cut). Lanes 1 and 15 contained a protein size ladder which is labelled with known molecular weights in kilodaltons (kDa) marked on the left of each image. The ALDH1A1 antibody showed binding at the relevant molecular weight in lanes 2-14 which contained protein lysate.

YAP/TAZ:

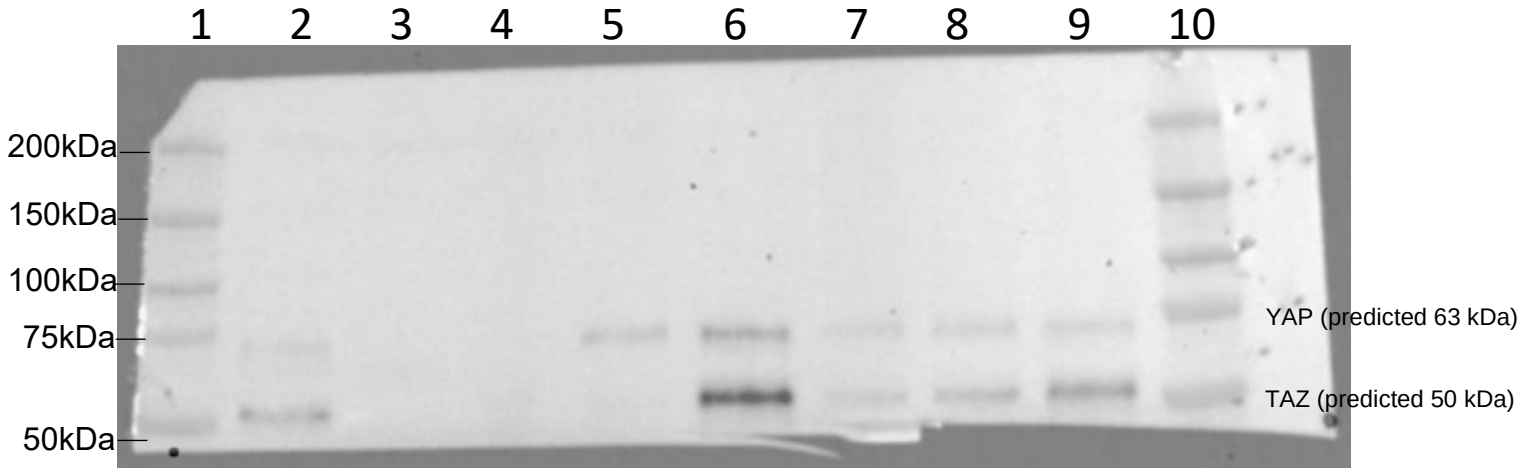

Figure 8.9: Uncropped scan of western blot membrane pieces to show antibody specificity for YAP and TAZ. This western blot consisted of 10 lanes (1-10, reading from left to right). Lanes 1 and 10 contained a protein size ladder which is labelled with known molecular weights in kilodaltons (kDa) marked on the left of each image. The YAP and TAZ antibodies showed binding at the relevant molecular weight in lanes 2-9, which contained protein lysate.

CTGF:

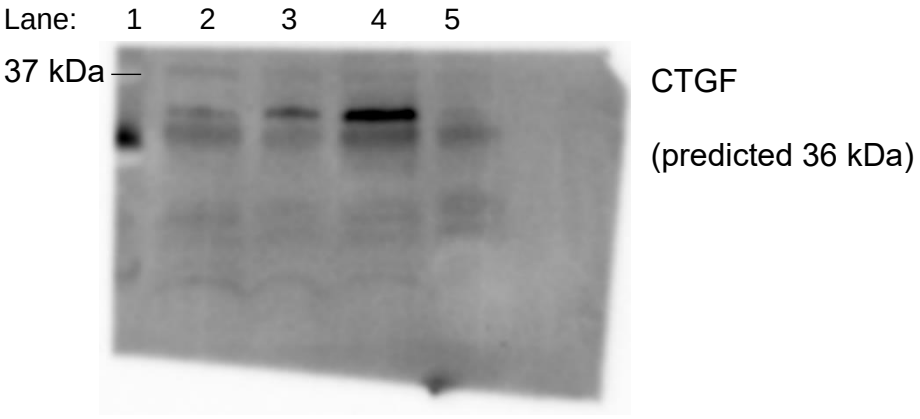

Figure 8.10: Uncropped scan of western blot membrane pieces to show antibody specificity for connective tissue growth factor (CTGF). This western blot consisted of 5 lanes (1-5, reading from left to right). Lane 1 contained a protein size ladder which is labelled with known molecular weights in kilodaltons (kDa) marked on the left of each image. The CTGF antibody showed binding at the relevant molecular weight in lanes 2-5, which contained protein lysate.

CyclinD1:

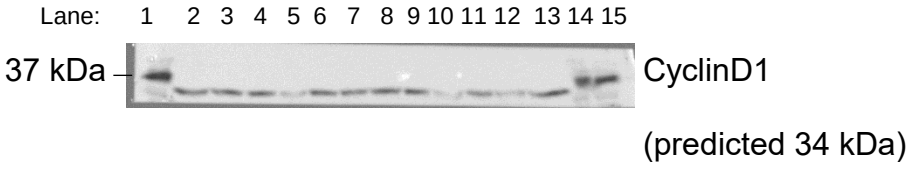

Figure 8.11: Uncropped scan of western blot membrane pieces to show antibody specificity for CyclinD1. This western blot consisted of 15 lanes (1-15, reading from left to right). Lanes 1, 14 and 15 contained a protein size ladder which is labelled with known molecular weights in kilodaltons (kDa) marked on the left of each image. The CyclinD1 antibody showed binding at the relevant molecular weight in lanes 2-13, which contained protein lysate.